

Eveline I.P. Volcke

**Modelling, analysis and control
of partial nitritation
in a SHARON reactor**

Thesis submitted in fulfillment of the requirements
for the degree of Doctor (PhD) in Applied Biological Sciences:
Environmental Technology

Promoters:

Prof. dr. ir. Peter A. Vanrolleghem

Department of Applied Mathematics, Biometrics and Process Control
Ghent University

Prof. dr. ir. Mark C.M. van Loosdrecht

Department of Biotechnology
Delft University of Technology

Dean:

Prof. dr. ir. Herman Van Langenhove

Rector:

Prof. dr. Paul Van Cauwenberge

*vo me broere, Corneel,
da 'k vor altied in m'n erte draeghe ...*

Dutch translation of the title:

Modelbouw, analyse en regeling van partiële nitrificatie
in een SHARON-reactor

Please refer to this work as follows:

Volcke E.I.P. (2006). Modelling, analysis and control of partial nitrification
in a SHARON reactor. PhD thesis, Ghent University, Belgium, pp. 300.

ISBN 90-5989-108-2

The author and the promoters give the authorization to consult and to
copy parts of this work for personal use only. Every other use is subject
to the copyright laws. Permission to reproduce any material contained
in this work should be obtained from the author.

Dankwoord

Het verrichten van doctoraatsonderzoek en het succesvol afronden ervan is slechts mogelijk dankzij de steun van en de samenwerking met vele mensen – het was in mijn geval niet anders. Een aantal van hen wil ik hierbij in het bijzonder bedanken.

Ik heb het voorrecht genoten begeleid te worden door twee waarlijk grootse promotoren, die mij tot tegen de grenzen van mijn kennis hebben geleid en mij zo in staat hebben gesteld deze te verleggen. Peter, bedankt om mij de kans te geven me te bekwamen in de milieutechnologie, meerbepaald waterzuivering, waar ik me al jaren voor interesseerde. Bedankt voor het vertrouwen en de vrijheid die ik heb gekregen, in het eigenlijke onderzoekswerk, bij deelname aan conferenties en projectvergaderingen en bij mijn onderwijstaken als assistent. Bedankt voor het enthousiasme, voor de vele ideeën, de interessante invalshoeken, voor de immer nuttige tips en verduidelijkende schema's. Mark, ook u was voor mij een promotor in de ware betekenis. Via e-mail was u nooit ver weg en tijdens vergaderingen in Gent of Delft leek u alle tijd te hebben, al ben ik zeker dat schijn bedriegt. Bedankt voor alle kritische opmerkingen, voor het beantwoorden van uiteenlopende vragen en voor het op de juiste momenten vrijgeven van stukjes uit een onuitputtelijke bron van kennis en inzichten, net zolang als ik die kon opslaan. Bedankt nog voor de gastvrijheid, die mijn verblijven in Delft mogelijk en aangenaam maakten.

Professor Noldus wil ik speciaal bedanken om me met veel geduld, methodisch en nauwgezet meer kennis van systeemtheorie bij te brengen. Voor de kennis en de rust die hij tegelijk uitstraalt, heb ik een diep respect, ik hoop ook van dat laatste wat te hebben overgenomen.

Het was me zeer aangenaam om samen met Stijn Van Hulle, mijn collega-nummer-1, te mogen werken rond autotrofe stikstofverwijdering in het algemeen en aan het IcoN-project in het bijzonder. Niet in het minst heb ik iets opgestoken van Stijns resultaatgerichtheid.

Een speciale vermelding verdienen ook de studenten, die ik heb mogen begeleiden tijdens het ‘maken’ van hun scriptie en die allen hebben bijgedragen tot algemene inzichten en/of concrete resultaten in dit werk: Ester, Sammy, Sabine, Kris, Josefa, Brecht en Nancy.

En er zijn nog een hele reeks mensen, met wie ik graag heb samengewerkt, zoals Stijn Wyffels en Mihaela Sbarciog. Chris Hellinga wil ik bedanken voor de oer-versie van het SHARON-model, waarop ik mocht verderbouwen. Jan-Willem Mulder en de rest van de mannen van Sluisjedijk worden bedankt voor het beschikbaar maken van de praktijkdata en om me met de SHARON-datacomputer te laten werken. *I want to thank Ulf Jeppsson for allowing me to use the BSM2 implementation in Matlab-Simulink, which allowed me to obtain very nice plant-wide results, as well as for his positive comments and remarks. I have also appreciated very much the interaction with Krist Gernaey and Darko Vrecko, leading to answers on a lot of small BSM2 questions.*

Zovele BIOMATHers (in de breedst mogelijke zin) wil ik van harte bedanken voor de leuke samenwerking op onderzoeks- en/of onderwijsvlak, voor het uitwisselen van ervaringen en gedachten, voor het zijn van een toffe bureaugenoot, voor de hulp bij administratieve of computerproblemen, voor korte en lange babbels, voor aangename lunches en koffiepauzes ... ik durf me niet aan een opsomming wagen maar weet heel goed hoeveel ik aan jullie heb. *My dear BIOMATH-colleagues, I don't dare to name names but I want to thank you for the nice cooperation, for exchanging experiences and thoughts, for being such a fine person to sit in the same room with, for helping me out with different types of problems, for short and long talks, for pleasant lunches and coffee-breaks.*

De ‘mensen uit Delft’ worden bedankt voor de gezellige uurtjes op de ‘kamer’ en daarbuiten. Ik heb me bij jullie thuisgevoeld.

Ma, pa, Annelies en Joery, . . . , moeke, Luc, Kristof, bedankt voor de steun, het vertrouwen en de doorgaans onuitgesproken trots. Bedankt voor jullie nuchtere kijk op de zaken op momenten dat ik wat minder goed kan relativeren. Bedankt voor alle hulp, dikwijls ongevraagd maar altijd welgekomen, en voor de goede zorgen, in het bijzonder voor Kamiel.

Bart-man, m’n beste vriend, lief, maatje, steun en toeverlaat. Al helemaal niet in woorden te vatten. Samen met Kamiel, onze lieve jongen, zorg je er elke dag opnieuw voor dat ik niet vergeet waar het leven eigenlijk om draait.

Eveline Volcke
Gent, 31 maart 2006

Contents

Summary	ix
Samenvatting	xiii
List of abbreviations	xvii
List of symbols	xix
1 Introduction - Outline	1
1.1 Introduction: the SHARON partial nitrification process . .	1
1.2 Outline of the thesis	4
2 What to do with reject water?	7
2.1 Introduction	8
2.2 Nitrification/denitrification over nitrate	10
2.2.1 Principle	10
2.2.2 Implementation and applications	11
2.3 Bio-augmentation processes	15
2.3.1 Principle	15
2.3.2 Applications	19
2.4 Nitrification/denitrification over nitrite	20
2.4.1 Principle	20
2.4.2 The SHARON process with complete nitrification and denitrification	22
2.4.3 SBRs	24
2.4.4 The 'Store And Treat' (SAT) process	25
2.5 Partial nitrification combined with an Anammox process .	27
2.5.1 Principle	27
2.5.2 Implementation and applications	27
2.6 Conclusions	31

3	The SHARON reactor model	33
3.1	Introduction	33
3.2	Liquid phase mass balances and heat balance	33
3.3	Biological conversion reactions	37
3.3.1	Process stoichiometry and kinetics	37
3.3.2	Heat production	41
3.4	pH calculation	43
3.4.1	General pH calculation procedure by means of a charge balance	43
3.4.2	Application to the SHARON reactor model	52
3.5	Gas phase mass balances	57
3.6	Transport between gas and liquid phase	59
3.7	Process control features	61
3.7.1	Aeration control	61
3.7.2	Acid and base addition	62
3.7.3	Liquid volume control	62
3.8	Model validation at the Sluisjesdijk SHARON reactor	63
3.8.1	Influent characteristics and reactor operation	63
3.8.2	Simulation results	64
3.9	Conclusions	70
4	Existence, uniqueness and stability of equilibrium points	71
4.1	Introduction	71
4.2	Stability concepts	72
4.2.1	Definitions of stability	72
4.2.2	Principle of contraction mappings	73
4.2.3	Linearization principle	74
4.3	The SHARON reactor model for constant pH	74
4.4	Equilibrium conditions	77
4.4.1	Equilibrium form of the SHARON reactor model	77
4.4.2	Equilibrium points in case $u_0 = 0$	78
4.4.3	Equilibrium points in case $u_0 > 0$	78
4.5	The contraction mapping theorem	79
4.5.1	Application to the 4-dimensional model	79
4.5.2	Application to a reduced 2-dimensional static mo- del	84
4.5.3	Comparison of the two methods	88
4.5.4	Simulation results	89
4.5.5	Calculation of the unique equilibrium point	92
4.5.6	Conclusions	94

4.6	Local asymptotic stability of equilibrium points	95
4.6.1	Local asymptotic stability and system behaviour	95
4.6.2	Simulation results	97
4.6.3	Conclusions	97
4.7	Direct calculation of equilibrium points	99
4.7.1	General model	99
4.7.2	Simplified model I: no inhibition	102
4.7.3	Simplified model II: nitrite inhibition of ammonium oxidation	113
4.7.4	Simplified model II _m : model II with small perturbations	122
4.7.5	Simplified model III: ammonium inhibition of ammonium oxidation	127
4.7.6	Practical implications	139
4.8	Discussion and conclusions	141
5	Controlling a SHARON reactor with fixed design	145
5.1	Introduction	146
5.2	Simulation study	147
5.2.1	Influent conditions	147
5.2.2	The SHARON and Anammox reactor models	148
5.2.3	SHARON reactor operating modes under study	149
5.3	Economic evaluation by means of an OCI	150
5.4	Simulation results	152
5.4.1	SHARON operating mode 1: no control	152
5.4.2	SHARON operating mode 2: O_2 -control	154
5.4.3	SHARON operating mode 3: cascade O_2 -control	156
5.4.4	SHARON operating mode 4: pH-control	158
5.4.5	SHARON operating mode 5: cascade pH-control	159
5.4.6	SHARON operating mode 6: O_2 -control + pH-control	160
5.4.7	SHARON operating mode 7: cascade O_2 -control + pH-control	163
5.4.8	SHARON operating mode 8: O_2 -control + cascade pH-control	166
5.5	Discussion and conclusions	168
6	Continuity-based model interfacing - reject water treatment	171
6.1	Introduction	172

6.2	Case study: implementation of a SHARON and Anammox model in BSM2	173
6.3	Application of the CBIM approach	175
6.3.1	Step 1: Elemental mass fractions and charge density	176
6.3.2	Step 2: Set-up of composition matrices	181
6.3.3	Step 3: Definition of transformation matrices	183
6.3.4	Step 4: Implementation of the transformations	201
6.4	Temperature and time in model interfacing	202
6.5	Conclusions	202
7	Plant-wide evaluation of reject water treatment	205
7.1	Introduction	206
7.2	The BSM2, SHARON and Anammox models	207
7.3	Economic evaluation by means of an operating cost index	209
7.4	Simulation results and discussion	213
7.5	Conclusions	219
8	Interaction between control and design of a SHARON reactor	221
8.1	Introduction	221
8.2	BSM2 reject water characteristics	221
8.3	SHARON reactor operating modes under study	222
8.4	Economic evaluation by means of OCIs	224
8.5	Simulation results	225
8.5.1	Operation of a SHARON reactor with $V=338 \text{ m}^3$	225
8.5.2	Operation of a SHARON reactor with $V=220 \text{ m}^3$	232
8.5.3	Operation of a SHARON reactor with $V=460 \text{ m}^3$	236
8.6	Discussion and conclusions	240
9	General discussion, conclusions and perspectives	243
	References	255
	Appendices	265
A	Equilibrium constants	267
A.1	Definition of equilibrium constants	267
A.1.1	Absolute equilibrium constants	267
A.1.2	Relative equilibrium constants in water	268
A.2	Temperature dependency of equilibria	269
A.2.1	The ammonium/ammonia equilibrium	269
A.2.2	The nitrous acid/nitrite equilibrium	270

B	Source code of Simulink c-mex function for pH calculation	273
C	Boundaries for the state variables of the SHARON model	283
C.1	Upper and lower boundaries under dynamic conditions	283
C.1.1	Boundaries for x_1	283
C.1.2	Boundaries for x_3	283
C.1.3	Boundaries for x_2	284
C.1.4	Boundaries for x_4	285
C.2	Upper boundaries under equilibrium conditions	285
D	The Anammox reactor model	287
D.1	State variables and mass balances	287
D.2	Biological conversion reactions	288
	Curriculum vitae	295

Summary

Biological techniques for nitrogen removal from wastewater streams that convert ammonium to nitrite only (i.e. the so-called nitritation reaction) and prevent further oxidation of nitrite to nitrate, display distinct advantages in comparison to conventional nitrification-denitrification over nitrate. In the SHARON process, stable nitrite formation is achieved by working at high temperature (about 35°C) and neutral pH (about 7). An appropriate sludge retention time is maintained to keep in ammonium oxidizing biomass, while washing out the nitrite oxidizing biomass, which grows slower than the ammonium oxidizing biomass under these conditions. In the last few years, the coupling of a partial nitritation process, in which about 50% of the ammonium is converted to nitrite, while the remaining 50% is not converted, with a so-called Anammox process, in which ammonium and nitrite are converted to nitrogen gas, has gained a lot of interest. With a combined partial nitritation-Anammox process, low nitrogen effluent concentrations can be obtained, while up to 63% aeration cost savings are realized, the need for external carbon source is completely omitted and sludge and CO_2 productions are very low in comparison with conventional nitrification-denitrification over nitrate.

The SHARON partial nitritation process for coupling with an Anammox process, is the focus of this thesis. It is very well suited to treat wastewater flows with high ammonium concentrations. A typical application is the reject water stream, originating from sludge digestion, dewatering and/or drying. In chapter 2, the SHARON partial nitritation process is compared with other biological treatment techniques for reject water. It is clear that the process selection strongly depends on the specific conditions and requirements in terms of efficiency, effluent quality, process compactness and associated operating and investment costs. The best option is mostly found among bio-augmentation

techniques and processes based on nitrification, the combined SHARON-Anammox process being an example of the latter.

An extensive model of a SHARON reactor has been developed (chapter 3), describing both liquid and gas phase dynamics, with special attention devoted to pH calculation, for which a general procedure has been developed. The resulting model has been validated at the full-scale SHARON reactor in Sluisjesdijk. For the simulation work carried out in this thesis, it has been judged sufficiently accurate to qualitatively represent the behaviour of a realistic SHARON reactor.

As a good knowledge of process dynamics is essential for control purposes, a theoretical study has been carried out with respect to the occurrence of multiple equilibrium points in SHARON partial nitrification models. The stability of these equilibrium points has been analyzed as well (chapter 4). Particular attention has been paid to the influence of microbial characteristics and to the translation of these findings into practical implications. Three equilibrium points have been found in case nitrite oxidizers are not limited by ammonium and no inhibition takes place: a wash-out point, an equilibrium point corresponding with only nitrite formation and an equilibrium point corresponding with nitrate formation. The dilution rate and the influent ammonium concentration determine which equilibrium point is (quasi) globally asymptotically stable and will usually be reached. Further results indicate that product inhibition does not affect the number of equilibrium points, while substrate inhibition is clearly a source of additional equilibrium points.

The usefulness of controlling a SHARON reactor with fixed design in view of its coupling with an Anammox process, is addressed in chapter 5. Several possible operating modes for the SHARON reactor, differing in control strategies for O_2 , pH and the produced nitrite:ammonium ratio and based on regulating the air flow rate and/or acid/base addition, are systematically evaluated. The results are quantified through an operating cost index (OCI). Best results are obtained by means of cascade feedback control of the nitrite:ammonium ratio produced by the SHARON reactor through setting an O_2 set point that is tracked by adjusting the air flow rate, combined with single loop pH-control through acid/base addition.

In chapter 6, the issue of coupling models with different state variables is addressed. The continuity-based interfacing method (CBIM) is applied to study the effect of reject water treatment with a SHARON-Anammox process on a plant-wide scale. The Benchmark Simulation

Model no. 2 (BSM2) is used to simulate the behaviour of a complete wastewater treatment plant, not only including the activated sludge process, but also the processes describing sludge treatment. The CBIM approach is followed to develop interfaces between the models ASM1/-SHARON, SHARON/Anammox and Anammox/ASM1. At the same time, this generally applicable approach is further refined and particular issues when coupling models in which pH is considered as a state variable, are pointed out.

The actual plant-wide evaluation of reject water treatment is described in chapter 7. A scenario without sludge treatment and therefore without reject water was compared with one in which untreated reject water is recycled to the main plant and one in which the reject water is treated with a combined SHARON-Anammox process before recirculation. It is shown that recirculation of the untreated reject water stream, representing 21% of the total influent ammonium load, unacceptably worsens the total nitrogen concentration in the effluent of the BSM2 WWTP. The effluent quality improves significantly by treatment of the reject water stream with a SHARON-Anammox process before recirculation. Although the yearly operating cost savings resulting from reject water treatment with a SHARON-Anammox process as such only partly warrant the associated investment costs, it is a promising option to meet the required effluent limits and prevent the WWTP from losing its permit.

In chapter 8, the control strategy of the SHARON reactor for treatment of the BSM2 reject water, is optimized and the interaction between reactor design and the usefulness of control is assessed. The best performance of the SHARON and Anammox reactor in terms of Anammox effluent quality (ammonium) is obtained with combined cascade O_2 -control and pH-control in the SHARON reactor. However, it has also been shown that a better conversion efficiency of the combined SHARON-Anammox process does not necessarily result in lower operating costs on a plant-wide scale. Besides, at different SHARON reactor volumes, different control strategies have been found optimal. For a moderately large reactor, good results have been obtained by controlling the aerobic retention time through cyclic reactor operation, and at the same time applying oxygen control during the aerobic phases. When using a smaller reactor volume, pH control becomes necessary as well.

Chapter 9 closes this thesis with general conclusions and perspectives for future research.

Samenvatting

Biologische technieken voor stikstofverwijdering uit afvalwater die ammonium omzetten tot nitriet (i.e. de zogenaamde nitritatie-reactie) en verdere oxidatie van nitriet tot nitraat vermijden, vertonen uitgesproken voordelen ten opzichte van technieken op basis van traditionele nitrificatie-denitrificatie over nitraat.

In het SHARON-proces wordt stabiele nitrietvorming bekomen bij hoge temperaturen (ca. 35°C) en neutrale pH (ongeveer 7). Een gepaste slibverblijftijd wordt aangehouden, zodat ammoniumoxideerders zich in de reactor handhaven en nitrietoxideerders, die onder de gegeven omstandigheden trager groeien, uitspoelen. De laatste jaren wordt een sterk toenemende interesse waargenomen voor de koppeling van processen voor partiële nitritatie, waarbij ongeveer 50% van het aanwezige ammonium wordt omgezet tot nitriet, terwijl de overige 50% niet wordt omgezet, met een zogenaamd Anammox-proces, waarin ammonium en nitriet worden gecombineerd tot stikstofgas. Met een gecombineerd proces voor partiële nitritatie en Anammox kunnen lage effluentconcentraties worden behaald, terwijl een besparing tot 63% aan beluchtingskosten wordt gerealiseerd, de noodzaak aan toevoeging van externe koolstofbron volledig verdwijnt en de productie van slib en CO_2 zeer laag is in vergelijking met traditionele nitrificatie-denitrificatie over nitraat.

Het SHARON-proces voor partiële nitritatie, met het oog op koppeling met een Anammox-proces, vormt de kern van dit werk. Het gecombineerde SHARON-Anammox-systeem is zeer geschikt voor de behandeling van afvalwaterstromen die hoge ammoniumconcentraties bevatten. Een typische toepassing vormt de behandeling van rejectiewater, afkomstig van slibvergisting, -ontwatering en/of -droging. In hoofdstuk 2, wordt het SHARON-proces voor partiële nitritatie vergeleken met andere biologische behandelingstechnieken voor rejectiewater. De processeselectie is duidelijk sterk afhankelijk van specifieke eigen-

schappen en vereisten in termen van efficiëntie, effluentkwaliteit, compactheid van de installatie en de ermee gepaard gaande werkings- en investeringskosten. De beste oplossing wordt meestal gevonden onder bio-augmentatieprocessen en processen gebaseerd op nitritatie, waarvan het gecombineerde SHARON-Anammox proces een voorbeeld is.

Een uitgebreid model van een SHARON-reactor werd ontwikkeld (hoofdstuk 3). Dit model beschrijft zowel de dynamica in de vloeistof als in de gasfase, met bijzondere aandacht voor de berekening van de pH, waarvoor een algemeen procedure werd ontwikkeld. Het resulterende model werd gevalideerd aan de volle-schaal SHARON-reactor te Sluisjesdijk. Voor de simulatiedoelinden in dit werk werd geoordeeld dat het model voldoende nauwkeurig het gedrag van een realistische SHARON-reactor beschrijft.

Aangezien een goede kennis van procesdynamica essentieel is voor regeldoeleinden, werd een theoretische studie uitgevoerd met betrekking tot het optreden van meerdere evenwichtspunten in SHARON-modellen met partiële nitritatie. De stabiliteit van deze evenwichtspunten werd eveneens geanalyseerd (hoofdstuk 4). Bijzondere aandacht werd besteed aan de invloed van microbiële karakteristieken en aan de vertaling van de bevindingen in de praktijk. In het geval nitrietoxideerders niet worden gelimiteerd door ammonium en geen enkele vorm van inhibitie plaatsvindt, trede drie evenwichtspunten op: een uitspoelingspunt, een evenwichtspunt waarin enkel nitriet wordt gevormd en een evenwichtspunt dat overeenstemt met nitraatvorming. De dilutiesnelheid en de ammoniumconcentratie in het influent bepalen welk evenwichtspunt (quasi) globaal asymptotisch stabiel is en doorgaans zal worden bereikt. Verdere resultaten wijzen erop dat productinhibitie het aantal evenwichtspunten niet beïnvloedt, terwijl substraat-inhibitie duidelijk bijkomende evenwichtspunten voor gevolg heeft.

In hoofdstuk 5 werd de noodzaak aan regeling van een SHARON-reactor met een vast ontwerp bestudeerd voor zijn koppeling met een Anammox-proces. Verschillende bedrijfsvoeringen voor de SHARON-reactor werden op systematische wijze geëvalueerd. Ze verschillen in de toegepaste regelstrategieën voor O_2 , pH en de geproduceerde nitriet:ammonium-verhouding, door aanpassing van het luchtdebiet en/of de toevoeging van zuur of base. De resultaten werden gekwantificeerd op economisch vlak door middel van een operationele kostenindex (OCI). De beste resultaten werden bekomen met een cascade-regeelaar, waarbij de nitriet:ammonium-verhouding in de SHARON-reactor de variabele wenswaarde bepaalt voor de zuurstofconcentratie, die be-

reikt wordt door aanpassing van het luchtdebiet, in combinatie met enkelvoudige pH-regeling door toevoeging van zuur of base.

In hoofdstuk 6 wordt aandacht besteed aan de koppeling van modellen met verschillende toestandsvariabelen. De CBIM (continuity-based interfacing method)-benadering werd toegepast om het effect van rejectiewaterbehandeling met een SHARON-Anammox-proces op een volledige waterzuiveringsinstallatie te bestuderen. Om het gedrag van een volledige waterzuiveringsinstallatie te bestuderen, werd het 'Benchmark'-simulatiemodel BSM2 gebruikt, dat niet enkel het actief-slibproces beschrijft, maar ook de slibbehandeling omvat. De CBIM-benadering werd gevolgd bij de ontwikkeling van koppelingen ('interfaces') tussen de modellen ASM1/SHARON, SHARON/Anammox and Anammox/ASM1. Terzelfdertijd werd deze algemeen toepasbare methode verder verfijnd en werd gewezen op bijzondere aandachtspunten bij het koppelen van modellen met de pH als toestandsvariabele.

De eigenlijke evaluatie van rejectiewaterbehandeling op het niveau van de volledige waterzuiveringsinstallatie, wordt beschreven in hoofdstuk 7. Een scenario zonder slibbehandeling en dus zonder rejectiewater wordt vergeleken met de recirculatie van onbehandeld rejectiewater naar de actief-slibbekkens en met recirculatie van rejectiewater na behandeling in een SHARON-Anammox-systeem. Er wordt aangetoond dat recirculatie van onbehandeld rejectiewater, dat ongeveer 21% van de totale inkomende ammoniumbelasting uitmaakt, leidt tot een onaanvaardbare toename van de totale stikstofconcentraties in het effluent van de BSM2-waterzuiveringsinstallatie. Een beduidende verbetering van de effluentkwaliteit wordt bekomen door behandeling van het rejectiewater met een SHARON-Anammox-proces voor recirculatie. Alhoewel de jaarlijkse besparingen in werkingskosten bij behandeling van het rejectiewater met een SHARON-Anammox-proces de ermee gepaard gaande investeringskosten slechts ten dele verantwoordt, is deze technologie veelbelovend voor het behalen van de vereiste effluentkwaliteit, zodat de waterzuiveringsinstallatie zijn vergunning niet verliest.

De toegepaste regelstrategie voor de SHARON-reactor voor de behandeling van het BSM2-rejectiewater, werd geoptimaliseerd in hoofdstuk 8. Hierbij komt eveneens de interactie tussen reactorontwerp en de noodzaak van regeling aan bod. De beste resultaten voor het gecombineerde SHARON-Anammox-systeem, in termen van de Anammox-effluentkwaliteit (ammonium), werden behaald met cascade O_2 -regeling, gecombineerd met pH-control, in de SHARON-reactor. Er wordt echter

aangetoond dat een betere omzetting in het gecombineerde SHARON-Anammox-proces niet noodzakelijk resulteert in lagere operationele kosten op het niveau van de volledige waterzuiveringsinstallatie. Voor verschillende volumes van de SHARON-reactor werden verschillende regelstrategieën optimaal bevonden. Voor een relatief grote reactor werden goede resultaten bekomen door regeling van de aërobe slibverblijftijd door cyclisch reactorbedrijf en het terzelfdertijd toepassen van zuurstofregeling tijdens de aërobe fasen. Indien een kleinere reactor wordt aangewend, blijkt pH-regeling eveneens noodzakelijk.

Hoofdstuk 9 sluit dit werk af met algemene conclusies en perspectieven voor verder onderzoek.

List of abbreviations

abbreviation	description
Anammox	ANAerobic (<i>also: ANoxic</i>) AMMONium OXidation
aerSRT	Aerobic Sludge Retention Time
ASM	Activated Sludge Model
ASM	Activated Sludge Model
BABE	Bio-Augmentation Batch Enhanced
BAS	Biofilm Airlift Suspension
BSM	Benchmark Simulation Model
CANON	Completely Autotrophic Nitrogen Removal Over Nitrite
CSTR	Continuous Stirred Tank Reactor
HRT	Hydraulic Residence Time
MBR	Membrane BioReactor
OCI	Operating Cost Index
OLAND	Oxygen Limited Autotrophic Nitrification Denitrification
OUR	Oxygen Uptake Rate
PE	Population Equivalents
PU	Pollution Units
RBC	Rotating Biological Contactor
RWQM	River Water Quality Model
SAT	Store And Treat
SBR	Sequencing Batch Reactor
SHARON	Single reactor High activity Ammonium Removal Over Nitrite
SRT	Sludge Residence Time
UASB	Upflow Anaerobic Sludge Blanket
VFA	Volatile Fatty Acid

List of symbols

symbol	characterization	dimension
AE	aeration energy	kWh d^{-1}
A_R	reactor cross section area	m^2
A_W	reactor (side) wall area	m^2
A_{ij}	stoichiometric coefficient of component i in reaction j	mole
C	concentration	mole m^{-3}
c_p	specific heat capacity	$\text{kJ kg}^{-1} \text{K}^{-1}$
D	diffusion coefficient	$\text{m}_R \text{s}^{-2}$
d	diameter	m
EC	external carbon addition	kg COD d^{-1}
EQ	effluent quality	kg PU d^{-1}
HE	heating energy	kWh d^{-1}
K	affinity constant	mole m^{-3}
K_e	equilibrium constant (acidity constant in water)	mole m^{-3}
K_w	water equilibrium constant	$\text{mole}^2 \text{m}^{-6}$
k_{La}	volumetric mass transfer coefficient	d^{-1}
L^+	net positive charges that take part in chemical equilibria	mole m^{-3}
M	molar mass	g mole^{-1}
ME	mixing energy	kWh d^{-1}
MP	methane production	$\text{kg CH}_4 \text{d}^{-1}$
N	molar flow rate	mole d^{-1}
n	total number of moles in gas phase	mole

OCI	operating cost index	€ year ⁻¹
PE	pumping energy	kWh d ⁻¹
R_X	retention fraction of insoluble components (in Anammox reactor)	–
r_i	volumetric conversion rate of component i	mole m _L ⁻³ d ⁻¹ ; gCOD m ⁻³ d ⁻¹ ; gN m ⁻³ d ⁻¹
SP	sludge production for disposal	kg SS d ⁻¹
TIC	total inorganic carbon	mole m ⁻³
TNH	total ammonium	mole m ⁻³
TNO_2	total nitrite	mole m ⁻³
U	overall heat transfer coefficient	kW m ⁻² K ⁻¹
V	volume	m ³
$v_{G,s}$	superficial gas velocity	m _G ³ m _R ⁻² d ⁻¹
X_{amm}	ammonium oxidizing biomass	mole m ⁻³
X_{nit}	nitrite oxidizing biomass	mole m ⁻³
Y_j	yield coefficient for reaction j	mole X (mole substrate) ⁻¹
Z^+	net positive charges that don't take part in chemical equilibria	mole m ⁻³
$(-\Delta_f H)$	enthalpy of formation	kJ mole ⁻¹
$(-\Delta_r H)$	reaction enthalpy (heat produced)	kJ mole ⁻¹
$\Delta_s H$	solution enthalpy (> 0 when heat is re- leased)	kJ mole ⁻¹
$\Delta_v H$	vaporization heat (> 0 when heat is re- leased)	kJ mole ⁻¹
δ	density	kg m ⁻³
Φ	volumetric flow rate	m ³ d ⁻¹
ρ_j	volumetric conversion rate of reaction j	mole m _L ⁻³ d ⁻¹
σ_j	volumetric conversion rate of reaction j in canonical state space model representation	mole m _L ⁻³ d ⁻¹

subscripts

0	initial (at time=0)
<i>as</i>	activated sludge tanks
<i>ad</i>	anaerobic digester
<i>An</i>	Anammox
<i>B</i>	bottom
<i>E</i>	environment
<i>e</i>	equilibrium
<i>eq</i>	equivalents
<i>G</i>	gas phase
<i>i</i>	for component <i>i</i>
<i>L</i>	liquid phase
<i>R</i>	reactor
<i>SH</i>	SHARON
<i>T</i>	top
<i>W</i>	wall

superscripts

<i>amm</i>	for ammonium oxidation
<i>in</i>	influent
<i>dNO₂</i>	for denitrification of nitrite
<i>dNO₃</i>	for denitrification of nitrate
<i>exchange</i>	exchange from gas phase to liquid phase
<i>met</i>	for methanol oxidation
<i>nit</i>	for nitrite oxidation
<i>opt</i>	optimal
<i>out</i>	outlet
0	initial (at time=0)
*	saturation
o	reference conditions (1 bar)

Chapter 1

Introduction - Outline

1.1 Introduction: the SHARON partial nitrification process for nitrogen removal from wastewater

Since the introduction around 1960 of the Haber-Bosch process, that lies on the basis of the production of synthetic nitrogen fertilizer from atmospheric N_2 to supply protein food for the increasing global population, man has had a substantial impact on the global nitrogen cycle. In the last century, the world's annual industrial output of nitrogenous fertilizer increased from 10 Mt N in 1960 to about 90 Mt N in 1998, where the global estimate for biological nitrogen fixation is in the range of 200-240 Mt (Gijzen and Mulder, 2001). Only 10-15% of the fertilizer applied to land ends up in food protein. The remainder is 'lost' into the air, soil and (ground)water, causing serious public health and environmental problems, of which eutrophication is the best known, besides the 'blue baby' syndrome and reported relationships between nitrates and some forms of cancer. Once fixed nitrogen has been incorporated into high quality protein and has been consumed as human food or animal feed, only a small fraction (1-2% for humans) is incorporated into the body, while the major part of the nitrogen is released again into the environment in the form of domestic wastewater and manure (Gijzen and Mulder, 2001).

Tertiary treatment of domestic wastewater is increasingly applied in industrialized nations. Over the last decades, legislation regarding nutrient levels in the effluent of wastewater treatment plants (WWTPs) has become more and more stringent and the need for nutrient removal besides the traditionally applied carbon removal in WWTPs has be-

come apparent. Already in the seventies, the European Union (EU) started issuing different regulations and directives, e.g. the Urban Waste Water Treatment Directive (91/271/EEC) issued in 1991 and its amending Directive 98/15/EEC, the Nitrates Directive (91/676/EEC) and, more recently, the Water Framework Directive (2000/60/EC). According to the Urban Waste Water Treatment Directive, target effluent values for plants with more than 100,000 PE should amount less than 10 mgN-tot/l. However, it is important that nitrogen removal processes not only meet these standards, but that they meet these standards in a sustainable way, regarding the substantial contribution of inorganic nitrogen in wastewater to the global nitrogen balance (Mulder, 2003).

Throughout the years, biological techniques for nitrogen removal from wastewater have proven their effectiveness and have been implemented widely in favour of the more expensive physicochemical techniques. Traditionally, biological nitrogen removal from wastewater is performed through nitrification/denitrification over nitrate (Figure 1.1). In the nitrification reaction, ammonium, the dominant form, is oxidized with oxygen via nitrite to nitrate. Subsequently, nitrate is denitrified to nitrogen gas. During denitrification, an organic carbon source is consumed, that should be supplied externally when necessary, while CO_2 is produced.

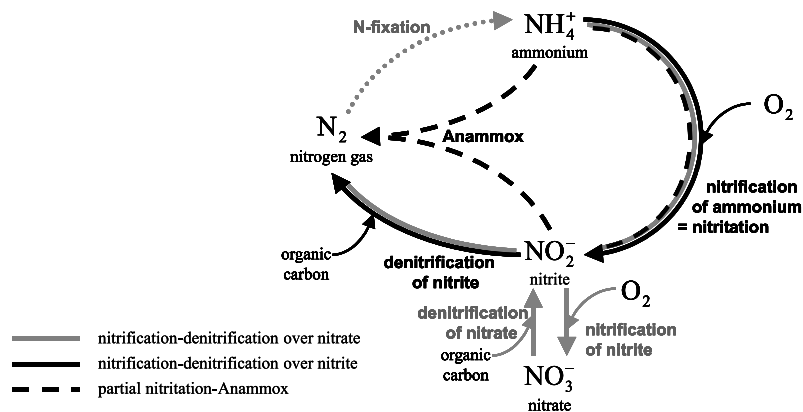


Figure 1.1: Simplified nitrogen cycle, indicating traditional and novel pathways for ammonium removal

In the search of improving the sustainability of nitrogen removal from wastewater, nitritation techniques have been denoted for quite a while as very promising (Abeling and Seyfried, 1992). Nitritation comprises conversion of ammonium to nitrite, while further oxidation

of nitrite to nitrate is prevented, thus realizing aeration cost savings in comparison with conventional nitrification to nitrate. In this way, significant aeration cost savings (up to 25%) are realized in comparison with conventional nitrification to nitrate, while less waste sludge is produced. When subsequent denitrification is applied (Figure 1.1), less carbon source (up to 40% less) must be added, while sludge and CO_2 productions are decreased.

However, nitrification processes can also be operated without denitrification. This operation mode is especially interesting in view of its coupling with a so-called Anammox (ANAerobic AMMONia OXidation) process, in which ammonium and nitrite are converted to nitrogen gas under anaerobic conditions by autotrophic micro-organisms (Jetten et al., 1999), and has gained a lot of interest in the last few years. For this purpose, in the first step, about 50% of the ammonium is converted to nitrite, while the remaining 50% is not converted. This process is denoted as partial nitrification. With a combined partial nitrification-Anammox process (Figure 1.1), low nitrogen effluent concentrations can be obtained, high savings on aeration energy (up to 63%) are realized, the need for external carbon source is completely omitted, while sludge and CO_2 -productions are negligible in comparison with conventional nitrification-denitrification.

Up till now, different strategies have been proposed to obtain persistent nitrite accumulation in nitrification:

- Control of the dissolved oxygen (DO) concentration (Garrido et al. 1997b, Kuai and Verstraete 1998, Bernet et al. 2000). Nitrite oxidizers have been shown to be more sensitive to oxygen limitation than ammonia oxidizers. Therefore, at low DO concentration, nitrite accumulation will be favored.
- pH control. Based on the results reported by Anthonisen et al. (1976), nitrite oxidizers are more sensitive than ammonia oxidizers to free ammonia and free nitrous acid. If the pH in the reactor is increased (higher free ammonia) or lowered (higher free nitrous acid) in a given range of values, inhibition of nitrite oxidizers will occur.
- SRT control. The relation between temperature and maximum growth rate is different between ammonium- and nitrite-oxidizing bacteria. At elevated temperature, ammonium oxidizers have a higher growth rate than nitrite oxidizers. Carefully controlling

the sludge age as a function of temperature has been shown to be a good operating parameter for a stable partial nitrification (Randall and Buth 1984, Hellinga et al. 1998).

In the SHARON (Single reactor High activity Ammonia Removal Over Nitrite) process (Hellinga et al., 1998), nitritation is achieved by maintaining an appropriate sludge retention time (SRT) in order to wash-out the nitrite oxidizing biomass, which grows slower than the ammonium oxidizing biomass at the prevailing high temperature (30-40°C) and neutral pH (about 7). The SHARON reactor can be operated as a continuously stirred tank reactor (CSTR, chemostat) without biomass retention, so the SRT equals the hydraulic retention time (HRT). The first full-scale SHARON process has been operational since January 1999 at the Rotterdam Sluisjesdijk sludge treatment plant (van Kempen et al., 2001). In its original configuration, the SHARON process has been operated under alternating aerobic and anoxic conditions, the latter serving for pH control by denitrification. However, the SHARON process can also be operated as a partial nitritation process for coupling with an Anammox process (van Dongen et al., 2001), realizing the abovementioned savings. A full-scale Anammox reactor has been successfully start-up in Rotterdam and is now operated at its full capacity (500 kgN/day).

1.2 Outline of the thesis

The SHARON partial nitritation process for coupling with an Anammox process, is the focus of this thesis.

In chapter 2, the SHARON-Anammox process is set in the whole of biological treatment techniques for reject water, originating from sludge digestion and dewatering. Different process categories are compared on the basis of their underlying principles, with an emphasis on process configuration and full-scale application.

Chapter 3 presents an extensive dynamic model of a SHARON reactor. Besides mass balances, also a heat balance has been set up for the liquid phase. Special attention is devoted to pH-calculation: a general procedure, assuming that chemical dissociation reactions are in equilibrium compared to biological conversion reactions, is presented and is subsequently applied to the SHARON reactor model. The model further considers gas phase dynamics and interphase transport. Finally, some control features can be added to the model as well. The resulting

model has been validated for the full-scale SHARON reactor at Sluisjesdijk (Rotterdam, The Netherlands).

A basic version of the SHARON model is used in chapter 4 to analyse the behaviour of a SHARON reactor with pH-control, using principles from system and control theory. More specifically, it is examined under which conditions a unique or multiple equilibrium points can be reached from different initial conditions in a two-step nitrification reactor, depending on the input space. The stability of these equilibria is also assessed. Special attention is paid to the influence of microbial kinetics and to the translation of these findings to practice.

The SHARON reactor model is further used in this thesis to evaluate different operating scenarios through simulation. The effect of the control strategies applied in the SHARON reactor on the performance of a subsequent Anammox reactor is also evaluated. In chapter 5 several possible operating modes for the SHARON reactor, differing in the applied control strategies, are systematically evaluated for realistic influent conditions. The results are quantified in an economic way through an operating cost index (OCI), weighing multiple criteria .

As optimization of the SHARON-Anammox process as such may not guarantee optimal overall process performance, plant-wide evaluation constitutes a following research interest that is addressed in this thesis. The Benchmark Simulation Model No. 2 (BSM2) has been judged very suitable for plant-wide evaluation, as it does not only describe traditional activated sludge tanks followed by a settler, but it also includes pre-treatment of wastewater as well as the processes describing sludge treatment.

However, the coupling of the BSM2, the SHARON model and the Anammox model, each containing their own state variables is not so straightforward. In chapter 6, the continuity-based interfacing method (CBIM) has been applied to couple these models through three different model interfaces. At the same time, the generally applicable CBIM approach is further refined and particular issues when coupling models in which pH is considered as a state variable, are pointed out.

The effect of reject water treatment with a SHARON-Anammox process on a plant-wide (BSM2) scale is evaluated in chapter 7. A scenario without sludge treatment and therefore without reject water is compared with one in which untreated reject water is recycled to the main plant and one in which the reject water is treated with a combined SHARON-Anammox process before recirculation.

Chapter 8 addresses the optimization of the control strategy applied to the SHARON reactor for treatment of the BSM2 reject water. The interaction between reactor design and the usefulness of control is also assessed. The results are quantified in terms of conversion efficiency of the SHARON and Anammox reactors, as well as in terms of operating costs on a plant-wide scale.

Chapter 9 closes this thesis with general conclusions and perspectives for future research.

Chapter 2

What to do with reject water?

A Dutch version of this chapter has been published as:

*Volcke E.I.P., Villez K., Van Hulle S.W.H., van Loosdrecht M.C.M. and Vanrolleghem P.A. (2004). Wat met rejectiewater? *Afwalwaterwetenschap*, 3 (4), 297-318.*

Anaerobic digestion of sludge produced at wastewater treatment plants is gaining ground. But what should one do with the associated sludge reject water, that contains high ammonia concentrations? This chapter compares biological treatment techniques for reject water on the basis of their underlying principles. Although recycling the reject water to the main treatment plant is the most obvious solution, separate treatment is often a better option. A first approach consists of 'conventional' nitrification/denitrification over nitrate in a separate process. A second process category, the one of the bio-augmentation processes, combines conventional nitrification and/or denitrification over nitrate with seeding nitrifiers in the main wastewater treatment plant. Third, there are also a number of techniques that short-circuit nitrification/denitrification over nitrite, resulting in significant savings in aeration costs and costs for carbon source addition. Even more pronounced operating cost savings are achieved in the fourth and last process category, combining partial nitrification to nitrite with an Anammox process. In this chapter, each of the above categories is discussed, with a focus on process configuration and full-scale application.

2.1 Introduction

The effluent limits for nitrogen species in the effluent of wastewater treatment plants, that are imposed by European legislation, become more and more stringent. In order to reach these limits, existing plants can be extended with additional nitrification and/or denitrification capacity. However, separate treatment of nitrogen-rich sidestreams, that represent a significant part of the nitrogen load of the influent, is often a cheaper option. The reject water stream, originating from sludge digestion and sludge dewatering, is an example of such nitrogen-rich side stream. It represents up to 25% of the nitrogen load of the main line, while its volume fraction is typically only 2% (Janus and van der Roest, 1997). In case sludge from other wastewater treatment plants is treated at the same site, the contribution of reject water to the plant's total nitrogen load, can become even higher.

The reject water can be recycled to the main wastewater treatment plant and is then treated together with the actual influent. The amount of nitrogen in the effluent is in this case determined by the spare aeration capacity of the main wastewater treatment plant, the aerobic sludge retention time and the presence of a denitrification zone. In case the main wastewater treatment plant has been designed for carbon removal only, its aeration capacity is mostly insufficient to convert all ammonium in the reject water. As the nitrification process is slow in comparison to carbon removal, the aerobic sludge retention time must also be sufficiently long, resulting in large reactor volumes. It is also possible that the wastewater treatment plant possesses insufficient denitrification capacity, for instance when the plant has been designed for carbon removal and nitrification only. In this case, the anoxic volume should be enlarged (if possible) or a carbon source should be added. Siegrist (1996) points out that a permanent anoxic zone of 25% of the activated sludge volume ensures a total nitrogen removal efficiency of 50-60%, while, for the diluted and pre-oxidized Swiss wastewater, more than 70% nitrogen removal through denitrification cannot be realized without a substantial increase of the anoxic zone or the addition of external carbon source. In the latter case, not only more sludge is produced, but also process control is required to avoid incomplete nitrate conversion or excess carbon source addition.

Separate reject water treatment displays several advantages:

- The nitrogen load of the main wastewater treatment plant is significantly reduced, as well as problematic variations in the nitro-

gen load, caused e.g. by discontinuous dewatering techniques. The effect is more pronounced in winter, at lower wastewater temperatures, as has been shown in a simulation study by Wett and Alex (2003). The same study also indicates that an equalization tank for reject water doesn't have the same effect as separate treatment, as domestic wastewater treatment plants lack denitrification capacity at night because of low concentrations of organic material.

- The high reject water temperature increases nitrification and denitrification rates, so smaller reactor volumes can suffice.
- Separate reject water treatment also enhances process stability (Wett and Alex, 2003): when reject water is recirculated to the main wastewater treatment plant, oxidation of ammonium peak loads can cause almost complete destruction of the buffer capacity, resulting in a pH-decrease and consequently a decrease of the nitrification capacity. This effect becomes even more pronounced when additional aeration in the main wastewater treatment plant is established at the expense of the denitrification zone.

Disadvantages of separate reject water treatment are an increased complexity of the wastewater treatment plant as a whole, as well as the investment costs for the construction of one or more reactors for separate reject water treatment. For this reason, in Flanders, where sludge digestion has been applied more widely in the last few years, the option of extending the main wastewater treatment plant is almost always chosen (AquaFin, pers. comm.), even if the associated investment costs are substantial.

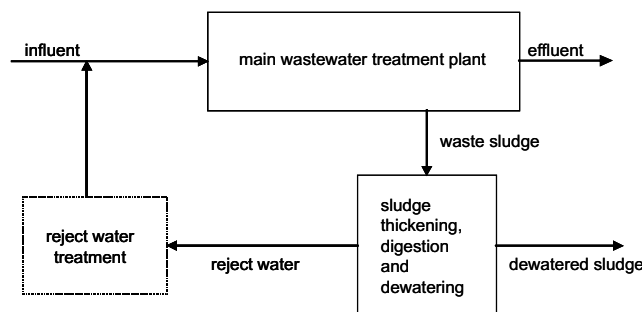


Figure 2.1: Implementation of reject water treatment in a wastewater treatment plant

Figure 2.1 locates the implementation of reject water treatment in a wastewater treatment plant. For separate reject water treatment, both physical-chemical and biological treatment techniques can be used. Biological techniques are usually more economical than physical-chemical techniques like MAP (magnesium-ammoniumphosphate, $MgNH_4PO_4$) precipitation or ammonia stripping (Siegrist 1996; Mulder 2003) and are listed in this chapter. The following process types are distinguished:

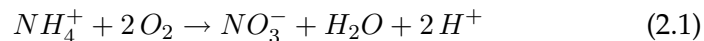
- Processes based on conventional nitrification/denitrification over nitrate
- Bio-augmentation techniques, that combine conventional nitrification/denitrification over nitrate with the seeding of nitrifiers to the activated sludge tanks of the main wastewater treatment plant
- Processes that promote nitrification/denitrification over nitrite
- Processes that combine partial nitrification over nitrite with anaerobic ammonium oxidation (Anammox)

Each of these categories is discussed in the next paragraphs.

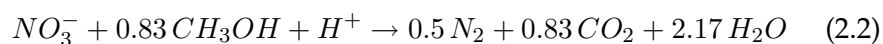
2.2 Nitrification/denitrification over nitrate

2.2.1 Principle

A first series of techniques is based on conventional nitrification/denitrification, i.e. a combination of autotrophic nitrification and heterotrophic denitrification over nitrate. During nitrification, ammonium (NH_4^+) is oxidized with oxygen via nitrite (NO_2^-) to nitrate (NO_3^-) by autotrophic bacteria:



Note that only the catabolic reaction is shown, bacterial growth is not considered in the simplified reaction stoichiometries in this chapter. The subsequent denitrification reaction consists of the reduction of nitrate via nitrite to nitrogen gas (N_2) by heterotrophic bacteria. In contrast to autotrophic bacteria, that use CO_2 for carbon source, heterotrophic bacteria use an organic carbon source, that should be supplied externally when necessary, e.g. as methanol (CH_3OH):

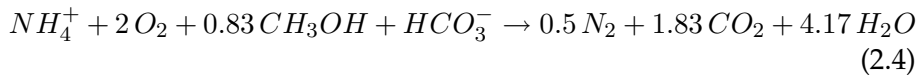


Conventional nitrification/denitrification over nitrate takes place in the activated sludge tanks of the main wastewater treatment plant, to which the reject water can be recycled, but it can also be established in separate units for reject water treatment.

The oxidation of high ammonium concentrations during separate reject water treatment, causes a significant pH-decrease, that limits further ammonium conversion due to a limitation of the free ammonia (NH_3), being the actual substrate (Anthonisen et al., 1976), and due to nitrous acid (HNO_2) inhibition. Sludge reject water typically contains equimolar amounts of bicarbonate and ammonium, so half of the produced protons (2 per mole of ammonium converted) is neutralized by CO_2 -stripping:



As a result, for streams containing bicarbonate and ammonium in equimolar amounts and without additional pH control in the reactor, typically half of the ammonium is converted before a significant pH-decrease occurs, that prevents further conversion. To obtain a higher ammonium conversion, pH-correction is necessary. This is realized by base addition or by including a denitrification phase in which an external carbon source (e.g. CH_3OH) is added. The latter option is cheaper (Hellinga et al. 1998, Mulder et al. 2001) and consequently is applied as much as possible in practice, even if denitrification is not strictly necessary because the main wastewater treatment plant possessed sufficient denitrification capacity. Complete denitrification compensates half of the protons produced during complete nitrification. As a result, for streams with equimolar amounts of ammonium and bicarbonate, all protons produced during nitrification are neutralized by combined CO_2 -stripping and denitrification. The overall reaction can then be written as:



2.2.2 Implementation and applications

'Conventional' nitrification/denitrification over nitrate can be applied to ammonium-rich streams such as reject water, provided that sufficient oxygen is supplied to the system and that sufficient carbon source is available for denitrification. As the COD:N ratio of the reject water is usually too low for denitrification (< 0.5 g/g, compared to about 20

for municipal wastewater, Wett et al. 1998) and the largest part of the present COD is usually not further degradable, the carbon source is mostly supplied externally.

Nitrification and denitrification either take place in one reactor, that is intermittently aerated, or in two separate reactors, usually with recirculation to compensate for pH-effects. When choosing between a one-reactor and a two-reactor system, the higher investment costs for aeration devices in one reactor (larger aeration devices are needed as they are only used part of the time) should be weighed against the additional investment costs for constructing two reactors instead of one.

The obtained effluent ammonium concentration is lower as the sludge retention time (SRT) in the reactor increases. A high SRT is applied if one wants to obtain very low effluent ammonium concentrations. However, since the reject water stream is usually recirculated to the main wastewater treatment plant after treatment, a significant ammonium conversion percentage rather than a low effluent ammonium concentration is required. In case the SRT is maintained relatively low, the nitrification/denitrification can be short-circuited over nitrite instead of nitrate, resulting in significant savings (see section 2.4). However, sometimes the option of nitrification/denitrification over nitrate at higher SRT values is chosen because of the somewhat simpler process configuration (less control needed) or because one aims to achieve low effluent concentrations, even if this is not always the most economical solution.

Different reactor types can be used and are discussed hereafter:

- Continuous stirred tank reactors (CSTRs)
- Sequencing batch reactor (SBRs)
- Biofilm airlift suspension (BAS) reactors
- Membrane bioreactors (MBRs)

CSTRs

For reject water treatment, either one intermittently aerated CSTR is used, with alternating aerobic phases for nitrification and anoxic phases for denitrification, or an aerobic CSTR and an anoxic CSTR in series, with recirculation between both (for pH-stabilization). Because of simplicity, CSTRs for reject water treatment are mostly operated without sludge retention, so the hydraulic retention time (HRT) equals the sludge

retention time (SRT). Operating a CSTR without sludge retention at a higher SRT corresponds with an increasing reactor volume for the same influent flow. If the aerobic retention time is kept sufficiently short (typically 1 day), nitrogen removal is mainly established via the nitrite route and the process is referred to as the SHARON process (see section 2.4.2).

At the 400,000 PE WWTP of Utrecht (The Netherlands), conventional extension was only feasible at relatively high investment costs, so a two reactor CSTR system has been applied for reject water treatment. As the reject water contains relatively low ammonium concentrations ($400\text{--}750 \text{ mg } NH_4^+ - N \text{ l}^{-1}$) and a nitrification efficiency of more than 95% was required, the aerobic retention time was kept higher than 1 day, so nitrite removal is mainly established via the nitrate route (van Kempen et al., 2001). For this reason, the implemented process is not a SHARON process in the strict sense, where nitrogen removal is mostly established through the nitrite route. By implementing this side stream process (maximum nitrogen load $0.2 \text{ kg N m}^{-3} \text{ d}^{-1}$), the nitrogen load of the main line has been reduced by 30%, while the mean effluent concentration has been decreased from 16 to 11 mg KjeldahlN/l (van Kempen et al., 2001).

SBRs

An SBR is an intermittently operated batch reactor, with an aeration phase for nitrification, an anoxic phase for denitrification, besides a sedimentation phase and a decantation phase. In comparison with an intermittently operated CSTR without sludge retention, the cycle length in an SBR is longer because of sedimentation and decantation. The volume of an SBR mainly depends on the required oxygen transfer capacity, that is determined by the influent nitrogen load, while the volume of a CSTR without sludge retention is only determined by the required SRT (=HRT), that is independent of the nitrogen load. The total reactor volume of an SBR (with sludge retention) can be smaller than the one of a CSTR without sludge retention: according to Siegrist (1996), the volume that is needed to treat the reject water of a 100,000 PE WWTP, with an SRT of 5 days amounts 1000 m^3 for a CSTR and 500 m^3 for an SBR. However, the difference in the necessary reactor volume decreases for decreasing SRT and for increasing nitrogen loads. It can also be noted that an SBR is less simple to operate than an CSTR without sludge retention and might involve higher costs for control and automation.

At the Linköping WWTP in Sweden (Karsson, 1994) reject water is treated separately in an SBR with intermittent nitrification/denitrification (SRT > 20 days; T > 18°C), in which hydrolysed starch is added as a carbon source. The total nitrogen removal efficiency is about 75%.

BAS reactors

A BAS reactor is a fluidized bed system, consisting of two concentric tubes, with reactor fluid rising in the inner tube and downflow taking place in the outer tube. Compressed air is supplied at the bottom of the inner tube to create this flow pattern. In this type of reactor, biologically active material adheres to inert carrier material. As a result, the biomass concentration can be up to 20 times higher compared to conventional activated sludge systems (Janus and van der Roest, 1997), so the hydraulic retention time can be kept low (Garrido et al., 1997a).

The maximum nitrogen load at 90% nitrification in a full-scale installation (height 15 m) amounts to $3.3 \text{ kg N m}^{-3} \text{ d}^{-1}$, while oxygen transfer is the limiting factor for ammonium conversion (Janus and van der Roest, 1997). If also denitrification should be established, an airlift reactor with integrated anoxic compartment can be used. In a full-scale BAS reactor (130 m^3) for wastewater from the potato-processing industry, high COD and ammonium conversion rates (mean $3 \text{ kg COD m}^{-3} \text{ d}^{-1}$ and $> 1 \text{ kg m}^{-3} \text{ d}^{-1}$ respectively) have been realized, together with a high denitrification efficiency (>90%) (Frijters et al., 2000).

No full-scale applications of this reactor type for reject water treatment are known to the author. This is probably because the treated reject water is usually recycled to the main wastewater treatment plant, so it is not needed to achieve very strict effluent standards.

MBRs

In a membrane bioreactor (MBR), the sludge is separated from the purified effluent by means of a membrane, in contrast to 'conventional' separation through sedimentation.

Membrane filtration ensures a high biomass concentration and a high temperature (35°C) because of energy dissipation. As for BAS reactors, oxygen transfer is again the limiting factor for ammonium conversion because of the high biomass concentration. This was shown in a study for the treatment of reject water in a MBR, described by Janus and van der Roest (1997), where a maximum nitrogen load for complete nitrification of $4.4 \text{ kg N m}^{-3} \text{ d}^{-1}$ was found for an oxygen trans-

fer rate of $1 \text{ kg O}_2 \text{ m}^{-3} \text{ h}^{-1}$. The optimum biomass concentration was $20 \text{ kg MLSS m}^{-3}$, so the maximum nitrogen load per unit of biomass amounted to $0.22 \text{ kg N (kg MLSS)}^{-1} \text{ d}^{-1}$.

During start-up of an MBR for reject water treatment ($293 \text{ mg Kjeldahl-N l}^{-1}$), Ghyoot et al. (1999) report complete nitrification at a comparable nitrogen load of $0.164 \text{ kg N (kg MLSS)}^{-1} \text{ d}^{-1}$, for a sludge concentration of $2.7 \text{ kg MLSS m}^{-3}$. In this case, nitrite accumulation has been observed and attributed to the high sludge load, that has been lowered subsequently.

Membrane bioreactors are mainly used in practice in case a very good effluent quality is required. As a result, this reactor type is rarely applied for reject water treatment.

2.3 Bio-augmentation processes

2.3.1 Principle

Nitrification/denitrification over nitrate for separate reject water treatment gains interest when an amount of surplus sludge from the reject water treatment, that contains both ammonium and nitrite oxidizers, is recycled to the main wastewater treatment plant. In this way, the nitrification capacity of the latter is augmented, a practice that is indicated with the term bio-augmentation. The nitrifiers in the side stream process are growing in flocs and in this way survive in the main wastewater treatment plant. In the side-stream process, complete nitrification to nitrate is required, as nitrification to nitrite only would result in only the growth of ammonium oxidizers, which could lead to nitrite accumulation in the effluent of the main plant (van Loosdrecht and Salem, 2006).

On the one hand, bio-augmentation techniques are interesting at low temperatures, when the nitrification rate decreases and either additional reactor volume (increasing SRT), or additional nitrifiers are required to improve the nitrification performance. On the other hand, when designing or expanding a WWTP with bio-augmentation, a shorter SRT can be applied than for plants without bio-augmentation, resulting in smaller reactors for the same loads.

By supplying return sludge of the main wastewater treatment plant to the bio-augmentation process, the dosing of external carbon source for denitrification of the reject water, that possesses an unfavourable C:N ratio, is minimized or even becomes unnecessary. In the absence

of oxygen, the electrons needed for denitrification of nitrate to nitrogen gas are supplied by endogenous respiration of the return sludge, a process that is further referred to as endogenous denitrification.

Different implementations of bio-augmentation processes are found in literature, such as the InNitri process (Kos, 1998), the BABE process (Salem et al. 2002 and Salem et al. 2003) and the ScanDeNi process (Rosén and Huijbregsen, 2003), all of which are patented.

The InNitri process (Fig. 2.2, Kos 1998) is realized in a single aerobic reactor, in which only nitrification takes place. The acidification from nitrification is compensated by base addition. Denitrification takes place in the main wastewater treatment plant. The sidestream reactor for reject water treatment is fed with primary settler effluent. According to the authors, this is done in order to lower the temperature (down to 25°C) and to add BOD. However, it is not clear what is the use of adding BOD (carbon source), as there is no denitrification phase for pH control. Note also that the primary settler effluent that is added cannot be used to grow nitrifiers. The reactor is operated at an SRT of 4 days and a temperature of 25°C and is followed by a settler with sludge recirculation. A part of this sludge is fed continuously or periodically to the main wastewater treatment plant to supply the latter with additional nitrifiers.

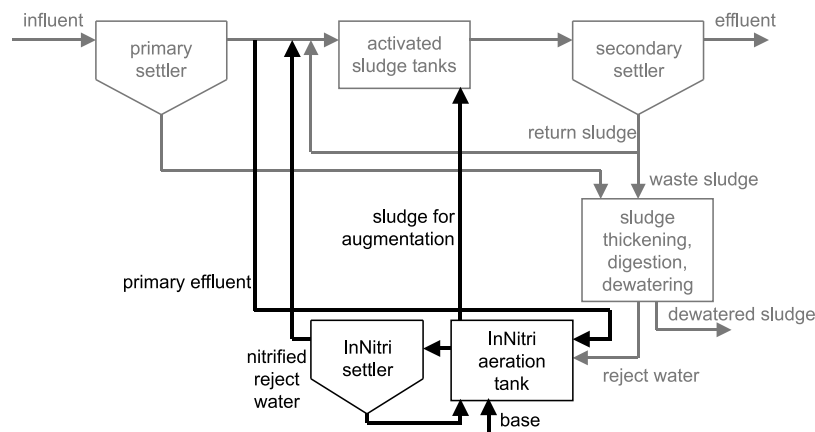


Figure 2.2: The InNitri process (from Kos 1998)

The BABE process and the ScanDeNi process are operated with denitrification besides nitrification, in order to control pH. Further, return sludge is used for growing nitrifiers. The main difference between BABE process and the ScanDeNi process lies in the process configura-

tion. The BABE (Bio-Augmentation Batch Enhanced) process can be operated as a one-reactor process as well as a two-reactor process. The one-reactor system (Berends et al., 2003) is operated cyclically. In the first, aerobic phase, the reject water and the return sludge are fed and nitrification takes place. During the second, anoxic phase, denitrification takes place and the sludge settles. At the end of this phase, the reactor liquid is fed to the main wastewater treatment plant. The sludge has not settled completely at this moment, so inoculation with nitrifying sludge is realized. The two-reactor BABE process configuration (Figure 2.3, Salem et al. 2002) consists of an anoxic reactor, followed by an aerobic reactor. In the first (anoxic) reactor, the reject water stream is mixed with return sludge, that also serves as carbon source. When necessary, an external carbon source can be added as well. To supply the first reactor with nitrite and nitrate, recirculation takes place between both reactors.

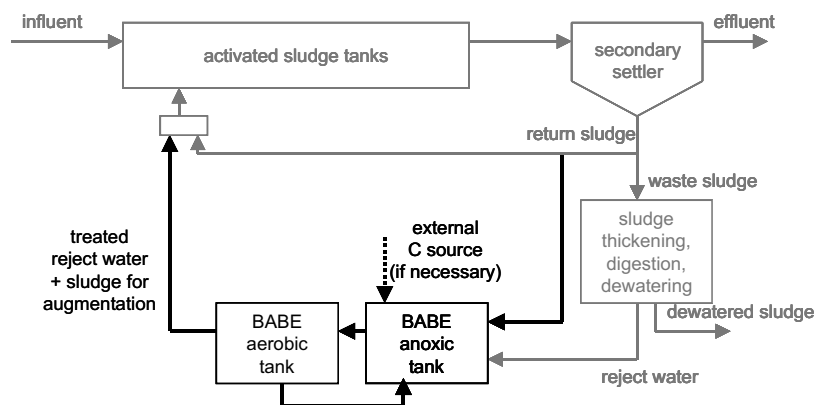


Figure 2.3: The two-reactor BABE process (from Salem et al. 2002 and Salem et al. 2003)

The ScanDeNi process (Figure 2.4, Rosén and Huijbregsen 2003) is only described as a two-reactor process. The first reactor is aerobic, the second one anoxic, without recirculation between both. No pH problems have been reported for this system, probably because the complete return sludge flow is sent to the process, so the ratio of return sludge over reject water is high. Note however that in this case no advantage is taken of the high reject water temperature. The reject water stream is mixed with return sludge in the first reactor, that is now aerobic. In the second tank, that is anoxic, a carbon source is added. This carbon source is either an internal one – typically a part of the influent –, or

an external one. As soon as all nitrate is denitrified, the second reactor becomes anaerobic and biological phosphate removal becomes feasible (Rosén and Huijbregsen, 2003). As an additional process advantage, the authors mention the reduction of surfactants from the return activated sludge, as well as in the reject stream, resulting in significant aeration cost savings. If this is indeed the case, this will also hold for other techniques for separate reject water treatment.

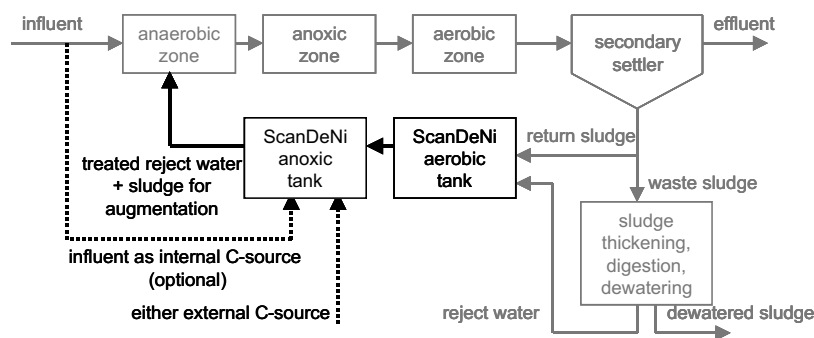


Figure 2.4: The ScanDeNi process (from Rosén and Huijbregsen 2003)

Apart from the order of the aerobic and the anoxic tank, the ScanDeNi process differs from the BABE process because the return sludge flow is treated completely in the ScanDeNi process, while only part of the return sludge flow is fed to the BABE process. The reason for this must probably be sought in the original and principal aim of the ScanDeNi process, that is improving the efficiency of an activated sludge process with poorly operating secondary clarifiers, by a hybrid arrangement of contact stabilisation (i.e. aeration of the return sludge before its contact with wastewater), combined with a sludge anoxic zone (Rosén and Huijbregsen, 2003).

The amount of return sludge versus the amount of reject water to be treated, influences the temperature of the sidestream process: higher amounts of return sludge decrease the temperature and thereby the sludge activity. This is however compensated by a higher sludge content in the reactor for increasing portions of return sludge. The combination of temperature and sludge determines the necessary reactor volume. At low ambient temperatures, the temperature effect prevails and the necessary reactor volume decreases for decreasing portions of return sludge added (down to 0.5%). At higher ambient temperatures (16-20°C), the necessary reactor volume decreases if less return sludge

is added, because of the lower sludge concentration in the reactor. If about 0.5% of the return sludge volume is sent to the reactor, the necessary volume of the latter is the same in summer and winter period (Salem et al., 2003).

The amount of carbon source that is needed for bio-augmentation processes with denitrification (BABE, ScanDeNi) is the same as for systems with nitrification/denitrification over nitrate without bio-augmentation (section 2.2). However, for the first process category, mainly internal carbon source is used and almost no external carbon source needs to be added, resulting in significant savings. The BABE process makes optimal use of the carbon content of the return sludge, that is added to the anoxic reactor, through endogenous denitrification, that proceeds fast at the prevailing high temperatures (20-30°C). In this way, for the BABE process, the need for external carbon dosage is significantly reduced. It is expected that more external carbon will need to be added to the ScanDeNi process, in which the anoxic tank comes behind the aerobic one, although this amount should still be less than for processes to which no return sludge or another stream containing carbon (such as incoming wastewater) is added. The most important influencing factors that determine the need for adding external carbon source are: the nitrogen load, the alkalinity, the amount and type of sludge fed and the desired ammonium conversion efficiency (Berends et al., 2003). As the influent alkalinity increases, less denitrification is needed for pH control. A larger amount of sludge in the reactors or a higher carbon source concentration in the sludge (high-loaded sludge contains more carbon source than low-loaded sludge) also decreases the need for external COD-addition.

The optimal SRT for bio-augmentation processes, maximizing the overall efficiency of the wastewater treatment plant as a whole, is determined by two opposite effects. On the one hand, a higher SRT results in a higher nitrification efficiency of the sidestream process. On the other hand, biomass decay also increases with increasing SRT. This results in less active biomass, which gives rise to a smaller augmentation effect on the activated sludge tanks (Berends et al., 2003).

2.3.2 Applications

No full-scale applications of the InNitri process have been found. This process, in which only nitrification takes place, does not seem very in-

teresting because of the costs of base addition and the subsequent settling tank.

The BABE process has been tested on full-scale for the 300.000 PE Garmerwolde WWTP (The Netherlands) (Berends et al., 2003). In this case study, an activated sludge line connected to a one-reactor BABE process has been compared with a second parallel line without reject water (as if the reject water treatment was ideal) and with a third line in which untreated reject water is sent back to the activated sludge tanks. The ammonium concentrations in the effluent of the WWTP amounted to 5.2, 9.9 en 13.3 mg $NH_4^+ - N l^{-1}$ respectively. Model simulations predict a further decrease of the effluent concentration down to $NH_4^+ - N l^{-1}$ if the BABE reactor volume is lowered from 1250 m³ (implementation in an existing thickener), for which a significant decay of nitrifiers takes place, down to 300 m³.

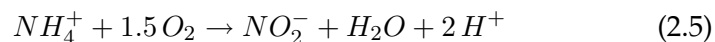
For the 350,000 PE WWTP of 's-Hertogenbosch (The Netherlands), nitrogen removal is not optimal due to a critical minimum aerobic sludge age, resulting in a present yearly average effluent N-total of 12 mg N l⁻¹, with large variation. Reject water treatment would bring the effluent N-total within the effluent standard (≤ 10 mg N l⁻¹). However, as in this case only bio-augmentation techniques are able to meet an expected future 15% load increase, the BABE technology has been selected for reject water treatment (van Loosdrecht and Salem, 2006) and is operational since October 2005.

The ScanDeNi process is operational since 1998 at the 150,000 PE WWTP of Västerås (Sweden), where it is fed with reject water. Even at low temperatures, down to 8-9°C, stable results are obtained and the effluent limits for nitrogen (< 10 mg l⁻¹), phosphorus (< 0.2 mg l⁻¹), and BOD and SS (< 5 mg l⁻¹) are met (Rosén and Huijbregsen, 2003).

2.4 Nitrification/denitrification over nitrite

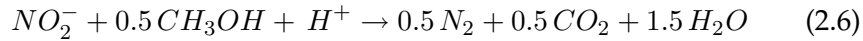
2.4.1 Principle

For the treatment of streams with high ammonium concentration, oxidizing ammonium to nitrite only (nitritation, Eq. 2.5) displays several economical advantages.



Up to 25% aeration cost savings for oxygen supply are realized in comparison with nitrification to nitrate (Eq. 2.1). As for nitrification to ni-

trite, 2 moles of protons are produced per mole of ammonium converted. For streams containing equimolar amounts of ammonium and bicarbonate, half of the protons produced can be compensated by CO_2 -stripping, corresponding to 50% ammonium conversion. Denitrification of nitrite to nitrogen gas:



results in 40% cost savings for external carbon source addition in comparison to denitrification of nitrate. As for denitrification of nitrate, half of the protons produced during nitrification, can be neutralized by denitrification of nitrite. So, in theory, 100% ammonium conversion can be realized by the overall reaction of nitrification/denitrification over nitrite, combined with CO_2 -stripping:



Note that also less CO_2 is emitted than for nitrification/denitrification over nitrate (Eq. 2.4). Further, less sludge is produced, although this is not clear from the above equations, that don't consider biomass growth. Table 2.1 summarizes the theoretical oxygen and COD consumption, as well as the CO_2 emission for different treatment techniques.

Table 2.1: Theoretical comparison of biological N-removal processes on stoichiometric grounds, for streams with equimolar amounts of ammonium and bicarbonate. * 1 g CH_3OH corresponds with 1.5 g COD.

	Oxygen consumption (kg O_2 kg ⁻¹ N)	COD consumption* (kg COD kg ⁻¹ N)	CO_2 emission (kg CO_2 kg ⁻¹ N)	sludge production (kg dry weight kg ⁻¹ N) (Mulder, 2003)
autotrophic nitrification – heterotrophic denitrification over nitrate (Eq. 2.4) (including bio-augmentation techniques)	4.57	2.86	5.76	1-1.2
autotrophic nitrification – heterotrophic denitrification over nitrite (Eq. 2.7)	3.43	1.71	4.72	0.8 - 0.9
partial autotrophic nitrification – Anammox (Eq. 2.9)	1.71	0	3.14	<0.1

The realization of stable nitrite formation by selecting ammonium oxidizers is based on differences in growth rate, oxygen affinity and/or inhibition characteristics between ammonium oxidizing and nitrite oxidizing bacteria.

2.4.2 The SHARON process with complete nitrification and denitrification

Principle

The SHARON (Single reactor High activity Ammonia Removal Over Nitrite) process (Hellinga et al., 1998) is operated at high temperature (30-40°C) and neutral pH (about 7.0). Under these conditions, nitrite oxidizers grow slower than ammonium oxidizers, so they are washed out by setting an appropriate sludge retention time (typically 1 day), preventing nitrate formation. Because of the short retention time, organisms with high activity are selected, that usually also possess a low affinity for ammonium. As a result, the SHARON process is very well suited for reducing the nitrogen load of streams with a high ammonium content ($> 500 \text{ mg } NH_4^+ \text{-N l}^{-1}$), rather than for obtaining strict effluent standards. Reject water is an excellent application for the SHARON process, because of its high temperature and high ammonium concentration, and as the effluent of the SHARON reactor is recycled to the activated sludge tanks for further reduction of the remaining ammonium.

Implementation and applications

The SHARON reactor is usually operated as a continuous, completely mixed tank reactor (CSTR, chemostat) without sludge retention, so the sludge retention time (SRT) equals the hydraulic retention time. This results in easy reactor operation and maintenance. The absence of sludge retention also makes the SHARON reactor insensitive towards the presence of suspended solids in the reject water.

Besides CO_2 stripping, denitrification is applied for pH control. Nitrification and denitrification either take place during intermittent aerobic and anoxic phases in the same reactor (Fig. 2.5), or in two separate reactors, an aerobic one and an anoxic one, with recirculation between both. Both process configurations have been applied successfully on full-scale. In a one-reactor system, the aerobic retention time is controlled by the duration of the aerated periods, and in this way can be maintained constant, independent of the inlet flow. The length of the aeration phase is determined by preset lower limits for the pH, at which the operation is switched to denitrification (van Kempen et al., 2001).

Table 2.2 (van Loosdrecht and Salem, 2006) gives an overview of the current implementations of the SHARON process. Note that in Utrecht,

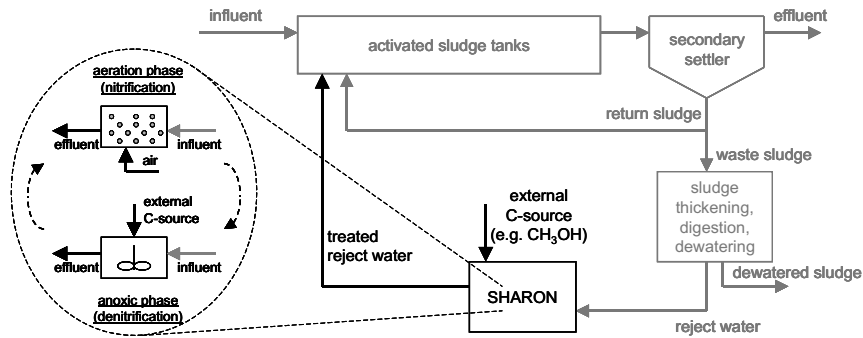


Figure 2.5: The cyclically operated one-reactor SHARON process for nitrification/denitrification

nitrification/denitrification takes place mainly over nitrate (see section 2.2), so the reject water treatment process is not a SHARON reactor in the strict sense (with nitrification to nitrite only).

Table 2.2: SHARON processes in operation/under construction (van Loosdrecht and Salem, 2006)

WWTP	Capacity (PE)	N-load (kgN/day)	Operational since
Utrecht	400,000	900	1997
Rotterdam	470,000	830	1999
Zwolle	150,000	540	2000
Beverwijk	320,000	1200	2004
Garmerwolde	300,000	700	2004
Den Haag	1,100,000	1200	2005
New York	3,000,000	5500	under construction

At the 470,000 PE WWTP of Rotterdam (The Netherlands), a one-reactor SHARON process has been operational since October 1998 (van Kempen et al., 2001). As expansion of the underground activated sludge tanks was not possible, it was decided to treat the reject water ($1230 \text{ mg } NH_4^+ - N \text{ l}^{-1}$) at the neighbouring sludge treatment plant to reach the nitrogen limits, that were becoming more stringent. During the second half of 2002, more than 95% ammonium was converted and the denitrification efficiency was about 90%, while methanol consumption figures showed that the nitrite route was followed (Warakomski et al., 2003). The same authors indicate that, by implementing the SHARON process, the effluent concentration of the main line was decreased from

7.5 to 3.9 mg Kjeldahl-N/l in the period 1995-2000. Currently, an Anammox reactor has been started up at the same plant (see section 2.5)

For the 320,000 PE WWTP of Beverwijk (The Netherlands), the SHARON process with nitrification/denitrification over nitrite has been selected as the best option to meet more stringent effluent limits. As the reject water at this plant originates from sludge digestion and thermal drying, it has acetate as the counterion of NH_4^+ . In this way, the reject water contains sufficient COD so there is no use in adding an Anammox-step (van Loosdrecht and Salem, 2006).

2.4.3 SBRs

Besides CSTRs, also SBRs (Sequencing Batch Reactors), with alternating aerated and anoxic phases, can be used for realizing nitrification/denitrification over nitrite (see Fig. 2.6). Wett et al. (1998) propose the following strategy for reject water treatment in an SBR: during a first phase, the SBR is intermittently aerated on the basis of pre-set upper and lower pH-limits, so alternating nitrification and denitrification take place. In the mean time, reject water is added until the storage tank is empty. During a second phase, mixing is performed and primary sludge is added as carbon source for endogenous denitrification. Wett et al. (1998) do not expect any significant augmentation effect, as the long sludge retention time hampers the selection of 'original' nitrifiers. Another reason is probably that primary sludge is not a suitable source for nitrifiers. The operation is finished by phases for sludge settling and effluent withdrawal. To ensure a continuous influent flow and intercept the discontinuous operation of an SBR, a storage tank is placed in front of the reactor (Wett et al., 1998). The associated investment cost is a disadvantage of this process configuration.

Fux et al. (2003) compared the operation of a pilot-scale CSTR and an SBR for reject water treatment at the Werdhoelzli WWTP (Switzerland), containing $650 \pm 70 \text{ g } NH_4^+ - N \text{ m}^{-3}$. They found that the volume of a CSTR (SHARON) needs to be more than twice as large as the one of an SBR to treat the same flow by nitrification/denitrification over nitrite. In this study, the overall costs were estimated at $1.63 \text{ € kg}^{-1}N$ and $1.4 \text{ € kg}^{-1}N$ in an SBR. It should however be noted that the estimated aerobic retention time of 2-2.5 days at 35°C in the SHARON reactor seems rather high. Also, investments costs for a storage tank when implementing an SBR have not been taken into account. Further, the ammonium concentration in the reject water on which this study

has been carried out, is rather low, while it is known that the difference in necessary reactor volume for a CSTR and an SBR decreases for increasing ammonium concentrations.

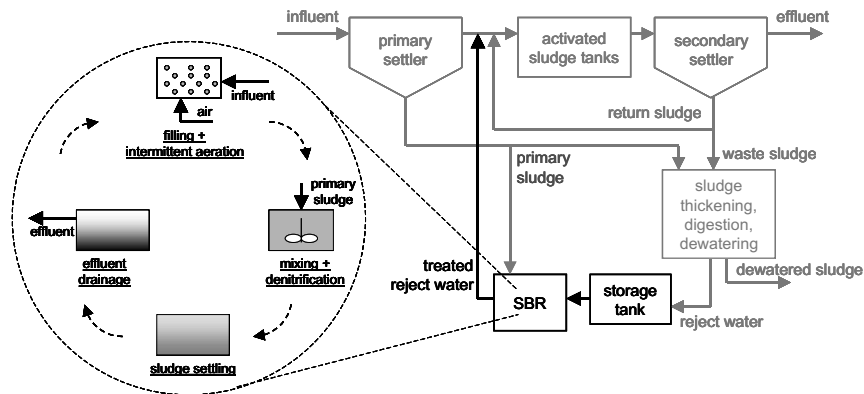


Figure 2.6: An SBR process for nitrification/denitrification (from Wett et al. 1998)

At the 200,000 PE WWTP of Strass (Austria), an SBR has been implemented for reject water treatment ($1250\text{--}1700\text{ mg } NH_4^+ - N\text{ l}^{-1}$, $700\text{--}1000\text{ gCOD l}^{-1}$) (Wett et al., 1998). A Kjeldahl-nitrogen removal efficiency of 80-83% is established and the nitrification/denitrification proceeds for 70% via the nitrite route, according to the authors because of inhibition of nitrite oxidizers by high ammonia concentrations. (about $1\text{ mg } NH_3 - N\text{ l}^{-1}$). Probably the low oxygen concentrations ($\leq 2\text{ mg } O_2/\text{l}$) also contribute to the nitrite accumulation. By implementing the SBR process for reject water treatment, the yearly nitrogen removal capacity of the overall WWTP of Strass has increased from 78% to 89% (Wett and Alex, 2003).

2.4.4 The 'Store And Treat' (SAT) process

The 'Store And Treat' (SAT) process (Laurich and Günner, 2003) combines reject water quantity management and treatment. Quantity management comprises the storage of reject water in storage tanks during periods with low BOD concentrations in the influent of the main WWTP (typically during weekends) to avoid nitrate peaks in the effluent (Ladiges and Bertram, 2004). It also comprises reject water equalization, improving the stability of the biological degradation processes and in this way the obtained efficiency (Laurich, 2004). Reject water storage only,

just shifts the nitrogen loads in time, without taking advantage of the favourable conditions (high temperature, high ammonium concentrations) for separate reject water treatment.

In the SAT process (Laurich, 2004), reject water is stored and treated in a cyclically operated tank. At the start of a cycle, the tank only contains the settled sludge from the previous cycle. During the filling phase, the reject water is mixed with this sludge and subsequently the tank is aerated for nitrification. Once the tank is completely filled, the treatment proceeds in continuous mode, during which the treated tank content, that also contains activated sludge, is removed. After a settling phase, the effluent is completely withdrawn. In the SAT process, the pH-decrease during nitrification is only compensated by CO_2 -stripping, without base addition or pH-control through denitrification. As a result, only about 50% of the ammonium load is nitrified. Denitrification of the produced nitrite/nitrate takes place in the main line of the WWTP.

The SAT process is operational at the 2,100,000 PE WWTP of Hamburg (Germany), where the reject water stream represents about 30% of the total nitrogen load of the main line. With the SAT process, the ammonium concentrations in the reject water are decreased from 1200-1600 mg $NH_4^+ - N l^{-1}$ to 800-1000 mg $NH_4^+ - N l^{-1}$, while 300-600 mg $NO_2^- - N l^{-1}$ and 100-200 mg $NO_3^- - N l^{-1}$ are formed (Laurich, 2004). Laurich and Günner (2003) attribute the relatively high amount of nitrite compared to nitrate formed in the SAT process to inhibition of nitrite oxidizers by the intermediate hydroxylamine. However, probably also growth rate selection plays a role. The full-scale SAT tank at the Hamburg WWTP is indeed operated long periods as a continuous reactor, as the amount of reject water is controlled by means of a second tank (Laurich, 2004). The given values for the reject water flow rates ($150 m^3 h^{-1}$) and the tank volume ($4000 m^3$) (Laurich, 2004) correspond with a hydraulic retention time of 1.11 days, so promotion of the nitrite route is indeed expected in case little or no sludge retention is applied.

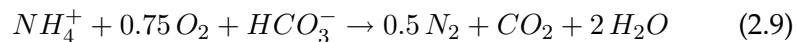
2.5 Partial nitrification combined with an Anammox process

2.5.1 Principle

In processes based on anaerobic ammonium oxidation (Anammox), even more aeration and carbon source addition cost savings are realized (see Table 2.1). Anaerobic ammonium oxidation (Mulder et al., 1995) comprises autotrophic conversion (with CO_2 as carbon source) of about equimolar amounts of ammonia and nitrite to form nitrogen gas, according to the simplified stoichiometry:



In reality, also a small amount of nitrate is formed. In order to implement the Anammox reaction, about half of the ammonium should be oxidized to nitrite in a preceding nitrification step. This is further denoted by the term 'partial nitrification'. For streams containing equimolar amounts of ammonium and bicarbonate, the associated proton production is compensated by CO_2 -stripping, so in principle no additional pH-control is necessary. The overall reaction for partial nitrification, CO_2 -stripping and Anammox becomes:



This means that 63%, resp. 50% aeration cost savings are realized in comparison with nitrification/denitrification over nitrate, resp. nitrite. Further, no COD-addition is necessary since the process is completely autotrophic, the CO_2 -production is further reduced and less sludge is produced.

2.5.2 Implementation and applications

The Anammox process is characterized by a low growth rate, low biomass yield and inhibition by oxygen and nitrite. Because of the low growth rate and biomass yield, start-up of an Anammox reactor takes quite long (100 to 300 days), while it is essential to use a reactor with high biomass retention. Up till now, various reactor types have been used: trickling filters, packed bed reactors, moving bed reactors, fluidized bed reactors, UASB (upflow anaerobic sludge blanket) reactors, SBRs, gas-lift reactors, MBRs (Strous et al. 2002; Wyffels et al. 2004a). Most of these studies have been carried out at lab-scale (1-15 l). The

reactors can be classified into reactor types in which Anammox bacteria grow on carrier material (the first 4 types) and reactor types with suspended sludge (the latter 4 types) (STOWA, 2000). While reactors with carrier material are well-suited for initial enrichment of Anammox, reactors with suspended sludge are advisable for further operation (Strous et al., 2002), as good mixing is necessary to avoid nitrite and oxygen inhibition.

As mentioned before, the Anammox process needs to be preceded by a partial nitrification step. This can take place in a separate reactor (two-reactor system) or in the same reactor in which the Anammox reaction proceeds (one-reactor system). Advantages of one-reactor systems are the higher volumetric nitrogen removal rates which are usually obtained (Wyffels et al., 2004a), so less space is required. Two-reactor systems are more flexible and result in more stable operation, as both steps can be controlled separately. Both possibilities are discussed in the next paragraphs.

Two-reactor systems

In two-reactor systems, nitrification and anaerobic ammonium oxidation are separated in space. In the first reactor, half of the ammonium is oxidized to nitrite. In the second reactor, anaerobic ammonium oxidation takes place. Regardless of the applied strategy to establish partial nitrification to feed the Anammox reactor, it is important that this influent has a constant composition, taking into account the sensitivity of the Anammox bacteria towards nitrite and oxygen. For this reason, in practice, control of the partial nitrification step will probably be necessary (see Chapters 5 and 8).

Partial nitrification in the first reactor can, for instance, be realized by selection on growth rate. Application of the SHARON process with CO_2 -stripping but without denitrification, to streams containing almost equimolar amounts of ammonium and bicarbonate, results in about 50% ammonium conversion to nitrite. The SHARON reactor, typically a CSTR without sludge retention, is either continuously aerated, or is intermittently aerated without carbon addition during the anoxic phases (Figure 2.7). The feasibility of the combined SHARON-Anammox process has been tested experimentally by van Dongen et al. (2001): in the SHARON reactor (CSTR, 10 liter), fed with reject water of the Rotterdam WWTP (The Netherlands), 53% of the ammonium load ($1.2 \text{ kg N m}^{-3} \text{ d}^{-1}$) was converted to nitrite, while all nitrite was converted

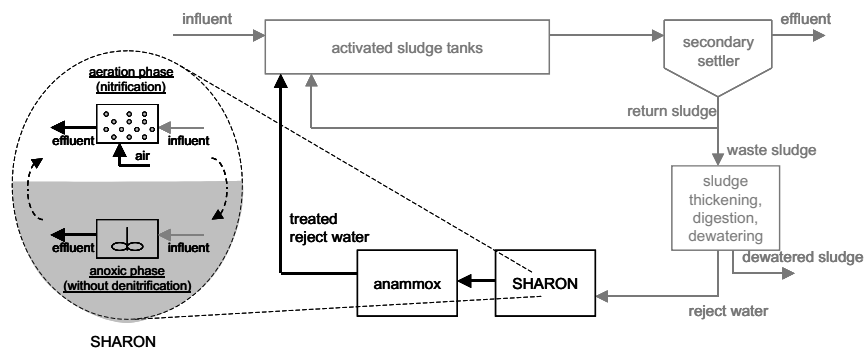


Figure 2.7: Cyclically operated SHARON process for partial nitritation, coupled with an Anammox-reactor

in the subsequent nitrite-limited Anammox reactor (granular sludge, SBR, load $0.75 \text{ kg N m}^{-3} \text{ d}^{-1}$). Within the scope of the EU IcoN project (no. EVK1-CT2000-054), a full-scale (70 m^3) Anammox-reactor has been started-up at the Rotterdam WWTP. The reactor influent is provided by the present SHARON reactor, that is now operated without denitrification. Since the beginning of 2006, the Anammox reactor is operated at full capacity (500 kgN/day ; Waterforum online, 02/2006).

Partial nitritation in the first reactor can also be realized on the basis of oxygen limitation with complete sludge retention (Wyffels et al., 2004b). Oxygen limitation favours ammonium oxidizers above nitrite oxidizers, as the latter have a lower affinity towards oxygen. At low oxygen concentrations, ammonium oxidizers are active at the expense of nitrite oxidizers, on the long term preventing nitrite oxidation (Kuai and Verstraete, 1998). The amount of ammonium converted is directly related to the oxygen supply. Wyffels et al. (2004a) have established partial nitritation and subsequent anaerobic ammonium oxidation in two membrane bioreactors (1.5 l each), that were fed with reject water ($862 \text{ mg NH}_4^+ - \text{N l}^{-1}$) from the Deurne WWTP (Belgium). An overall nitrogen removal efficiency of 82% was obtained, corresponding with a removal rate of $0.55 \text{ kg N m}^{-3} \text{ d}^{-1}$. The authors mention the following advantages for the two-step OLAND (oxygen-limited autotrophic nitrification denitrification) process: its independence of the volumetric load of the nitritation step and the growth rate of ammonium oxidizers (as sludge retention is applied), the possibility to treat reject water at relatively low temperatures ($20\text{-}30^\circ\text{C}$), as well as the fact that no sludge will enter the subsequent Anammox-reactor. A disadvantage of sys-

tems with partial nitrification based on oxygen supply is that the air flow rate cannot be used to control CO_2 -stripping, for instance to limit nitrite formation for streams with an excess of buffer capacity. Also, even though the process is independent of the growth rate of ammonium oxidizers, it is instead dependent on their oxygen affinity constant.

Combination of the SAT-process, in which 50% of the ammonium is converted, mainly to nitrite, with an Anammox-process also seems possible and is suggested by Ladiges and Bertram (2004) for future implementation at the Hamburg WWTP (Germany).

One-reactor biofilm systems

In one-reactor systems, partial nitrification and anaerobic ammonium oxidation take place in the same reactor, in a biofilm configuration. Ammonium oxidizers are located at the biofilm outer side, while Anammox bacteria are active in the inside of the biofilm, that is anoxic. Promotion of the nitrite route is based on the differences in oxygen affinity between ammonium and nitrite oxidizers. Examples of applications are the OLAND process (Pynaert et al., 2003), the CANON (completely autotrophic nitrogen removal over nitrite) process (Sliekers et al., 2003) and the 'aerobic deammonification' process (Hippen et al., 1997). Both for the OLAND process and for the aerobic deammonification process, aerobic nitrifiers were initially indicated as the organisms responsible for carrying out the anaerobic ammonium oxidation mechanism under micro-aerobic conditions (Kuai and Verstraete 1998; Helmer et al. 1999). However, in later studies (Pynaert et al. 2003; Helmer-Madhok et al. 2002) FISH analyses have revealed that in all systems anaerobic ammonium oxidation is carried out by Anammox-bacteria, even though Pynaert et al. (2003) do not exclude a permanent role of the aerobic ammonium oxidizers. It can be concluded that the three processes are essentially the same, i.e. in each of them Anammox bacteria play an important role.

In one-reactor systems, the oxygen concentration is a key variable. A too high oxygen level not only allows nitrite oxidation, but exposure of the Anammox population to aerobic conditions should also be avoided because of inhibition effects. If the oxygen level is too low, the ammonium conversion will be insufficient to provide enough nitrite for the anaerobic ammonium oxidation.

In a study of the OLAND process, carried out in a 44 l RBC (rotating biological contactor) reactor, fed with a synthetic influent load of 675 to

1189 mg $NH_4^+ - N l^{-1} d^{-1}$, a mean removal rate of 86% was obtained (Pynaert et al., 2003), corresponding to 0.58-1.022 kg N $m^{-3} d^{-1}$.

Up till now, the highest nitrogen removal rate in a one-reactor system for partial nitrification and Anammox, 1.5 kg N $m_{reactor}^{-3} d^{-1}$, has been found in a lab-scale gas-lift reactor, fed with synthetic influent (1.3 g $(NH_4)_2SO_4 - N l^{-1}$; 1.3 g $NaNO_2 - N l^{-1}$) (Sliemers et al., 2003). The authors indicate oxygen transfer as the main limiting factor for obtaining even higher removal rates.

Hippen et al. (2001) describe the application of aerobic deammonification for reject water treatment on pilot-scale (40 l). In a one-reactor system with a specific biofilm area of 100 $m^2 m^{-3}$, nitrogen removal amounted to 1.2 g N $m_{biofilm}^{-2} d^{-1}$ or 0.12 kg N $m_{reactor}^{-3} d^{-1}$.

2.6 Conclusions

In this chapter, different alternatives for biological nitrogen removal from reject water have been described. It is clear that the process choice strongly depends on the specific conditions and requirements in terms of efficiency, effluent quality, process compactness and associated operating and investment costs. As a result, choosing one system or another is only possible on an ad-hoc basis.

Separate reject water treatment with nitrification/denitrification over nitrate is rarely the most economical solution. It is only applied because of the somewhat simpler process configuration or in case low effluent concentrations are aimed for, even if this is mostly not the case for reject water, that is recirculated to the main WWTP.

Bio-augmentation techniques ensure a reduction of the ammonium and/or nitrate concentration in the effluent of the WWTP by combining reject water treatment, resulting in a reduced nitrogen load that is recirculated to the activated sludge tanks in the main line, with the supply of additional nitrifiers to the latter. Bio-augmentation processes are essentially applied when the aerobic retention time in the activated sludge process is insufficient for nitrification or its anoxic retention time is insufficient for denitrification. In the latter case, bio-augmentation allows extension of the denitrification space in the main line at the expense of the aerobic retention time.

Other reject water treatment techniques only reduce the nitrogen load that is recirculated to the main line. They are especially suitable in case the retention time in the main line is sufficient, but its aeration capacity or the amount of carbon source is limited. In comparison with

processes based on nitrification/denitrification over nitrate, techniques establishing nitrification/denitrification over nitrite or combining partial nitrification and Anammox, realize significant cost savings for aeration and carbon source addition. The latter techniques, that are based on the nitrite route, cannot be applied if bio-augmentation is aimed for, in order not to risk nitrite build-up in the effluent of the WWTP.

Both bio-augmentation techniques and techniques based on nitrification/denitrification over nitrite have already been applied successfully at full-scale. The combination of partial nitrification and anaerobic ammonium oxidation is very promising and a full-scale Anammox reactor has been successfully started-up in Rotterdam and is operated at its full capacity since the beginning of 2006. It is expected that many more full-scale Anammox reactors will be constructed in the near future.

Chapter 3

The SHARON reactor model

3.1 Introduction

This chapter describes the SHARON reactor model, that has been developed and implemented in Matlab-Simulink to carry out the simulation work described in this thesis. The SHARON reactor is of the CSTR (continuous stirred tank reactor) type and consists of a liquid phase and a gas phase (i.e. the bubbles in the liquid phase), both assumed to be perfectly mixed. Interphase transport of oxygen, carbon dioxide and nitrogen is considered. The following sections describe the mass balances and the heat balance in the liquid phase (section 3.2), the biological conversion reactions considered (section 3.3), the pH-calculation procedure (section 3.4), the gas phase mass balances (section 3.5) and the interphase transport terms (section 3.6). Some control features that can be added to the model, are described in section 3.7. The resulting model has been validated for the full-scale SHARON reactor at Sluisjesdijk (section 3.8).

3.2 Liquid phase mass balances and heat balance

The liquid phase volume, concentrations and temperature are calculated from the global and individual mass balances and the heat balance respectively.

The following liquid phase components are considered: H^+ (pH), NH_4^+ , NH_3 , HNO_2 , NO_2^- , CO_2 , HCO_3^- , CO_3^{2-} , $H_2PO_4^-$, HPO_4^{2-} , NO_3^- , O_2 , N_2 , ammonia oxidizing bacteria (X_{amm}), nitrite oxidizing bacteria (X_{nit}), heterotrophic bacteria (X_{het}), CH_3OH and Z^+ . Methanol can be

added to the process as an external carbon source. Z^+ is an artificial component, that represents the amount of net positive charges, originating from strong acids or bases. Its concentration is negative if there are more negative than positive charges present. This component plays a role in the pH calculation (see section 3.4). Acid or base addition influences the pH through the Z^+ concentration. Water is not considered as a component of interest for the conversion model.

The overall liquid phase mass balance is given by

$$\begin{aligned} \frac{dV_L}{dt} &= \Phi_L^{in} + \Phi_{acid} + \Phi_{base} + \Phi_{CH_3OH} - \Phi_L^{out} \\ &\triangleq \Phi_L^{in,net} - \Phi_L^{out} \end{aligned} \quad (3.1)$$

expressing that the liquid phase volume is determined by the volumetric flow rates in and out of the liquid phase, as well as by the amounts of methanol, acid and/or base streams added to the liquid phase. Eq. 3.1 implicitly assumes equal and constant density for all streams. As the added acid, base and methanol streams are small and have a high water content, the error made by the equal density assumption will be negligible. It is further reasonable to assume that watery streams have a constant density since the density of water only varies little with temperature (from 999.7 at 10°C to 992.2 at 40°C; Perry and Green, 1984).

Lumped components are defined, of which the concentrations equal the total concentration of the components, active in an equilibrium:

$$C_{TNH} = C_{NH_3} + C_{NH_4^+} \quad (3.2)$$

$$C_{TNO_2} = C_{HNO_2} + C_{NO_2^-} \quad (3.3)$$

$$C_{TIC} = C_{CO_2} + C_{HCO_3^-} + C_{CO_3^{2-}} \quad (3.4)$$

$$C_{TIP} = C_{HPO_4^{2-}} + C_{H_2PO_4^-} \quad (3.5)$$

Note that for the phosphorus equilibrium, only the dissociation reaction between HPO_4^{2-} and $H_2PO_4^-$ is taken into account, which means that these components are the only equilibrium forms considered. Indeed, the pKa-values of the $H_3PO_4/H_2PO_4^-$ and the HPO_4^{2-}/PO_4^{3-} equilibrium, that lie around 2 and 12 respectively, are so far from the normal pH operating range (typically 6-7.5) of a SHARON reactor that the fraction of inorganic phosphorus present as H_3PO_4 or PO_4^{3-} can be neglected.

Individual mass balances are set up for lumped components rather than for all corresponding equilibrium forms, as every change in the

concentration of a component involved in a chemical equilibrium, causes changes in the concentrations of all components taking part in that equilibrium. The individual liquid phase mass balance for a component i (TNH , TNO_2 , TIC , TIP , NO_3^- , O_2 , N_2 , X_{amm} , X_{nit} , X_{het}) with concentration C_i reads as

$$\frac{d(V_L \cdot C_{L,i})}{dt} = \Phi_L^{in} \cdot C_{L,i}^{in} - \Phi_L^{out} \cdot C_{L,i} + k_L a_i \cdot (C_{L,i}^* - C_{L,i}) \cdot V_L + r_{i,L} \cdot V_L \quad (3.6)$$

expressing that accumulation (decrease) of a certain component in the liquid phase is due to the net influx (outflux) of this component through incoming and outgoing liquid stream, as well as transport from this component from (to) the gas phase, and production (consumption) of this component in biological conversion reactions. Considering

$$\frac{d(V_L \cdot C_{L,i})}{dt} = V_L \cdot \frac{dC_{L,i}}{dt} + C_{L,i} \cdot \frac{dV_L}{dt} \quad (3.7)$$

and substituting Eq. 3.1, Eq. 3.6 is rewritten as

$$\frac{dC_{L,i}}{dt} = \frac{1}{V_L} \cdot \left[\Phi_L^{in} \cdot C_{L,i}^{in} - \Phi_L^{in,net} \cdot C_{L,i} \right] + k_L a_i \cdot (C_{L,i}^* - C_{L,i}) + r_{i,L} \quad (3.8)$$

which is valid for a variable liquid phase volume.

In the same way, the mass balance for CH_3OH is given by

$$\frac{dC_{L,CH_3OH}}{dt} = \frac{1}{V_L} \cdot \left[\Phi_L^{in} \cdot C_{L,CH_3OH}^{in} + \Phi_{CH_3OH} \cdot C_{CH_3OH} - \Phi_L^{in,net} \cdot C_{L,CH_3OH} \right] + r_{CH_3OH,L} \quad (3.9)$$

in which C_{L,CH_3OH} is the methanol concentration in the liquid phase, while C_{CH_3OH} represents the methanol concentration in the incoming methanol stream.

Analogously, the mass balance for Z^+ reads as

$$\frac{dC_{L,Z^+}}{dt} = \frac{1}{V_L} \cdot \left[\Phi_L^{in} \cdot C_{L,Z^+}^{in} + \Phi_{acid} \cdot C_{acid} + \Phi_{base} \cdot C_{base} - \Phi_L^{in,net} \cdot C_{L,Z^+} \right] \quad (3.10)$$

Note that the acid concentration C_{acid} is negative (adding negative charges), while the base concentration C_{base} is positive (adding positive charges).

The liquid phase heat balance is given by

$$\begin{aligned}
\frac{d(\delta_L \cdot c_{p,L} \cdot V_L \cdot T_L)}{dt} &= \delta_L^{in} \cdot c_{p,L}^{in} \cdot \Phi_L^{in} \cdot T_L^{in} - \delta_L \cdot c_{p,L} \cdot \Phi_L^{out} \cdot T_L \\
&+ \delta_{CH_3OH} \cdot c_{p,CH_3OH} \cdot \Phi_{CH_3OH} \cdot T_{CH_3OH} \\
&+ \Delta_s H_{CH_3OH} \cdot \Phi_{CH_3OH} \cdot C_{CH_3OH} \\
&+ \delta_{acid} \cdot c_{p,acid} \cdot \Phi_{acid} \cdot T_{acid} + \delta_{base} \cdot c_{p,base} \cdot \Phi_{base} \cdot T_{base} \\
&+ \Delta_s H_{acid} \cdot \Phi_{acid} \cdot C_{acid} + \Delta_s H_{base} \cdot \Phi_{base} \cdot C_{base} \\
&- U_W \cdot A_W \cdot (T_L - T_{env}) + \sum_j (-\Delta_r H)_j \cdot \rho_j \cdot V_L \\
&+ \Delta_v H_{H_2O} \cdot N_{H_2O}
\end{aligned} \tag{3.11}$$

expressing that heat accumulation (decrease) in the reactor is due to the temperature difference between the incoming and outgoing liquid stream, the temperature and heat of solution of the added methanol, acid and/or base streams, the heat transport through the reactor wall, the heat release during biological conversion reactions and the heat loss due to water evaporation.

The area of the reactor side wall can be written in terms of the reactor height and diameter:

$$A_W = \pi \cdot d_R \cdot H_L \tag{3.12}$$

The heat balance is further simplified, neglecting the heat content of incoming methanol and acid or base streams and the heat of solution during addition of methanol, acid or base. Also, heat loss due to evaporation of water is not considered. However, this heat loss can be considerable when the reactor is aerated with dry air, supplied by a compressor. In this case also the compressor heat should be taken into account. As for the density (see Eq. 3.1), the heat capacity of the liquid phase is assumed to be equal to the one of water and its temperature dependency is neglected. The heat capacity of water indeed remains quite constant ($\approx 4.184 \text{ kJ kg}^{-1} \text{ K}^{-1}$; Perry and Green, 1984) in a broad temperature range.

Taking into account these assumptions and substituting Eqs. 3.1 and 3.12, the liquid phase heat balance 3.11 is simplified to

$$\begin{aligned}
\frac{dT_L}{dt} &= \frac{1}{V_L} \cdot \left[\Phi_L^{in} \cdot T_L^{in} - \Phi_L^{in,net} \cdot T_L \right] \\
&- \frac{U_W \cdot \pi \cdot d_R \cdot H_L \cdot (T_L - T_{env})}{\delta_L \cdot c_{p,L} \cdot V_L} + \sum_j \frac{(-\Delta_r H)_j}{\delta_L \cdot c_{p,L}} \cdot \rho_j
\end{aligned} \tag{3.13}$$

The mass balances and the heat balance are implemented in Simulink in the form of the Eqs. 3.1, 3.8, 3.9, 3.10 and 3.13.

During a dynamic simulation, some concentrations may show negative values because of certain conditions and disturbances of the system in combination with the selected tolerance for the numerical solver, which allows the solver to take a time step that may be slightly too large. This problem was reported by Jeppsson for Matlab/Simulink simulations with the COST Benchmark simulation model (Copp, 2002, Chapter 8) and has also been detected during dynamic simulations with the SHARON model, more particular for oxygen concentrations in oxygen-limited conditions. As proposed by Jeppsson for the Benchmark case, the problem was solved in the SHARON model using a concentration of zero instead of a negative value for the state variable(s) of concern for the calculation of the reaction rates. In this way, the effect of a negative state variable on the concentration of other state variables is minimized. In the mass balances, the original values of all state variables are used and no additional limitations are used in the model output description. Of course an exception is made for the state variable Z^+ , of which a negative concentration is possible and is used to express a concentration of negatively charged ions.

3.3 Biological conversion reactions

Five different biological conversion reactions, taking place in the liquid phase only, are considered in the SHARON reactor model. The nitrification process is modelled in two steps: oxidation of ammonia to nitrite by ammonia oxidizers and subsequent oxidation of nitrite to nitrate by nitrite oxidizers. Denitrification of both nitrite and nitrate directly to nitrogen gas is considered. Finally, also oxidation of methanol, that is typically added as an external carbon source, is taken up.

3.3.1 Process stoichiometry and kinetics

The stoichiometry of the biological conversion reactions is summarized in the form of the stoichiometric matrix (A_{ij}) in Table 3.1.

Table 3.1: Stoichiometric matrix (A_{ij}) in terms of yield coefficients and biomass composition

i variable: temperature [K] or concentration [mole m_L^{-3}]	j process considered				
A_{ij}	1 ammonium oxidation	2 nitrite oxidation	3 denitrification nitrite	4 denitrification nitrate	5 methanol oxidation
1 T	$\frac{(-\Delta_r H)_1}{\rho \cdot c_p}$	$\frac{(-\Delta_r H)_2}{\rho \cdot c_p}$	$\frac{(-\Delta_r H)_3}{\rho \cdot c_p}$	$\frac{(-\Delta_r H)_4}{\rho \cdot c_p}$	$\frac{(-\Delta_r H)_5}{\rho \cdot c_p}$
2 $TNH(NH_4^+)$	$-\frac{1}{Y_1}$	$-n_{nit}$	$-n_{het}$	$-n_{het}$	$-n_{het}$
3 $TNO_2(NO_2^-)$	$\frac{1}{Y_1} - n_{amm}$	$-\frac{1}{Y_2}$	$-\frac{1}{Y_3}$	0	0
4 $TIC(CO_2)$	-1	-1	$-\frac{1}{3} + \frac{0.5}{Y_3} + \frac{h_{het}}{6}$ $-\frac{o_{het}}{3} - \frac{n_{het}}{2}$	$-\frac{1}{3} + \frac{5}{6 \cdot Y_4} + \frac{h_{het}}{6}$ $-\frac{o_{het}}{3} - \frac{n_{het}}{2}$	$-1 + \frac{1}{Y_5}$
5 TIP	0	0	0	0	0
6 NO_3	0	$\frac{1}{Y_2}$	0	$-\frac{1}{Y_4}$	0
7 O_2	$-\left(-1 + \frac{1.5}{Y_1} - \frac{h_{amm}}{4} + \frac{o_{amm}}{2} - \frac{3}{4} \cdot n_{amm}\right)$	$-\left(-1 + \frac{0.5}{Y_2} - \frac{h_{nit}}{4} + \frac{o_{nit}}{2} + \frac{3}{4} \cdot n_{nit}\right)$	0	0	$-\left(-1 + \frac{1.5}{Y_5} - \frac{h_{het}}{4} + \frac{o_{het}}{2} + \frac{3}{4} \cdot n_{het}\right)$
8 N_2	0	0	$\frac{0.5}{Y_3}$	$\frac{0.5}{Y_4}$	0
9 X_{amm}	1	0	0	0	0
10 X_{nit}	0	1	0	0	0
11 X_{het}	0	0	1	1	1
12 CH_3OH	0	0	$-\left(\frac{2}{3} + \frac{0.5}{Y_3} + \frac{h_{het}}{6} - \frac{o_{het}}{3} - \frac{n_{het}}{2}\right)$	$-\left(\frac{2}{3} + \frac{5}{6 \cdot Y_4} + \frac{h_{het}}{6} - \frac{o_{het}}{3} - \frac{n_{het}}{2}\right)$	$-\frac{1}{Y_5}$
13 Z^+	0	0	0	0	0
H^+	$\frac{2}{Y_1} - n_{amm}$	n_{nit}	$-\left(\frac{1}{Y_3} - n_{het}\right)$	$-\left(\frac{1}{Y_4} - n_{het}\right)$	n_{het}
H_2O	$\frac{1}{Y_1} - \frac{h_{amm}}{2} + \frac{n_{amm}}{2}$	$\frac{3}{2} \cdot n_{nit} - \frac{h_{nit}}{2}$	$\frac{4}{3} + \frac{1.5}{Y_3} - \frac{h_{het}}{6} - \frac{2}{3} \cdot o_{het} + \frac{n_{het}}{2}$	$\frac{4}{3} + \frac{13}{6 \cdot Y_4} - \frac{h_{het}}{6} - \frac{2}{3} \cdot o_{het} + \frac{n_{het}}{2}$	$\frac{2}{Y_5} - \frac{h_{het}}{2} + \frac{3}{2} \cdot n_{het}$

Although mass balances are set up for lumped compounds, the stoichiometric coefficients given in Table 3.1 are calculated for a certain equilibrium form, given between brackets. The inclusion of coefficients for protons and for water in the stoichiometric matrix of Table 3.1 is necessary for calculation of the reaction enthalpy values (see section 3.3.2). However, no mass balances are set up for these components: the proton concentration and the related pH is calculated every time step from a charge balance for all components (see section 3.4), while water is not considered as a component of interest.

The stoichiometric coefficients A_{ij} are expressed in terms of the corresponding yield coefficients Y_j for each reaction j (Table 3.2) and in terms of the biomass composition $CH_hO_oN_n$. A fixed biomass composition of $CH_{1.8}O_{0.5}N_{0.2}$ has been assumed for ammonium oxidizers, nitrite oxidizers as well as heterotrophs.

Table 3.2: Yield coefficients (Lochtman, 1995)

symbol	characterization	value	unit
Y_1	yield of ammonia oxidation	$0.11 \cdot \frac{14}{M_{amm}}$	$\frac{\text{mole } X_{amm}}{\text{mole } NH_4^+}$
Y_2	yield of nitrite oxidation	$0.03 \cdot \frac{14}{M_{nit}}$	$\frac{\text{mole } X_{nit}}{\text{mole } NO_2^-}$
Y_3	yield of denitrification of nitrite	0.23	$\frac{\text{mole } X_{het}}{\text{mole } NO_2^-}$
Y_4	yield of denitrification of nitrate	0.33	$\frac{\text{mole } X_{het}}{\text{mole } NO_3^-}$
Y_5	yield of methanol oxidation	0.29	$\frac{\text{mole } X_{het}}{\text{mole } CH_3OH}$

The biological process rates ρ_j for each reaction j (expressed in mole $m_L^{-3} d^{-1}$) are summarized in Table 3.3. The values of the kinetic parameters are given in Table 3.4.

Mind that ammonia rather than ammonium and nitrous acid rather than nitrite are the real substrates for the nitrification process, as biomass can only transport the uncharged components over its membrane (Anthonisen et al. 1976, confirmed by Van Hulle et al. 2004). Monod terms for NH_3 and HNO_2 are therefore included in the kinetic growth rate expressions. This formulation contrasts with the one in the ASM models, where e.g. S_{NH} accounts for both NH_3 and NH_4^+ and the resulting models are only valid for constant pH, at which the ratio $\frac{NH_3}{NH_3+NH_4^+}$ is constant. The formulation in this model assures satisfying description of the pH influence during oxidation of high amounts of ammonium. Inhibition experiments with nitrite have revealed that at

Table 3.3: Kinetic rate expressions

process rate equation ρ_j
$\rho_1 = \mu_{max}^{amm} \cdot \frac{C_{NH_3}}{K_{NH_3}^{amm} + C_{NH_3}} \cdot \frac{C_{O_2}}{K_{O_2}^{amm} + C_{O_2}} \cdot \frac{K_{I,HNO_2}^{amm}}{K_{I,HNO_2}^{amm} + C_{HNO_2}} \cdot X^{amm}$
$\rho_2 = \mu_{max}^{nit} \cdot \frac{C_{HNO_2}}{K_{HNO_2}^{nit} + C_{HNO_2}} \cdot \frac{C_{O_2}}{K_{O_2}^{nit} + C_{O_2}} \cdot X^{nit}$
$\rho_3 = \mu_{max}^{dNO_2} \cdot \frac{C_{TNO_2}}{K_{NO_2}^{dNO_2} + C_{TNO_2}} \cdot \frac{C_{CH_3OH}}{K_{CH_3OH}^{het,an} + C_{CH_3OH}} \cdot \frac{C_{TNO_2}}{C_{TNO_2} + C_{NO_3}} \cdot \frac{K_{I,O_2}}{K_{I,O_2} + C_{O_2}} \cdot X^{het}$
$\rho_4 = \mu_{max}^{dNO_3} \cdot \frac{C_{NO_3}}{K_{NO_3}^{dNO_3} + C_{NO_3}} \cdot \frac{C_{CH_3OH}}{K_{CH_3OH}^{het,an} + C_{CH_3OH}} \cdot \frac{C_{NO_3}}{C_{TNO_2} + C_{NO_3}} \cdot \frac{K_{I,O_2}}{K_{I,O_2} + C_{O_2}} \cdot X^{het}$
$\rho_5 = \mu_{max}^{met} \cdot \frac{C_{CH_3OH}}{K_{CH_3OH}^{het,ox} + C_{CH_3OH}} \cdot \frac{C_{O_2}}{K_{O_2}^{het} + C_{O_2}} \cdot X^{het}$

the prevailing nitrite concentration levels in the SHARON process, an inhibition term has to be included, with unionized HNO_2 as the actual inhibiting compound (Van Hulle et al., 2004). Inhibition of ammonia is not taken into account, as it has not been detected at the prevailing ammonia concentrations.

The pH dependency of maximum specific growth rates is taken into account using the relationship from Van Hulle et al. (2004), determined for ammonium oxidizers in a partial nitritation SHARON process and shown in Figure 3.1:

$$OUR = OUR_{max} \cdot \frac{K_{pH}}{K_{pH} - 1 + 10^{|pH_{opt} - pH|}} \quad (3.14)$$

in which $K_{pH} = 8.21$ and $pH_{opt} = 7.23$. This relationship is applied here for the maximum specific growth rate μ instead of the oxygen uptake rate. Note that in this way the pH dependency of the maintenance coefficient is neglected. Besides, it is not only applied for ammonium oxidizers but for all microbial growth rates (μ_{max}^{amm} , μ_{max}^{nit} , $\mu_{max}^{dNO_2}$, $\mu_{max}^{dNO_3}$ and μ_{max}^{met}) assuming they all have the same pH dependency profile.

From the process rates, the volumetric conversion rate $r_{i,L}$ of a component i (TNH , TNO_2 , TIC , TIP , NO_3^- , O_2 , N_2 , X_{amm} , X_{nit} , X_{het}) is calculated as

$$r_{i,L} = \sum_{j=1}^5 A_{ij} \cdot \rho_j \quad (3.15)$$

Note that the conversion rate is positive for components that are produced, and negative for components that undergo net consumption.

Table 3.4: Kinetic parameter values

symbol	characterization	value at 35C	unit	reference
μ_{max}^{amm}	maximum growth rate ammonia oxidizers	2.1	d ⁻¹	(1)
$K_{NH_3}^{amm}$	ammonia substrate saturation for ammonia oxidizers	0.054	mol m ⁻³	(2)
$K_{O_2}^{amm}$	oxygen substrate saturation for ammonia oxidizers	0.0294	mol m ⁻³	(2)
K_{I,HNO_2}^{amm}	nitrous acid inhibition constant for ammonia oxidizers	0.146	mol m ⁻³	(2)
μ_{max}^{nit}	maximum growth rate nitrite oxidizers	1.05	d ⁻¹	(1)
$K_{HNO_2}^{nit}$	nitrous acid substrate saturation for nitrite oxidizers	0.019	mol m ⁻³	(3)
$K_{O_2}^{nit}$	oxygen substrate saturation for nitrite oxidizers	0.034	mol m ⁻³	(3)
$\mu_{max}^{dNO_2}$	maximum growth rate nitrite denitrifiers	1.5	d ⁻¹	(1)
$K_{NO_2}^{dNO_2}$	nitrite substrate saturation for nitrite denitrifiers	0.0085	mol m ⁻³	(3)
$K_{CH_3OH}^{het,an}$	methanol substrate saturation during denitrification	0.521	mol m ⁻³	(3)
K_{I,O_2}	oxygen 'inhibition constant' for denitrifiers	0.0063	mol m ⁻³	(4)
$\mu_{max}^{dNO_3}$	maximum growth rate nitrate denitrifiers	1.5	d ⁻¹	(5)
$K_{NO_3}^{dNO_3}$	nitrate substrate saturation for nitrate denitrifiers	0.01	mol m ⁻³	(3)
μ_{max}^{met}	maximum growth rate methanol oxidizers	2.5	d ⁻¹	(6)
$K_{CH_3OH}^{het,ox}$	methanol substrate saturation during aerobic growth	2.083	mol m ⁻³	(3)
$K_{O_2}^{het}$	oxygen substrate saturation for methanol oxidizers	0.0025	mol m ⁻³	(3)

(1) Lochtman (1995)

(2) Van Hulle et al. (2004)

(3) Wiesmann (1994)

(4) Henze et al. (2000, ASM3)

(5) Taken equal to $\mu_{max}^{dNO_2}$ (6) In correspondance with $\eta = \frac{\mu_{max}^{dNO_3}}{\mu_{max}^{met}} = 0.6$, analogous to Henze et al. (2000, ASM3)

3.3.2 Heat production

Comparing the individual mass balances (Eq. 3.8) with the heat balance (Eq. 3.13), one notices the analogy between the component concentrations on the one hand and the temperature on the other hand. Also, the stoichiometric coefficients A_{ij} in the individual mass balances are analogous to the term $\frac{(-\Delta_r H)_j}{\delta_L \cdot c_{p,L}}$ in the heat balance. The 'stoichiometric' matrix (A_{ij}) is extended with these insights, so the heat production from reactions is calculated together with the conversion rates of the components.

The reaction enthalpy values are calculated from the formation enthalpy values of all components (including H_2O and H^+) involved in

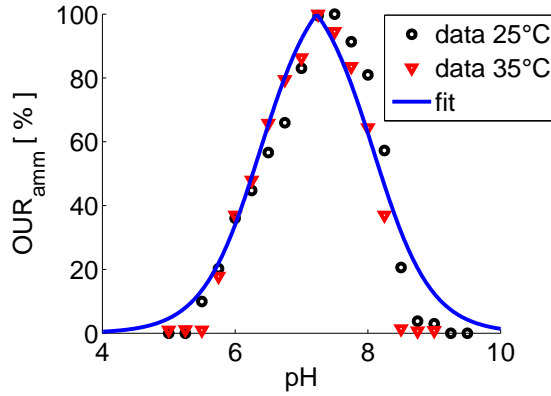


Figure 3.1: pH-dependency of the oxygen uptake rate (OUR) of ammonium oxidizers (Van Hulle et al., 2004)

the corresponding reaction:

$$(-\Delta_r H)_j = \sum_i A_{ij} \cdot (-\Delta_f H)_i \quad (3.16)$$

Different equilibrium forms of a certain compound (e.g. NH_3 and NH_4^+) have different formation enthalpy values. However, the reaction enthalpy values are calculated considering the formation enthalpies of the equilibrium forms, to which the stoichiometric coefficients correspond, i.e. NH_4^+ , NO_2^- and CO_2 , as if they were the only forms present. For the amount of equilibrium components, present in another form, i.e. NH_3 , HNO_2 , HCO_3^- and CO_3^{2-} the error made by this assumption amounts up to the reaction enthalpy for the equilibrium reaction between the different forms. This error will be small because the equilibrium forms NH_4^+ , NO_2^- and HCO_3^- of which the formation enthalpies are used, are the dominant forms in the pH range of the SHARON process.

Further, the reaction heat of ammonium oxidation is added up to the reaction heat of CO_2 -stripping, assuming that all protons produced result in an equimolar amount of CO_2 stripped, hereby neglecting the (relatively very small) amount of protons that stays in the liquid phase and results in a pH decrease.

3.4 pH calculation

Biological conversion reactions that involve proton consumption or production affect the pH of the medium in which they take place and as a result at the same time also the concentrations of all components that are involved in chemical equilibria. Vice versa, significant pH effects and resulting equilibrium component concentration changes will also influence the biological conversion rates. Consequently, when modelling systems in which significant pH changes are to be expected, chemical dissociation reactions (acid/base chemistry) must be modelled adequately in order to obtain realistic results. Section 3.4.1 describes a general procedure for the calculation of pH and corresponding equilibrium concentrations. This procedure is applied to the SHARON process in section 3.4.2.

3.4.1 General pH calculation procedure by means of a charge balance

Biological conversion reactions and chemical dissociation reactions occur on a different time-scale (typically hours-days and seconds respectively). The model of a biological system with varying pH consequently exhibits different time constants. The model is said to be stiff. In order to avoid computational problems associated with stiff models, the fastest reactions in the model can be assumed to be in steady state (equilibrium).

During dynamic simulation of a system in which both (slow) biological and (fast) chemical transformations occur, the chemical dissociation reactions can be considered to be in steady state in comparison to the biological conversion reactions. In this approach, the pH and the concentrations of equilibrium components are calculated by means of a charge balance (electro-neutrality equation) in the reactor, that is an algebraic equation. Lumped components are introduced, of which the concentrations equal the total concentration of all equilibrium forms of a certain component. Mass balances (differential equations) are set up for lumped components and for components that are not involved in chemical equilibrium reactions. As the chemical dissociation reactions are considered to be in steady state, only biological conversion reactions are taken up in the mass balances. The stoichiometry of the biological conversion reactions is expressed in terms of the lumped components, the biological process rates are expressed in the actual form by

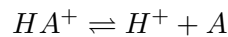
which they are influenced, typically the unionized form. The mass balances are solved for the concentration of the lumped components and the components that are not involved in equilibria. Subsequently, the pH is calculated from the concentrations of the lumped components and the components that don't take part in equilibria by means of a charge balance. Once the pH is known, besides the concentrations of the lumped components, the corresponding concentrations of individual components involved in equilibria can be calculated as well.

The application of this procedure to the SHARON process was first suggested and implemented in Matlab 4.0/Simulink 1.2 by Hellinga et al. (1999). The method has been generalized and is explained in detail in this section.

Identification of chemical equilibria and definition of lumped components

The following 'general' procedure includes the following types of chemical dissociation reactions:

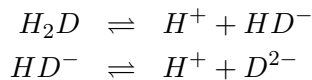
1. Monoprotic acid with monovalent positive charge, dissociates into neutral base form:



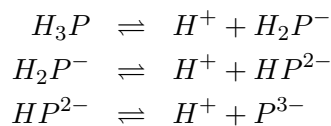
2. Monoprotic neutral acid, dissociates into base with monovalent negative charge:



3. Biprotic neutral acid, dissociates in two steps into base with bivalent negative charge:



4. Triprotic neutral acid, dissociates in three steps into base with trivalent negative charge:



Besides, also the water equilibrium is taken into account:



As chemical equilibrium reactions proceed much faster than the biological conversion reactions, they are assumed to be in steady state, so the following equations apply:

$$K_{e,A} = \frac{C_A \cdot C_{H^+}}{C_{HA^+}} \quad (3.17)$$

$$K_{e,B} = \frac{C_{H^+} \cdot C_{B^-}}{C_{HB}} \quad (3.18)$$

$$K_{e,D1} = \frac{C_{H^+} \cdot C_{HD^-}}{C_{H_2D}} \quad (3.19)$$

$$K_{e,D2} = \frac{C_{H^+} \cdot C_{D^{2-}}}{C_{HD^-}} \quad (3.20)$$

$$K_{e,P1} = \frac{C_{H^+} \cdot C_{H_2P^-}}{C_{H_3P}} \quad (3.21)$$

$$K_{e,P2} = \frac{C_{H^+} \cdot C_{HP^{2-}}}{C_{H_2P^-}} \quad (3.22)$$

$$K_{e,P3} = \frac{C_{H^+} \cdot C_{P^{3-}}}{C_{HP^{2-}}} \quad (3.23)$$

$$K_w = C_{H^+} \cdot C_{OH^-} \quad (3.24)$$

Note that C_{H^+} is written where essentially $C_{H_3O^+}$ is meant, as the above equilibrium constants represent the acidity constants in water (See appendix A.1 for the rigorous definition of equilibrium constants).

When significant temperature changes occur in the system under study, the temperature will be considered as a separate state variable, besides the concentrations of the components of interest. The temperature dependency of the equilibrium constants K_a will be taken into account, typically by means of an Arrhenius equation, and their value will be calculated every time step from the prevailing temperature.

Lumped components are defined, of which the concentrations equal the total concentration of all equilibrium forms of a certain component:

$$C_{TA} = C_{HA^+} + C_A \quad (3.25)$$

$$C_{TB} = C_{HB} + C_{B^-} \quad (3.26)$$

$$C_{TD} = C_{H_2D} + C_{HD^-} + C_{D^{2-}} \quad (3.27)$$

$$C_{TP} = C_{H_3P} + C_{H_2P^-} + C_{HP^{2-}} + C_{P^{3-}} \quad (3.28)$$

Set-up of the electro-neutrality equation (charge balance)

The electro-neutrality equation or charge balance in the reactor can be written as

$$\begin{aligned} \Delta_{ch} = & C_{H^+} - C_{OH^-} + C_{HA^+} - C_{B^-} - C_{HD^-} - 2 \cdot C_{D^{2-}} \\ & - C_{H_2P^-} - 2 \cdot C_{HP^{2-}} - 3 \cdot C_{P^{3-}} + C_{L^+} + C_{Z^+} \quad (3.29) \end{aligned}$$

in which Δ_{ch} stands for the 'gap' in the charge balance, which should be close to zero.

If multiple components of one or more type(s) are present, additional analogous terms (e.g. $C_{HA_1^+}$, $C_{HA_2^+}$) are inserted in the charge balance and in the subsequent calculation.

Z^+ is a lumped component that represents the concentration of net positive charges that are not influenced by the establishment of an equilibrium pH and that are not involved in any biological conversion reaction.

L^+ is a lumped component that represents the concentration of net positive charges that are not influenced by the establishment of an equilibrium pH but are involved in one or more biological conversion reactions. It is further assumed that all components involved in biological reactions are considered in the model, so that it is exactly known which components L^+ consists of. This is not the case for Z^+ , of which the composition is not known as one usually doesn't consider components that do not effect the biological conversion reactions. Note that the concentrations of Z^+ and L^+ are negative if there are more negative than positive charges present.

The charge balance can be rewritten in terms of the known concentrations of the lumped components, the components L^+ and Z^+ , and the concentration of H^+ , that needs to be calculated. By substituting the concentrations of the lumped components (Eqs. 3.25-3.28) into the steady state expressions for equilibria (Eqs. 3.17-3.23), the concentration of every charged component is rewritten in terms of the concentration

of protons and lumped components:

$$C_{HA^+} = \frac{C_{TA} \cdot C_{H^+}}{N_A} \quad (3.30)$$

$$C_{B^-} = \frac{C_{TB} \cdot K_{e,B}}{N_B} \quad (3.31)$$

$$C_{HD^-} = \frac{C_{TD} \cdot C_{H^+} \cdot K_{e,D1}}{N_D} \quad (3.32)$$

$$C_{D^{2-}} = \frac{C_{TD} \cdot K_{e,D1} \cdot K_{e,D2}}{N_D} \quad (3.33)$$

$$C_{H_2P^-} = \frac{C_{TP} \cdot C_{H^+}^2 \cdot K_{e,P1}}{N_P} \quad (3.34)$$

$$C_{HP^{2-}} = \frac{C_{TP} \cdot C_{H^+} \cdot K_{e,P1} \cdot K_{e,P2}}{N_P} \quad (3.35)$$

$$C_P^{3-} = \frac{C_{TP} \cdot K_{e,P1} \cdot K_{e,P2} \cdot K_{e,P3}}{N_P} \quad (3.36)$$

in which

$$N_A \triangleq C_{H^+} + K_{e,A} \quad (3.37)$$

$$N_B \triangleq C_{H^+} + K_{e,B} \quad (3.38)$$

$$N_D \triangleq C_{H^+}^2 + C_{H^+} \cdot K_{e,D1} + K_{e,D1} \cdot K_{e,D2} \quad (3.39)$$

$$N_P \triangleq C_{H^+}^3 + C_{H^+}^2 \cdot K_{e,P1} + C_{H^+} \cdot K_{e,P1} \cdot K_{e,P2} + K_{e,P1} \cdot K_{e,P2} \cdot K_{e,P3} \quad (3.40)$$

After substitution of the above equations 3.30-3.36 and the OH^- -concentration through Eq. 3.24, the charge balance becomes

$$\begin{aligned} \Delta_{ch} = & C_{H^+} - \frac{K_w}{C_{H^+}} + \frac{C_{TA} \cdot C_{H^+}}{N_A} - \frac{C_{TB} \cdot K_{e,B}}{N_B} \\ & - \frac{C_{TD} \cdot C_{H^+} \cdot K_{e,D1}}{N_D} - 2 \cdot \frac{C_{TD} \cdot K_{e,D1} \cdot K_{e,D2}}{N_D} \\ & - \frac{C_{TP} \cdot C_{H^+}^2 \cdot K_{e,P1}}{N_P} - 2 \cdot \frac{C_{TP} \cdot C_{H^+} \cdot K_{e,P1} \cdot K_{e,P2}}{N_P} \\ & - 3 \cdot \frac{C_{TP} \cdot K_{e,P1} \cdot K_{e,P2} \cdot K_{e,P3}}{N_P} + C_{L^+} + C_{Z^+} \quad (3.41) \end{aligned}$$

The concentrations of the lumped components TA , TB , TD , TP , L^+ and Z^+ are calculated every time step from the corresponding mass balances. As it is not known which components Z^+ comprises, its influent concentration $C_{Z^+}^{in}$ and its initial concentration $C_{Z^+}^0$, that need to

be known to solve the corresponding mass balance, are calculated from the charge balances for the influent and for the initial concentrations respectively. This is demonstrated for $C_{Z^+}^{in}$:

$$\begin{aligned}
C_{Z^+}^{in} = & -C_{H^+}^{in} + \frac{K_w}{C_{H^+}^{in}} - \frac{C_{TA}^{in} \cdot C_{H^+}^{in}}{N_A^{in}} + \frac{C_{TB}^{in} \cdot K_{e,B}^{in}}{N_B^{in}} \\
& + \frac{C_{TD}^{in} \cdot C_{H^+}^{in} \cdot K_{e,D1}^{in}}{N_D^{in}} + 2 \cdot \frac{C_{TD}^{in} \cdot K_{e,D1}^{in} \cdot K_{e,D2}^{in}}{N_D^{in}} \\
& + \frac{C_{TP}^{in} \cdot (C_{H^+}^{in})^2 \cdot K_{e,P1}^{in}}{N_P^{in}} + 2 \cdot \frac{C_{TP}^{in} \cdot C_{H^+}^{in} \cdot K_{e,P1}^{in} \cdot K_{e,P2}^{in}}{N_P^{in}} \\
& + 3 \frac{C_{TP}^{in} \cdot K_{e,P1}^{in} \cdot K_{e,P2}^{in} \cdot K_{e,P3}^{in}}{N_P^{in}} - C_{L^+}^{in} \quad (3.42)
\end{aligned}$$

The calculation of $C_{Z^+}^0$ is performed completely analogously.

Note that temperature changes can cause the initial equilibrium constants and the equilibrium constants for the influent to be different from the ones in the reactor. This is not only the case when temperature effects are taken into account explicitly, i.e. temperature is a state variable, but also when the reactor temperature is assumed constant in time but not equal to the constant temperature of the reactor influent.

Once the concentrations of the lumped components C_{TA} , C_{TB} , C_{TD} , C_{TP} , C_{L^+} and C_{Z^+} have been calculated, the proton concentration C_{H^+} remains the only unknown in the charge balance (Eq. 3.41):

$$\Delta_{ch} = \Delta_{ch}(C_{H^+}) \quad (3.43)$$

Calculation of pH and equilibrium concentrations

The algebraic equation 3.43 has to be solved for the proton concentration C_{H^+} for which the sum of all charges is zero:

$$\Delta_{ch}(C_{H^+}) = 0 \quad (3.44)$$

Since this is an implicit equation in C_{H^+} , it has to be solved iteratively. Different numerical solution methods can be applied, e.g. the Newton-Raphson method. The Newton-Raphson method starts from an initial guess $C_{H^+,0}$, that deviates from the actual value of C_{H^+} , for which the charge balance is fulfilled:

$$C_{H^+} = C_{H^+,0} + \delta C_{H^+} \quad (3.45)$$

Performing a Taylor approximation of Eq. 3.43 around Eq. 3.45 yields

$$\Delta_{ch}(C_{H^+}) \approx \Delta_{ch}(C_{H^+,0}) + \left. \frac{d\Delta_{ch}(C_{H^+})}{dC_{H^+}} \right|_{C_{H^+,0}} \cdot (C_{H^+} - C_{H^+,0}) \quad (3.46)$$

To close the gap in the charge balance, C_{H^+} is calculated from Eq. 3.46 as

$$C_{H^+} \approx C_{H^+,0} - \frac{\Delta_{ch}(C_{H^+,0})}{\left. \frac{d\Delta_{ch}(C_{H^+})}{dC_{H^+}} \right|_{C_{H^+,0}}} \quad (3.47)$$

The derivative of the gap in the charge balance (Eq. 3.41) to C_{H^+} can be calculated analytically; one finds

$$\begin{aligned} \frac{d\Delta_{ch}(C_{H^+})}{dC_{H^+}} = & 1 + \frac{K_w}{C_{H^+}^2} + \frac{C_{TA} \cdot K_{e,A}}{N_A^2} + \frac{C_{TB} \cdot K_{e,B}}{N_B^2} \\ & + \frac{C_{TD} \cdot K_{e,D1} \cdot (C_{H^+}^2 - K_{e,D1} \cdot K_{e,D2})}{N_D^2} \\ & + 2 \cdot \frac{C_{TD} \cdot K_{e,D1} \cdot K_{e,D2} \cdot (2 \cdot C_{H^+} + K_{e,D1})}{N_D^2} \\ & + \frac{C_{TP} \cdot C_{H^+} \cdot K_{e,P1}}{N_P^2} \\ & \quad \cdot (C_{H^+}^3 - C_{H^+} \cdot K_{e,P1} \cdot K_{e,P2} - 2 \cdot K_{e,P1} \cdot K_{e,P2} \cdot K_{e,P3}) \\ & + 2 \cdot \frac{C_{TP} \cdot K_{e,P1} \cdot K_{e,P2}}{N_P^2} \\ & \quad \cdot (2 \cdot C_{H^+}^3 + C_{H^+}^2 \cdot K_{e,P1} - K_{e,P1} \cdot K_{e,P2} \cdot K_{e,P3}) \\ & + 3 \cdot \frac{C_{TP} \cdot K_{e,P1} \cdot K_{e,P2} \cdot K_{e,P3}}{N_P^2} \\ & \quad \cdot (3 \cdot C_{H^+}^2 + 2 \cdot C_{H^+} \cdot K_{e,P1} + K_{e,P1} \cdot K_{e,P2}) \end{aligned} \quad (3.48)$$

considering C_{Z^+} and C_{L^+} are not dependent on pH.

Evaluating the gap in the charge balance (Eq. 3.41) and its derivative (Eq. 3.48) in $C_{H^+,0}$ and substituting these expressions in Eq. 3.45 yields a new estimation for C_{H^+} , noted as $C_{H^+,1}$:

$$C_{H^+,1} = C_{H^+,0} - \frac{\Delta_{ch}(C_{H^+,0})}{\left. \frac{d\Delta_{ch}(C_{H^+})}{dC_{H^+}} \right|_{C_{H^+,0}}}$$

Because of the Taylor series approximation, H_1^+ will not be the value of H^+ that sets $\Delta_{ch}(H^+) = 0$. Therefore, in a next iteration step, the gap

in the charge balance and its derivative are evaluated for the latest estimation of the proton concentration H_1^+ . This yields another estimation for H^+ , now noted as H_2^+

$$C_{H^+,2} = C_{H^+,1} - \frac{\Delta_{ch}(C_{H^+,1})}{\left. \frac{d\Delta_{ch}(C_{H^+})}{dC_{H^+}} \right|_{C_{H^+,1}}}$$

The iteration is repeated until the absolute value of the gap in the charge balance is smaller than a predefined tolerance value, TOL:

$$|\Delta_{ch}(C_{H^+,i})| < \text{TOL}$$

To avoid endless loops when the solution doesn't converge, the iteration is also stopped when exceeding a predefined maximum number of iteration steps. However, the algorithm usually converges very fast (typically in 3-5 iterations).

Once the pH is known besides the concentrations of the lumped components, the concentration of the individual components, involved in an equilibrium, can be calculated from Eqs. 3.30-3.36 and Eqs. 3.25-3.28.

Simplification for biprotic and triprotic acids

The general procedure explained above can be applied to all systems that contain chemical equilibria of one of the forms given by Eqs. 3.17-3.24 by selecting the appropriate terms in the expressions for the charge balance (Eq. 3.41) and its derivative (Eq. 3.48).

Instead of taking into account all dissociation reactions for biprotic and triprotic acids, one can also choose to consider only those dissociation reactions that are likely to occur in the normal pH operating range of the system. E.g. for the diprotic acid H_3Q , one could choose only to consider the second reaction:



with equilibrium constant

$$K_{e,Q2} = \frac{C_{H^+} \cdot C_{HQ^{2-}}}{C_{H_2Q^-}}$$

which means that H_2Q^- and HQ^{2-} are the only equilibrium forms considered for the component TQ :

$$C_{TQ} = C_{H_2Q^-} + C_{HQ^{2-}}$$

The corresponding terms in the charge balance and in its derivative to the proton concentration are found as:

$$\begin{aligned}\Delta_{ch} &= \dots - C_{H_2Q} - 2 \cdot C_{HQ^{2-}} + \dots \\ &= \dots - \frac{C_{TQ} \cdot C_{H^+}}{C_{H^+} + K_{e,Q2}} - 2 \cdot \frac{C_{TQ} \cdot K_{e,Q2}}{C_{H^+} + K_{e,Q2}} + \dots\end{aligned}\quad (3.49)$$

$$\frac{d\Delta_{ch}(C_{H^+})}{dC_{H^+}} = \dots + \frac{C_{TQ} \cdot K_{e,Q2}}{(C_{H^+} + K_{e,Q2})^2} + \dots \quad (3.50)$$

This procedure might be preferred over the one in which all dissociation reactions of the multiprotic acid are considered, as the calculation of very small concentrations of equilibrium forms, that are not likely to occur under the operating conditions considered, might cause numerical problems.

Applicability of the charge balance method

As stated, the above reasoning assumes the concentration of net positive charges not to vary with varying pH, assuming these net positive charges originate from strong acids or bases (e.g. Na^+ , K^+ , Cl^- , F^-). In reality, weak acids or bases of which the equilibrium reactions were not considered (because they were assumed to be negligible at the prevailing nominal pH concentrations) could contribute to the concentration of these net positive charges. The same is valid for equilibrium forms of biprotic or triprotic acids that were not considered in case of applying the simplifications mentioned above.

Another possible reason for deviations from reality is that the steady state assumption might not be appropriate for equilibria that are rather slow, e.g. the bicarbonate/carbon dioxide equilibrium, .

These assumptions can explain possible differences in the pH calculated by the model from acid-base equilibria and the measured pH.

Despite the abovementioned limitations, the use of the charge balance method for calculation of pH and equilibrium concentrations, in which the fast chemical equilibrium reactions are assumed to be in steady state, is a powerful technique. The combination of algebraic and differential equations to be solved, results in a significant reduction in simulation time compared to an approach in which all chemical equilibria are modelled dynamically, resulting in differential equations with strong varying time constants. Section 3.4.2 discusses the application of the generalised pH calculation procedure to the SHARON model and its implementation in Matlab 6.5/Simulink 5.0 (R13).

The method of steady state assumption for fast dynamics is also applicable to other systems. Rosén et al. (2006) used it to reduce the simulation time for the anaerobic digestion model no. 1 (ADMI) implementation in Matlab/Simulink. In this case, the charge balance method was used for calculation of pH and equilibrium concentrations. At the same time, also the fast hydrogen (H_2) dynamics was approximated by an algebraic equation in a completely analogous way. Their implementation of the routines for solving the algebraic equations has been based on the c-mex file for solving the charge balance of the SHARON model, written in this study and discussed in section 3.4.2. When calculating both the pH and the H_2 concentration from algebraic equations, Rosén et al. (2006) obtained an increase in simulation speed by a factor 8 for simulation of the ADM 1 model in comparison to a model containing only differential equations.

3.4.2 Application to the SHARON reactor model

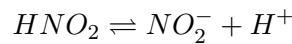
Identification of equilibria and set-up of the charge balance

The SHARON model considers the following chemical equilibria

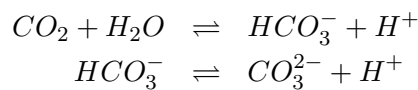
- of type 1:



- of type 2:



- of type 3:

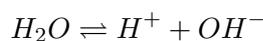


Note that the first reaction includes the formation of H_2CO_3 from H_2O and CO_2 as well as the dissociation of H_2CO_3 into H^+ and HCO_3^-

- of type 4 (only the second dissociation reaction is considered here):



- the water equilibrium:



The corresponding equilibrium constants are given in Table 3.5. Appendix A.2 illustrates the temperature dependency of the ammonium/ammonia and the nitrous acid/nitrite equilibrium.

Table 3.5: Chemical equilibrium coefficients

symbol [unit]	expression	ref.
K_{e,NH_4} [mmole m ⁻³]	$\exp\left(-\frac{6344}{T}\right)$	(1)
K_{e,HNO_2} [mmole m ⁻³]	$\exp\left(-\frac{2300}{T}\right)$	(1)
K_{e,CO_2} [mmole m ⁻³]	$10^{(-356.3094 - 0.06091964 \cdot T + \frac{21834.37}{T} + 126.8339 \cdot \log_{10} T - \frac{1684915}{T^2})}$	(2)
K_{e,HCO_3} [mmole m ⁻³]	$10^{(-107.8871 - 0.03252849 \cdot T + \frac{5151.79}{T} + 38.92561 \cdot \log_{10} T - \frac{563713.9}{T^2})}$	(2)
$K_{e,H_2PO_4^-}$ [mmole m ⁻³]	$-\frac{1979.5}{T} + 5.3541 - 0.01984 \cdot T$	(3)
K_w [mmole ² m ⁻⁶]	$10^{(-283.971 + \frac{13323}{T} - 0.05069842 \cdot T + 102.24447 \cdot \log T - \frac{1119669}{T^2})}$	(2)

(1) Anthonisen et al. (1976)
(2) Stumm and Morgan (1996)
(3) Helgeson (1967)

Nitrate is the only charged component that is involved in the biological conversion reactions but doesn't take part in chemical equilibrium reactions:

$$C_{L+} = -C_{NO_3^-}$$

Consequently, the charge balance in the reactor is written as:

$$\begin{aligned} \Delta_{ch} = & C_{H^+} - C_{OH^-} + C_{NH_4^+} - C_{NO_2^-} - C_{HCO_3^-} - 2 \cdot C_{CO_3^{2-}} \\ & - C_{H_2PO_4^-} - 2 \cdot C_{HPO_4^{2-}} - C_{NO_3^-} + C_{Z^+} \end{aligned} \quad (3.51)$$

or in terms of the lumped components (defined by Eqs. 3.2-3.5), equilibrium constants and C_{H^+} as the only unknown:

$$\begin{aligned} \Delta_{ch} = & C_{H^+} - \frac{K_w}{C_{H^+}} + \frac{C_{TNH} \cdot C_{H^+}}{C_{H^+} + K_{e,NH_4}} - \frac{C_{TNO_2} \cdot K_{e,HNO_2}}{C_{H^+} + K_{e,HNO_2}} \\ & - \frac{C_{TIC} \cdot C_{H^+} \cdot K_{e,CO_2} + 2 \cdot C_{TIC} \cdot K_{e,CO_2} \cdot K_{e,HCO_3}}{C_{H^+}^2 + C_{H^+} \cdot K_{e,CO_2} + K_{e,CO_2} \cdot K_{e,HCO_3}} \\ & - \frac{C_{TIP} \cdot C_{H^+} + 2 \cdot C_{TIP} \cdot K_{e,H_2PO_4}}{C_{H^+} + K_{e,H_2PO_4}} - C_{NO_3^-} + C_{Z^+} \end{aligned} \quad (3.52)$$

The derivative of the gap in the charge balance (3.52) to C_{H^+} can be calculated analytically; one finds

$$\begin{aligned} \frac{d\Delta_{ch}(C_{H^+})}{dC_{H^+}} = & 1 + \frac{K_w}{C_{H^+}^2} + \frac{C_{TNH} \cdot K_{e,NH_4}}{(C_{H^+} + K_{e,NH_4})^2} + \frac{C_{TNO_2} \cdot K_{e,HNO_2}}{(C_{H^+} + K_{e,HNO_2})^2} \\ & + \frac{C_{TIC} \cdot K_{e,CO_2} \cdot (C_{H^+}^2 + 4 \cdot C_{H^+} \cdot K_{e,HCO_3} + K_{e,CO_2} \cdot K_{e,HCO_3})}{(C_{H^+}^2 + C_{H^+} \cdot K_{e,CO_2} + K_{e,CO_2} \cdot K_{e,HCO_3})^2} \\ & + \frac{C_{TIP} \cdot K_{e,H_2PO_4}}{(C_{H^+} + K_{e,H_2PO_4})^2} \end{aligned} \quad (3.53)$$

Every time step, the concentrations of the lumped components TNH , TNO_2 , TIC , TIP , NO_3^- and Z^+ are calculated from the corresponding mass balances (differential equations). Subsequently, the pH and the concentrations of the equilibrium components NH_4^+ , NH_3 , HNO_2 , NO_2^- , CO_2 , HCO_3^- , CO_3^{2-} , $H_2PO_4^-$ and HPO_4^{2-} are calculated according to the general procedure explained in section 3.4.1. Regarding the stopping criterion, the tolerance value is set to $TOL = 10^{-12}$ mole m^{-3} ; the maximum number of iteration steps is set to 1000.

Implementation in Matlab/Simulink

The procedure for calculating pH and corresponding equilibrium concentrations is implemented in Simulink by means of a c-mex S-function, of which the code is listed in Appendix B. This function has been written on the basis of the c-mex S-function template provided by Matlab R13 (`sfuntmpl_basic.c`, in the `matlabroot/simulink/src` directory), that contains skeleton implementations of all the required and optional callback routines that a c-mex-file S-function can implement.

The simulation stages in a Simulink S-function are the same as the general simulation stages in Simulink and are shown in Figure 3.2. First comes the initialization phase, in which the numbers of parameters, continuous and discrete states, input and output variables are defined (function `mdlInitializeSizes`), as well as the sample time (`mdlInitializeSampleTimes`). In this phase, also initial values are given to the state variables (in `mdlInitializeConditions`). Then a simulation loop is entered. During each simulation step, Simulink computes the block's states (`mdlUpdate`, for discrete states), derivatives (`mdlDerivatives`, for continuous states), and outputs (`mdlOutputs`) for the current sample time. This continues until the simulation is complete.

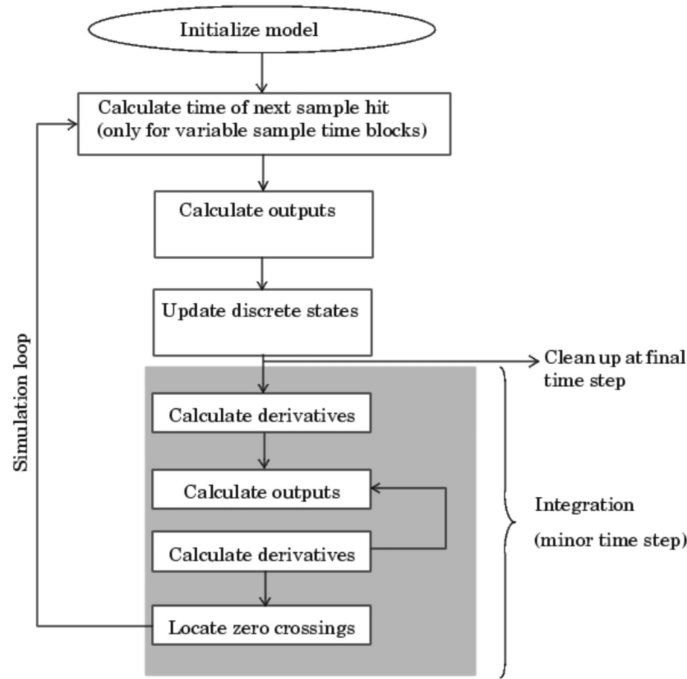


Figure 3.2: Simulation stages in Simulink (from Matlab R13 help)

The inputs for the S-function block for pH-calculation in Simulink are the equilibrium constants K_w , K_{e,NH_4} , K_{e,HNO_2} , K_{e,CO_2} , K_{e,HCO_3} , K_{e,H_2PO_4} , that are calculated every time step for the current temperature, and the concentrations of the lumped components TNH , TNO_2 , TIC , TIP , NO_3^- and Z^+ . The block outputs are the concentrations of H^+ , NH_4^+ , NH_3 , HNO_2 , NO_2^- , CO_2 , HCO_3^- , CO_3^{2-} , $H_2PO_4^-$ and HPO_4^{2-} (all in given order). The initial estimations for the concentrations of the components H^+ , NH_4^+ , NH_3 , HNO_2 , NO_2^- , CO_2 , HCO_3^- , CO_3^{2-} , $H_2PO_4^-$ and HPO_4^{2-} are passed on as block parameters and are in this way the same for every time step. All states in the S-function block for pH-calculation are discrete states, of which the values are updated through the function. This function calls for the user-defined functions `NewtonRaphson`, `Gap` and `dGapdH` in order to calculate the current block states, i.e. the pH and the equilibrium concentrations, according to the iterative Newton Raphson procedure explained above.

Figure 3.3 visualizes the equilibria by means of a buffer capacity curve for a mixture of 60 mole m^{-3} TNH, 20 mole m^{-3} TNO₂, 40 mole m^{-3} TIC, 40 mole m^{-3} TIP, 10 mole m^{-3} NO_3^- and 10 mole m^{-3} Z^+ .

m^{-3} TIC and 40 mole m^{-3} TIP in water. The buffer capacity indicates the differential amount of (strong) acid or base that needs to be added to cause a differential change in pH. The area of the composing peaks correspond to the concentrations of the corresponding equilibrium components. Note that the buffer capacity is always positive.

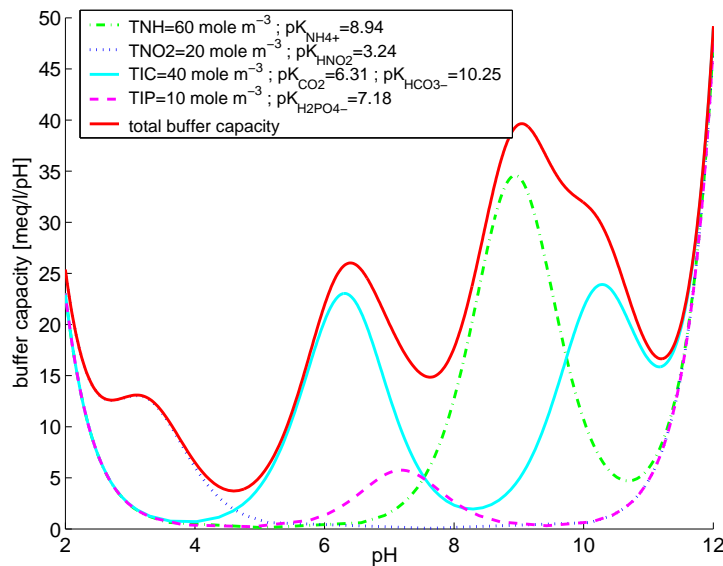


Figure 3.3: Buffer capacity curve for a given mixture of *TNH*, *TNO2*, *TIC* and *TIP* in water

The current implementation differs from the one of Hellinga et al. (1999) in the following aspects:

- Two types of charged components that are not involved in chemical equilibria are considered: components that take part in biological conversions (lumped in L^+) and components that are not affected by biological conversion (lumped in Z^+). This distinction was necessary to take into account the effect of nitrate, of which the concentration changes due to biological conversion.
- The implementation of the pH calculation algorithm as a Simulink S-function was upgraded to a level 2 S-function. It was found necessary to implement the states in discrete form (while they were implemented as continuous states previously) to get the c-mex function running.

- The phosphorus equilibrium was not considered previously. In the current implementation, the equilibrium between $H_2PO_4^-$ and HPO_4^{2-} is considered.

3.5 Gas phase mass balances

The gas phase is assumed to be perfectly mixed. This is a reasonable assumption for reactors with low aspect ratios (column height over diameter less than 3, van der Lans, 2000), as is the case in the simulation study performed in this work. No reactions are assumed to take place in the gas phase. Individual gas phase mass balances for oxygen, carbon dioxide and nitrogen (component i) are considered:

$$\frac{d(V_G^\circ \cdot C_{G,i}^\circ)}{dt} = \Phi_G^{in,\circ} \cdot C_{G,i}^{in,\circ} - \Phi_G^{out,\circ} \cdot C_{G,i}^\circ - k_L a_i \cdot (C_{L,i}^* - C_{L,i}) \cdot V_L$$

The superscript \circ indicates that gas phase concentrations and volumes correspond to the same reference pressure, p^0 .

Considering the short gas residence time relative to the time constants for interphase mass transport and moreover relative to the biological conversion rates, the gas phase is assumed to be in steady state:

$$0 = \Phi_G^{in,\circ} \cdot C_{G,i}^{in,\circ} - \Phi_G^{out,\circ} \cdot C_{G,i}^\circ - k_L a_i \cdot (C_{L,i}^* - C_{L,i}) \cdot V_L \quad (3.54)$$

This assumption is justified in view of the application of this model, that will be used for design and control purposes.

The gas outflow rate $\Phi_G^{out,\circ}$ is calculated from the overall gas phase mass balance for substitution in Eq. 3.54. An overall gas phase mass balance can be set up as

$$\frac{dn_G}{dt} = N_G^{in} - N_G^{out} + N^{exchange} \quad (3.55)$$

The overall gas phase mass balance equals the sum of all individual gas phase mass balances. In this way, the -steady state - overall gas phase mass balance can also be written as:

$$0 = \Phi_G^{in,\circ} \cdot \sum_i C_{G,i}^{in,\circ} - \Phi_G^{out,\circ} \cdot \sum_i C_{G,i}^\circ - \sum_i [k_L a_i \cdot (C_{L,i}^* - C_{L,i})] \cdot V_L \quad (3.56)$$

Note that the summons not only include the components of interest (oxygen, carbon dioxide and nitrogen) but also all other components

that are present in the gas phase e.g. water. The summons of transport terms only include the components that are considered to be transported between gas phase and liquid phase, in this case oxygen, carbon dioxide and nitrogen. Water evaporation is not considered.

Considering two possible ways of calculating the total number of moles present in the gas phase

$$n_G = V_G \cdot \sum_i C_{G,i} \quad \text{or} \quad n_G = \frac{V_G}{V_M} \quad (3.57)$$

it is clear that

$$\sum_i C_{G,i} = \frac{1}{V_M} \quad (3.58)$$

so the overall gas phase mass balance 3.56 can be rewritten as

$$0 = \Phi_G^{in,\circ} \cdot \frac{1}{V_M^{in,\circ}} - \Phi_G^{out,\circ} \cdot \frac{1}{V_M^\circ} - \sum_i [k_L a_i \cdot (C_{L,i}^* - C_{L,i})] \cdot V_L \quad (3.59)$$

The molar gas volume, V_M° , corresponding with (reference) pressure p° , is calculated from the ideal gas law as

$$V_M^\circ = \frac{\mathcal{R} \cdot T}{p^\circ} \quad (3.60)$$

on the basis of the prevailing reactor temperature.

The molar gas volume of the incoming gas stream ($V_M^{in,\circ}$) is the same as the molar gas volume of the gas phase in the reactor (V_M°), as they are calculated according to the same reference pressure and the temperature of these streams can be assumed to be the same (equal to the liquid phase temperature). Consequently, the molar gas outflow rate is calculated from Eq. 3.59 as

$$\Phi_G^{out,\circ} = \Phi_G^{in,\circ} - \sum_i [k_L a_i \cdot (C_{L,i}^* - C_{L,i})] \cdot V_L \cdot V_M^\circ \quad (3.61)$$

After substitution of Eq. 3.61 in the individual mass balances 3.54, the gas phase concentration of component i is calculated as

$$C_{G,i}^\circ = \frac{\Phi_G^{in,\circ} \cdot C_{G,i}^{in,\circ} - k_L a_i \cdot (C_{L,i}^* - C_{L,i}) \cdot V_L}{\Phi_G^{in,\circ} - \sum_i [k_L a_i \cdot (C_{L,i}^* - C_{L,i})] \cdot V_L \cdot V_M^\circ} \quad (3.62)$$

Eq. 3.62 is implemented in Simulink to calculate the gas phase concentrations at every time step. The molar gas volume is calculated from

Eq. 3.60. The transport terms between gas phase and liquid phase, require some special attention and are discussed in the next paragraph.

Note that no heat balance is considered for the gas phase. Its heat capacity is so small that one can assume that the gas phase temperature instantaneously equals the liquid phase temperature.

3.6 Transport between gas and liquid phase

Oxygen is transported from the gas phase to the liquid phase, carbon dioxide and nitrogen (if denitrification takes place) from the liquid phase to the gas phase. The net transport rate from the gas phase to the liquid phase is expressed by the exchange term

$$TR_i = k_L a_i \cdot (C_{L,i}^* - C_{L,i}) \quad (3.63)$$

Mass transport coefficients The mass transport coefficient for oxygen, $k_L a_{O_2}$, expressed in d^{-1} , is related to the superficial gas velocity, v_{Gs} , expressed in $m d^{-1}$. For relatively low, but commonly used gas flow rates $v_{Gs} < 0.1 m s^{-1}$ and for air/water bubble columns with coarse (about 6 mm diameter) bubbles, the linear relationship (van der Lans, 2000)

$$k_L a_{O_2} = 0.6 \cdot v_{Gs} \quad (3.64)$$

can be used, resulting in the value for the mass transfer coefficient at 293.15 K. The temperature dependency of the mass transport coefficient is taken into account through the relationship

$$k_L a_{O_2}(T) = k_L a_{O_2}(293.15 K) \cdot \theta_{kLa}^{T-293.15}$$

in which a value of $\theta_{kLa} = 1.024$ is typical for both diffused and mechanical aeration devices (Tchobanoglous and Burton, 1991). Note that the resulting mass transport coefficient is valid for air/clean water systems and is assumed to be applicable for the specific wastewater treated in the SHARON-process.

The mass transport coefficients for carbon dioxide and nitrogen gas (indicated as component i) are related to the mass transport coefficient for oxygen through their diffusion coefficients, according to the relationship

$$k_L a_i = k_L a_{O_2} \cdot \sqrt{\frac{D_i}{D_{O_2}}} \quad (3.65)$$

valid for low water soluble components and a liquid interphase that is in turbulent motion (De heyder et al., 1997).

The superficial gas flow rate is equal to the ratio of the (influent) gas flow rate to the reactor cross section area. Taking into account its pressure dependency by means of the correlation given by van der Lans (2000) for a bubble column, the following expression is obtained:

$$\begin{aligned} v_{G,s} &= \frac{\Phi_G^{in,\circ}}{A_R} \cdot p^0 \cdot \frac{\ln \frac{p_B}{p_T}}{p_B - p_T} \\ &= \frac{\Phi_G^{in,\circ}}{A_R} \cdot p^0 \cdot \frac{\ln(1 + \frac{\delta_{H_2O} \cdot g \cdot H_L}{p^0})}{\delta_{H_2O} \cdot g \cdot H_L} \end{aligned} \quad (3.66)$$

Eq. 3.66 is substituted in Eq. 3.64 to calculate the mass transport coefficients. The latter simplification is valid in case the pressure on top of the gas phase, p^T , equals the atmospheric pressure, p^0 , chosen as the reference pressure. The liquid height in the reactor can be reasonably approximated as

$$H_L = \frac{V_L + V_G}{A_R} \approx \frac{V_L}{A_R} \quad (3.67)$$

Note that the use of V_G to calculate H_L would lead to an algebraic loop since the knowledge of V_G requires the knowledge of ϵ and thus the knowledge of $v_{G,s}$, requiring on its turn the knowledge of H_L .

Saturation concentration The saturation concentration $C_{L,i}^*$ of a component i at the gas/liquid interphase represents the liquid phase concentration of that component at the interphase, that is assumed to be in equilibrium with its gas phase concentration $C_{G,i}$. It is related to the gas phase concentration of this component by means of its Henry coefficient m_i

$$m_i = \frac{C_{G,i}^\circ}{C_{L,i}^{*,\circ}}$$

The Henry coefficients are temperature dependent. Their values are calculated on the basis of the prevailing temperature according to the correlations given in Table 3.6. The superscript \circ indicates that the saturation concentration and the gas phase concentration correspond to the same reference pressure.

The influence of gas phase pressure (reactor height) on the saturation concentration is taken into account through the following expres-

Table 3.6: Temperature dependency of Henry coefficients (Lochtman, 1995, Appendix V)

symbol	expression
m_{O_2}	$-403 + 2.52 \cdot T - 3.56 \cdot 10^{-3} \cdot T^2$
m_{CO_2}	$2.8 - 3.87 \cdot 10^{-2} \cdot T + 1.12 \cdot 10^{-4} \cdot T^2$
m_{N_2}	$-747 + 4.74 \cdot T - 6.77 \cdot 10^{-3} \cdot T^2$

sion (van der Lans, 2000)

$$\begin{aligned}
 C_{L,i}^* &= \frac{C_{G,i}^o}{m_i} \cdot \frac{p^T + \frac{1}{2} \delta_{H_2O} \cdot g \cdot H_L}{p^0} \\
 &= \frac{C_{G,i}^o}{m_i} \cdot \left(1 + \frac{\delta_{H_2O} \cdot g \cdot H_L}{2 \cdot p^0} \right) \quad (3.68)
 \end{aligned}$$

assuming the top pressure in the reactor, p_T equals the reference pressure, p_0 , in the model chosen as the atmospheric pressure. The expression 3.68 is only valid for an ideally mixed gas phase, an assumption that is reasonable for low aspect ratios ($\frac{H_L}{d_R} < 3$). The effect of liquid composition (β -factor) on the saturation concentrations has not been taken into account.

Eq. 3.68 is implemented in Simulink to calculate the saturation concentration at every time step. However, the combination of Eq. 3.62 and Eq. 3.68 leads to an algebraic loop, as they need to be solved simultaneously. A 'memory'-block was connected to the block with output $C_{L,i}^*$, so the saturation concentration from the previous time step is used to calculate the gas phase concentrations in order to overcome this problem. However, this led to erroneous results (negative gas phase concentrations). The problem was eventually solved by using a first order system with very small time constant (1 s) to impose an imperceptibly small delay to $C_{L,i}^*$ as suggested by Devisscher (personal communication).

3.7 Process control features

3.7.1 Aeration control

The effect of a varying influent air flow rate $\Phi_G^{in,o}$ on the superficial gas velocity through Eq. 3.66 and consequently on the mass transport

coefficients through Eqs. 3.64 and 3.65 is taken up in the model. As an influent air flow rate of zero would cause a numerical error because of division by zero in Eq. 3.62, the minimum air flow rate is limited to a very small but nonzero value ($10^{-10} \text{ m}^3 \text{ s}^{-1}$). A maximum air flow rate is also defined by the user, according to the maximum aeration capacity installed in the reactor under study.

The model further includes the possibility to simulate cyclic operation of the SHARON reactor, with alternating aerobic and anoxic phases. For instance, the SHARON reactor can be operated with alternating aerobic-anoxic periods in such a way that a fixed mean aerobic retention time is established for a varying influent flow rate and or reactor volume.

3.7.2 Acid and base addition

Acid or base addition is mimiced by adding negative resp. positive concentrations of the lumped component Z^+ , corresponding with the added volumes and given concentration of the added streams. The addition of these streams influences the reactor volume through the overall liquid phase balance Eq. 3.1, its dilution effect on the liquid phase concentrations is accounted for through the Eqs. 3.8-Eqs. 3.10. Note that the temperature effect of acid/base addition has been neglected in the liquid phase heat balance Eq. 3.13.

3.7.3 Liquid volume control

The SHARON reactor can be operated with constant (liquid) volume. In this case, the outgoing liquid flow rate is calculated from the ingoing flow rate and the liquid volume through the overall mass balance (Eq. 3.1). The SHARON reactor can also be operated with variable liquid volume, calculated through Eq. 3.1 from given in- and outgoing mass flow rates.

3.8 Model validation at the Sluisjesdijk SHARON reactor

The developed SHARON reactor model has been validated at the full-scale SHARON reactor ($V=1710 \text{ m}^3$; $H_L=5.5 \text{ m}$) at Sluisjesdijk (Rotterdam). Since mid-December 2004, this reactor has been operated without denitrification (no methanol addition) in view of its coupling with the Anammox reactor at the same site, which start-up phase is reaching its end.

3.8.1 Influent characteristics and reactor operation

For model validation, the period of 1 April - 31 August 2005 (153 days) has been selected, while the previous 60 days (1 February - 31 March 2005) served to initialize the model. No parameter adjustments have been made so the comparison of the model predictions with the actual data can be considered a true validation. Daily averaged on-line measurements for flow rate and ammonium concentrations, as well as weekly lab analyses (linearly interpolated to obtain daily values) for alkalinity, pH, BOD and total phosphorus were used. The influent inorganic carbon concentration has been calculated from the alkalinity measurement taking into account pH, as explained in Chapter 6. The influent COD concentration was reasonably assumed to be twice the measured total BOD content. However, as the SHARON reactor model considers CH_3OH as the only COD-source, the influent COD has been expressed as CH_3OH -equivalents. In this transformation, the lower biomass production associated with growth on CH_3OH ($Y_{X_{het}}^{CH_3OH} = 0.29 \text{ mole } X_{het} / \text{mole } CH_3OH = 0.20 \text{ gCOD } X_{het} / \text{gCOD } CH_3OH$) compared to 'regular' COD-sources (typically $Y_{X_{het}}^{SS} = 0.4 \text{ gCOD } X_{het} / \text{gCOD}$) has been compensated by adding heterotrophic biomass to the influent, in such a way that the overall oxygen consumption and biomass production remains the same and using influent TNH , TIC , TIP and Z^+ concentrations as compensation terms to close the balances (see Chapter 6). As temperature measurements in the SHARON reactor indicated a constant temperature of $\pm 35^\circ\text{C}$, the SHARON reactor model with constant temperature has been applied.

Figure 3.4 displays the profiles for the influent flow rate (mean $524 \text{ m}^3 \text{ d}^{-1}$), total ammonium concentration (mean¹ 86.7 mole m^{-3}), total inorganic carbon concentration (mean 98.9 mole m^{-3}), pH (mean 8.32),

¹given mean concentrations are all load-averaged values

TIC:TNH ratio (mean 1.16) as well as COD concentration (mean 281 gCOD m⁻³) translated into *CH₃OH* equivalents (mean 4.4 mole m⁻³). Note that in the simulations, all influent variables were kept constant for each day at their corresponding daily-mean value.

The liquid influent stream was assumed not to contain nitrite, nitrate, or oxygen. Its nitrogen concentration was set to 0.44 mole m⁻³, the equilibrium concentration with air for atmospheric pressure and 35°C. Further, a negligible amount of ammonium and nitrite oxidizers (0.01 mole m⁻³ each) has been included in the influent, to be able to simulate biomass re-growth following wash-out.

The SHARON reactor has been operated with alternating aerobic-anoxic periods in such a way that a mean aerobic retention time of 1.25 days is established, regardless of the influent flow rate. For this purpose, the reactor is operated in 2-hour cycles, where the aeration time per cycle is determined on the basis of the influent flow rate of the previous cycle and the (constant) reactor volume. The air flow rate has been controlled to meet an oxygen set point of 1.4 gO₂ m⁻³ during aerobic periods, while the maximum air flow rate amounts 6600 m³ h⁻¹, as in practice.

3.8.2 Simulation results

The simulation results are summarized in Figure 3.5. The simulated ammonium concentration in the reactor is lower (mean 27.5 mole m⁻³) than the measured ammonium concentration (mean 30.8 mole m⁻³). In the simulations, more nitrite is formed (mean 53.6 mole m⁻³) than the measurements indicate (mean 39.1 mole m⁻³). It is striking however that, although on average only 3.3 mole m⁻³ more ammonium is converted in the model than in reality, 14.5 mole m⁻³ more nitrite is formed. As a result, the predicted nitrite:ammonium ratio (mean 2.03) also deviates from the measured one (mean 1.29). Nitrate formation (results not shown) is negligible both in simulations (mean 0.2 mole m⁻³) and in reality (mean 0.7 mole m⁻³). Very little inorganic carbon remains in the reactor (mean 4.9 mole m⁻³ for simulations and 6.2 mole m⁻³ in reality, results not shown). The applied controllers showed a very good performance: the set-point for the aerobic retention time and the oxygen set point during aerobic periods were reached very well, although the simulated air flow rate that was needed to reach the oxygen set point (mean 5200 m³ d⁻¹) was higher than in reality (mean 3230 m³ d⁻¹) (results not shown).

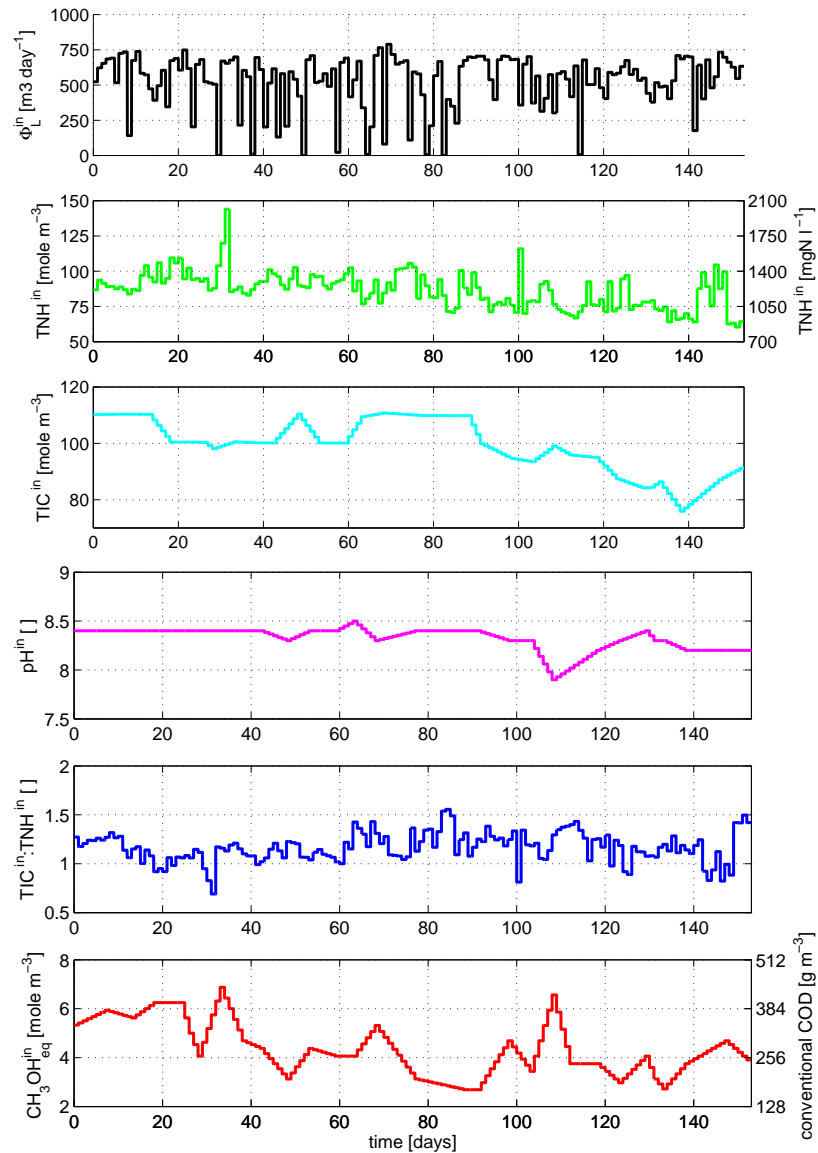


Figure 3.4: SHARON influent characteristics (from top to bottom): flow rate, total ammonium concentration (TNH), total inorganic carbon concentration (TIC), pH, bicarbonate:ammonium molar ratio ($TIC : TNH$) and influent COD translated into methanol equivalents (CH_3OH_{eq}).

The difference between the influent ammonium concentration and the sum of ammonium, nitrite and nitrate concentrations in the reac-

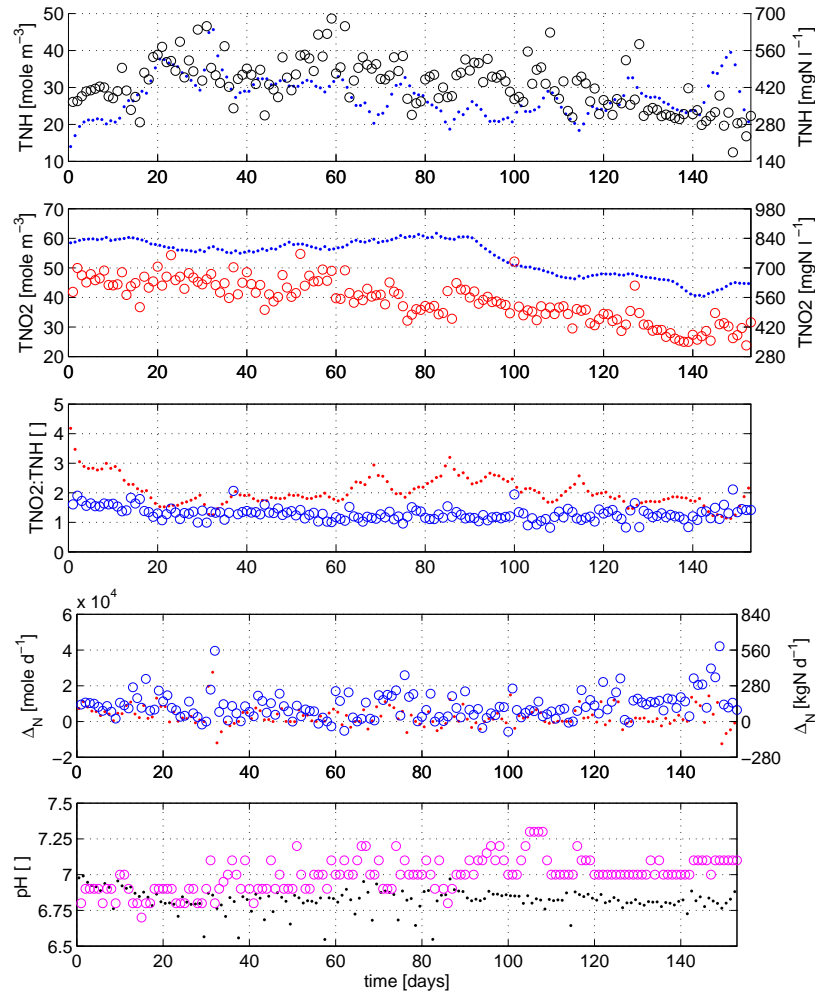


Figure 3.5: SHARON reactor daily mean characteristics (from top to bottom): total ammonium concentration (TNH), total nitrite concentration ($TNO2$), $TNO2 : TNH$ ratio, $\Delta_N = TNH^{in} - TNH - TNO2 - NO_3^-$, pH. Simulation results (●) versus on-site measurements (○).

tor, denote $\Delta_N = TNH^{in} - TNH - TNO2 - NO_3^-$, corresponds to the amount of N_2 formed during denitrification, at least during simulation. In reality, the difference could also be explained by NO_x and/or N_2O formation, taking into account the findings of Stüven and Bock (2001) that significant amounts of particularly NO_2 can be formed during combined nitrification/denitrification of sludge liquor. During simulation Δ_N amounted to, on average, 5.4 mole m^{-3} (or 2838 mole

d^{-1}), while measurements correspond with a mean value of 16.5 mole m^{-3} (or 8638 mole d^{-1}). The difference between these values corresponds with about 5800 mole d^{-1} of N_2 and possibly also some NO_x that is formed more in reality than is predicted by the simulations. Several *hypotheses* have been considered to explain this difference:

- *Significant formation of NO, NO₂ and/or N₂O.* Gas samples at different time instants during an aerobic/anoxic cycle have been analyzed, indicating $\text{NO} + \text{NO}_2$ formation of about 150 mole d^{-1} , and about the same amount of N_2O formation (Kampschreur and Van Der Star, personal communication). It is clear that formation of these gases does not explain the discrepancy between simulation and measurement results.
- *During simulation, not all influent COD has been converted.* This is not the case, since the mean CH_3OH concentration in the reactor amounts to 0.13 mole m^{-3} , which means that 97% of the influent COD has been converted.
- *In reality, the influent contains more COD than has been assumed during simulation.* Although the assumption that the influent COD concentration is twice the measured BOD content, seems quite reasonable, it should be kept in mind that this assumption has quite a strong effect: if the COD concentration would be 2.5 times the measured BOD content, this would result in an additional denitrification of about $700 \text{ mole NO}_2^- \text{ d}^{-1}$, but still about 8 times this amount is needed to close the gap. Note that the measured BOD is total BOD and in this way also includes biomass coming from the anaerobic digester, that decays in the SHARON reactor and subsequently can be used as a carbon source for denitrification.
- *During simulation, the part of the COD that is oxidized in the aerobic phase compared to the amount of COD that is used for denitrification of NO₂⁻ is too high.* Consumption of all influent COD during the anoxic phase would correspond with denitrification of $3483 \text{ mole NO}_2^- \text{ d}^{-1}$, while this is currently 2838 mole d^{-1} . This means that, according to the simulation results, 81% of the influent COD is used during denitrification, while 19% is oxidized in the aerobic phase (cfr. the reactor is operated under anoxic and aerobic conditions, 62% and 38% of time respectively). The fraction of COD

used for denitrification will increase e.g. for a decreasing maximum growth rate of methanol oxidizers (μ_{max}^{met}) and an increasing maximum growth rate of nitrite denitrifiers ($\mu_{max}^{dNO_2}$). But it is clear that, even if all influent COD would be used for denitrification, this could not explain the gap.

- *Denitrification on biomass decay products may explain the deviations.* Indeed, biomass decay is not included in the SHARON model. Given a simulated mean biomass concentration in the reactor of about 6 mole m^{-3} and assuming a rather high decay rate of 0.2 d^{-1} (value at 20°C Salem et al. 2006), this corresponds with denitrification of about $1500 \text{ mole NO}_2^- \text{ d}^{-1}$ in case 81% of the influent COD is used for denitrification.
- *The amount of NO_2^- that is denitrified per amount of COD consumed, as calculated by the model, is too low.* This is directly related to the biomass yield coefficient: as the biomass yield coefficient decreases, more NO_2^- is denitrified per unit of COD converted. For instance, whereas 1.51 mole NO_2^- is denitrified per mole of CH_3OH converted for the current value $Y_3 = 0.23 \frac{\text{mole } X_{het}}{\text{mole } \text{NO}_2^-}$, this would be 2 mole NO_2^- in case no biomass would be formed, which gives an idea of the sensitivity of the parameter Y_3 : if 1.75 mole NO_2^- is denitrified per mole of CH_3OH , this would result in additional denitrification of about $300 \text{ mole NO}_2^- \text{ d}^{-1}$.
- *The transformation of influent COD into methanol equivalents is not correct.* This transformation is based on the lower heterotrophic yield coefficient on 'regular' COD compared to methanol. If the difference is not as large as expected, the amount of methanol equivalents for the given influent COD content will be higher. The extreme case, with equal yield coefficients for 'regular' COD sources as for methanol, would yield 33.3% additional methanol equivalents. In case 81% of the influent COD is used for denitrification, this corresponds with additional denitrification of $940 \text{ mole NO}_2^- \text{ d}^{-1}$.
- *Some N_2 is produced by Anammox bacteria.* Although the biomass in the SHARON reactor grows in suspension, it is not unrealistic that Anammox bacteria are present in the biofilm attached to the reactor wall and bottom. Assuming a rather high Anammox conversion efficiency of about 7.5 gN d^{-1} , as detected by Wyffels

et al. (2003) in a rotating biological contactor (RBC), this means that about 360 mole d^{-1} nitrogen could be removed for the given reactor wall and bottom area of about 670 m^2 , which is a rather small amount.

- Finally, sample handling and/or measurement errors (e.g. of influent BOD) may also contribute to the differences between the simulation and measurement results.

The above statements clearly indicate how the current model can be improved, especially in terms of denitrification kinetics, to better predict the gaseous nitrogen losses. However, denitrification does not play a major role in the simulations described in this work, as the simulated SHARON reactor is not as much overdimensioned as the one at Sluisjesdijk and is aerated most of the time. As modelling denitrification is not so important for the simulation work described in this thesis, the current model was judged to sufficiently describe the reactor behaviour.

Regarding the higher ammonium conversion during simulation than in reality, this could be remedied by adjusting parameters that influence the ammonium conversion rate such as the maximum growth rate of ammonium oxidizers, their oxygen affinity constant, as well as their nitrous acid inhibition constant. For instance, when applying $K_{O_2}^{amm} = 1.45 \text{ g m}^{-3}$ (Lochtman, 1995) instead of $0.0294 \text{ mole m}^{-3} \approx 1 \text{ g m}^{-3}$ (Van Hulle et al., 2004), 28.4 mole m^{-3} ammonium on average remains unconverted. A further decrease of the ammonium conversion is expected when applying stronger nitrous acid inhibition: $K_{I,HNO_2}^{amm} = 0.0145 \text{ mole m}^{-3}$ (Lochtman, 1995) instead of 0.146 (Van Hulle et al., 2004). It is also possible that the amount of total inorganic carbon in the influent is overestimated during simulations, as a part of the measured alkalinity may consist of volatile fatty acids (VFAs). Although VFAs also possess a buffering capacity, their pK_e -values are lower (typically 4.8) than the one for the CO_2/HCO_3^- equilibrium (6.3), leading to an overestimation of the pH, in this way also enhancing ammonium conversion.

The higher ammonium conversion and probably lower amount of denitrification in the model compared to the simulations, is in correspondance with the lower simulated pH (mean 6.82) compared to the measured one (mean 7.0), although the difference can be considered to be within the pH measurement accuracy (the deviation between the two pH sensors in the tank amounts up to 0.2-0.3)

From the above reasoning, it is clear that, taking into account a combined effect of several of the above factors, it will be possible to calibrate the model by adapting microbial parameters in such a way that the simulation results reflect the measurements more closely. However, as the developed model is not intended for optimization of the specific SHARON reactor in Sluisjesdijk and as microbial characteristics are likely to vary from case to case, no calibration has been performed in this study.

3.9 Conclusions

In this chapter, the SHARON reactor model used for the simulations performed in this work, has been described. Both the liquid phase and the gas phase as well as interphase transport have been modelled. Special attention has been devoted to pH calculation. The resulting model has been validated at the full-scale SHARON reactor in Sluisjesdijk. Although the simulation results did not quantitatively reproduce the measurements, in particular concerning the denitrification process, the model was judged sufficiently accurate to qualitatively represent the behaviour of a realistic SHARON reactor for the given purposes.

Chapter 4

Existence, uniqueness and stability of equilibrium points of a SHARON reactor model for constant pH

This chapter has been based on:

Volcke E.I.P., Loccupier M., Vanrolleghem P.A. and Noldus E.J.L. (2006). Existence, uniqueness and stability of the equilibrium points of a SHARON bioreactor model. Submitted.

4.1 Introduction

In this chapter, the existence, uniqueness and stability of the equilibrium points of a SHARON bioreactor model are studied.

In the SHARON (Single reactor High activity Ammonium Removal Over Nitrite) process, ammonium is converted to nitrite while further conversion of nitrite to nitrate is prevented. This is realized by operating the reactor at a suitable dilution rate. At the prevailing pH (about 7) and high temperature (30-40°C), ammonium oxidizers grow faster than nitrite oxidizers. For this reason, it is possible to establish ammonium oxidation to nitrite only and prevent further oxidation of nitrite to nitrate by setting an appropriate dilution rate. In this way, substantial savings in aeration costs are realized, in comparison with oxidation of ammonium to nitrate. Additional savings can be made when the SHARON reactor is coupled with an Anammox process, in which am-

monium and nitrite are combined to form nitrogen gas. In order to obtain both a good conversion efficiency and to prevent inhibition of the Anammox process, the SHARON reactor must be operated in such a way that its effluent contains a nitrite:ammonium ratio of about 1:1.

The question rises whether the nitrite:ammonium ratio obtained in the SHARON process is unique and stable for constant input variables. For this reason, the existence, uniqueness and stability of the reactor's equilibrium points is addressed in this chapter.

In a first stage, operating regions in the input space for which there exists a unique equilibrium point are identified, as these often provide easy reactor operation. For this purpose, the contraction mapping theorem is used, resulting in a sufficient but not necessary criterion for the uniqueness of equilibrium points. The local asymptotic stability of the equilibrium point and the dynamic behaviour of the system in its neighbourhood are also examined.

The obtained results are verified in a second stage analysis by direct calculation of the SHARON reactor model's equilibrium points in a number of simplified cases. In particular, the effect of biological conversion kinetics on the number of equilibrium points and on their stability, is addressed. For the case of nitrite inhibition of ammonium conversion, as in the SHARON reactor model that has been used in chapters 5 and 8, the effect of slightly varying parameter and input values on the position of the equilibrium points, is also investigated. The analytically obtained results are verified by simulations. Phase trajectories illustrate the process behaviour.

4.2 Stability concepts

4.2.1 Definitions of stability

Consider a nonlinear, continuous-time and autonomous system with order n :

$$\dot{\mathbf{x}} = \mathbf{f}(\mathbf{x}) \quad (4.1)$$

$\mathbf{x} \in \mathbb{R}^{n \times 1}$ represents the system's state vector and \mathbf{f} a nonlinear function.

The solution of 4.1 for a given initial condition \mathbf{x}_0 at $t = 0$ is noted as $\mathbf{x}(t, \mathbf{x}_0)$ with $-\infty < t < +\infty$. Note that, in this work, only $0 < t < +\infty$ is considered.

Equilibrium points of the system 4.1 are state vectors \mathbf{x}_e that satisfy the equation

$$0 = \mathbf{f}(\mathbf{x}_e) \quad (4.2)$$

Stability An equilibrium point \mathbf{x}_e is *stable* if for every positive ϵ , there exists a positive $\delta(\epsilon)$, such that $|\mathbf{x}_0 - \mathbf{x}_e| < \delta$ implies that $|\mathbf{x}(t, \mathbf{x}_0) - \mathbf{x}_e| < \epsilon$, $\forall t > 0$

Local convergence An equilibrium point \mathbf{x}_e is *locally convergent* if there exists a positive δ_0 , such that $|\mathbf{x}_0 - \mathbf{x}_e| < \delta_0$ implies that $\mathbf{x}(t, \mathbf{x}_0) \rightarrow \mathbf{x}_e$ for $t \rightarrow +\infty$

Local asymptotic stability An equilibrium point is locally asymptotically stable if it is stable and locally convergent.

Global convergence An equilibrium point \mathbf{x}_e is *globally convergent* if every $\mathbf{x}(t, \mathbf{x}_0) \rightarrow \mathbf{x}_e$ for $t \rightarrow +\infty$

Global asymptotic stability An equilibrium point is globally asymptotically stable if it is stable and globally convergent.

4.2.2 Principle of contraction mappings

The uniqueness of equilibrium states can be investigated by means of the principle of contraction mappings, as formulated by Hale (1963):

Every contraction mapping \mathbf{g} defined in a complete metric space \mathbf{X} has one and only one fixed point in \mathbf{X} , that is, there is one and only one point in \mathbf{X} such that $\mathbf{x} = \mathbf{g}(\mathbf{x})$

The n -dimensional Euclidian space $\mathbb{R}^{n \times 1}$ is an example of a complete metric space.

A mapping \mathbf{g} of a metric space \mathbf{X} with distance ℓ into itself is called a *contraction mapping* if there exists a positive number $K < 1$ such that for all \mathbf{x}, \mathbf{w} in \mathbf{X} :

$$\ell[\mathbf{g}(\mathbf{x}), \mathbf{g}(\mathbf{w})] \leq K \cdot \ell(\mathbf{x}, \mathbf{w}) \quad (4.3)$$

The above theorem shows that one can find a *fixed point* of a mapping \mathbf{g} in \mathbf{X} if one shows that, for any \mathbf{x} in \mathbf{X} , $\mathbf{g}(\mathbf{x})$ is in \mathbf{X} and \mathbf{g} is a contraction mapping. The fixed point is obtained by the method of successive approximations

$$\mathbf{x}_{n+1} = \mathbf{g}(\mathbf{x}_n) \quad n = 0, 1, 2, \dots \quad (4.4)$$

where the starting value \mathbf{x}_0 is completely arbitrary.

4.2.3 Linearization principle

An equilibrium point \mathbf{x}_e of the system 4.1 is locally asymptotically stable if all eigenvalues of the Jacobian matrix

$$\left. \frac{\partial \mathbf{f}(\mathbf{x})}{\partial \mathbf{x}} \right|_{\mathbf{x}=\mathbf{x}_e} \triangleq \begin{bmatrix} \left. \frac{\partial f_1}{\partial x_1} \right|_{\mathbf{x}=\mathbf{x}_e} & \cdots & \left. \frac{\partial f_1}{\partial x_n} \right|_{\mathbf{x}=\mathbf{x}_e} \\ \vdots & & \vdots \\ \left. \frac{\partial f_n}{\partial x_1} \right|_{\mathbf{x}=\mathbf{x}_e} & \cdots & \left. \frac{\partial f_n}{\partial x_n} \right|_{\mathbf{x}=\mathbf{x}_e} \end{bmatrix} \quad (4.5)$$

are in the open left phase plane, i.e. have strictly negative real parts.

The linearization principle provides a necessary and sufficient condition for local asymptotic stability in case there are no eigenvalues on the imaginary axis, i.e. of which the real part is equal to zero. Such an equilibrium point is said to be *hyperbolic*.

The *index* of a hyperbolic equilibrium point is the number of unstable eigenvalues (with strictly positive real parts) of the Jacobian matrix 4.5.

4.3 The SHARON reactor model for constant pH

In this chapter, a simplified SHARON reactor model is used to investigate the applicability of the theoretical criteria. To the model described in chapter 3, the following additional, realistic assumptions are made:

- The SHARON reactor is controlled at a constant pH.
- The SHARON reactor is continuously aerated and oxygen is always present in excess.
- The reactor temperature is constant (at 35°C).
- The reactor liquid volume is constant

The resulting model only considers the two nitrification reactions. Only mass balances for total ammonium (TNH), total nitrite (TNO_2),

ammonium oxidizers (X_{amm}) and nitrite oxidizers (X_{nit}), of which the concentrations are identified as the system's states, are retained:

$$\dot{x}_1 = u_0 \cdot (u_1 - x_1) - a \cdot \rho_1 - b \cdot \rho_2 \triangleq f_1(\mathbf{x}) \quad (4.6)$$

$$\dot{x}_2 = u_0 \cdot (u_2 - x_2) + c \cdot \rho_1 - d \cdot \rho_2 \triangleq f_2(\mathbf{x}) \quad (4.7)$$

$$\dot{x}_3 = u_0 \cdot (u_3 - x_3) + \rho_1 \triangleq f_3(\mathbf{x}) \quad (4.8)$$

$$\dot{x}_4 = u_0 \cdot (u_4 - x_4) + \rho_2 \triangleq f_4(\mathbf{x}) \quad (4.9)$$

in which

$$\mathbf{u}^* \triangleq \begin{bmatrix} u_0 \\ u_1 \\ u_2 \\ u_3 \\ u_4 \end{bmatrix} \triangleq \begin{bmatrix} \frac{\Phi_{in}(t)}{V} \\ C_{TNH}^{in}(t) \\ C_{TNO_2}^{in}(t) \\ C_{X_{amm}}^{in}(t) \\ C_{X_{nit}}^{in}(t) \end{bmatrix} ; \quad \mathbf{x} \triangleq \begin{bmatrix} x_1 \\ x_2 \\ x_3 \\ x_4 \end{bmatrix} \triangleq \begin{bmatrix} C_{TNH}(t) \\ C_{TNO_2}(t) \\ C_{X_{amm}}(t) \\ C_{X_{nit}}(t) \end{bmatrix} \quad (4.10)$$

with

$$u_0(t), u_1(t) \geq 0 ; \quad u_2 = 0 ; \quad u_3, u_4 \text{ constant} ; \quad x_i(t) \geq 0 \quad \forall i \quad (4.11)$$

and

$$a = \frac{1}{Y_1} > 0 \quad b = n > 0 \quad c = \left(\frac{1}{Y_1} - n \right) > 0 \quad d = \frac{1}{Y_2} > 0 \quad (4.12)$$

Note that the process inputs are defined generally, also taking into account constant and zero inputs. The reaction rates for ammonium oxidation and nitrite oxidation respectively are written as

$$\rho_1 = a_1 \cdot \frac{x_1}{b_1 + x_1} \cdot \frac{c_1}{c_1 + x_2} \cdot x_3 \quad (4.13)$$

$$\rho_2 = a_2 \cdot \frac{x_2}{b_2 + x_2} \cdot \frac{x_1}{c_2 + x_1} \cdot \frac{d_2}{d_2 + x_2} \cdot \frac{e_2}{e_2 + x_1} \cdot x_4 \quad (4.14)$$

with

$$\begin{aligned} a_1 &\triangleq \mu_{max}^{amm} > 0 & b_1 &\triangleq K_{TNH}^{amm} > 0 & c_1 &\triangleq K_{I,TNO_2}^{amm} > 0 \\ a_2 &\triangleq \mu_{max}^{nit} > 0 & b_2 &\triangleq K_{TNO_2}^{nit} > 0 & c_2 &\triangleq K_{TNH}^{nit} > 0 \\ d_2 &\triangleq K_{I,TNO_2}^{nit} > 0 & e_2 &\triangleq K_{I,TNH}^{nit} > 0 \end{aligned} \quad (4.15)$$

Eq. 4.13 expresses that ammonium oxidation is inhibited by nitrous acid but not by ammonia, in accordance with the findings of Van Hulle

et al. (2004). For nitrite oxidation, a general expression for inhibition of both ammonia and nitrous acid is used in Eq. 4.14. Although no inhibition of nitrite oxidation was considered in the model of chapter 3, these terms were taken up here in order to obtain more general results. In case a certain component is not inhibiting, the corresponding inhibition constant will have a high value.

Typical ranges for input variables and parameter values at pH 7 and $T=35^\circ$ are summarized in Table 4.1

Table 4.1: Parameter values at pH 7 and input ranges

symbol	value	unit	
a_1	μ_{max}^{amm}	2.1	day^{-1}
b_1	K_{TNH}^{amm}	4.73	mole m^{-3}
c_1	K_{I,TNO_2}^{amm}	837	mole m^{-3}
a_2	μ_{max}^{nit}	1.05	day^{-1}
b_2	$K_{TNO_2}^{nit}$	109	mole m^{-3}
c_2	K_{TNH}^{nit}	0.01	mole m^{-3}
d_2	K_{I,TNO_2}^{nit}	1000	mole m^{-3}
e_2	$K_{I,TNH}^{nit}$	1000	mole m^{-3}
a	$\frac{1}{Y_1}$	16	mole mole^{-1}
b	n	0.2	mole mole^{-1}
c	$\left(\frac{1}{Y_1} - n\right)$	15.8	mole mole^{-1}
d	$\frac{1}{Y_2}$	58.6	mole mole^{-1}
u_0	$\frac{\Phi_{in}(t)}{V}$	0.25 \rightarrow 2.5	day^{-1}
u_1	TNH_{in}	0 \rightarrow 140	mole m^{-3}

The state equations 4.6-4.9 are summarized in the following matrix form:

$$\dot{\mathbf{x}} = (\mathbf{u} - \mathbf{x}) \cdot u_0 + \mathbf{M} \cdot \rho(\mathbf{x}) \triangleq \mathbf{f}(\mathbf{x}) \quad (4.16)$$

with

$$\mathbf{u} \triangleq \begin{bmatrix} u_1 \\ u_2 \\ u_3 \\ u_4 \end{bmatrix}; \mathbf{M} \triangleq \begin{bmatrix} -a & -b \\ c & -d \\ 1 & 0 \\ 0 & 1 \end{bmatrix}; \rho(\mathbf{x}) \triangleq \begin{bmatrix} \rho_1(\mathbf{x}) \\ \rho_2(\mathbf{x}) \end{bmatrix} \quad (4.17)$$

The model 4.16 is nonlinear, because of the product $(\mathbf{u} - \mathbf{x}) \cdot u_0$ and as the vector of specific growth rates $\rho(\mathbf{x})$ is a nonlinear function of the state variables. The question addressed in this chapter is whether the nitrite:ammonium ratio obtained in the SHARON process is unique and stable for constant input variables, being the dilution rate (u_0) and influent concentrations of (total) ammonium (u_1), (total) nitrite ($u_2 = 0$), ammonium oxidizing biomass (u_3) and nitrite oxidizing biomass (u_4). Note that for constant state values x_i , the nitrite:ammonium $x_2:x_1$ ratio in the SHARON effluent is also constant. For this reason, the subsequent analysis focuses on the existence, uniqueness and stability of the equilibrium states.

4.4 Equilibrium conditions

4.4.1 Equilibrium form of the SHARON reactor model

The equilibrium states x_{ei} of the SHARON reactor model, corresponding with constant input values u_i , satisfy Eq. 4.16 or the Eqs. 4.6-4.9 in which $\dot{x}_i = 0$:

$$0 = (\mathbf{u} - \mathbf{x}_e) \cdot u_0 + \mathbf{M} \cdot \rho(\mathbf{x}_e) \triangleq \mathbf{f}(\mathbf{x}_e) \quad (4.18)$$

or

$$0 = u_0 \cdot (u_1 - x_{e1}) - a \cdot \rho_1(\mathbf{x}_e) - b \cdot \rho_2(\mathbf{x}_e) \quad (4.19)$$

$$0 = u_0 \cdot (u_2 - x_{e2}) + c \cdot \rho_1(\mathbf{x}_e) - d \cdot \rho_2(\mathbf{x}_e) \quad (4.20)$$

$$0 = u_0 \cdot (u_3 - x_{e3}) + \rho_1(\mathbf{x}_e) \quad (4.21)$$

$$0 = u_0 \cdot (u_4 - x_{e4}) + \rho_2(\mathbf{x}_e) \quad (4.22)$$

A distinction is made between the case in which $u_0 = 0$ and the case in which $u_0 \neq 0$.

4.4.2 Equilibrium points in case $u_0 = 0$

If $u_0 = 0$, the equilibrium points can easily be calculated directly from Eqs. 4.19-4.22:

$$\dot{\mathbf{x}} = 0 \Leftrightarrow \rho_1(\mathbf{x}_e) = \rho_2(\mathbf{x}_e) = 0 \Leftrightarrow x_{e1} \cdot x_{e3} = x_{e1} \cdot x_{e2} \cdot x_{e4} = 0$$

This condition is fulfilled in each of the following cases:

- $x_{e1} = 0$; x_{e2}, x_{e3}, x_{e4} arbitrary
- $x_{e2} = x_{e3} = 0$; x_{e1}, x_{e4} arbitrary
- $x_{e3} = x_{e4} = 0$; x_{e1}, x_{e2} arbitrary

So in case $u_0 = 0$, there are a number $\infty^3 + 2 \cdot \infty^2$ equilibrium solutions.

4.4.3 Equilibrium points in case $u_0 > 0$

In case $u_0 \neq 0$, the equilibrium points cannot easily be calculated directly. In the next section, the contraction mapping theorem is used to determine the region(s) in the input space where there exists a unique equilibrium point in this case.

However, for an infinitely high dilution rate, Eqs. 4.19-4.22 show that there is a unique equilibrium point, corresponding with the influent conditions:

$$u_0 \rightarrow \infty \Rightarrow \begin{cases} x_{e1} \rightarrow u_1 \\ x_{e2} \rightarrow u_2 \\ x_{e3} \rightarrow u_3 \\ x_{e4} \rightarrow u_4 \end{cases} \quad (4.23)$$

Note the contrast with the case $u_0 = 0$ (section 4.4.2), where the model possesses three infinite families of equilibrium points.

4.5 Uniqueness of equilibrium points for $u_0 \neq 0$; The contraction mapping theorem

4.5.1 Application of the contraction mapping theorem to the 4-dimensional model

Principle

Assuming $u_0 \neq 0$, Eqs. 4.19-4.22 can be rewritten as:

$$x_{e1} = u_1 - \frac{1}{u_0} \cdot [a \cdot \rho_1(\mathbf{x}_e) + b \cdot \rho_2(\mathbf{x}_e)] \triangleq \varphi_1(\mathbf{x}_e) \quad (4.24)$$

$$x_{e2} = u_2 + \frac{1}{u_0} \cdot [c \cdot \rho_1(\mathbf{x}_e) - d \cdot \rho_2(\mathbf{x}_e)] \triangleq \varphi_2(\mathbf{x}_e) \quad (4.25)$$

$$x_{e3} = u_3 + \frac{1}{u_0} \cdot \rho_1(\mathbf{x}_e) \triangleq \varphi_3(\mathbf{x}_e) \quad (4.26)$$

$$x_{e4} = u_4 + \frac{1}{u_0} \cdot \rho_2(\mathbf{x}_e) \triangleq \varphi_4(\mathbf{x}_e) \quad (4.27)$$

and are summarized in the following matrix equation:

$$\mathbf{x}_e = \mathbf{u} + \frac{1}{u_0} \cdot \mathbf{M} \cdot \rho(\mathbf{x}_e) \triangleq \varphi(\mathbf{x}_e) \quad (4.28)$$

with

$$\varphi(\mathbf{x}) \triangleq \begin{bmatrix} \varphi_1(\mathbf{x}) \\ \varphi_2(\mathbf{x}) \\ \varphi_3(\mathbf{x}) \\ \varphi_4(\mathbf{x}) \end{bmatrix} \quad (4.29)$$

Define a mapping

$$\mathbb{R}^{4 \times 1} \mapsto \mathbb{R}^{4 \times 1} : \mathbf{y} = \varphi(\mathbf{x}) \quad (4.30)$$

Define the Euclidian norm as distance in $\mathbb{R}^{4 \times 1}$ (Euclidian space):

$$\ell(\mathbf{x}, \mathbf{w}) \triangleq |\mathbf{x} - \mathbf{w}| = \sqrt{\sum_{i=1}^4 (x_i - w_i)^2} \quad (4.31)$$

If the mapping φ possesses a point \mathbf{x}_e for which

$$\mathbf{x}_e = \varphi(\mathbf{x}_e) \quad (4.32)$$

then \mathbf{x}_e is an equilibrium point of this system.

Moreover, if one can show that the mapping φ is a *contraction mapping* according to Eq. 4.3, then this mapping possesses a *unique* fixed point (Eq. 4.32), i.e. a unique equilibrium point for the SHARON reactor. The value of this unique equilibrium point can subsequently be determined through Eq. 4.4. This procedure is followed in the following paragraphs.

Finding a contraction mapping - condition for a unique equilibrium point

From Eq. 4.28, the following relationship for the distances between two arbitrary elements \mathbf{x} and \mathbf{w} in $\mathbb{R}^{4 \times 1}$ results:

$$\ell^2 [\varphi(\mathbf{x}), \varphi(\mathbf{w})] = \frac{1}{u_0^2} \cdot [\rho(\mathbf{x}) - \rho(\mathbf{w})]^T \mathbf{M}^T \mathbf{M} [\rho(\mathbf{x}) - \rho(\mathbf{w})] \quad (4.33)$$

The largest eigenvalue of the real-symmetric matrix $\mathbf{M}^T \mathbf{M}$ is determined as

$$s_0 = \frac{(\alpha + \beta) + \sqrt{(\alpha - \beta)^2 + 4 \cdot \gamma^2}}{2} \quad (4.34)$$

with

$$\alpha \triangleq a^2 + c^2 + 1 \quad (4.35)$$

$$\beta \triangleq b^2 + d^2 + 1 \quad (4.36)$$

$$\gamma \triangleq a \cdot b - c \cdot d \quad (4.37)$$

For a real-symmetric matrix $\mathbf{A} \in \mathbb{R}^{n \times n}$ with largest eigenvalue λ_{max} , the following relationship holds for every vector $\mathbf{x} \in \mathbb{R}^{n \times 1}$:

$$\mathbf{x}^T \mathbf{A} \mathbf{x} \leq \lambda_{max} \cdot \mathbf{x}^T \mathbf{x} \quad (4.38)$$

Applying the relationship 4.38 to the real-symmetric matrix $\mathbf{M}^T \mathbf{M}$ with largest eigenvalue s_0 , Eq. 4.33 is rewritten as

$$\ell^2 [\varphi(\mathbf{x}), \varphi(\mathbf{w})] \leq \frac{s_0}{u_0^2} \cdot [\rho(\mathbf{x}) - \rho(\mathbf{w})]^T [\rho(\mathbf{x}) - \rho(\mathbf{w})] \quad (4.39)$$

According to the mean value theorem, there exist vectors $\tilde{\mathbf{x}}_{ij}$ in the hyperrectangle with opposite corners \mathbf{x} and \mathbf{w} for which

$$\rho(\mathbf{x}) = \rho(\mathbf{w}) + \mathbf{J} (\mathbf{x} - \mathbf{w}) \quad (4.40)$$

with

$$\mathbf{J} = \begin{bmatrix} \left. \frac{\partial \rho_1}{\partial x_1} \right|_{\mathbf{x}=\tilde{\mathbf{x}}_{11}} & \left. \frac{\partial \rho_1}{\partial x_2} \right|_{\mathbf{x}=\tilde{\mathbf{x}}_{12}} & \left. \frac{\partial \rho_1}{\partial x_3} \right|_{\mathbf{x}=\tilde{\mathbf{x}}_{13}} & \left. \frac{\partial \rho_1}{\partial x_4} \right|_{\mathbf{x}=\tilde{\mathbf{x}}_{14}} \\ \left. \frac{\partial \rho_2}{\partial x_1} \right|_{\mathbf{x}=\tilde{\mathbf{x}}_{21}} & \left. \frac{\partial \rho_2}{\partial x_2} \right|_{\mathbf{x}=\tilde{\mathbf{x}}_{22}} & \left. \frac{\partial \rho_2}{\partial x_3} \right|_{\mathbf{x}=\tilde{\mathbf{x}}_{23}} & \left. \frac{\partial \rho_2}{\partial x_4} \right|_{\mathbf{x}=\tilde{\mathbf{x}}_{24}} \end{bmatrix} \\ \triangleq \begin{bmatrix} \delta_1 & \delta_2 & \delta_3 & 0 \\ \delta_5 & \delta_6 & 0 & \delta_8 \end{bmatrix} \quad (4.41)$$

Consequently, one can write

$$[\rho(\mathbf{x}) - \rho(\mathbf{w})]^T [\rho(\mathbf{x}) - \rho(\mathbf{w})] = [\mathbf{x} - \mathbf{w}]^T \mathbf{J}^T \mathbf{J} [\mathbf{x} - \mathbf{w}] \quad (4.42)$$

Substitution of Eq. 4.42 in Eq. 4.39 yields

$$\ell^2 [\varphi(\mathbf{x}), \varphi(\mathbf{w})] \leq \frac{s_0}{u_0^2} \cdot [\mathbf{x} - \mathbf{w}]^T \mathbf{J}^T \mathbf{J} [\mathbf{x} - \mathbf{w}] \quad (4.43)$$

The largest eigenvalue of the real-symmetric matrix $\mathbf{J}^T \mathbf{J}$ is found as

$$s_1 = \frac{(\mu + \nu) + \sqrt{(\mu - \nu)^2 + 4 \cdot \xi^2}}{2} \quad (4.44)$$

with

$$\mu \triangleq \delta_1^2 + \delta_2^2 + \delta_3^2 \quad (4.45)$$

$$\nu \triangleq \delta_5^2 + \delta_6^2 + \delta_8^2 \quad (4.46)$$

$$\xi \triangleq \delta_1 \cdot \delta_5 + \delta_2 \cdot \delta_6 \quad (4.47)$$

Applying the relationship 4.38 to the real-symmetric matrix $\mathbf{J}^T \mathbf{J}$ with largest eigenvalue s_1 and taking into account the definition of distance (Eq. 4.31), Eq. 4.43 is rewritten as

$$\ell^2 [\varphi(\mathbf{x}), \varphi(\mathbf{w})] \leq \frac{s_0 \cdot s_1}{u_0^2} \cdot \ell^2 [\mathbf{x}, \mathbf{w}] \quad (4.48)$$

As the relation 4.48 holds for all \mathbf{x}, \mathbf{w} in $\mathbb{R}^{4 \times 1}$, the mapping φ is a *contraction mapping* according to the definition (Eq. 4.3) if

$$\frac{s_0 \cdot s_1}{u_0^2} < 1 \quad \Leftrightarrow \quad u_0 > \sqrt{s_0 \cdot s_1} \quad (4.49)$$

Under this condition that is sufficient but not necessary, the mapping φ possesses a unique fixed point that is a unique equilibrium point for the SHARON reactor.

Upper boundaries for the partial derivatives of the reaction rates to the state variables

In order to evaluate the condition 4.49 for a unique equilibrium, s_0 and s_1 must be known. While the calculation of s_0 is straightforward, the calculation of s_1 is more complicated since the values of μ , ν and ξ depend on the values of δ_i^2 and thus on the absolute values of the partial derivatives $\frac{\partial \rho_i}{\partial x_j}$, evaluated in the unknown \hat{x}_{ij} (see Eq. 4.41).

It is however possible to define maximum absolute values for the partial derivatives (so there is no need to know the exact values of \hat{x}_{ij}) and in this way also maximum values for μ , ν and ξ :

$$\begin{aligned} \left| \frac{\partial \rho_1}{\partial x_1} \right| &= \left| a_1 \cdot \frac{b_1}{(b_1 + x_1)^2} \cdot \frac{c_1}{c_1 + x_2} \cdot x_3 \right| \\ &\leq \frac{a_1}{b_1} \cdot x_{3,max} = |\delta_1|_{max} \end{aligned} \quad (4.50)$$

$$\begin{aligned} \left| \frac{\partial \rho_1}{\partial x_2} \right| &= \left| a_1 \cdot \frac{x_1}{b_1 + x_1} \cdot \frac{-c_1}{(c_1 + x_2)^2} \cdot x_3 \right| \\ &\leq \frac{a_1}{c_1} \cdot \frac{x_{1,max}}{b_1 + x_{1,max}} \cdot x_{3,max} \triangleq \frac{\hat{a}_1}{c_1} \cdot x_{3,max} = |\delta_2|_{max} \end{aligned} \quad (4.51)$$

$$\begin{aligned} \left| \frac{\partial \rho_1}{\partial x_3} \right| &= \left| a_1 \cdot \frac{x_1}{b_1 + x_1} \cdot \frac{c_1}{c_1 + x_2} \right| \\ &\leq a_1 \cdot \frac{x_{1,max}}{b_1 + x_{1,max}} \triangleq \hat{a}_1 = |\delta_3|_{max} \end{aligned} \quad (4.52)$$

$$\begin{aligned} \left| \frac{\partial \rho_2}{\partial x_1} \right| &= \left| a_2 \cdot \frac{x_2}{(b_2 + x_2)} \cdot \frac{d_2}{(d_2 + x_2)} \cdot \frac{e_2 \cdot (c_2 \cdot e_2 - x_1^2)}{(c_2 + x_1)^2 \cdot (e_2 + x_1)^2} \cdot x_4 \right| \\ &\leq \frac{a_2}{c_2} \cdot m_2 \cdot x_{4,max} = |\delta_5|_{max} \end{aligned} \quad (4.53)$$

$$\begin{aligned} \left| \frac{\partial \rho_2}{\partial x_2} \right| &= \left| a_2 \cdot \frac{x_1}{(c_2 + x_1)} \cdot \frac{e_2}{(e_2 + x_1)} \cdot \frac{d_2 \cdot (b_2 \cdot d_2 - x_2^2)}{(b_2 + x_2)^2 \cdot (d_2 + x_2)^2} \cdot x_4 \right| \\ &\leq \frac{a_2}{b_2} \cdot m_1 \cdot x_{4,max} = |\delta_6|_{max} \end{aligned} \quad (4.54)$$

$$\begin{aligned} \left| \frac{\partial \rho_2}{\partial x_4} \right| &= \left| a_2 \cdot \frac{x_1}{(c_2 + x_1)} \cdot \frac{e_2}{(e_2 + x_1)} \cdot \frac{x_2}{(b_2 + x_2)} \cdot \frac{d_2}{(d_2 + x_2)} \right| \\ &\leq a_2 \cdot m_1 \cdot m_2 = |\delta_8|_{max} \end{aligned} \quad (4.55)$$

with

$$\begin{aligned}
 m_1 &\triangleq \max \left\{ \frac{x_1}{(c_2 + x_1)} \cdot \frac{e_2}{(e_2 + x_1)} \right\} \\
 &= \begin{cases} \frac{e_2}{(\sqrt{c_2} + \sqrt{e_2})^2} & \text{if } x_{1,max} > \sqrt{c_2 \cdot e_2} \\ \frac{x_{1,max}}{c_2 + x_{1,max}} \cdot \frac{e_2}{e_2 + x_{1,max}} & \text{if } x_{1,max} < \sqrt{c_2 \cdot e_2} \end{cases} \quad (4.56)
 \end{aligned}$$

$$\begin{aligned}
 m_2 &\triangleq \max \left\{ \frac{x_2}{(b_2 + x_2)} \cdot \frac{d_2}{(d_2 + x_2)} \right\} \\
 &= \begin{cases} \frac{d_2}{(\sqrt{b_2} + \sqrt{d_2})^2} & \text{if } x_{2,max} > \sqrt{b_2 \cdot d_2} \\ \frac{x_{2,max}}{b_2 + x_{2,max}} \cdot \frac{d_2}{d_2 + x_{2,max}} & \text{if } x_{2,max} < \sqrt{b_2 \cdot d_2} \end{cases} \quad (4.57)
 \end{aligned}$$

After substitution of the Eqs. 4.50-4.55, the equilibrium uniqueness condition Eq. 4.49 becomes independent of \tilde{x}_{ij} . Still, values for $x_{1,max}$, $x_{3,max}$ and $x_{4,max}$ must be known before the resulting equilibrium condition can be evaluated. For the upper boundaries for x_3 and x_4 , one can use either the maximum values under dynamic conditions, determined in appendix C.1, or the values for equilibrium conditions, determined in appendix C.2, since the condition 4.32 with φ a contraction mapping is an equilibrium condition. An evident choice is to choose the lowest value for the upper boundary of each state variable, so the resulting equilibrium condition is the least stringent:

$$x_{1,max} = u_1 \quad (4.58)$$

$$x_{3,max} = \begin{cases} \min \left\{ \frac{u_0 \cdot u_3}{u_0 - \hat{a}_1}, u_3 + \frac{u_1}{a} \right\} & \text{if } u_0 > \hat{a}_1 \\ u_3 + \frac{u_1}{a} & \text{if } u_0 \leq \hat{a}_1 \end{cases} \quad (4.59)$$

$$x_{2,max} = \min \left\{ u_2 + \frac{c}{u_0} \cdot \hat{a}_1 \cdot x_{3,max}, u_2 + \frac{c}{a} \cdot u_1 \right\} \quad (4.60)$$

$$x_{4,max} = \begin{cases} \min \left\{ \frac{u_0 \cdot u_4}{u_0 - a_2 \cdot m_1 \cdot m_2}, u_4 + \frac{c \cdot u_1 + a \cdot u_2}{a \cdot d + b \cdot c} \right\} & \text{if } u_0 > a_2 \cdot m_1 \cdot m_2 \\ u_4 + \frac{c \cdot u_1 + a \cdot u_2}{a \cdot d + b \cdot c} & \text{if } u_0 \leq a_2 \cdot m_1 \cdot m_2 \end{cases} \quad (4.61)$$

in which m_2 is determined through (4.57) using the value of $x_{2,max}$ given by (4.60).

The condition 4.49 for a unique equilibrium, can now be evaluated and results in a sufficient, but not necessary criterion for the existence of a unique equilibrium point.

4.5.2 Application of the contraction mapping theorem to a reduced 2-dimensional static model

In section 4.5.1, the application of the contraction mapping theorem to the 4-dimensional SHARON reactor model has resulted in a criterion that assures the existence of a unique equilibrium point. However, the resulting criterion gives a sufficient but not necessary condition, as upper boundaries have been estimated for several variables. The question arises whether it would be possible to determine a less restrictive criterion for the existence of a unique equilibrium point by applying the contraction mapping on a reduced reactor model. In this section, a reduced 2-dimensional model, valid under equilibrium conditions, is set up and an alternative criterion for the existence of a unique equilibrium point is deduced. Both criteria will be compared in section 4.5.3.

Principle

In case $u_0 \neq 0$, the equilibrium concentrations of ammonium oxidizers (x_{e3}) and nitrite oxidizers (x_{e4}) can be written in terms of the equilibrium concentrations of ammonium (x_{e1}) and nitrite (x_{e2}). This is achieved by calculating the reaction terms $\rho_1(\mathbf{x}_e)$ and $\rho_2(\mathbf{x}_e)$ from Eqs. 4.21 and 4.22 respectively, subsequent substitution in Eqs. 4.19 and 4.20 and solving the obtained equations for x_{e3} and x_{e4} :

$$x_{e3} = u_3 + \frac{1}{a \cdot d + b \cdot c} \cdot [d \cdot (u_1 - x_{e1}) - b \cdot (u_2 - x_{e2})] \quad (4.62)$$

$$x_{e4} = u_4 + \frac{1}{a \cdot d + b \cdot c} \cdot [c \cdot (u_1 - x_{e1}) + a \cdot (u_2 - x_{e2})] \quad (4.63)$$

Define

$$\mathbf{y} \triangleq \begin{bmatrix} x_1 \\ x_2 \end{bmatrix}; \quad \mathbf{w} \triangleq \begin{bmatrix} u_1 \\ u_2 \end{bmatrix} \quad (4.64)$$

Taking into account 4.62 and 4.63 the reaction rates under equilibrium conditions can also be written in terms of x_{e1} and x_{e2} and are denoted

as $\hat{\rho}_i(\mathbf{y}_e)$:

$$\hat{\rho}_1(\mathbf{y}_e) = a_1 \cdot \frac{x_{e1}}{b_1 + x_{e1}} \cdot \frac{c_1}{c_1 + x_{e2}} \cdot \left[u_3 + \frac{d \cdot (u_1 - x_{e1}) - b \cdot (u_2 - x_{e2})}{a \cdot d + b \cdot c} \right] \quad (4.65)$$

$$\hat{\rho}_2(\mathbf{y}_e) = a_2 \cdot \frac{x_{e2}}{b_2 + x_{e2}} \cdot \frac{x_{e1}}{c_2 + x_{e1}} \cdot \frac{d_2}{d_2 + x_{e2}} \cdot \frac{e_2}{e_2 + x_{e1}} \cdot \left[u_4 + \frac{c \cdot (u_1 - x_{e1}) + a \cdot (u_2 - x_{e2})}{a \cdot d + b \cdot c} \right] \quad (4.66)$$

The equilibrium equations 4.24 and 4.25 are now rewritten as

$$x_{e1} = u_1 - \frac{1}{u_0} \cdot [a \cdot \hat{\rho}_1(\mathbf{y}_e) + b \cdot \hat{\rho}_2(\mathbf{y}_e)] \triangleq \hat{\varphi}_1(\mathbf{y}_e) \quad (4.67)$$

$$x_{e2} = u_2 + \frac{1}{u_0} \cdot [c \cdot \hat{\rho}_1(\mathbf{y}_e) - d \cdot \hat{\rho}_2(\mathbf{y}_e)] \triangleq \hat{\varphi}_2(\mathbf{y}_e) \quad (4.68)$$

and are summarized in the following matrix equation:

$$\mathbf{y}_e = \mathbf{w} + \frac{1}{u_0} \cdot \hat{\mathbf{M}} \hat{\rho}(\mathbf{y}_e) \triangleq \hat{\varphi}(\mathbf{y}_e) \quad (4.69)$$

in which

$$\hat{\varphi}(\mathbf{y}_e) \triangleq \begin{bmatrix} \hat{\varphi}_1(\mathbf{y}_e) \\ \hat{\varphi}_2(\mathbf{y}_e) \end{bmatrix}; \quad \hat{\mathbf{M}} \triangleq \begin{bmatrix} -a & -b \\ c & -d \end{bmatrix}; \quad \hat{\rho}(\mathbf{y}_e) \triangleq \begin{bmatrix} \rho_1(\mathbf{y}_e) \\ \rho_2(\mathbf{y}_e) \end{bmatrix} \quad (4.70)$$

Every fixed point of the mapping

$$\mathbf{y}_e = \hat{\varphi}(\mathbf{y}_e) \quad (4.71)$$

is an equilibrium point of the system. If the mapping $\hat{\varphi}$ is a *contraction mapping* according to Eq. 4.3, the unique fixed point of the mapping is a unique equilibrium point for the SHARON reactor and its value can subsequently be determined through Eq. 4.4. This procedure is followed in the following paragraphs.

Finding a contraction mapping - condition for a unique equilibrium point

Define the Euclidian norm as a distance in $\mathbb{R}^{2 \times 1}$:

$$\ell(\mathbf{y}, \mathbf{z}) \triangleq |\mathbf{y} - \mathbf{z}| = \sqrt{\sum_{i=1}^2 (y_i - z_i)^2} \quad (4.72)$$

From Eq. 4.69, the following relationship for the distances between two arbitrary elements \mathbf{y} and \mathbf{z} in $\mathbb{R}^{2 \times 1}$ results:

$$\ell^2 [\hat{\varphi}(\mathbf{y}_e), \hat{\varphi}(\mathbf{z}_e)] = \frac{1}{u_0^2} \cdot [\hat{\rho}(\mathbf{y}_e) - \hat{\rho}(\mathbf{z}_e)]^T \hat{\mathbf{M}}^T \hat{\mathbf{M}} [\hat{\rho}(\mathbf{y}_e) - \hat{\rho}(\mathbf{z}_e)] \quad (4.73)$$

The largest eigenvalue of the real-symmetric matrix $\hat{\mathbf{M}}^T \hat{\mathbf{M}}$ is determined as

$$\hat{s}_0 = \frac{(\hat{\alpha} + \hat{\beta}) + \sqrt{(\hat{\alpha} - \hat{\beta})^2 + 4 \cdot \hat{\gamma}^2}}{2} \quad (4.74)$$

with

$$\hat{\alpha} \triangleq a^2 + c^2 \quad (4.75)$$

$$\hat{\beta} \triangleq b^2 + d^2 \quad (4.76)$$

$$\hat{\gamma} \triangleq a \cdot b - c \cdot d \quad (4.77)$$

Applying the relationship 4.38 to the real-symmetric matrix $\hat{\mathbf{M}}^T \hat{\mathbf{M}}$ with largest eigenvalue \hat{s}_0 , Eq. 4.73 is rewritten as

$$\ell^2 [\hat{\varphi}(\mathbf{y}_e), \hat{\varphi}(\mathbf{z}_e)] \leq \frac{\hat{s}_0}{u_0^2} \cdot [\hat{\rho}(\mathbf{y}_e) - \hat{\rho}(\mathbf{z}_e)]^T [\hat{\rho}(\mathbf{y}_e) - \hat{\rho}(\mathbf{z}_e)] \quad (4.78)$$

According to the mean value theorem, there exist vectors $\tilde{\mathbf{y}}_{eij}$ in the rectangle with opposite corners \mathbf{y}_e and \mathbf{z}_e for which

$$\hat{\rho}(\mathbf{y}_e) = \hat{\rho}(\mathbf{z}_e) + \hat{\mathbf{J}} (\mathbf{y}_e - \mathbf{z}_e) \quad (4.79)$$

with

$$\hat{\mathbf{J}} = \begin{bmatrix} \left. \frac{\partial \hat{\rho}_1}{\partial x_{e1}} \right|_{\mathbf{y}=\tilde{\mathbf{y}}_{11}} & \left. \frac{\partial \hat{\rho}_1}{\partial x_{e2}} \right|_{\mathbf{y}=\tilde{\mathbf{y}}_{12}} \\ \left. \frac{\partial \hat{\rho}_2}{\partial x_{e1}} \right|_{\mathbf{y}=\tilde{\mathbf{y}}_{21}} & \left. \frac{\partial \hat{\rho}_2}{\partial x_{e2}} \right|_{\mathbf{y}=\tilde{\mathbf{y}}_{22}} \end{bmatrix} \triangleq \begin{bmatrix} \lambda_1 & \lambda_2 \\ \lambda_3 & \lambda_4 \end{bmatrix} \quad (4.80)$$

Consequently, one can write

$$[\hat{\rho}(\mathbf{y}_e) - \hat{\rho}(\mathbf{z}_e)]^T [\hat{\rho}(\mathbf{y}_e) - \hat{\rho}(\mathbf{z}_e)] = [\mathbf{y}_e - \mathbf{z}_e]^T \hat{\mathbf{J}}^T \hat{\mathbf{J}} [\mathbf{y}_e - \mathbf{z}_e] \quad (4.81)$$

Substitution of Eq. 4.81 in Eq. 4.78 yields

$$\ell^2 [\varphi(\mathbf{y}_e), \varphi(\mathbf{z}_e)] \leq \frac{\hat{s}_0}{u_0^2} \cdot [\mathbf{y}_e - \mathbf{z}_e]^T \hat{\mathbf{J}}^T \hat{\mathbf{J}} [\mathbf{y}_e - \mathbf{z}_e] \quad (4.82)$$

The largest eigenvalue of the real-symmetric matrix $\hat{\mathbf{J}}^T \hat{\mathbf{J}}$ is found as

$$\hat{s}_1 = \frac{(\hat{\mu} + \hat{\nu}) + \sqrt{(\hat{\mu} - \hat{\nu})^2 + 4 \cdot \hat{\xi}^2}}{2} \quad (4.83)$$

with

$$\hat{\mu} \triangleq \lambda_1^2 + \lambda_3^2 \quad (4.84)$$

$$\hat{\nu} \triangleq \lambda_2^2 + \lambda_4^2 \quad (4.85)$$

$$\hat{\xi} \triangleq \lambda_1 \cdot \lambda_2 + \lambda_3 \cdot \lambda_4 \quad (4.86)$$

Applying the relationship 4.38 to the real-symmetric matrix $\hat{\mathbf{J}}^T \hat{\mathbf{J}}$ with largest eigenvalue \hat{s}_1 and taking into account the definition of distance (Eq. 4.72), Eq. 4.82 is rewritten as

$$\ell^2 [\varphi(\mathbf{y}_e), \varphi(\mathbf{z}_e)] \leq \frac{\hat{s}_0 \cdot \hat{s}_1}{u_0^2} \cdot \ell^2[\mathbf{y}_e, \mathbf{z}_e] \quad (4.87)$$

As the relation 4.87 holds for all $\mathbf{y}_e, \mathbf{z}_e$ in $\mathbb{R}^{2 \times 1}$, the mapping $\hat{\varphi}$ is a *contraction mapping* according to the definition (Eq. 4.3) if

$$\frac{\hat{s}_0 \cdot \hat{s}_1}{u_0^2} < 1 \quad \Leftrightarrow \quad u_0 > \sqrt{\hat{s}_0 \cdot \hat{s}_1} \quad (4.88)$$

Under this condition that is sufficient but not necessary, the mapping $\hat{\varphi}$ possesses a unique fixed point that is a unique equilibrium point for the SHARON reactor.

Upper boundaries for the partial derivatives of the reaction rates to the state variables

The values of $\hat{\mu}$, $\hat{\nu}$ and $\hat{\xi}$ depend on the values of λ_i^2 and thus on the absolute values of the partial derivatives $\frac{\partial \hat{p}_i}{\partial x_{ej}}$, evaluated in the unknown \tilde{y}_{ij} (see Eq. 4.80). Consequently, the equilibrium uniqueness condition 4.88 cannot be used as such.

It is however possible to define maximum absolute values for the partial derivatives (so there is no need to know the exact values of \tilde{y}_{ij})

and in this way also maximum values for $\hat{\mu}$, $\hat{\nu}$ and $\hat{\xi}$:

$$\begin{aligned} \left| \frac{\partial \hat{\rho}_1}{\partial x_{e1}} \right| &= \left| a_1 \cdot \frac{c_1}{c_1 + x_{e2}} \cdot \left[\frac{b_1}{(b_1 + x_{e1})^2} \cdot x_3 - \frac{d}{a \cdot d + b \cdot c} \cdot \frac{x_{e1}}{b_1 + x_{e1}} \right] \right| \\ &\leq a_1 \cdot \max \left\{ \frac{x_{3,max}}{b_1}, \frac{d}{a \cdot d + b \cdot c} \cdot \frac{x_{e1,max}}{b_1 + x_{e1,max}} \right\} \\ &= |\lambda_1|_{max} \end{aligned} \quad (4.89)$$

$$\begin{aligned} \left| \frac{\partial \hat{\rho}_1}{\partial x_{e2}} \right| &= \left| a_1 \cdot \frac{x_{e1}}{b_1 + x_{e1}} \cdot \left[\frac{-c_1}{(c_1 + x_{e2})^2} \cdot x_{e3} + \frac{c_1}{c_1 + x_{e2}} \cdot \frac{b}{a \cdot d + b \cdot c} \right] \right| \\ &\leq a_1 \cdot \frac{x_{1,max}}{b_1 + x_{1,max}} \cdot \max \left\{ \frac{x_{3,max}}{b_1}, \frac{b}{a \cdot d + b \cdot c} \right\} \\ &= |\lambda_2|_{max} \end{aligned} \quad (4.90)$$

$$\begin{aligned} \left| \frac{\partial \hat{\rho}_2}{\partial x_{e1}} \right| &= \left| a_2 \cdot \frac{x_{e2}}{(b_2 + x_{e2})} \cdot \frac{d_2}{(d_2 + x_{e2})} \cdot \left[\frac{e_2 \cdot (c_2 \cdot e_2 - x_{e1}^2)}{(c_2 + x_{e1})^2 \cdot (e_2 + x_{e1})^2} \cdot x_{e4} \right. \right. \\ &\quad \left. \left. + \frac{x_{e1} \cdot e_2}{(c_2 + x_{e1})(e_2 + x_{e1})} \cdot \frac{c}{a \cdot d + b \cdot c} \right] \right| \\ &\leq a_2 \cdot m_2 \cdot \left[\frac{x_{4,max}}{c_2} + m_1 \cdot \frac{c}{a \cdot d + b \cdot c} \right] = |\lambda_3|_{max} \end{aligned} \quad (4.91)$$

$$\begin{aligned} \left| \frac{\partial \hat{\rho}_2}{\partial x_{e2}} \right| &= \left| a_2 \cdot \frac{x_1}{(c_2 + x_{e1})} \cdot \frac{e_2}{(e_2 + x_{e1})} \cdot \left[\frac{d_2 \cdot (b_2 \cdot d_2 - x_{e2}^2)}{(b_2 + x_{e2})^2 \cdot (d_2 + x_{e2})^2} \cdot x_{e4} \right. \right. \\ &\quad \left. \left. + \frac{x_{e2} \cdot d_2}{(b_2 + x_{e2})(d_2 + x_{e2})} \cdot \frac{a}{a \cdot d + b \cdot c} \right] \right| \\ &\leq a_2 \cdot m_1 \cdot \left[\frac{x_{4,max}}{b_2} + m_2 \cdot \frac{a}{a \cdot d + b \cdot c} \right] = |\lambda_4|_{max} \end{aligned} \quad (4.92)$$

with m_1 and m_2 defined by Eqs. 4.56 and 4.57 respectively.

The criterion for uniqueness of the equilibrium point, Eq. 4.88, is now relaxed by substituting Eqs. 4.89-4.92. For the upper boundaries for the state variables $x_{i,max}$, again the values given by Eqs. 4.58, 4.59, 4.60 and 4.61 are used. In this way, the criterion Eq. 4.88 can be evaluated.

4.5.3 Comparison of the two methods

The calculations in the previous sections have resulted in two criteria, given by Eqs. 4.49 and 4.88, for the uniqueness of the equilibrium point

in a SHARON reactor with constant pH:

$$\begin{aligned} u_0 &> \sqrt{s_0 \cdot s_1} \\ u_0 &> \sqrt{\hat{s}_0 \cdot \hat{s}_1} \end{aligned}$$

Comparing Eq. 4.34 with Eq. 4.74, it is clear that

$$\hat{s}_0 < s_0$$

However, considering Eq. 4.44 and Eq. 4.83, one cannot easily draw a conclusion about the relative magnitudes of s_1 and \hat{s}_1 . Consequently, it is not possible either to decide a priori which condition for the uniqueness of the equilibrium point is the most stringent. For this reason, both criteria will be evaluated. Note however, that intuitively, the '2-dimensional' criterion (derived on the basis of the reduced 2-dimensional model) is expected to give the best result, since less relaxations have been made in the 2-dimensional space.

Considering Eqs. 4.59-4.61, it is clear that for increasing u_0 , the values of $x_{3,max}$, $x_{2,max}$ and $x_{4,max}$ become independent of u_0 :

$$u_0 \rightarrow +\infty \Rightarrow \begin{cases} x_{3,max} \rightarrow u_3 \\ x_{2,max} \rightarrow u_2 \\ x_{4,max} \rightarrow u_4 \end{cases} \quad (4.93)$$

As a result, the upper boundaries for μ , ν and ξ (as well as for $\hat{\mu}$, $\hat{\nu}$ and $\hat{\xi}$) and consequently the upper boundaries for s_1 (\hat{s}_1) become independent of u_0 . As a result, the criterion 4.49 (4.88) is certainly fulfilled for sufficiently large values of u_0 . This means that *for a sufficiently large value of the dilution rate u_0 , there always exists a unique equilibrium point*, which also corresponds with the finding of a unique equilibrium point for $u_0 \rightarrow \infty$ in section 4.4.3. As the criteria 4.49 and 4.88 are certainly fulfilled for sufficiently large u_0 , it makes sense to calculate a lower limit of u_0 for which the criteria are fulfilled, as it is now certain that such a value exists.

4.5.4 Simulation results

The criteria for a unique equilibrium point, Eqs. 4.49 and 4.88, have been evaluated in Matlab (R13) for the parameter values given in Table 4.1. The influence of the input variable $u_1 = C_{TNH}^{in}$ on the uniqueness criterion has been investigated and is described in this paragraph. The influence of the input variables $u_2 = C_{TNO_2}^{in}$, $u_3 = C_{Xamm}^{in}$, $u_4 = C_{Xnit}^{in}$ is not discussed, as they are not likely to vary a lot in practice.

Calculation of dilution rates for which there exists a unique equilibrium

The criteria 4.49 and 4.88 for a unique equilibrium can be evaluated in terms of the dilution rates, u_0 . The minimum value of the dilution rate above which a unique equilibrium point exists, $u_{0,crit}$, is calculated as

$$u_{0,crit}^{Adim} \triangleq \sqrt{s_0 \cdot s_1} \quad (4.94)$$

or as

$$u_{0,crit}^{2dim} \triangleq \sqrt{\hat{s}_0 \cdot \hat{s}_1} \quad (4.95)$$

Figure 4.1 gives the profiles of $u_0 - \sqrt{s_0 \cdot s_1}$ and $u_0 - \sqrt{\hat{s}_0 \cdot \hat{s}_1}$ in case $u_1 = C_{TNH}^{in} = 70 \text{ mole m}^{-3}$; $u_2 = C_{TNO_2}^{in} = 0$; $u_3 = C_{X_{amm}}^{in} = u_4 = C_{X_{nit}}^{in} = 0.01 \text{ mole m}^{-3}$. The values of $u_{0,crit}^{Adim}$ and $u_{0,crit}^{2dim}$ are found as the values of u_0 where these functions become zero, i.e. 120.1 day^{-1} and 7.5 day^{-1} respectively. The discontinuity in the graphs near $u_0 = 2 \text{ day}^{-1}$ is caused by the discontinuity in the calculation of $x_{3,max}$ (Eq. 4.59).

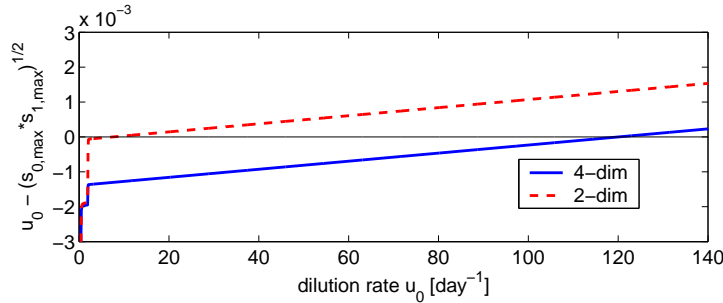


Figure 4.1: Evaluation of the criteria for a unique equilibrium in terms of u_0 for $u_1 = C_{TNH}^{in} = 70 \text{ mole m}^{-3}$; $u_2 = C_{TNO_2}^{in} = 0$; $u_3 = C_{X_{amm}}^{in} = u_4 = C_{X_{nit}}^{in} = 0.01 \text{ mole m}^{-3}$

For the given parameter and input values, the 2-dimensional criterion performs better than the 4-dimensional one, as it results in a lower (critical) value of the dilution rate above which there exists a unique equilibrium point. From these results, it can be concluded that for the given influent conditions, a unique equilibrium will be obtained for dilution rates higher than 7.5 day^{-1} . Such a high dilution rate will however cause wash-out of both ammonium oxidizing and nitrite oxidizing biomass, as demonstrated in the following paragraph.

Conditions for biomass wash-out

During wash-out, the biomass loss with the outgoing stream is higher than the biomass growth due to conversion¹. Normal operation of a SHARON reactor aims at wash-out of the nitrite oxidizing biomass (x_4) while maintaining the ammonium oxidizing biomass (x_3) in the reactor.

Considering Eq. 4.8, wash-out of ammonium oxidizers occurs if

$$u_0 \cdot x_3 > \rho_1 \quad (4.96)$$

A fortiori, wash-out of ammonium oxidizers occurs if

$$u_0 > \hat{a}_1 \triangleq a_1 \cdot \frac{x_{1,max}}{b_1 + x_{1,max}} = a_1 \cdot \frac{u_1}{b_1 + u_1} \quad (4.97)$$

as in this case (Eq. C.4 gives the latter inequality)

$$u_0 \cdot x_3 > \hat{a}_1 \cdot x_3 \geq \rho_1$$

Considering Eq. 4.9, wash-out of nitrite oxidizers occurs if

$$u_0 \cdot x_4 > \rho_2 \quad (4.98)$$

A fortiori, wash-out of nitrite oxidizers occurs if

$$u_0 > a_2 \cdot m_1 \cdot m_2 \quad (4.99)$$

as in this case (Eq. C.12 gives the latter inequality)

$$u_0 \cdot x_4 > a_2 \cdot m_1 \cdot m_2 \cdot x_4 \geq \rho_2$$

It is clear that moreover, wash-out of ammonium oxidizers occurs if (taking into account Eq. C.8)

$$u_0 > a_1 \quad (4.100)$$

while wash-out of nitrite oxidizers takes place if (taking into account Eq. C.15)

$$u_0 > a_2 \quad (4.101)$$

Since $a_1 (= 2.10 \text{ d}^{-1}) > a_2 (= 1.05 \text{ d}^{-1})$, stating that ammonium oxidizers grow faster than nitrite oxidizers, both ammonium and nitrite oxidizers are washed out if Eq. 4.100 is fulfilled, i.e. if $u_0 > 2.10 \text{ d}^{-1}$. This is certainly the case for $u_0 = 7.5 \text{ day}^{-1}$, as determined in the previous paragraph, which means that the unique equilibrium state for such high dilution rates corresponds with wash-out of all biomass. This equilibrium state obviously is not interesting for operational purposes, as there is no conversion of ammonium.

¹Reasonably assuming the effect of biomass present in the influent, is negligible

Influence of the influent ammonium concentration, $C_{TNH}^{in} = u_1$ on the uniqueness of equilibrium points

The criteria for a unique equilibrium have been evaluated in terms of the dilution rates, u_0 for different values of the ammonium influent concentration, $C_{TNH}^{in} = u_1$. Figure 4.2 gives the resulting minimum value of the dilution rate above which there exists a unique equilibrium point, $u_{0,crit}$, in terms of $C_{TNH}^{in} = u_1$. In all cases, the 2-dimensional criterion performs better, i.e. is less stringent, than the 4-dimensional one (or equally well in case $C_{TNH}^{in} = u_1 = 0$).

For the range of influent conditions examined, the minimum value for the dilution rate, above which there exists a unique equilibrium point, is too high to prevent wash-out of ammonium oxidizing biomass. Indeed, the values of the dilution rate u_0 higher than the critical dilution rate, for which there exists a unique equilibrium point, are clearly higher than \hat{a}_1 (Figure 4.2). Considering the condition for wash-out of ammonium oxidizers, Eq. 4.97, it is therefore highly likely that, for these values, the wash-out states will be found as the unique equilibrium point. This is confirmed in section 4.5.5.

Figure 4.2 further shows that the critical dilution rate above which there exists a unique equilibrium point, increases as C_{TNH}^{in} increases, according to a Monod-like relationship. This can be explained considering that a higher ammonium influent concentration, $C_{TNH}^{in} = u_1$, results in a higher ammonium concentration in the reactor, $C_{TNH} = x_1$, at least before reaching equilibrium, on its turn increasing the reaction rate ρ_1 up to a certain value according to Monod's kinetics (Eq. 4.13). As long as the reaction rate ρ_1 increases, a higher value of u_0 is necessary to fulfill the wash-out condition Eq. 4.96, corresponding with the unique equilibrium state.

4.5.5 Calculation of the unique equilibrium point

In case the contraction mapping possesses a unique fixed point, corresponding with the unique equilibrium point of the SHARON reactor model, the value of this point for a given dilution rate u_0 is calculated using the method of successive approximations (Eq. 4.4), applied to the 4-dimensional contraction mapping (Eq. 4.28):

$$\begin{aligned} \mathbf{x}_{n+1} &= \varphi(\mathbf{x}_n) \\ &= \mathbf{u} + \frac{1}{u_0} \cdot \mathbf{M} \rho(\mathbf{x}_n) \quad n = 0, 1, 2, \dots \end{aligned}$$

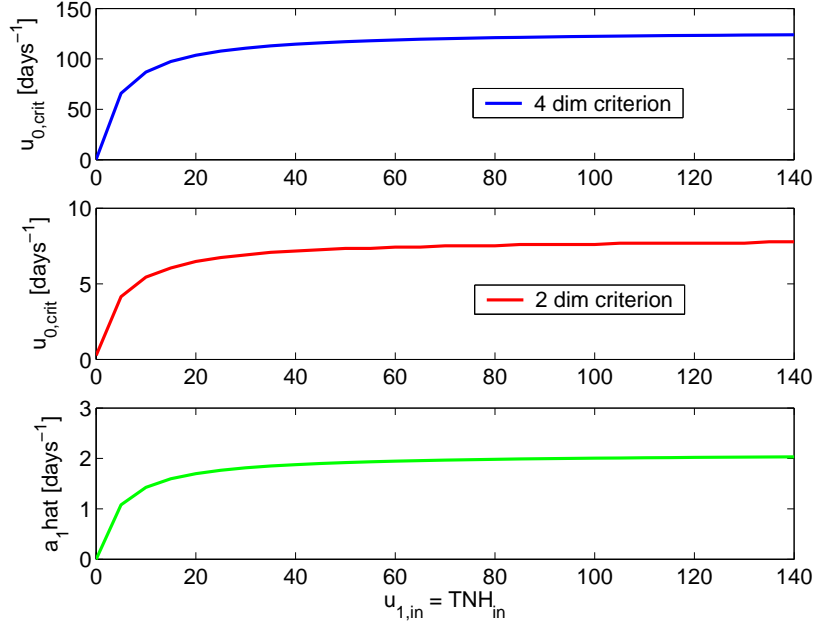


Figure 4.2: Minimum dilution rate $u_{0,crit}$ required for a unique equilibrium point in terms of $u_1 = C_{TNH}^{in}$; $u_2 = TNNO2_{in} = 0$; $u_3 = C_{X_{amm}}^{in} = u_4 = C_{X_{nit}}^{in} = 0.01 \text{ mole m}^{-3}$

starting from a vector \mathbf{x}_0 with arbitrary state values.

For $C_{TNH}^{in} = u_1 = 70 \text{ mole m}^{-3}$, $C_{TNNO2}^{in} = u_2 = 0$, $C_{X_{amm}}^{in} = u_3 = 0.01 \text{ mole m}^{-3}$ and $C_{X_{nit}}^{in} = u_4 = 0.01 \text{ mole m}^{-3}$, there exists a unique equilibrium for dilution rates higher than $u_{0,crit} = 7.5 \text{ day}^{-1}$. The values of the equilibrium states have been calculated with the principle of contraction mapping for $u_0 = 7.6 \text{ day}^{-1}$ as

$$\begin{aligned} C_{TNH,e} = x_{e1} &= 69.94 \text{ mole m}^{-3} \\ C_{TNNO2,e} = x_{e2} &= 0.0551 \text{ mole m}^{-3} \\ C_{X_{amm},e} = x_{e3} &= 0.135 \text{ mole m}^{-3} \\ C_{X_{nit},e} = x_{e4} &= 0.0100 \text{ mole m}^{-3} \end{aligned}$$

The equilibrium states indeed correspond with biomass wash-out, as expected. Only a very small amount of ammonium is converted by the ammonium oxidizers present in the influent. This result has been verified through steady state simulation of the reactor model in Simulink, giving exactly the same values for the equilibrium states.

Figure 4.3 shows the values of the equilibrium states in terms of the influent ammonium concentration. The equilibrium states have been calculated for values of the dilution rates just above (1%) the critical dilution rate, that guarantees a unique equilibrium. Each time, the unique equilibrium state is identified as the wash-out state with a negligible ammonium conversion. It has been verified that the state values of the starting vector x_0 indeed do not influence the results.

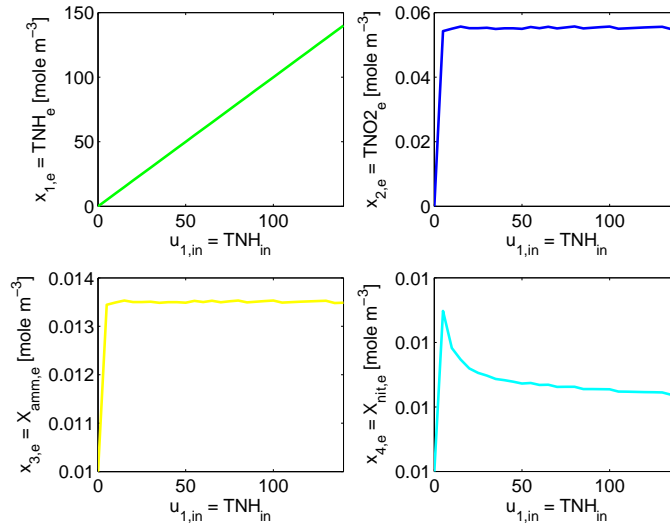


Figure 4.3: Values of the unique equilibrium states in terms of $u_1 = C_{TNH}^{in}$; $u_0 = 1.01 \cdot u_{0,crit}$; $u_2 = C_{TNO2}^{in} = 0$; $u_3 = C_{X_{amm}}^{in} = u_4 = C_{X_{nit}}^{in} = 0.01 \text{ mole m}^{-3}$

4.5.6 Conclusions

In this section, criteria for the uniqueness of equilibrium points of a SHARON reactor model with constant pH have been deduced according to the principle of contraction mapping. A first criterion was derived from the original 4-dimensional model, a second one from a reduced 2-dimensional model form, valid in case of equilibrium. Both criteria identify a minimum value of the dilution rate above which the model possesses a unique equilibrium point. As neither of the two criteria could be identified a priori as being better than the other, both criteria were used in the subsequent evaluation. Simulation results have revealed that, in all practical cases, the 2-dimensional criterion performs better, i.e. is more stringent, than the 4-dimensional one. This

corresponds to what could be expected intuitively, since it is likely that less relaxations are made in a 2-dimensional space compared to a 4-dimensional one.

Simulation results show that the critical dilution rate above which a unique equilibrium point exists, increases with increasing influent ammonium concentrations. The results further indicate that the unique equilibrium point at high dilution rates corresponds with wash-out of both ammonium and nitrite oxidizers, i.e. the trivial equilibrium point where the reactor fails. This is confirmed when calculating the exact values of the unique equilibrium states.

As expected, calculation of the unique equilibrium states according to the contraction mapping theorem gives the same results as obtained through a corresponding steady state simulation with the reactor model, implemented in Matlab-Simulink.

It is important to remember that the criteria derived on the basis of the contraction mapping principle give sufficient but not necessary conditions for the existence of a unique equilibrium. So this result does not mean that there do not exist any other operating regions with only one equilibrium point but it means that no conclusions can be drawn concerning the uniqueness of equilibrium points for values below the critical dilution rate. In particular, no conclusions could be drawn for the practical operating region, in which the dilution rate (u_0) should be larger than the growth rate of nitrite oxidizers (a_2), but smaller than the growth rate of ammonium oxidizers (a_1).

4.6 Local asymptotic stability of equilibrium points

4.6.1 Local asymptotic stability and system behaviour

Criterion for local asymptotic stability The linearization principle is used to investigate the local asymptotic stability of equilibrium points. An equilibrium point \mathbf{x}_e of the SHARON reactor model (Eq. 4.16) is locally asymptotically stable if the eigenvalues of the Jacobian matrix

$$\left. \frac{\partial \mathbf{f}(\mathbf{x})}{\partial \mathbf{x}} \right|_{\mathbf{x}=\mathbf{x}_e} \triangleq \begin{bmatrix} \left. \frac{\partial f_1}{\partial x_1} \right|_{\mathbf{x}=\mathbf{x}_e} & \cdots & \left. \frac{\partial f_1}{\partial x_4} \right|_{\mathbf{x}=\mathbf{x}_e} \\ \vdots & & \vdots \\ \left. \frac{\partial f_4}{\partial x_1} \right|_{\mathbf{x}=\mathbf{x}_e} & \cdots & \left. \frac{\partial f_4}{\partial x_4} \right|_{\mathbf{x}=\mathbf{x}_e} \end{bmatrix} \quad (4.102)$$

all are in the open left half plane, i.e. have a strictly negative real part.

It can easily be found that

$$s = -u_0 \quad (4.103)$$

is a double eigenvalue of the Jacobian matrix and that its remaining two eigenvalues are the solutions of the quadratic equation

$$s^2 + (2 \cdot u_0 - \alpha - \delta) \cdot s + (u_0 - \alpha) \cdot (u_0 - \delta) - \gamma \cdot \beta = 0 \quad (4.104)$$

in which

$$\alpha = -a \cdot \left. \frac{\partial \rho_1}{\partial x_1} \right|_{\mathbf{x}=\mathbf{x}_e} + c \cdot \left. \frac{\partial \rho_1}{\partial x_2} \right|_{\mathbf{x}=\mathbf{x}_e} + \left. \frac{\partial \rho_1}{\partial x_3} \right|_{\mathbf{x}=\mathbf{x}_e} \quad (4.105)$$

$$\beta = -b \cdot \left. \frac{\partial \rho_1}{\partial x_1} \right|_{\mathbf{x}=\mathbf{x}_e} - d \cdot \left. \frac{\partial \rho_1}{\partial x_2} \right|_{\mathbf{x}=\mathbf{x}_e} \quad (4.106)$$

$$\gamma = -a \cdot \left. \frac{\partial \rho_2}{\partial x_1} \right|_{\mathbf{x}=\mathbf{x}_e} + c \cdot \left. \frac{\partial \rho_2}{\partial x_2} \right|_{\mathbf{x}=\mathbf{x}_e} \quad (4.107)$$

$$\delta = -b \cdot \left. \frac{\partial \rho_2}{\partial x_1} \right|_{\mathbf{x}=\mathbf{x}_e} - d \cdot \left. \frac{\partial \rho_2}{\partial x_2} \right|_{\mathbf{x}=\mathbf{x}_e} + \left. \frac{\partial \rho_2}{\partial x_4} \right|_{\mathbf{x}=\mathbf{x}_e} \quad (4.108)$$

The eigenvalues 4.103 are strictly negative for $u_0 \neq 0$). The eigenvalues given by Eq. 4.104 have a negative real part if their sum is strictly negative and their product is strictly positive, i.e. if

$$(2 \cdot u_0 - \alpha - \delta) > 0 \quad \text{and} \quad (u_0 - \alpha) \cdot (u_0 - \delta) - \gamma \cdot \beta > 0 \quad (4.109)$$

If this criterion is fulfilled, this assures local asymptotic stability of the equilibrium point \mathbf{x}_e for $u_0 \neq 0$.

For $u_0 \rightarrow \infty$, the unique equilibrium point approaches the influent conditions (Eq. 4.23). As a result, the values of α , β , γ and δ in this case become independent of u_0 . Consequently, the conditions 4.109 are always fulfilled for $u_0 \rightarrow \infty$, which means that *for sufficiently high values of the dilution rate u_0 , the equilibrium point is always locally asymptotically stable.*

System behaviour around the equilibrium point The characteristic equation 4.104 can be written in its standard form for a second order system:

$$s^2 + 2 \cdot \zeta \cdot \omega_n \cdot s + \omega_n^2 = 0 \quad (4.110)$$

with

$$\omega_n = \sqrt{(u_0 - \alpha) \cdot (u_0 - \beta) - \gamma \cdot \beta} \quad (4.111)$$

$$\zeta = \frac{(2 \cdot u_0 - \alpha - \delta)}{2 \cdot \sqrt{(u_0 - \alpha) \cdot (u_0 - \beta) - \gamma \cdot \beta}} \quad (4.112)$$

Close to the equilibrium point, the system exhibits linear behaviour. If $\zeta < 1$, the state variables converge to the equilibrium point with an oscillatory transient behaviour, following trajectories that are described by

$$x_i(t) = x_{ei} + \exp(-u_0 \cdot t) \cdot (a_i \cdot t + b_i) + c_i \cdot \exp(-\zeta \cdot \omega_n \cdot t) \cdot \sin(\omega_n \cdot \sqrt{1 - \zeta^2} \cdot t + d_i) \quad (4.113)$$

in which the values of a_i , b_i , c_i and d_i are determined by the initial state values. If $\zeta = 1$, the transient behaviour exhibits critical damping; if $\zeta > 1$ the system is overdamped.

4.6.2 Simulation results

Criterion for local asymptotic stability The condition for local asymptotic stability 4.109 is evaluated for the equilibrium points, calculated in section 4.5.5 in terms of the influent ammonium concentration and for corresponding values of the dilution rate just above the critical values calculated. Figure 4.4 shows that the opposite of (i.e. minus) the sum of the eigenvalues is always strictly negative and their product is always strictly positive, which means that these equilibrium points are all locally asymptotically stable.

Note that the conditions for local asymptotic stability (Eq. 4.109) indicate (not rigorously prove!) that, if the equilibrium point corresponding with a dilution rate just above the critical values is locally asymptotically stable, then the equilibrium points corresponding with higher values of the dilution rate are also locally asymptotically stable.

System behaviour around the equilibrium point Figure 4.5 shows that the damping factor ζ is larger than 1 for all equilibrium points, calculated in section 4.5.5 in terms of the influent ammonium concentration and for corresponding values of the dilution rate just above the critical values. So in these cases, the system's states will converge to the equilibrium states in a non-oscillatory way.

4.6.3 Conclusions

Using the linearization principle, conditions for local asymptotic stability of the equilibrium points of the SHARON reactor model for constant pH have been derived. Evaluation of this criterion has shown that

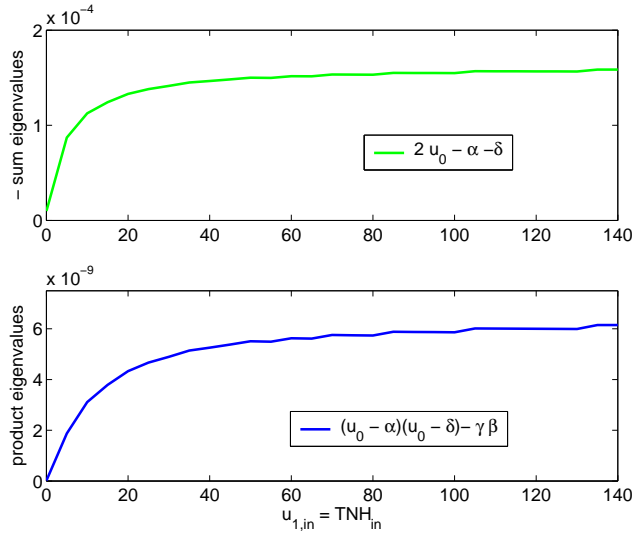


Figure 4.4: Negative sum and product of eigenvalues, corresponding with the system behaviour around the unique equilibrium point in terms of $u_1 = C_{\text{TNH}}^{\text{in}}$; $u_0 = 1.01 \cdot u_{0,\text{crit}}$; $u_2 = C_{\text{TN}O_2}^{\text{in}} = 0$; $u_3 = C_{\text{X}_{\text{amm}}}^{\text{in}} = u_4 = C_{\text{X}_{\text{nit}}}^{\text{in}} = 0.01 \text{ mole m}^{-3}$

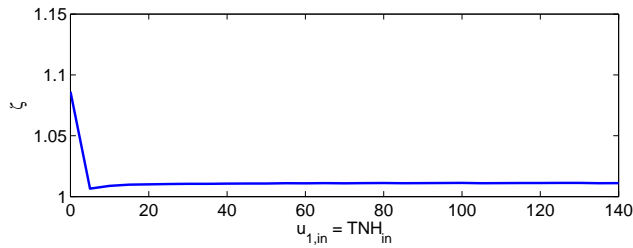


Figure 4.5: ζ corresponding with the system behaviour around the unique equilibrium point in terms of $u_1 = C_{\text{TNH}}^{\text{in}}$; $u_0 = 1.01 \cdot u_{0,\text{crit}}$; $u_2 = C_{\text{TN}O_2}^{\text{in}} = 0$; $u_3 = C_{\text{X}_{\text{amm}}}^{\text{in}} = u_4 = C_{\text{X}_{\text{nit}}}^{\text{in}} = 0.01 \text{ mole m}^{-3}$

the unique equilibrium points, calculated in section 4.5.5, are all locally asymptotically stable and that the system's states will converge to the equilibrium states in a non-oscillatory way.

4.7 Direct calculation of equilibrium points

In section 4.5, criteria derived on the basis of the contraction mapping principle showed that the SHARON reactor model defined by Eqs. 4.6-4.9 possesses a unique equilibrium point for sufficiently high dilution rates. This unique equilibrium point was identified as the wash-out point and was shown to be locally asymptotically stable (section 4.6). However, because of the 'sufficient but not necessary' nature of the derived criteria, no conclusions could be drawn concerning the uniqueness of equilibrium points for values below the critical dilution rate. For this reason, it was decided to calculate the equilibrium points of the SHARON reactor model directly for a simplified reactor model. The general SHARON reactor model is first transformed into a so-called canonical state space representation. Subsequently, the number of equilibrium points is calculated directly and their stability is examined in a number of simplified cases.

4.7.1 General model

Canonical state space representation

Define new state variables

$$y_1 \triangleq x_1 + a \cdot x_3 + b \cdot x_4 \quad (4.114)$$

$$y_2 \triangleq x_2 - c \cdot x_3 + d \cdot x_4 \quad (4.115)$$

$$y_3 \triangleq x_3 \quad (4.116)$$

$$y_4 \triangleq x_4 \quad (4.117)$$

By introducing these new state variables, it is easily shown that the SHARON reactor model given by Eqs. 4.6-4.9 is equivalent with

$$\dot{y}_1 = u_0 \cdot (w_1 - y_1) \quad (4.118)$$

$$\dot{y}_2 = u_0 \cdot (w_2 - y_2) \quad (4.119)$$

$$\dot{y}_3 = u_0 \cdot (u_3 - y_3) + \sigma_1(\mathbf{y}) \quad (4.120)$$

$$\dot{y}_4 = u_0 \cdot (u_4 - y_4) + \sigma_2(\mathbf{y}) \quad (4.121)$$

in which

$$\mathbf{y} \triangleq \begin{bmatrix} y_1 \\ y_2 \\ y_3 \\ y_4 \end{bmatrix} \quad (4.122)$$

$$w_1 \triangleq u_1 + a \cdot u_3 + b \cdot u_4 \quad (4.123)$$

$$w_2 \triangleq u_2 - c \cdot u_3 + d \cdot u_4 \quad (4.124)$$

$$\sigma_1(\mathbf{y}) = \rho_1(\mathbf{x}) \left| \begin{array}{l} x_1 = y_1 - a \cdot y_3 - b \cdot y_4 \\ x_2 = y_2 + c \cdot y_3 - d \cdot y_4 \\ x_3 = y_3 \end{array} \right. \quad (4.125)$$

$$\sigma_2(\mathbf{y}) = \rho_2(\mathbf{x}) \left| \begin{array}{l} x_1 = y_1 - a \cdot y_3 - b \cdot y_4 \\ x_2 = y_2 + c \cdot y_3 - d \cdot y_4 \\ x_4 = y_4 \end{array} \right. \quad (4.126)$$

with $\rho_1(\mathbf{x})$ and $\rho_2(\mathbf{x})$ defined by Eqs. 4.13 and 4.14 respectively.

The state space of the system defined by Eqs. 4.6-4.9 is

$$\mathbb{R}^{+4} \triangleq \{\mathbf{x} \in \mathbb{R}^4 \mid x_i \geq 0, i = 1, \dots, 4\}$$

Call \mathbf{S}_y the image of \mathbb{R}^{+4} under the transformation $\mathbf{x} \mapsto \mathbf{y}$. \mathbf{S}_y is the state space of the system 4.118-4.121. It is defined by the inequalities:

$$x_1 = y_1 - a \cdot y_3 - b \cdot y_4 \geq 0 \quad (4.127)$$

$$x_2 = y_2 + c \cdot y_3 - d \cdot y_4 \geq 0 \quad (4.128)$$

$$x_3 = y_3 \geq 0 \quad (4.129)$$

$$x_4 = y_4 \geq 0 \quad (4.130)$$

Every trajectory that starts at $t = 0$ in a point \mathbf{y}_0 of \mathbf{S}_y , stays in \mathbf{S}_y for $t \geq 0$. Under constant inputs, for $t \rightarrow +\infty$ (steady state), every trajectory converges to the cross-section Δ of \mathbf{S}_y with the plane $\{y_1 = w_1, y_2 = w_2\}$, as can be seen from Eqs. 4.118 and 4.119:

$$\Delta \triangleq \{\mathbf{y} \in \mathbf{S}_y ; y_1 = w_1 ; y_2 = w_2\} \quad (4.131)$$

The cross-section Δ is defined by the inequalities

$$w_1 - a \cdot y_3 - b \cdot y_4 \geq 0 \quad (4.132)$$

$$w_2 + c \cdot y_3 - d \cdot y_4 \geq 0 \quad (4.133)$$

$$y_3 \geq 0 \quad (4.134)$$

$$y_4 \geq 0 \quad (4.135)$$

After completing this convergence, the process exhibits a secondary order behaviour that is determined by the dynamics of y_3 and y_4 .

Local asymptotic stability of equilibrium points

The local asymptotic stability of the equilibrium points is assessed using the linearization principle (Section 4.2.3). An equilibrium point \mathbf{y}_e of the system 4.118-4.121 is locally asymptotically stable if all eigenvalues of the system's Jacobian matrix, evaluated in this equilibrium point, are in the open left phase plane, i.e. have strictly negative real parts. This Jacobian matrix is defined as

$$\mathbf{J}(\mathbf{y}_e) \triangleq \begin{bmatrix} \left. \frac{\partial f_1}{\partial y_1} \right|_{\mathbf{y}=\mathbf{y}_e} & \left. \frac{\partial f_1}{\partial y_2} \right|_{\mathbf{y}=\mathbf{y}_e} & \left. \frac{\partial f_1}{\partial y_3} \right|_{\mathbf{y}=\mathbf{y}_e} & \left. \frac{\partial f_1}{\partial y_4} \right|_{\mathbf{y}=\mathbf{y}_e} \\ \left. \frac{\partial f_2}{\partial y_1} \right|_{\mathbf{y}=\mathbf{y}_e} & \left. \frac{\partial f_2}{\partial y_2} \right|_{\mathbf{y}=\mathbf{y}_e} & \left. \frac{\partial f_2}{\partial y_3} \right|_{\mathbf{y}=\mathbf{y}_e} & \left. \frac{\partial f_2}{\partial y_4} \right|_{\mathbf{y}=\mathbf{y}_e} \\ \left. \frac{\partial f_3}{\partial y_1} \right|_{\mathbf{y}=\mathbf{y}_e} & \left. \frac{\partial f_3}{\partial y_2} \right|_{\mathbf{y}=\mathbf{y}_e} & \left. \frac{\partial f_3}{\partial y_3} \right|_{\mathbf{y}=\mathbf{y}_e} & \left. \frac{\partial f_3}{\partial y_4} \right|_{\mathbf{y}=\mathbf{y}_e} \\ \left. \frac{\partial f_4}{\partial y_1} \right|_{\mathbf{y}=\mathbf{y}_e} & \left. \frac{\partial f_4}{\partial y_2} \right|_{\mathbf{y}=\mathbf{y}_e} & \left. \frac{\partial f_4}{\partial y_3} \right|_{\mathbf{y}=\mathbf{y}_e} & \left. \frac{\partial f_4}{\partial y_4} \right|_{\mathbf{y}=\mathbf{y}_e} \end{bmatrix} \quad (4.136)$$

in which

$$f_1 \triangleq u_0 \cdot (w_1 - y_1) \quad (4.137)$$

$$f_2 \triangleq u_0 \cdot (w_2 - y_2) \quad (4.138)$$

$$f_3 \triangleq u_0 \cdot (u_3 - y_3) + \sigma_1(\mathbf{y}) \quad (4.139)$$

$$f_4 \triangleq u_0 \cdot (u_4 - y_4) + \sigma_2(\mathbf{y}) \quad (4.140)$$

with $\sigma_1(\mathbf{y})$ and $\sigma_2(\mathbf{y})$ determined by Eqs. 4.125 and 4.126 respectively. The partial derivatives $\frac{\partial f_1}{\partial y_i}$ and $\frac{\partial f_2}{\partial y_i}$ are constant $\forall i$ (independent of the equilibrium point). As a result, the Jacobian matrix 4.136 becomes

$$\mathbf{J}(\mathbf{y}_e) = \begin{bmatrix} -u_0 & 0 & 0 & 0 \\ 0 & -u_0 & 0 & 0 \\ \left. \frac{\partial f_3}{\partial y_1} \right|_{\mathbf{y}=\mathbf{y}_e} & \left. \frac{\partial f_3}{\partial y_2} \right|_{\mathbf{y}=\mathbf{y}_e} & \left. \frac{\partial f_3}{\partial y_3} \right|_{\mathbf{y}=\mathbf{y}_e} & \left. \frac{\partial f_3}{\partial y_4} \right|_{\mathbf{y}=\mathbf{y}_e} \\ \left. \frac{\partial f_4}{\partial y_1} \right|_{\mathbf{y}=\mathbf{y}_e} & \left. \frac{\partial f_4}{\partial y_2} \right|_{\mathbf{y}=\mathbf{y}_e} & \left. \frac{\partial f_4}{\partial y_3} \right|_{\mathbf{y}=\mathbf{y}_e} & \left. \frac{\partial f_4}{\partial y_4} \right|_{\mathbf{y}=\mathbf{y}_e} \end{bmatrix} \quad (4.141)$$

It is now clear that $\mathbf{J}(\mathbf{y}_e)$ has a double eigenvalue $-u_0$. Its remaining two eigenvalues are the eigenvalues of the 2-dimensional Jacobian matrix

$$\mathbf{J}_{34}(\mathbf{y}_e) = \begin{bmatrix} \left. \frac{\partial f_3}{\partial y_3} \right|_{\mathbf{y}=\mathbf{y}_e} & \left. \frac{\partial f_3}{\partial y_4} \right|_{\mathbf{y}=\mathbf{y}_e} \\ \left. \frac{\partial f_4}{\partial y_3} \right|_{\mathbf{y}=\mathbf{y}_e} & \left. \frac{\partial f_4}{\partial y_4} \right|_{\mathbf{y}=\mathbf{y}_e} \end{bmatrix} \quad (4.142)$$

and should be calculated separately for each equilibrium point. If both eigenvalues of $\mathbf{J}_{34}(\mathbf{y}_e)$ of an equilibrium point of the given system are in the open left phase plane (have strictly negative real parts), the equilibrium point is locally asymptotically stable. This procedure will be followed for all equilibrium points of each of the models studied below.

4.7.2 Simplified model I: no inhibition

The SHARON reactor model is simplified, realistically assuming the incoming stream does not contain any nitrite, ammonium oxidizers or nitrite oxidizers. Further, ammonium limitation of nitrite oxidizers is not considered ($c_2 = 0$). Finally, it is assumed that no inhibition of any kind takes place. This is expressed mathematically as

$$\begin{aligned} u_2 &= u_3 = u_4 = 0 \\ c_2 &= 0 \\ c_1 &= d_2 = e_2 = +\infty \end{aligned}$$

so the canonical state space representation 4.118-4.121 is simplified to

$$\dot{y}_1 = u_0 \cdot (u_1 - y_1) \quad (4.143)$$

$$\dot{y}_2 = -u_0 \cdot y_2 \quad (4.144)$$

$$\dot{y}_3 = -u_0 \cdot y_3 + \sigma_1(\mathbf{y}) \quad (4.145)$$

$$\dot{y}_4 = -u_0 \cdot y_4 + \sigma_2(\mathbf{y}) \quad (4.146)$$

with

$$\sigma_1(\mathbf{y}) = a_1 \cdot \frac{x_1}{b_1 + x_1} \cdot y_3 \quad (4.147)$$

$$\sigma_2(\mathbf{y}) = \begin{cases} a_2 \cdot \frac{x_2}{b_2 + x_2} \cdot y_4 & \text{for } x_1 > 0 \\ 0 & \text{for } x_1 = 0 \end{cases} \quad (4.148)$$

in which

$$x_1 = y_1 - a \cdot y_3 - b \cdot y_4 \quad (4.149)$$

$$x_2 = y_2 + c \cdot y_3 - d \cdot y_4 \quad (4.150)$$

$$x_3 = y_3 \quad (4.151)$$

$$x_4 = y_4 \quad (4.152)$$

Equilibrium points in case $u_1 = 0$

In case the influent does not contain ammonium ($u_1 = 0$), it follows from Eqs. 4.143, 4.144, 4.149 and 4.150 that

$$\dot{y} = 0 \Leftrightarrow y_{e1} = y_{e2} = y_{e3} = y_{e4} = 0 \Leftrightarrow x_{e1} = x_{e2} = x_{e3} = x_{e4} = 0$$

indicating a unique (trivial) equilibrium point corresponding with biomass wash-out.

Equilibrium points in case $u_0 > 0$ and $u_1 > 0$

As the cases $u_0 = 0$ and $u_1 = 0$ have already been considered in section 4.4.2 and in this section respectively, the equilibrium points of the SHARON reactor model with constant pH will now be calculated for $u_0 > 0$ and $u_1 > 0$. In this case, there exists no equilibrium point for which $x_{e1} = 0$. Indeed:

$$\begin{aligned} (4.147), (4.148) \quad (4.145), (4.146) \quad (4.149) \\ x_{e1} = 0 \Rightarrow \sigma_1(\mathbf{y}_e) = \sigma_2(\mathbf{y}_e) = 0 \Rightarrow y_{e3} = y_{e4} = 0 \Rightarrow y_{e1} = 0 \\ (4.143) \\ \Rightarrow u_0 \cdot u_1 = 0 \end{aligned}$$

Consequently, it results from Eqs. 4.143-4.148 that the equilibrium points fulfill the following set of equations:

$$y_{e1} = u_1 \quad (4.153)$$

$$y_{e2} = 0 \quad (4.154)$$

$$\left(-u_0 + a_1 \cdot \frac{x_{e1}}{b_1 + x_{e1}} \right) \cdot y_{e3} = 0 \quad (4.155)$$

$$\left(-u_0 + a_2 \cdot \frac{x_{e2}}{b_2 + x_{e2}} \right) \cdot y_{e4} = 0 \quad (4.156)$$

It can be shown that $y_{e3} = 0$ also implies $y_{e4} = 0$. As a result, three equilibrium points are obtained:

1. The first equilibrium point corresponds with $y_{e3} = y_{e4} = 0$:

$$\mathbf{y}_e^{\mathbf{A},\mathbf{I}} = \begin{bmatrix} u_1 \\ 0 \\ 0 \\ 0 \end{bmatrix} \Leftrightarrow \mathbf{x}_e^{\mathbf{A},\mathbf{I}} = \begin{bmatrix} u_1 \\ 0 \\ 0 \\ 0 \end{bmatrix} \quad (4.157)$$

This equilibrium point, corresponding with biomass wash-out, is always a physical equilibrium point.

2. The second equilibrium point corresponds with $y_{e4} = 0$, while $y_{e3} \neq 0$:

$$\mathbf{y}_e^{\mathbf{B},\mathbf{I}} = \begin{bmatrix} u_1 \\ 0 \\ \frac{1}{a} \cdot \left(u_1 - \frac{b_1 \cdot u_0}{a_1 - u_0} \right) \\ 0 \end{bmatrix} \\ \Leftrightarrow \mathbf{x}_e^{\mathbf{B},\mathbf{I}} = \begin{bmatrix} \frac{b_1 \cdot u_0}{a_1 - u_0} \\ \frac{c}{a} \cdot \left(u_1 - \frac{b_1 \cdot u_0}{a_1 - u_0} \right) \\ \frac{1}{a} \cdot \left(u_1 - \frac{b_1 \cdot u_0}{a_1 - u_0} \right) \\ 0 \end{bmatrix} \quad (4.158)$$

This equilibrium point is a physical equilibrium point, i.e. $y_{ei}^{\mathbf{B},\mathbf{I}} > 0$ and $x_{ei}^{\mathbf{B},\mathbf{I}} > 0$, $i = 1, \dots, 4$, if and only if

$$u_0 < \frac{a_1 \cdot u_1}{b_1 + u_1} \\ \Leftrightarrow \\ u_1 > \frac{b_1 \cdot u_0}{a_1 - u_0} \quad \text{and} \quad u_0 < a_1 \quad (4.159)$$

This equilibrium point corresponds with a situation without nitrite oxidizers ($x_{e4}^{\mathbf{B},\mathbf{I}} = 0$) and consequently without nitrate production. This is exactly the aim of a SHARON reactor.

In case $u_0 = \frac{a_1 \cdot u_1}{b_1 + u_1}$, $\mathbf{y}_e^{\mathbf{B},\mathbf{I}}$ coincides with $\mathbf{y}_e^{\mathbf{A},\mathbf{I}}$, the wash-out equilibrium point.

3. The third equilibrium point corresponds with both $y_{e3} \neq 0$ and $y_{e4} \neq 0$:

$$\begin{aligned} \mathbf{y}_e^{C,I} &= \begin{bmatrix} u_1 \\ 0 \\ \frac{d \cdot (u_1 - x_{e1}^{C,I}) + b \cdot x_{e2}^{C,I}}{a \cdot d + b \cdot c} \\ \frac{c \cdot (u_1 - x_{e1}^{C,I}) - a \cdot x_{e2}^{C,I}}{a \cdot d + b \cdot c} \end{bmatrix} \\ \Leftrightarrow \mathbf{x}_e^{C,I} &= \begin{bmatrix} \frac{b_1 \cdot u_0}{a_1 - u_0} \\ \frac{b_2 \cdot u_0}{a_2 - u_0} \\ \frac{d \cdot (u_1 - x_{e1}^{C,I}) + b \cdot x_{e2}^{C,I}}{a \cdot d + b \cdot c} \\ \frac{c \cdot (u_1 - x_{e1}^{C,I}) - a \cdot x_{e2}^{C,I}}{a \cdot d + b \cdot c} \end{bmatrix} \end{aligned} \quad (4.160)$$

The equilibrium point $\mathbf{x}_e^{C,I}$ is a physical equilibrium point if and only if Eq. 4.159 is fulfilled, i.e. if $\mathbf{x}_e^{B,I}$ is a physical equilibrium point, and if at the same time

$$\begin{aligned} u_0 &< \frac{a_2 \cdot \frac{c}{a} \cdot (u_1 - \frac{b_1 \cdot u_0}{a_1 - u_0})}{b_2 + \frac{c}{a} \cdot (u_1 - \frac{b_1 \cdot u_0}{a_1 - u_0})} \\ &\Leftrightarrow \\ u_1 &> \frac{b_1 \cdot u_0}{a_1 - u_0} + \frac{a}{c} \cdot \frac{b_2 \cdot u_0}{a_2 - u_0} \text{ and } u_0 < a_2 \end{aligned} \quad (4.161)$$

Taking into account that the growth rate of ammonium oxidizers is larger than that of nitrite oxidizers ($a_1 > a_2$) at the prevailing temperatures in a SHARON reactor, it is clear that condition 4.161 is more stringent than condition 4.159. This means that the occurrence of $\mathbf{y}_e^{C,I}$ implies the occurrence of $\mathbf{y}_e^{B,I}$, while $\mathbf{y}_e^{B,I}$ can be a physical equilibrium point without $\mathbf{y}_e^{C,I}$ being one. The equilibrium point $\mathbf{x}_e^{C,I}$ corresponds with a situation with both ammonium and nitrite oxidizers ($x_{e3}^{C,I}, x_{e4}^{C,I} \neq 0$), which means that at least part of the formed nitrite will be further oxidized to nitrate.

The equilibrium concentration of ammonium is the same for the equilibrium points $\mathbf{y}_e^{\text{B,I}}$ and $\mathbf{y}_e^{\text{C,I}}$: $x_{e1}^{\text{B,I}} = x_{e1}^{\text{C,I}}$.

$$\text{In case } u_0 = \frac{a_2 \cdot \frac{c}{a} \cdot (u_1 - x_{e1}^{\text{C,I}})}{b_2 + \frac{c}{a} \cdot (u_1 - x_{e1}^{\text{C,I}})}, \mathbf{y}_e^{\text{C,I}} \text{ coincides with } \mathbf{y}_e^{\text{B,I}}.$$

Figure 4.6 shows the occurrence of equilibrium points in terms of the dilution rate u_0 and the influent ammonium concentration u_1 . For high dilution rates or low influent ammonium concentrations, only the wash-out equilibrium $\mathbf{y}_e^{\text{A,I}}$ occurs. This corresponds with the findings of section 4.5. As the dilution rate decreases, a second equilibrium point $\mathbf{y}_e^{\text{B,I}}$ appears, corresponding with only nitrite production. If the dilution rate becomes sufficiently low, also a third equilibrium point $\mathbf{y}_e^{\text{C,I}}$ occurs. The maximum values of the dilution rate below which a second or a third equilibrium point occur, increase with increasing influent ammonium concentration u_1 . This means that u_0 must be sufficiently low and u_1 sufficiently large to obtain a second or a third equilibrium point.

Local asymptotic stability of equilibrium points

The local asymptotic stability of the equilibrium points of model I is assessed using the linearization principle. Taking into account the kinetic rate expressions 4.147 and 4.148 for this simplified model, the expressions for the partial derivatives in the reduced Jacobian matrix 4.142 become:

$$\frac{\partial f_3}{\partial y_3} = -u_0 + a_1 \cdot \frac{x_1}{b_1 + x_1} - a_1 \cdot y_3 \cdot \frac{b_1 \cdot a}{(b_1 + x_1)^2} \quad (4.162)$$

$$\frac{\partial f_3}{\partial y_4} = -a_1 \cdot y_3 \cdot \frac{b_1 \cdot b}{(b_1 + x_1)^2} \quad (4.163)$$

$$\frac{\partial f_4}{\partial y_3} = a_2 \cdot y_4 \cdot \frac{b_2 \cdot c}{(b_2 + x_2)^2} \quad (4.164)$$

$$\frac{\partial f_4}{\partial y_4} = -u_0 + a_2 \cdot \frac{x_2}{b_2 + x_2} - a_2 \cdot y_4 \cdot \frac{b_2 \cdot d}{(b_2 + x_2)^2} \quad (4.165)$$

Subsequently, the expressions 4.162-4.165 are evaluated in each of the three equilibrium points. The position of the eigenvalues of the resulting reduced Jacobian matrix 4.142 then determines the stability of the corresponding equilibrium point.

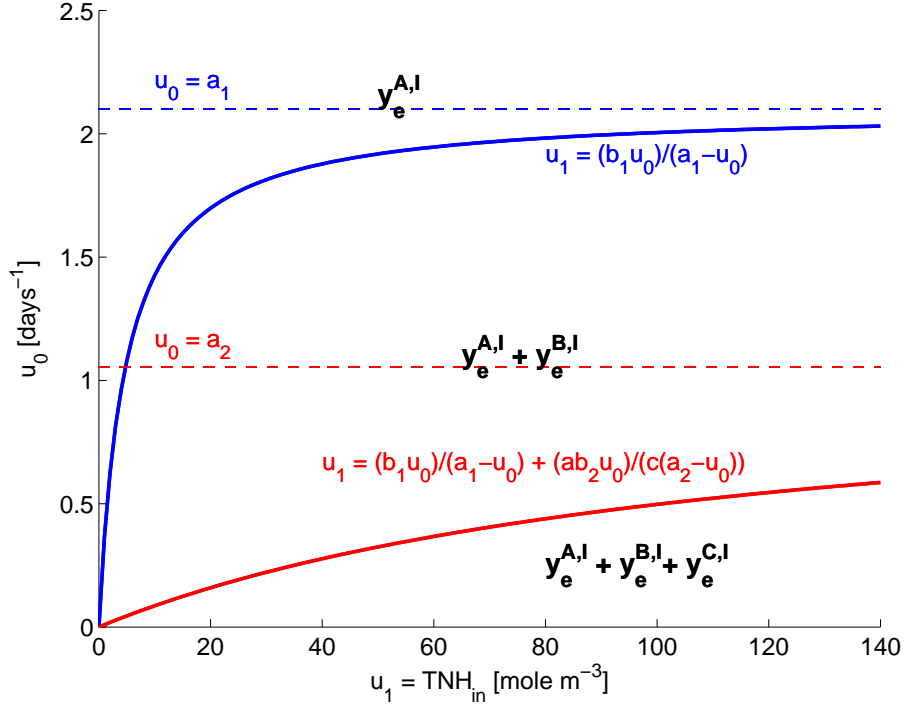


Figure 4.6: Equilibrium points of model I in terms of $u_0 = \Phi_{in}/V$ and $u_1 = C_{TNH}^{in}$

For the wash-out equilibrium point, $y_e^{A,I}$, the reduced Jacobian matrix becomes

$$\mathbf{J}_{34}(y_e^{A,I}) = \begin{bmatrix} -u_0 + \frac{a_1 \cdot u_1}{b_1 + u_1} & 0 \\ 0 & -u_0 \end{bmatrix} \quad (4.166)$$

It is clear that both eigenvalues of $\mathbf{J}_{34}(y_e^{A,I})$ are strictly negative in case $u_0 > \frac{a_1 \cdot u_1}{b_1 + u_1}$. This corresponds with the case in which $y_e^{A,I}$ is the only physical equilibrium point, i.e. when 4.159 is *not* fulfilled. $y_e^{A,I}$ is then locally asymptotically stable. However, even a more general conclusion can be drawn, taking into account that every trajectory inside a bounded region should converge to either an equilibrium point, or a limit cycle. According to the theory of the index (Jordan and Smith, 1977, Chapter 3), a limit cycle cannot surround a region containing no equilibrium points. But no limit cycle can occur around the equilibrium point $y_e^{A,I}$, that is lying on the boundary of S_y , since this would imply

that a trajectory is leaving the system's state space Δ , which is impossible. Consequently, all trajectories starting in S_y converge to $y_e^{A,I}$. As a result, in case $y_e^{A,I}$ is the only equilibrium point, $y_e^{A,I}$ is also globally asymptotically stable in the sense that every trajectory starting in the interior of S_y converges to $y_e^{A,I}$ as $t \rightarrow +\infty$.

On the other hand, in case 4.159 is fulfilled, corresponding with a situation in which at least one other physical equilibrium point exists besides $y_e^{A,I}$, $y_e^{A,I}$ is unstable with index 1. In this case only trajectories on the y_4 -axis converge to $y_e^{A,I}$. However, these trajectories are not located within the physical boundaries of the system.

For the equilibrium point $y_e^{B,I}$ corresponding with only nitrite production, one calculates $\left. \frac{\partial f_4}{\partial y_3} \right|_{y=y_e^{B,I}} = 0$. As a result, the eigenvalues of the reduced Jacobian matrix equal its diagonal elements

$$\left. \frac{\partial f_3}{\partial y_3} \right|_{y=y_e^{B,I}} = - \left(u_1 - \frac{b_1 \cdot u_0}{a_1 - u_0} \right) \cdot \frac{a_1 \cdot b_1}{(b_1 + x_{e1}^{B,I})^2} \quad (4.167)$$

and

$$\left. \frac{\partial f_4}{\partial y_4} \right|_{y=y_e^{B,I}} = -u_0 + a_2 \cdot \frac{\frac{c}{a} \cdot \left(u_1 - \frac{b_1 \cdot u_0}{a_1 - u_0} \right)}{b_2 + \frac{c}{a} \cdot \left(u_1 - \frac{b_1 \cdot u_0}{a_1 - u_0} \right)} \quad (4.168)$$

The eigenvalue 4.167 is strictly negative in case $u_1 > \frac{b_1 \cdot u_0}{a_1 - u_0}$ and $u_0 < a_1$, which is equivalent to the condition 4.159 for $y_e^{B,I}$ to be a physical equilibrium point. The eigenvalue 4.168 is strictly negative in case $u_0 >$

$a_2 \cdot \frac{\frac{c}{a} \cdot \left(u_1 - \frac{b_1 \cdot u_0}{a_1 - u_0} \right)}{b_2 + \frac{c}{a} \cdot \left(u_1 - \frac{b_1 \cdot u_0}{a_1 - u_0} \right)}$, corresponding with the situation in which

$y_e^{C,I}$ is not a physical equilibrium point (see Eq. 4.161). As a result, the equilibrium point $y_e^{B,I}$ is locally asymptotically stable if and only if it is the only physical equilibrium point besides $y_e^{A,I}$. As $y_e^{B,I}$ lies on the boundary of system's state space, no limit cycle can occur around this equilibrium point. As a result, $y_e^{B,I}$ is then *quasi* globally asymptotically stable, in the sense that all trajectories starting inside S_y converge to $y_e^{B,I}$, except for the trajectory consisting of the point $y_e^{A,I}$.

In case the system possesses three equilibrium points, $y_e^{B,I}$ is unstable with index 1: only trajectories on the y_3 -axis converge to $y_e^{B,I}$.

For the equilibrium point $\mathbf{y}_e^{C,I}$, corresponding with nitrate formation, the reduced Jacobian matrix can be written as

$$\mathbf{J}_{34}(\mathbf{y}_e^{C,I}) = \begin{bmatrix} -\gamma \cdot a & -\gamma \cdot b \\ \zeta \cdot c & -\zeta \cdot d \end{bmatrix} \quad (4.169)$$

in which

$$\gamma \triangleq a_1 \cdot y_{e3}^{C,I} \cdot \frac{b_1}{(b_1 + x_{e1}^{C,I})^2} > 0 \quad (4.170)$$

$$\zeta \triangleq a_2 \cdot y_{e4}^{C,I} \cdot \frac{b_2}{(b_2 + x_{e2}^{C,I})^2} > 0 \quad (4.171)$$

The eigenvalues of $\mathbf{J}_{34}(\mathbf{y}_e^{C,I})$ are the solutions of the equation

$$s^2 + (\gamma \cdot a + \zeta \cdot d) \cdot s + \gamma \cdot \zeta \cdot (a \cdot d + b \cdot c) = 0 \quad (4.172)$$

It is clear that the sum of the eigenvalues is always negative, while their product is positive. This means that both eigenvalues always have strictly negative real parts, so the equilibrium point $\mathbf{y}_e^{C,I}$ is locally asymptotically stable. In case $\mathbf{y}_e^{C,I}$ is not surrounded by a limit cycle (this will be verified through simulation), all solutions that start in \mathbf{S}_y will converge to $\mathbf{y}_e^{C,I}$, except for the trajectories for $y_4(t=0) = 0$. The latter converge to $\mathbf{y}_e^{B,I}$, except for the trajectory coinciding with $\mathbf{y}_e^{A,I}$. In this sense, $\mathbf{y}_e^{C,I}$ is quasi globally asymptotically stable.

Phase trajectories of the system

From an arbitrary starting value in \mathbf{S}_y , every trajectory of the system defined by Model I converges to the cross-section Δ of \mathbf{S}_y with the plane $\{y_1 = w_1 = u_1, y_2 = w_2 = 0\}$, described by the inequalities 4.132-4.135 in which now $w_1 = u_1$ and $w_2 = 0$:

$$u_1 - a \cdot y_3 - b \cdot y_4 \geq 0 \quad (4.173)$$

$$c \cdot y_3 - d \cdot y_4 \geq 0 \quad (4.174)$$

$$y_3 \geq 0 \quad (4.175)$$

$$y_4 \geq 0 \quad (4.176)$$

After reaching convergence, the system's behaviour is governed by the dynamics of y_3 and y_4 . Figure 4.7 shows the system boundaries, the

equilibrium points and trajectory fields in Δ for different values of the dilution rate u_0 and the influent ammonium concentration u_1 . The system boundaries are only dependent on u_1 (note the different scales for different u_1 values). The simulation results confirm the calculations in terms of the number of equilibrium points, their values as well as their stability.

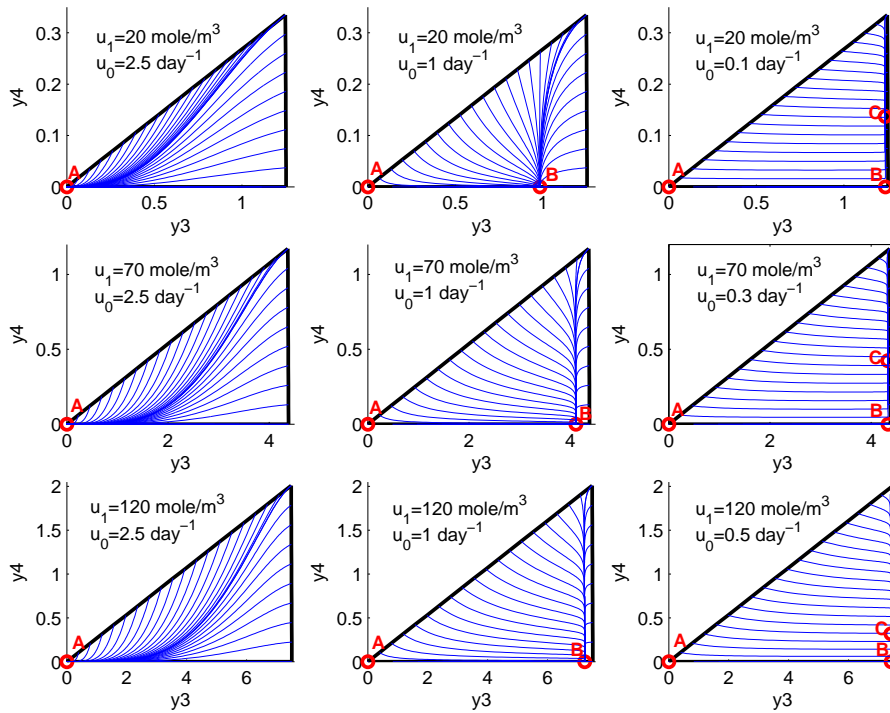


Figure 4.7: Trajectory fields for model I in terms of u_0 and u_1

For high values of the dilution rate ($u_0 = 2.5 \text{ day}^{-1}$), only the equilibrium point $y_e^{A,I}$, corresponding with biomass wash-out occurs and is globally asymptotically stable. For lower values of the dilution rate ($u_0 = 1 \text{ day}^{-1}$), the equilibrium point $y_e^{A,I}$ is no longer the only equilibrium point and becomes unstable. Within the physical boundaries of the system, there aren't any trajectories that converge to $y_e^{A,I}$ (except from the point $y_e^{A,I}$ itself), which means that biomass wash-out will not occur no matter what the initial values of the system's states are. If the dilution rate is still sufficiently high, only the equilibrium point $y_e^{B,I}$, corresponding with only nitrite production (and therefore lying on the

y_3 -axis since no nitrite oxidizers are present) appears besides $y_e^{A,I}$ and is asymptotically stable. If the dilution rate becomes even lower, $y_e^{B,I}$ becomes unstable and a third equilibrium point $y_e^{C,I}$, appears. The simulation results indicate that no limit cycle occurs around $y_e^{C,I}$, which means that this equilibrium point is quasi globally asymptotically stable. In this case nitrite oxidizers grow in the system so nitrate will be produced. However, since $y_e^{B,I}$ has stability index 1 there is one situation in which only nitrite will be produced, namely when initially no nitrite oxidizers are present in the system ($y_4(t=0) = 0$). Indeed, trajectories starting on the y_3 -axis converge to $y_e^{B,I}$ (except for $y_e^{B,I}$). This was to be expected, since nitrite oxidizers are not present in the reactor influent: $u_4 = 0$.

The main advantages of a SHARON reactor are established when only nitrite and no nitrate is formed. To obtain this result, one needs to set the dilution rate u_0 (according to the influent ammonium concentration u_1 , which mostly cannot be controlled) in such a way that the equilibrium point $y_e^{B,I}$ is the only equilibrium point and locally asymptotically stable.

Conclusions

For a simplified SHARON reactor model, without inhibition, the equilibrium points have been calculated directly. Three different cases are distinguished:

1. For high dilution rates u_0 or low influent ammonium concentrations u_1 :

$$\frac{a_1 \cdot u_1}{b_1 + u_1} < u_0$$

only one equilibrium point ($y_e^{A,I}$, Eq. 4.157) occurs, corresponding with biomass wash-out. This equilibrium point is globally asymptotically stable.

2. For moderately high dilution rates u_0 and somewhat high influent ammonium concentrations u_1 :

$$\frac{a_2 \cdot \frac{c}{a} \cdot \left(u_1 - \frac{b_1 \cdot u_0}{a_1 - u_0}\right)}{b_2 + \frac{c}{a} \cdot \left(u_1 - \frac{b_1 \cdot u_0}{a_1 - u_0}\right)} < u_0 < \frac{a_1 \cdot u_1}{b_1 + u_1}$$

the system possesses two physical equilibrium points. These are

- the wash-out equilibrium point $y_e^{A,I}$, that is now unstable with index 1. This means that within the physical boundaries of the system, only the trajectory consisting of the point $y_e^{A,I}$, stays in this point. This corresponds with a situation in which initially no biomass is present in the reactor.
 - an equilibrium point $y_e^{B,I}$ (Eq. 4.158), corresponding with only nitrite formation. This equilibrium point is quasi globally asymptotically stable, in the sense that all trajectories within the physical boundaries of the system converge to this point, except from the equilibrium point $y_e^{A,I}$.
3. For sufficiently low dilution rates u_0 and corresponding influent ammonium concentrations u_1 :

$$u_0 < \frac{a_2 \cdot \frac{c}{a} \cdot (u_1 - \frac{b_1 \cdot u_0}{a_1 - u_0})}{b_2 + \frac{c}{a} \cdot (u_1 - \frac{b_1 \cdot u_0}{a_1 - u_0})}$$

three equilibrium points occur, namely

- the wash-out equilibrium point $y_e^{A,I}$, that is still unstable with index 1. Within the physical boundaries of the system, there are no trajectories converging to $y_e^{A,I}$, except for the trajectory consisting of the point $y_e^{A,I}$ itself, which stays in this point, corresponding with a situation in which initially no biomass is present in the reactor.
- the equilibrium point $y_e^{B,I}$, corresponding with only nitrite formation. This equilibrium point is also unstable with index 1: only trajectories on the y_3 -axis converge to $y_e^{B,I}$. This corresponds with a reactor in which initially only ammonium oxidizers are present (note that this model assumes that the influent does not contain biomass).
- an equilibrium point $y_e^{C,I}$ (Eq. 4.160), corresponding with nitrate formation, while the ammonium conversion is the same as for $y_e^{B,I}$. The equilibrium point $y_e^{C,I}$ is quasi globally asymptotically stable, in the sense that all trajectories within the physical boundaries of the system converge to this point, except for the equilibrium point $y_e^{A,I}$ and the trajectories on the y_3 -axis.

4.7.3 Simplified model II: nitrite inhibition of ammonium oxidation

This SHARON reactor model adds nitrite inhibition of ammonium oxidation to the model from section 4.7.2, which means that now $c_1 \neq \infty$. The canonical state space representation is still given by Eqs. 4.143-4.146 but the reaction rates in these equations are now given by

$$\sigma_1(\mathbf{y}) = a_1 \cdot \frac{x_1}{b_1 + x_1} \cdot \frac{c_1}{c_1 + x_2} \cdot y_3 \quad (4.177)$$

$$\sigma_2(\mathbf{y}) = \begin{cases} a_2 \cdot \frac{x_2}{b_2 + x_2} \cdot y_4 & \text{for } x_1 > 0 \\ 0 & \text{for } x_1 = 0 \end{cases} \quad (4.178)$$

for which Eqs. 4.149-4.152 are still valid.

Equilibrium points in case $u_0 > 0$ and $u_1 > 0$

In case no ammonium is present in the influent ($u_1 = 0$), the same reasoning as in section 4.7.2 holds, indicating a unique (trivial) equilibrium point corresponding with biomass wash-out. So in the following, the equilibrium points of the SHARON reactor model with constant pH will be calculated for $u_0 > 0$ and $u_1 > 0$. It is again easy to show that, in this case, there exists no equilibrium point for which $x_{e1} = 0$. Consequently, it results from Eqs. 4.143-4.146 and 4.177-4.178 that the equilibrium points fulfill the following set of equations:

$$y_{e1} = u_1 \quad (4.179)$$

$$y_{e2} = 0 \quad (4.180)$$

$$\left(-u_0 + a_1 \cdot \frac{x_{e1}}{b_1 + x_{e1}} \cdot \frac{c_1}{c_1 + x_{e2}} \right) \cdot y_{e3} = 0 \quad (4.181)$$

$$\left(-u_0 + a_2 \cdot \frac{x_{e2}}{b_2 + x_{e2}} \right) \cdot y_{e4} = 0 \quad (4.182)$$

Just like in section 4.7.2, three equilibrium points are obtained:

1. A wash-out equilibrium point, that always occurs and is the same as for model I (section 4.7.2):

$$\mathbf{y}_e^{\text{A,II}} = \begin{bmatrix} u_1 \\ 0 \\ 0 \\ 0 \end{bmatrix} \Leftrightarrow \mathbf{x}_e^{\text{A,II}} = \begin{bmatrix} u_1 \\ 0 \\ 0 \\ 0 \end{bmatrix} \quad (4.183)$$

2. An equilibrium point that corresponds with a situation without nitrite oxidizers and consequently without nitrate production:

$$\begin{aligned}
 \mathbf{y}_e^{B,II} &= \begin{bmatrix} u_1 \\ 0 \\ \frac{1}{a} \cdot (u_1 - x_{e1}^{B,II}) \\ 0 \end{bmatrix} \\
 \Leftrightarrow \mathbf{x}_e^{B,II} &= \begin{bmatrix} x_{e1}^{B,II} \\ \frac{c}{a} \cdot (u_1 - x_{e1}^{B,II}) \\ \frac{1}{a} \cdot (u_1 - x_{e1}^{B,II}) \\ 0 \end{bmatrix}
 \end{aligned} \tag{4.184}$$

in which $x_{e1}^{B,II}$ is obtained from

$$a_1 \cdot \frac{x_{e1}^{B,II}}{b_1 + x_{e1}^{B,II}} \cdot \frac{c_1}{c_1 + \frac{c}{a} \cdot (u_1 - x_{e1}^{B,II})} = u_0 \tag{4.185}$$

It can be seen that

$$x_{e1}^{B,II} > x_{e1}^{B,I} \quad \text{and} \quad x_{e2}^{B,II} < x_{e2}^{B,I} \tag{4.186}$$

which means that the ammonium concentration will be higher and the nitrite concentration will be lower for model II than for model I. This is exactly what is to be expected, since inhibition of the ammonium oxidation by its product nitrite leads to less ammonium conversion. The condition for this equilibrium point to be a physical equilibrium point is the same as for model I:

$$\begin{aligned}
 u_0 &< \frac{a_1 \cdot u_1}{b_1 + u_1} \\
 &\Leftrightarrow \\
 u_1 &> \frac{b_1 \cdot u_0}{a_1 - u_0} \quad \text{and} \quad u_0 < a_1
 \end{aligned} \tag{4.187}$$

Again, in case $u_0 = \frac{a_1 \cdot u_1}{b_1 + u_1}$, $\mathbf{y}_e^{B,II}$ coincides with $\mathbf{y}_e^{A,II}$, the wash-out equilibrium point.

3. The third equilibrium point corresponds with a situation with both ammonium oxidizers and nitrite oxidizers, in which at least part of the formed nitrite is further oxidized to nitrate:

$$\begin{aligned}
 \mathbf{y}_e^{C,II} &= \begin{bmatrix} u_1 \\ 0 \\ \frac{d \cdot (u_1 - x_{e1}^{C,II}) + b \cdot x_{e2}^{C,II}}{a \cdot d + b \cdot c} \\ \frac{c \cdot (u_1 - x_{e1}^{C,II}) - a \cdot x_{e2}^{C,II}}{a \cdot d + b \cdot c} \end{bmatrix} \\
 \Leftrightarrow \mathbf{x}_e^{C,II} &= \begin{bmatrix} \frac{b_1 \cdot f(u_0)}{a_1 - f(u_0)} \\ \frac{b_2 \cdot u_0}{a_2 - u_0} \\ \frac{d \cdot (u_1 - x_{e1}^{C,II}) + b \cdot x_{e2}^{C,II}}{a \cdot d + b \cdot c} \\ \frac{c \cdot (u_1 - x_{e1}^{C,II}) - a \cdot x_{e2}^{C,II}}{a \cdot d + b \cdot c} \end{bmatrix} \quad (4.188)
 \end{aligned}$$

in which

$$f(u_0) = u_0 + \frac{b_2 \cdot u_0^2}{c_1 \cdot (a_2 - u_0)} \quad (4.189)$$

Note that $f(u_0) > u_0$ (as $a_2 > u_0$ for a physical $x_{e2}^{C,II}$) and $f(u_0) \approx u_0$ for small u_0 -values. It is clear that

$$x_{e2}^{C,II} = x_{e2}^{C,I} \quad \text{and} \quad x_{e1}^{C,II} > x_{e1}^{C,I} \quad (4.190)$$

which means that in case of nitrite inhibition of ammonium oxidation (model II), less ammonium will be converted but the same amount of nitrite will be formed, so less nitrate will be formed compared to the case without inhibition (model I).

This equilibrium point is a physical equilibrium point if and only if

$$u_1 > \frac{b_1 \cdot f(u_0)}{a_1 - f(u_0)} + \frac{a}{c} \cdot \frac{b_2 \cdot u_0}{a_2 - u_0} \quad (4.191)$$

It can be shown that the curve defined by Eq. 4.191 has a horizontal asymptote, \hat{u}_0 , that is the unique solution of

$$(c_1 - b_2) \cdot \hat{u}_0^2 - c_1 \cdot (a_1 + a_2) \cdot \hat{u}_0 + c_1 \cdot a_1 \cdot a_2 = 0 \quad (4.192)$$

in the interval $0 < \hat{u}_0 < a_2$ and for which $a_1 = f(\hat{u}_0)$ holds. As $f(u_0) > u_0$, the condition for the occurrence of a third equilibrium point is (slightly) more stringent in a system described by model II (Eq. 4.191) than in a system described by model I (Eq. 4.161). In case there is no nitrite inhibition ($c_1 = +\infty$), $f(u_0) = u_0$ and $\hat{u}_0 = a_2$, so both conditions are equivalent. In this way, a continuous transient exists between model I and model II. It can be shown that $\mathbf{y}_e^{\text{C,II}}$ and $\mathbf{y}_e^{\text{B,II}}$ coincide if

$$u_1 = \frac{b_1 \cdot f(u_0)}{a_1 - f(u_0)} + \frac{a}{c} \cdot \frac{b_2 \cdot u_0}{a_2 - u_0}$$

In case $\mathbf{y}_e^{\text{C,II}}$ and $\mathbf{y}_e^{\text{B,II}}$ are distinctive physical equilibrium points, it is found that the ammonium concentration corresponding with $\mathbf{y}_e^{\text{C,II}}$ is slightly lower than for $\mathbf{y}_e^{\text{B,II}}$: as some nitrite is further oxidized to nitrate in $\mathbf{y}_e^{\text{C,II}}$, less nitrite is present, so the corresponding microbial growth rate, that includes nitrite inhibition, is higher, resulting in a (slightly) higher ammonium conversion. This was not the case for model I (without inhibition), where the ammonium concentration is the same for both equilibrium points $\mathbf{y}_e^{\text{C,I}}$ and $\mathbf{y}_e^{\text{B,I}}$.

Figure 4.8 shows the occurrence of equilibrium points in terms of the dilution rate u_0 and the influent ammonium concentration u_1 . For high dilution rates, only the wash-out equilibrium $\mathbf{y}_e^{\text{A,II}}$ occurs. The boundary conditions for the appearance of a second equilibrium point $\mathbf{y}_e^{\text{B,II}}$, corresponding with only nitrite production, are exactly the same as for model I (Fig. 4.6). The condition for the occurrence of a third equilibrium point $\mathbf{y}_e^{\text{C,II}}$ is more stringent for model II than for model I. This is clear when comparing Figures 4.6 and 4.8: the curve for model II lies below the one for model I, which means the third equilibrium point will be obtained for (just a little) lower values of the dilution rate and (just a little) higher values of the influent ammonium concentration. This difference becomes larger for stronger inhibition kinetics (lower c_1 values).

Local asymptotic stability of equilibrium points

The linearization principle is used again to assess the local asymptotic stability of the equilibrium points.

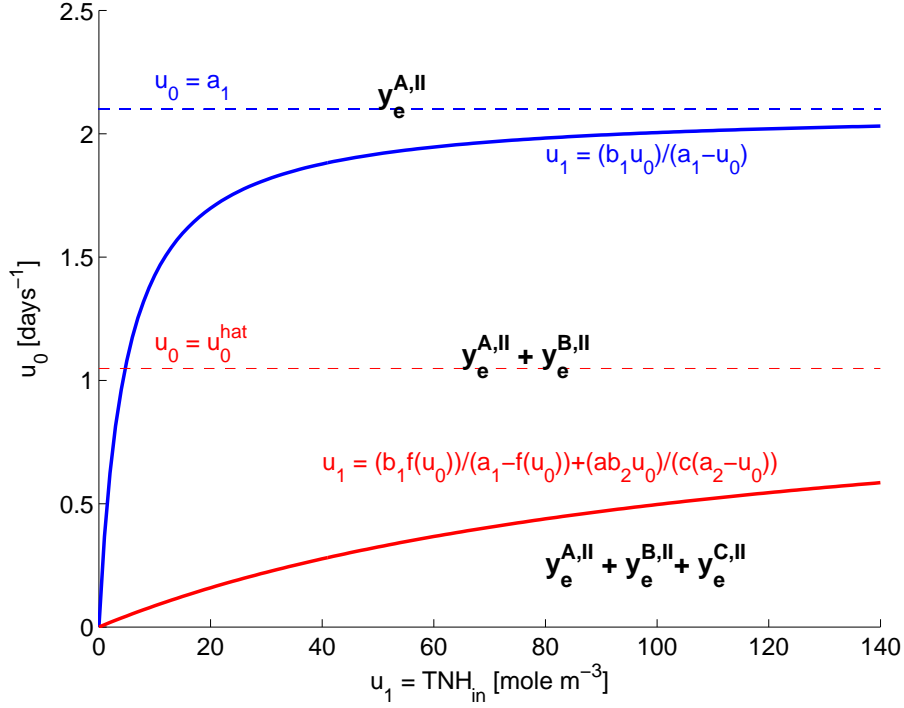


Figure 4.8: Equilibrium points of model II in terms of $u_0 = \Phi_{in}/V$ and $u_1 = C_{TNH}^{in}$

The expressions for the partial derivatives of f_3 in the reduced Jacobian matrix 4.142, evaluated for the kinetic rate expressions 4.177 and 4.178, become

$$\begin{aligned} \frac{\partial f_3}{\partial y_3} &= -u_0 + a_1 \cdot \frac{x_1}{b_1 + x_1} \cdot \frac{c_1}{c_1 + x_2} \\ &\quad - a_1 \cdot y_3 \cdot a \cdot \frac{b_1}{(b_1 + x_1)^2} \cdot \frac{c_1}{(c_1 + x_2)} \\ &\quad - a_1 \cdot y_3 \cdot c \cdot \frac{x_1}{(b_1 + x_1)} \cdot \frac{c_1}{(c_1 + x_2)^2} \end{aligned} \quad (4.193)$$

$$\begin{aligned} \frac{\partial f_3}{\partial y_4} &= -a_1 \cdot b \cdot y_3 \cdot \frac{b_1}{(b_1 + x_1)^2} \cdot \frac{c_1}{(c_1 + x_2)} \\ &\quad + a_1 \cdot d \cdot y_3 \cdot \frac{x_1}{(b_1 + x_1)} \cdot \frac{c_1}{(c_1 + x_2)^2} \end{aligned} \quad (4.194)$$

The expressions 4.164 and 4.165 for the partial derivatives of f_4 remain valid.

For the wash-out equilibrium point, $\mathbf{y}_e^{A,II}$, the same reduced Jacobian matrix (Eq. 4.166) as for model I is obtained. Both eigenvalues of this matrix are strictly negative in case $u_0 > \frac{a_1 \cdot u_1}{b_1 + u_1}$. As for model I, this corresponds with the case in which $\mathbf{y}_e^{A,II}$ is the only physical equilibrium point, i.e. when 4.187 is *not* fulfilled. In this case, $\mathbf{y}_e^{A,II}$ is globally asymptotically stable: every trajectory starting in the interior of \mathbf{S}_y converges to $\mathbf{y}_e^{A,II}$ as $t \rightarrow +\infty$. On the other hand, in case at least one other physical equilibrium point exists besides $\mathbf{y}_e^{A,II}$ (i.e. 4.187 fulfilled), $\mathbf{y}_e^{A,II}$ is unstable with index 1: only trajectories on the y_4 -axis converge to $\mathbf{y}_e^{A,II}$ but these trajectories are not located within the physical boundaries of the system.

For the equilibrium point $\mathbf{y}_e^{B,II}$ corresponding with only nitrite production, the eigenvalues of the reduced Jacobian matrix equal its diagonal elements

$$\begin{aligned} \left. \frac{\partial f_3}{\partial y_3} \right|_{\mathbf{y}=\mathbf{y}_e^{B,II}} &= -a_1 \cdot (u_1 - x_{e1}^{B,II}) \cdot \left[\frac{b_1}{(b_1 + x_{e1}^{B,II})^2} \cdot \frac{c_1}{(c_1 + x_{e2}^{B,II})} \right. \\ &\quad \left. + \left(\frac{u_0}{a_1} + \frac{u_0 \cdot c}{a \cdot a_1 \cdot c_1} \cdot (u_1 - x_{e1}^{B,II}) \right) \cdot \frac{c_1 \cdot c}{(c_1 + x_{e1}^{B,II}) \cdot a} \right] \end{aligned} \quad (4.195)$$

and

$$\left. \frac{\partial f_4}{\partial y_4} \right|_{\mathbf{y}=\mathbf{y}_e^{B,II}} = -u_0 + a_2 \cdot \frac{x_{e2}^{B,II}}{b_2 + x_{e2}^{B,II}} \quad (4.196)$$

The eigenvalue 4.195 is strictly negative in case $x_{e1}^{B,II} < u_1$. This condition is fulfilled for each physical equilibrium point. The eigenvalue 4.196 has been found strictly negative in case $u_0 > a_2$ or in case $u_0 < a_2$ and $u_1 < \frac{b_1 \cdot f(u_0)}{a_1 - f(u_0)} + \frac{a}{c} \cdot \frac{b_2 \cdot u_0}{a_2 - u_0}$. Taking into account $a_2 > \hat{u}_0$ and Eq. 4.191, this corresponds with a situation in which $\mathbf{y}_e^{C,II}$ is not a physical equilibrium point. In the latter case, the equilibrium point $\mathbf{y}_e^{B,II}$ is *quasi* globally asymptotically stable: trajectories starting inside \mathbf{S}_y converge to $\mathbf{y}_e^{B,II}$, except for the equilibrium point $\mathbf{y}_e^{A,II}$. In case the system possesses three equilibrium points, $\mathbf{y}_e^{B,II}$ is unstable with index 1: only trajectories on the y_3 -axis converge to $\mathbf{y}_e^{B,II}$.

For the equilibrium point $\mathbf{y}_e^{C,II}$, the reduced Jacobian matrix becomes

$$\mathbf{J}_{34}(\mathbf{y}_e^{C,II}) = \begin{bmatrix} -\kappa \cdot a - \nu \cdot c & -\kappa \cdot b - \nu \cdot d \\ \mu \cdot c & -\mu \cdot d \end{bmatrix} \quad (4.197)$$

in which

$$\kappa \triangleq a_1 \cdot y_{e3}^{C,II} \cdot \frac{b_1}{(b_1 + x_{e1}^{C,II})^2} \cdot \frac{c_1}{(c_1 + x_{e2}^{C,II})} > 0 \quad (4.198)$$

$$\mu \triangleq a_2 \cdot y_{e4}^{C,II} \cdot \frac{b_2}{(b_2 + x_{e2}^{C,II})^2} > 0 \quad (4.199)$$

$$\nu \triangleq a_1 \cdot y_{e3}^{C,II} \cdot \frac{x_{e1}^{C,II}}{(b_1 + x_{e1}^{C,II})} \cdot \frac{c_1}{(c_1 + x_{e2}^{C,II})^2} > 0 \quad (4.200)$$

The eigenvalues of $\mathbf{J}_{34}(\mathbf{y}_e^{C,II})$ are the solutions of the equation

$$s^2 + (\kappa \cdot a + \nu \cdot c + \mu \cdot d) \cdot s + (\kappa \cdot a + \nu \cdot c) \cdot \mu \cdot d + \mu \cdot c \cdot (\kappa \cdot b + \nu \cdot d) = 0 \quad (4.201)$$

and always have strictly negative real parts. As a result, the equilibrium point $\mathbf{y}_e^{C,II}$ is locally asymptotically stable, and even quasi globally asymptotically stable in case $\mathbf{y}_e^{C,II}$ is not surrounded by a limit cycle (this will be verified through simulation). This means that trajectories within the physical boundaries of the system will converge to $\mathbf{y}_e^{C,II}$, except for the trajectories on the y_3 -axis, that converge to $\mathbf{y}_e^{B,II}$, and except for the trajectory coinciding with $\mathbf{y}_e^{A,II}$.

Phase trajectories of the system

From an arbitrary starting value in \mathbf{S}_y , every trajectory of the system defined by model II converges to the cross-section Δ of \mathbf{S}_y with the plane $\{y_1 = w_1 = u_1, y_2 = w_2 = 0\}$, described as for model I by the inequalities 4.173-4.176.

The phase trajectories are qualitatively the same as for model I. Figure 4.9 shows the system boundaries, the equilibrium points and trajectory fields for different values of the dilution rate u_0 and the influent ammonium concentration u_1 . The simulations revealed that the equilibrium point $\mathbf{y}_e^{C,II}$ is not surrounded by a limit cycle, so it is quasi globally asymptotically stable.

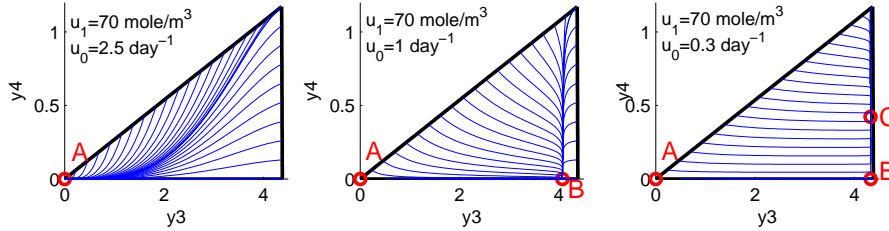


Figure 4.9: Trajectory fields for model II in terms of u_0 ; $u_1=70$

Conclusions

The equilibrium points of a SHARON two-step nitrification model with product (nitrite) inhibition have been calculated directly. Compared to the model without inhibition (section 4.7.2), addition of product inhibition leaves the number of equilibrium points unchanged, as well as their stability. However, the position of the equilibrium points corresponding with biomass growth is affected. The condition for the occurrence of an equilibrium point with only nitrite production remains the same, while the condition for the occurrence of an additional equilibrium point, corresponding with nitrate formation, becomes more stringent. The results are summarized as follows:

1. For high dilution rates u_0 or low influent ammonium concentrations u_1 :

$$\frac{a_1 \cdot u_1}{b_1 + u_1} < u_0$$

only one equilibrium point ($y_e^{A,II}$, Eq. 4.183) occurs, corresponding with biomass wash-out. This equilibrium point is globally asymptotically stable.

2. For moderately high dilution rates u_0 and not too high influent ammonium concentrations u_1 :

$$u_0 < \frac{a_1 \cdot u_1}{b_1 + u_1}$$

and

$$u_1 < \frac{b_1 \cdot f(u_0)}{a_1 - f(u_0)} + \frac{a}{c} \cdot \frac{b_2 \cdot u_0}{a_2 - u_0}$$

the system possesses two physical equilibrium points. These are

- the wash-out equilibrium point $y_e^{A,II}$, that is now unstable with index 1. Within the physical boundaries of the system, only the trajectory consisting of the point $y_e^{A,II}$, stays in this point. This corresponds with a situation in which initially no biomass is present in the reactor.
- an equilibrium point $y_e^{B,II}$ (Eq. 4.184), corresponding with only nitrite formation. The ammonium concentration in this equilibrium point is higher and the nitrite concentration is lower for the model with nitrite inhibition than for the model without inhibition. This equilibrium point is quasi globally asymptotically stable, in the sense that all trajectories within the physical boundaries of the system converge to this point, except from the equilibrium point $y_e^{A,II}$.

3. For sufficiently low dilution rates u_0 and corresponding influent ammonium concentrations u_1 :

$$u_1 > \frac{b_1 \cdot f(u_0)}{a_1 - f(u_0)} + \frac{a}{c} \cdot \frac{b_2 \cdot u_0}{a_2 - u_0} b_2 + \frac{c}{a} \cdot \left(u_1 - \frac{b_1 \cdot u_0}{a_1 - u_0} \right)$$

three equilibrium points occur, namely

- the wash-out equilibrium point $y_e^{A,II}$, that is still unstable with index 1. Within the physical boundaries of the system, only the trajectory consisting of the point $y_e^{A,II}$ stays in the neighbourhood of this point, corresponding with a situation in which initially no biomass is present in the reactor.
- the equilibrium point $y_e^{B,II}$, corresponding with only nitrite formation. This equilibrium point is also unstable with index 1: only trajectories on the y_3 -axis converge to $y_e^{B,II}$. This corresponds with a reactor in which initially only ammonium oxidizers are present (note that this model assumes that the influent does not contain biomass).
- an equilibrium point $y_e^{C,II}$ (Eq. 4.188), corresponding with nitrate formation. This equilibrium point corresponds with less ammonium conversion, the same amount of nitrite produced and less nitrate produced than for the corresponding equilibrium point in case there is no inhibition. This equilibrium point is quasi globally convergent, in the sense that all trajectories within the physical boundaries of the system

converge to this point, except for the equilibrium point $y_e^{A,II}$ and the trajectories on the y_3 -axis.

4.7.4 Simplified model II_m: model II with small perturbations

For biological systems, it is often difficult to determine exact parameter values. Also, parameter values may change in time, e.g. because of biomass adaptation. Besides, also the input values may be uncertain. For this reason, the effect of changing parameter and input values on the number of equilibrium points and their stability is assessed in this section.

Consider model II as described in section 4.7.3, but now assume that $u_2, u_3, u_4, c_2, d_3 = \frac{1}{d_2}$ and $e_3 = \frac{1}{e_2}$ are no longer zero but have small positive values. In this section, the effect of these changes on the position of the equilibrium points will be studied. The resulting model is the same as used for the simulation studies discussed in the remaining chapters of this PhD thesis, except that the possibility of ammonium and/or nitrite inhibition of nitrite oxidation ($d_3, e_3 \neq 0$) is left open here while pH is kept constant.

It is important to note that the index and thus the local asymptotic stability properties of the equilibrium points are not influenced by these parameters as the equilibrium points are hyperbolic.

The canonical state space representation of this system is given by Eqs. 4.118-4.121, in which the reaction rates are now given by

$$\sigma_1(\mathbf{y}) = a_1 \cdot \frac{x_1}{b_1 + x_1} \cdot \frac{c_1}{c_1 + x_2} \cdot y_3 \quad (4.202)$$

$$\sigma_2(\mathbf{y}) = a_2 \cdot \frac{x_2}{b_2 + x_2} \cdot \frac{x_1}{c_2 + x_1} \cdot \frac{1}{1 + d_3 \cdot x_2} \cdot \frac{1}{1 + e_3 \cdot x_1} \cdot y_4 \quad (4.203)$$

The state space of this system is \mathbf{S}_y , defined by Eqs. 4.127-4.130.

The equilibrium points of this system are given by

$$y_1 = w_1 = u_1 + a \cdot u_3 + b \cdot u_4 \quad (4.204)$$

$$y_2 = w_2 = u_2 - c \cdot u_3 + d \cdot u_4 \quad (4.205)$$

$$0 = u_0 \cdot u_3 + \left(-u_0 + a_1 \cdot \frac{x_{e1}}{b_1 + x_{e1}} \cdot \frac{c_1}{c_1 + x_{e2}} \right) \cdot y_{e3} \quad (4.206)$$

$$0 = u_0 \cdot u_4 + \left(-u_0 + a_2 \cdot \frac{x_{e2}}{b_2 + x_{e2}} \cdot \frac{x_{e1}}{c_2 + x_{e1}} \cdot \frac{1}{1 + d_3 \cdot x_{e2}} \cdot \frac{1}{1 + e_3 \cdot x_{e1}} \right) \cdot y_{e4} \quad (4.207)$$

and can be written as variations of the equilibrium points of model II:

1. The wash-out equilibrium

$$\mathbf{y}_e^{\mathbf{A},\text{IIIm}} = \mathbf{y}_e^{\mathbf{A},\text{II}} + \Delta\mathbf{y}_e^{\mathbf{A},\text{II}} \quad (4.208)$$

Substitution of $y_{e3}^{\mathbf{A},\text{II}} = y_{e4}^{\mathbf{A},\text{II}} = 0$ and Eqs. 4.204-4.205 in Eq. 4.208, neglecting higher order terms in the variations of the parameters and variables ($\Delta y_{e3}^{\mathbf{A},\text{II}}, \Delta y_{e4}^{\mathbf{A},\text{II}}, u_2, u_3, u_4, c_2, d_3$ and e_3) eventually yields the value of the equilibrium point

$$\mathbf{y}_e^{\mathbf{A},\text{IIIm}} = \begin{bmatrix} u_1 + a \cdot u_3 + b \cdot u_4 \\ u_2 - c \cdot u_3 + d \cdot u_4 \\ \frac{u_0 \cdot u_3}{u_0 - a_1 \cdot \frac{u_1}{b_1 + u_1}} \\ u_4 \end{bmatrix} \quad (4.209)$$

The only conversion realized in this equilibrium point is caused by the biomass present in the influent. This equilibrium point does not always occur (like for model II) but is a physical equilibrium point if and only if

$$u_0 > \frac{a_1 \cdot u_1}{b_1 + u_1} \quad (4.210)$$

which is exactly the same condition for it to be the only equilibrium point. In this case, the equilibrium point is globally asymptotically stable. The condition 4.210 arises from $u_3 \neq 0$: in case ammonium oxidizers are present in the influent, the wash-out equilibrium point only occurs for high dilution rates u_0 , determined by 4.210. In case $u_3 = 0$ the wash-out equilibrium point occurs independent of the values of u_0 and u_1 . Note however that in practice, there will always be some ammonium oxidizers present ('at least one') in the influent ($u_3 \neq 0$).

2. An equilibrium corresponding with (almost) only nitrite production, where nitrate is produced only because of nitrite oxidizers present in the influent:

$$\mathbf{y}_e^{\mathbf{B},\text{IIIm}} = \mathbf{y}_e^{\mathbf{B},\text{II}} + \Delta\mathbf{y}_e^{\mathbf{B},\text{II}} \quad (4.211)$$

Combining Eqs. 4.211, 4.204-4.207, 4.184, 4.114 and 4.115, neglecting higher order terms in the variations of the parameters and

variables $(\Delta x_{e1}^{B,II}, \Delta x_{e2}^{B,II}, \Delta y_{e3}^{B,II}, \Delta y_{e4}^{B,II}, u_2, u_3, u_4, c_2, d_3$ and $e_3)$ eventually yields the value of the equilibrium point

$$\mathbf{y}_e^{B,II} = \begin{bmatrix} u_1 + a \cdot u_3 + b \cdot u_4 \\ u_2 - c \cdot u_3 + d \cdot u_4 \\ y_{e3}^{B,II} + \Delta y_{e3}^{B,II} \\ \Delta y_{e4}^{B,II} \end{bmatrix} \quad (4.212)$$

with

$$\Delta y_{e4}^{B,II} = \frac{u_0 \cdot u_4}{u_0 - a_2 \cdot \frac{x_{e2}^{B,II}}{b_2 + x_{e2}^{B,II}}} \quad (4.213)$$

$\Delta y_{e3}^{B,II}$ is obtained from

$$\begin{aligned} u_0 \cdot u_3 - a_1 \cdot \frac{x_{e1}^{B,II}}{b_1 + x_{e1}^{B,II}} \cdot \frac{c_1 \cdot \Delta x_{e2}^{B,II}}{(c_1 + x_{e2}^{B,II})^2} \cdot y_{e3}^{B,II} \\ + a_1 \cdot \frac{b_1 \cdot \Delta x_{e1}^{B,II}}{(b_1 + x_{e1}^{B,II})^2} \cdot \frac{c_1}{c_1 + x_{e2}^{B,II}} \cdot y_{e3}^{B,II} = 0 \end{aligned} \quad (4.214)$$

after substitution of

$$\Delta x_{e1}^{B,II} = a \cdot u_3 + b \cdot u_4 - a \cdot \Delta y_{e3}^{B,II} - b \cdot \Delta y_{e4}^{B,II} \quad (4.215)$$

$$\Delta x_{e2}^{B,II} = u_2 - c \cdot u_3 + d \cdot u_4 + c \cdot \Delta y_{e3}^{B,II} - d \cdot \Delta y_{e4}^{B,II} \quad (4.216)$$

and taking into account Eq. 4.213.

The equilibrium point $\mathbf{y}_e^{B,II}$ is a physical equilibrium point if $\mathbf{y}_e^{B,II}$ is a physical equilibrium point (Eq. 4.187) and if at the same time

$$u_0 > a_2 \cdot \frac{x_{e2}^{B,II}}{b_2 + x_{e2}^{B,II}} \quad (4.217)$$

It can be shown that condition 4.217 is equivalent with condition 4.191 not to be fulfilled, so for $\mathbf{y}_e^{C,II}$ not to be a physical equilibrium point. So, if $\mathbf{y}_e^{B,II}$ is an equilibrium point, it is also the only equilibrium point. It is then globally asymptotically stable. Condition 4.217 arises from $u_4 \neq 0$: if nitrite oxidizers are present in the influent, the equilibrium point corresponding with only nitrite production is only a physical equilibrium point in the range

of dilution rates u_0 and influent ammonium concentrations u_1 determined by Eqs. 4.187 and 4.217. This will always be the case in practice, since there will always be some nitrite oxidizers present in the influent ($u_4 \neq 0$).

3. An equilibrium point corresponding with (substantial) nitrate production:

$$\begin{aligned} \mathbf{y}_e^{C,IIIm} &= \mathbf{y}_e^{C,II} + \Delta \mathbf{y}_e^{C,II} \\ &= \begin{bmatrix} u_1 + a \cdot u_3 + b \cdot u_4 \\ u_2 - c \cdot u_3 + d \cdot u_4 \\ y_{e3}^{C,IIIm} \\ y_{e4}^{C,IIIm} \end{bmatrix} \end{aligned} \quad (4.218)$$

This equilibrium point is a physical equilibrium point if $\mathbf{y}_e^{C,II}$ is a physical equilibrium point (condition 4.191), since the small parameter differences between both models will not significantly effect the position of the equilibrium point, that lies in the interior of the physical boundaries of the system. Its value can be obtained analogously to the values of $\mathbf{y}_e^{A,IIIm}$ and $\mathbf{y}_e^{B,IIIm}$, but this gives rise to more complicated calculations. For this reason, it seems more advisable to calculate its value with a numerical search algorithm, that calculates $y_{e3}^{C,IIIm}$ and $y_{e4}^{C,IIIm}$ from Eqs. 4.206 and 4.207, taking into account Eqs. 4.127 and 4.128. As small parameter and input changes will only slightly change the position of the equilibrium point, the values $y_{e3}^{C,II}$ and $y_{e4}^{C,II}$ can be used to initialize the search algorithm.

It is important to note that the parameters c_2 , d_3 and e_3 , of which the values are assumed small, do not appear in the (approximate) expressions that determine the position of the equilibrium points $\mathbf{y}_e^{A,IIIm}$ and $\mathbf{y}_e^{B,IIIm}$. Their effect has been neglected by neglecting higher order terms in the variations of the parameters and input variables, that are assumed small. When the values of these parameters become relatively high, their effect on the position of the equilibrium points cannot be neglected any more. The occurrence of additional inhibition terms in the kinetic rate expressions $\sigma_1(\mathbf{y})$ and $\sigma_2(\mathbf{y})$ may even give rise to additional equilibrium points, as is clear from the work of Sbarciog et al. (2006). For this reason, in case additional inhibition terms occur, it is advisable to explicitly calculate the number of equilibrium points for the corresponding model.

Conclusions

In this section, the effect of nonzero parameter and input values $u_2, u_3, u_4, c_2, d_3 = \frac{1}{d_2}$ and $e_3 = \frac{1}{e_2}$ on the number of equilibrium points and their stability, has been evaluated in comparison to the model with nitrite inhibition (model II, section 4.7.3). The position of the equilibrium points is only slightly affected. However, the equilibrium points \mathbf{y}_e^A and \mathbf{y}_e^B , that are lying on the physical system boundaries for model II now shift outside the physical boundaries under certain conditions, which means they then no longer occur. Summarizing:

1. For high dilution rates u_0 or low influent ammonium concentrations u_1 :

$$\frac{a_1 \cdot u_1}{b_1 + u_1} < u_0$$

only one equilibrium point ($\mathbf{y}_e^{A,IIIm}$, Eq. 4.209) occurs, corresponding with biomass wash-out. This equilibrium point is globally asymptotically stable.

2. For moderately high dilution rates u_0 and not too high influent ammonium concentrations u_1 :

$$u_0 < \frac{a_1 \cdot u_1}{b_1 + u_1}$$

and

$$u_0 > a_2 \cdot \frac{x_{e2}^{B,II}}{b_2 + x_{e2}^{B,II}}$$

\Leftrightarrow

$$u_1 < \frac{b_1 \cdot f(u_0)}{a_1 - f(u_0)} + \frac{a}{c} \cdot \frac{b_2 \cdot u_0}{a_2 - u_0}$$

the equilibrium point $\mathbf{y}_e^{B,IIIm}$ (Eq. 4.212), corresponding with only nitrite formation, is the only equilibrium point and is globally asymptotically stable.

3. For sufficiently low dilution rates u_0 and corresponding influent ammonium concentrations u_1 :

$$u_1 > \frac{b_1 \cdot f(u_0)}{a_1 - f(u_0)} + \frac{a}{c} \cdot \frac{b_2 \cdot u_0}{a_2 - u_0} b_2 + \frac{c}{a} \cdot \left(u_1 - \frac{b_1 \cdot u_0}{a_1 - u_0} \right)$$

the equilibrium point $\mathbf{y}_e^{C,IIIm}$ (Eq. 4.218), corresponding with nitrate formation, is the only equilibrium point. It is globally asymptotically stable.

4.7.5 Simplified model III: ammonium inhibition of ammonium oxidation

Comparing the results of sections 4.7.2 and 4.7.3, it is clear that product inhibition does not affect the number of equilibrium point of the model. From these results, the question rises whether substrate inhibition affects the number of equilibrium points, an issue that is addressed in this section. For this purpose, ammonium inhibition of ammonium oxidation is added to the model without inhibition (section 4.7.2), which means that now $d_1 \neq \infty$. It must be stressed that this addition is only made to study the effect of substrate inhibition on the number of equilibrium points. In the SHARON reactor model used for the simulation work described in Chapters 5 and 8, ammonium inhibition is not taken up as it was found not to be significant (Van Hulle et al., 2004). However, SHARON models presented by other authors (e.g. Magri et al. 2005) do consider ammonium inhibition of ammonium oxidation, so its study is certainly relevant.

The canonical state space representation is unvaryingly given by Eqs. 4.143-4.146, while the reaction rates in these equations become

$$\sigma_1(\mathbf{y}) = a_1 \cdot \frac{x_1}{b_1 + x_1} \cdot \frac{d_1}{d_1 + x_1} \cdot y_3 \quad (4.219)$$

$$\sigma_2(\mathbf{y}) = \begin{cases} a_2 \cdot \frac{x_2}{b_2 + x_2} \cdot y_4 & \text{for } x_1 > 0 \\ 0 & \text{for } x_1 = 0 \end{cases} \quad (4.220)$$

Eqs. 4.149-4.152 remain valid.

Equilibrium points in case $u_0 > 0$ and $u_1 > 0$

For the same reason as in model I and II, the equilibrium points are calculated in case $u_0 > 0$ and $u_1 > 0$. Invariably, there exists no equilibrium point for which $x_{e1} = 0$. The equilibrium points fulfill the following set of equations (see Eqs. 4.143-4.146 and 4.219-4.220) :

$$y_{e1} = u_1 \quad (4.221)$$

$$y_{e2} = 0 \quad (4.222)$$

$$\left(-u_0 + a_1 \cdot \frac{x_{e1}}{b_1 + x_{e1}} \cdot \frac{d_1}{d_1 + x_{e1}} \right) \cdot y_{e3} = 0 \quad (4.223)$$

$$\left(-u_0 + a_2 \cdot \frac{x_{e2}}{b_2 + x_{e2}} \right) \cdot y_{e4} = 0 \quad (4.224)$$

In this case, five equilibrium points are obtained:

1. The wash-out equilibrium point, that always occurs and is the same as for model I (section 4.7.2):

$$\mathbf{y}_e^{\mathbf{A},\text{III}} = \begin{bmatrix} u_1 \\ 0 \\ 0 \\ 0 \end{bmatrix} \Leftrightarrow \mathbf{x}_e^{\mathbf{A},\text{III}} = \begin{bmatrix} u_1 \\ 0 \\ 0 \\ 0 \end{bmatrix} \quad (4.225)$$

2. Two equilibrium points, $\mathbf{y}_e^{\mathbf{B},\text{III}}$ and $\mathbf{y}_e^{\mathbf{C},\text{III}}$, that correspond with a situation without nitrite oxidizers and consequently without nitrate production:

$$\mathbf{y}_e^{\alpha,\text{III}} = \begin{bmatrix} u_1 \\ 0 \\ \frac{1}{a} \cdot (u_1 - x_{e1}^{\alpha,\text{III}}) \\ 0 \end{bmatrix} \\ \Leftrightarrow \mathbf{x}_e^{\alpha,\text{III}} = \begin{bmatrix} x_{e1}^{\alpha,\text{III}} \\ \frac{c}{a} \cdot (u_1 - x_{e1}^{\alpha,\text{III}}) \\ \frac{1}{a} \cdot (u_1 - x_{e1}^{\alpha,\text{III}}) \\ 0 \end{bmatrix} \quad (4.226)$$

in which α denotes B or C .

$x_{e1}^{\mathbf{B},\text{III}}$ and $x_{e1}^{\mathbf{C},\text{III}}$ are obtained from (say $x_{e1}^{\mathbf{B},\text{III}} < x_{e1}^{\mathbf{C},\text{III}}$)

$$a_1 \cdot \frac{x_{e1}^{\alpha,\text{III}}}{b_1 + x_{e1}^{\alpha,\text{III}}} \cdot \frac{d_1}{d_1 + x_{e1}^{\alpha,\text{III}}} = u_0 \quad (4.227)$$

These equilibrium points are physical equilibrium points if and only if

$$u_0 < \frac{a_1 \cdot d_1}{(\sqrt{b_1} + \sqrt{d_1})^2} \quad (4.228)$$

and

$$x_{e1}^{\alpha,\text{III}} < u_1 \quad (4.229)$$

If = instead of < in Eq. 4.228, then $\mathbf{y}_e^{\mathbf{B},\text{III}} = \mathbf{y}_e^{\mathbf{C},\text{III}}$.

Regarding condition 4.229 and $x_{e1}^{\mathbf{B},\text{III}} < x_{e1}^{\mathbf{C},\text{III}}$, it is possible that

$\mathbf{y}_e^{B,III}$ is a physical equilibrium point and $\mathbf{y}_e^{C,III}$ is not. It is interesting to note that the boundary condition $x_{e1}^{\alpha,III} = u_1$ for the occurrence of $x_{e1}^{\alpha,III}$ is equivalent with

$$a_1 \cdot \frac{u_1}{b_1 + u_1} \cdot \frac{d_1}{d_1 + u_1} = u_0 \quad (4.230)$$

3. Two equilibrium points, $\mathbf{y}_e^{D,III}$ and $\mathbf{y}_e^{E,III}$, for which both ammonium and nitrite oxidizers are present, so at least part of the formed nitrite is further oxidized to nitrate:

$$\begin{aligned} \mathbf{y}_e^{\beta,III} &= \begin{bmatrix} u_1 \\ 0 \\ \frac{d \cdot (u_1 - x_{e1}^{\beta,III}) + b \cdot x_{e2}^{\beta,III}}{a \cdot d + b \cdot c} \\ \frac{c \cdot (u_1 - x_{e1}^{\beta,III}) - a \cdot x_{e2}^{\beta,III}}{a \cdot d + b \cdot c} \end{bmatrix} \\ \Leftrightarrow \mathbf{x}_e^{\beta,III} &= \begin{bmatrix} x_{e1}^{\beta,III} \\ \frac{b_2 \cdot u_0}{a_2 - u_0} \\ \frac{d \cdot (u_1 - x_{e1}^{\beta,III}) + b \cdot x_{e2}^{\beta,III}}{a \cdot d + b \cdot c} \\ \frac{c \cdot (u_1 - x_{e1}^{\beta,III}) - a \cdot x_{e2}^{\beta,III}}{a \cdot d + b \cdot c} \end{bmatrix} \end{aligned} \quad (4.231)$$

in which β denotes D or E .

$x_{e1}^{D,III}$ and $x_{e1}^{E,III}$ are obtained from Eq. 4.227 (say $x_{e1}^{D,III} < x_{e1}^{E,III}$), so

$$x_{e1}^{D,III} = x_{e1}^{B,III} \quad \text{and} \quad x_{e1}^{E,III} = x_{e1}^{C,III}$$

These equilibrium points are physical equilibrium points if and only if

$$u_0 < \frac{a_1 \cdot d_1}{(\sqrt{b_1} + \sqrt{d_1})^2} \quad (4.232)$$

and

$$u_0 < a_2 \quad (4.233)$$

and

$$x_{e1}^{\beta,III} < u_1 - \frac{a}{c} \cdot \frac{b_2 \cdot u_0}{a_2 - u_0} \quad (4.234)$$

If $=$ instead of $<$ in Eq. 4.232, then $y_e^{D,III} = y_e^{E,III}$.

Regarding condition 4.234 and $x_{e1}^{D,III} < x_{e1}^{E,III}$, it is possible that $y_e^{D,III}$ occurs but $y_e^{E,III}$ does not.

Comparison of the conditions 4.229 and 4.234, and taking into account 4.233, it is clear that $y_e^{D,III}$ is only a physical equilibrium point if $y_e^{B,III}$ is a physical equilibrium point, and that the occurrence of $y_e^{E,III}$ implies the occurrence of $y_e^{C,III}$. If $=$ instead of $<$ in Eq. 4.234, then $y_e^{D,III} = y_e^{B,III}$ and $y_e^{E,III} = y_e^{C,III}$.

Figures 4.10 and 4.11 show the occurrence of equilibrium points in terms of the dilution rate u_0 and the influent ammonium concentration u_1 for different values of the nitrite inhibition constant d_1 . From Figure 4.10, it is clear that, if there is no strong nitrite inhibition, maximally three equilibrium points simultaneously occur in the range of dilution rates u_0 and influent ammonium concentration u_1 that can reasonably be expected. For significant nitrite inhibition however, it is possible that five equilibrium points occur at the same time, as shown in Figure 4.11. Note that one cannot a priori say which one of the conditions 4.232 and 4.233 is the most stringent, as this depends on the numerical values of the parameters: for the given values of a_1 , b_1 and a_2 , condition 4.232 is most stringent for $d_1 = 10$, while condition 4.233 is most stringent for $d_1 = 1000$.

Local asymptotic stability of equilibrium points

The expressions for the partial derivatives of f_3 in the reduced Jacobian matrix 4.142, evaluated for the kinetic rate expressions 4.219 and 4.220 are now given by

$$\frac{\partial f_3}{\partial y_3} = -u_0 + a_1 \cdot \frac{x_1}{b_1 + x_1} \cdot \frac{d_1}{d_1 + x_1} - a_1 \cdot d_1 \cdot y_3 \cdot \frac{(b_1 \cdot d_1 - x_1^2) \cdot a}{(b_1 + x_1)^2 \cdot (d_1 + x_1)^2} \quad (4.235)$$

$$\frac{\partial f_3}{\partial y_4} = -a_1 \cdot d_1 \cdot y_3 \cdot \frac{(b_1 \cdot d_1 - x_1^2) \cdot b}{(b_1 + x_1)^2 \cdot (d_1 + x_1)^2} \quad (4.236)$$

The expressions 4.164 and 4.165 for the partial derivatives of f_4 remain valid.

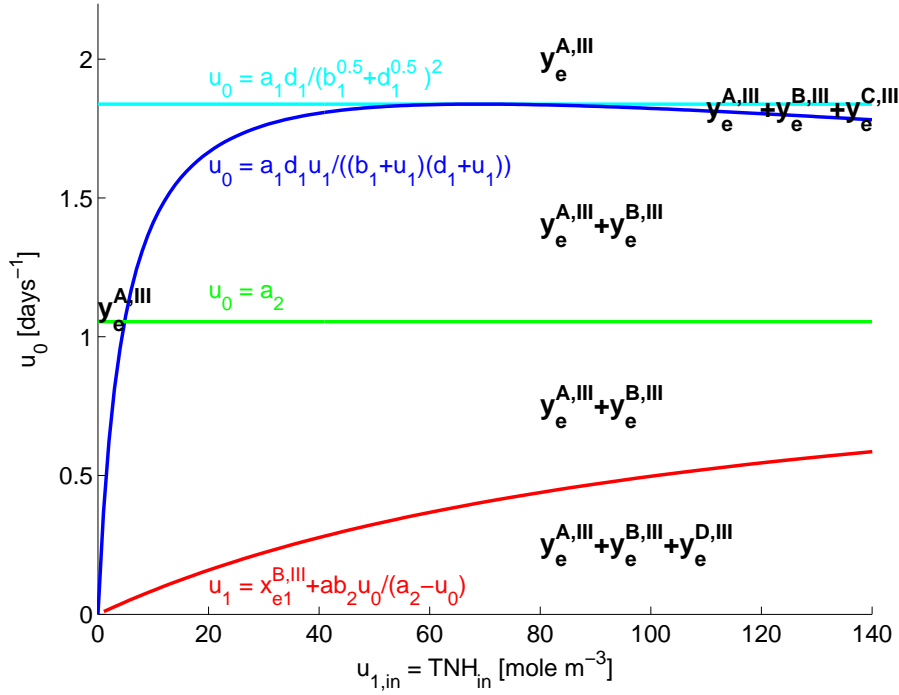


Figure 4.10: Equilibrium points of model III in terms of $u_0 = \Phi_{in}/V$ and $u_1 = C_{TNH}^{in}$; $d_1 = 1000 \text{ mole m}^{-3}$

For the wash-out equilibrium point, $y_e^{A,III}$, the reduced Jacobian matrix becomes

$$\mathbf{J}_{34}(y_e^{A,III}) = \begin{bmatrix} -u_0 + \frac{a_1 \cdot u_1}{b_1 + u_1} \cdot \frac{d_1}{d_1 + u_1} & 0 \\ 0 & -u_0 \end{bmatrix} \quad (4.237)$$

As a result, $y_e^{A,III}$ is locally asymptotically stable (both eigenvalues of $\mathbf{J}_{34}(y_e^{A,III})$ are strictly negative) in case $u_0 > \frac{a_1 \cdot u_1}{b_1 + u_1} \cdot \frac{d_1}{d_1 + u_1}$. If not, $y_e^{A,III}$ is unstable with index 1: only the trajectories on the y_4 -axis converge to $y_e^{A,III}$, of which only the equilibrium point $y_e^{A,III}$ itself lies within the physical system boundaries.

For the equilibrium points $y_e^{\alpha,III}$ ($\alpha = B, C$) corresponding with only nitrite production, the eigenvalues of the reduced Jacobian matrix

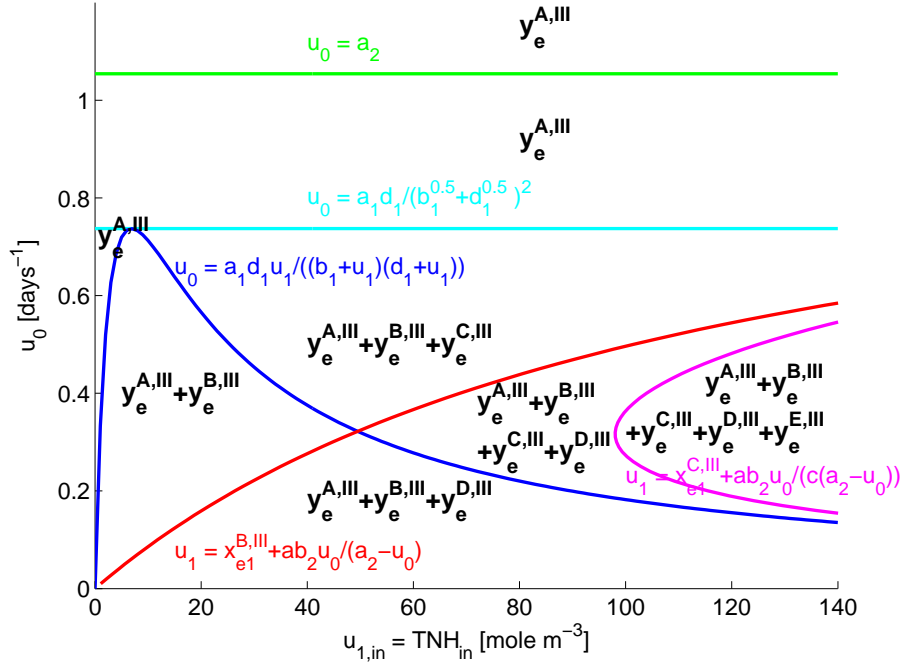


Figure 4.11: Equilibrium points of model III in terms of $u_0 = \Phi_{in}/V$ and $u_1 = C_{TNH}^{in}$; $d_1 = 10 \text{ mole m}^{-3}$

equal its diagonal elements

$$\left. \frac{\partial f_3}{\partial y_3} \right|_{\mathbf{y}=\mathbf{y}_e^{B,III}} = -a_1 \cdot d_1 \cdot \frac{(u_1 - x_{e1}^{\alpha,III}) \cdot (b_1 \cdot d_1 - (x_{e1}^{\alpha,I})^2)}{(b_1 + x_{e1}^{\alpha,III})^2 \cdot (d_1 + x_{e1}^{\alpha,III})^2}$$

and

$$\left. \frac{\partial f_4}{\partial y_4} \right|_{\mathbf{y}=\mathbf{y}_e^{B,III}} = -u_0 + a_2 \cdot \frac{x_{e2}^{\alpha,III}}{b_2 + x_{e2}^{\alpha,III}} \quad (4.239)$$

Considering the condition 4.229 for physical equilibria $\mathbf{y}_e^{\alpha,III}$, and considering $x_{e1}^{B,III} < \sqrt{b_1 \cdot d_1} < x_{e1}^{C,III}$ (resulting from 4.227), the eigenvalue 4.238 is strictly negative for $\mathbf{y}_e^{B,III}$ and strictly positive for $\mathbf{y}_e^{C,III}$. It can be shown that the eigenvalue 4.239 is strictly negative in case $u_0 > a_2$ or in case $u_0 < a_2$ and $u_1 < x_{e1}^{\beta,III} + \frac{a}{c} \cdot \frac{b_2 \cdot u_0}{a_2 - u_0}$. Regarding 4.233 and 4.234, this means that the eigenvalue 4.239 for $\mathbf{y}_e^{B,III}$ is strictly negative in case $\mathbf{y}_e^{D,III}$ does not occur and the eigenvalue for $\mathbf{y}_e^{C,III}$ is

strictly negative in case $\mathbf{y}_e^{\text{E,III}}$ does not occur. Interpreting and summarizing these results, $\mathbf{y}_e^{\text{B,III}}$ is locally asymptotically stable if $\mathbf{y}_e^{\text{D,III}}$ is not a physical equilibrium point and else is instable with index 1: in the latter case, only the trajectories on the y_3 -axis converge to $\mathbf{y}_e^{\text{B,III}}$. If $\mathbf{y}_e^{\text{E,III}}$ is not a physical equilibrium point, $\mathbf{y}_e^{\text{C,III}}$ is instable with index 1: only trajectories parallel to the y_4 -axis and with $y_{e3}^{\text{C,III}}$ as y_3 -coordinate converge to $\mathbf{y}_e^{\text{C,III}}$. In case $\mathbf{y}_e^{\text{E,III}}$ is a physical equilibrium point, $y_{e3}^{\text{C,III}}$ is instable with index 2: the only trajectory converging to $y_{e3}^{\text{C,III}}$ is then this point itself.

For the equilibrium point $\mathbf{y}_e^{\beta,\text{III}}$, the reduced Jacobian matrix can be written as

$$\mathbf{J}_{34}(\mathbf{y}_e^{\text{C,III}}) = \begin{bmatrix} -\eta \cdot a & -\eta \cdot b \\ \xi \cdot c & -\xi \cdot d \end{bmatrix} \quad (4.240)$$

in which

$$\begin{aligned} \eta &\triangleq a_1 \cdot d_1 \cdot y_{e3}^{\beta,\text{III}} \cdot \frac{b_1 \cdot d_1 - (x_{e1}^{\beta,\text{III}})^2}{(b_1 + x_{e1}^{\beta,\text{III}})^2 \cdot (d_1 + x_{e1}^{\beta,\text{III}})^2} \\ &> 0 \text{ for } x_{e1}^{\beta,\text{III}} < \sqrt{b_1 \cdot d_1} \Leftrightarrow \mathbf{y}_e^{\beta,\text{III}} = \mathbf{y}_e^{\text{D,III}} \\ &< 0 \text{ for } x_{e1}^{\beta,\text{III}} > \sqrt{b_1 \cdot d_1} \Leftrightarrow \mathbf{y}_e^{\beta,\text{III}} = \mathbf{y}_e^{\text{E,III}} \end{aligned} \quad (4.241)$$

$$\xi \triangleq a_2 \cdot y_{e4}^{\beta,\text{III}} \cdot \frac{b_2}{(b_2 + x_{e2}^{\beta,\text{III}})^2} > 0 \quad (4.242)$$

The eigenvalues of $\mathbf{J}_{34}(\mathbf{y}_e^{\beta,\text{III}})$ are the solutions of the equation

$$s^2 + (\eta \cdot a + \xi \cdot d) \cdot s + \eta \cdot \xi \cdot (a \cdot d + b \cdot c) = 0 \quad (4.243)$$

For $\mathbf{y}_e^{\text{D,III}}$, the sum of the eigenvalues is always negative, while their product is positive. This means that both eigenvalues have strictly negative real parts, so the equilibrium point $\mathbf{y}_e^{\text{D,III}}$ is locally asymptotically stable. For $\mathbf{y}_e^{\text{E,III}}$, the product of the eigenvalues is negative, which means that the eigenvalues are real with opposite sign. Consequently $\mathbf{y}_e^{\text{E,III}}$ is unstable with index 1. In this case, it is not possible to say a priori which trajectories will converge to this equilibrium point. However, this would be interesting to know, as this trajectory constitutes the stability boundary, that separates the attraction regions of the equilibrium points $\mathbf{y}_e^{\text{A,III}}$ and $\mathbf{y}_e^{\text{D,III}}$. One way to estimate this stability boundary, is by the trajectory reversing technique, as described e.g. by Chiang et al. (1998).

Phase trajectories and stability boundaries of the system

Figure 4.12 shows the system boundaries, the equilibrium points and trajectory fields in Δ for different values of the dilution rate u_0 and the influent ammonium concentration u_1 . The simulation results confirm the calculations. In case 3, 5 and 6, each time two locally asymptotically stable equilibrium points occur. The stability boundary, that separates their attraction regions, determines from which initial states the process will converge to which equilibrium point.

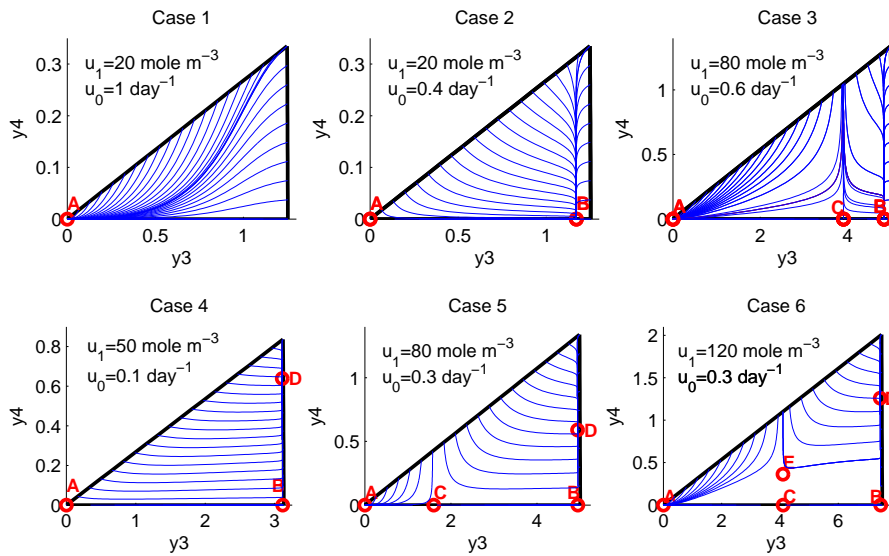


Figure 4.12: Trajectory fields for model III in terms of u_0 and u_1 ($d_1 = 10 \text{ mole m}^{-3}$)

Conclusions

In this section, the effect of substrate (ammonium) inhibition on the number of equilibrium points of a SHARON two-step nitrification model has been studied. In contrast to product inhibition (section 4.7.3), that leaves the number of equilibrium points unchanged in comparison with a model without inhibition (section 4.7.2), addition of substrate inhibition (combined with substrate limitation, resulting in Haldane kinetics) does affect the number of equilibrium points. The results are summarized as follows:

1. For high dilution rates u_0 :

$$u_0 > \frac{a_1 \cdot d_1}{(\sqrt{b_1} + \sqrt{d_1})^2}$$

there is one equilibrium physical point ($y_e^{A,III}$, Eq. 4.225), corresponding with biomass wash-out. This equilibrium point is globally asymptotically stable. This is also the case for lower dilution rates

$$u_0 < \frac{a_1 \cdot d_1}{(\sqrt{b_1} + \sqrt{d_1})^2}$$

and low influent ammonium concentrations, in the sense that the equation

$$a_1 \cdot \frac{x_{e1}^{\alpha,III}}{b_1 + x_{e1}^{\alpha,III}} \cdot \frac{d_1}{d_1 + x_{e1}^{\alpha,III}} = u_0$$

has only solutions for which $x_{e1}^{\alpha,III} > u_1$ holds.

2. For moderately high dilution rates u_0 :

$$u_0 < \frac{a_1 \cdot d_1}{(\sqrt{b_1} + \sqrt{d_1})^2}$$

and in case the equation

$$a_1 \cdot \frac{x_{e1}^{\alpha,III}}{b_1 + x_{e1}^{\alpha,III}} \cdot \frac{d_1}{d_1 + x_{e1}^{\alpha,III}} = u_0$$

yields solutions $x_{e1}^{B,III}$ and $x_{e1}^{C,III}$ (say $x_{e1}^{B,III} < x_{e1}^{C,III}$) that fulfill the equations

$$u_1 - \frac{a}{c} \cdot \frac{b_2 \cdot u_0}{a_2 - u_0} < x_{e1}^{B,III} < u_1$$

and

$$u_1 < x_{e1}^{C,III}$$

the system possesses two physical equilibrium points. These are

- the wash-out equilibrium point $y_e^{A,III}$, that is now unstable with index 1: the equilibrium point itself is the only physical trajectory that stays in the neighbourhood of this point.

- an equilibrium point $y_e^{B,III}$ (Eq. 4.226), corresponding with only nitrite formation. This equilibrium point is quasi globally asymptotically stable: within the physical boundaries of the system, all trajectories converge to this point, except for the equilibrium point $y_e^{A,III}$.

3. For moderately high dilution rates u_0 :

$$u_0 < \frac{a_1 \cdot d_1}{(\sqrt{b_1} + \sqrt{d_1})^2}$$

and in case the equation

$$a_1 \cdot \frac{x_{e1}^{\alpha,III}}{b_1 + x_{e1}^{\alpha,III}} \cdot \frac{d_1}{d_1 + x_{e1}^{\alpha,III}} = u_0$$

yields solutions $x_{e1}^{B,III}$ and $x_{e1}^{C,III}$ (say $x_{e1}^{B,III} < x_{e1}^{C,III}$) that fulfill the equations

$$u_1 - \frac{a}{c} \cdot \frac{b_2 \cdot u_0}{a_2 - u_0} < x_{e1}^{B,III} < u_1$$

and

$$u_1 - \frac{a}{c} \cdot \frac{b_2 \cdot u_0}{a_2 - u_0} < x_{e1}^{C,III} < u_1$$

the system possesses three physical equilibrium points. These are

- the wash-out equilibrium point $y_e^{A,III}$, that is now locally asymptotically stable.
- the equilibrium point $y_e^{B,III}$, corresponding with only nitrite formation, that is also locally asymptotically stable.
- an equilibrium point $y_e^{C,III}$ (Eq. 4.226), also corresponding with only nitrite formation, that is unstable with index 1: only trajectories parallel to the y_4 -axis and with $y_{e3}^{C,III}$ as y_3 -coordinate converge to $y_e^{C,III}$. These trajectories separate the regions of attraction of the equilibrium points $y_e^{A,III}$ and $y_e^{B,III}$.

4. For dilution rates u_0 :

$$u_0 < \frac{a_1 \cdot d_1}{(\sqrt{b_1} + \sqrt{d_1})^2}$$

and in case the equation

$$a_1 \cdot \frac{x_{e1}^{\alpha,III}}{b_1 + x_{e1}^{\alpha,III}} \cdot \frac{d_1}{d_1 + x_{e1}^{\alpha,III}} = u_0$$

yields solutions $x_{e1}^{B,III}$ and $x_{e1}^{C,III}$ (say $x_{e1}^{B,III} < x_{e1}^{C,III}$) that fulfill the equations

$$x_{e1}^{B,III} < u_1 - \frac{a}{c} \cdot \frac{b_2 \cdot u_0}{a_2 - u_0}$$

and

$$u_1 < x_{e1}^{C,III}$$

the system possesses three physical equilibrium points. These are

- the wash-out equilibrium point $y_e^{A,III}$, that is unstable with index 1: the equilibrium point itself is the only physical trajectory that stays in the neighbourhood of this point.
- the equilibrium point $y_e^{B,III}$, corresponding with only nitrite formation, that is now unstable with index 1: only trajectories on the y_3 -axis converge to this point.
- an equilibrium point $y_e^{D,III}$ (Eq. 4.231), in which nitrate is formed. This equilibrium point is quasi globally asymptotically stable: except from the equilibrium point $y_e^{A,III}$ and the trajectories on the y_3 -axis, all trajectories within the physical boundaries of the system converge to this point.

5. For moderately low dilution rates u_0 and rather high influent ammonium concentrations:

$$u_0 < \frac{a_1 \cdot d_1}{(\sqrt{b_1} + \sqrt{d_1})^2}$$

and in case the equation

$$a_1 \cdot \frac{x_{e1}^{\alpha,III}}{b_1 + x_{e1}^{\alpha,III}} \cdot \frac{d_1}{d_1 + x_{e1}^{\alpha,III}} = u_0$$

yields solutions $x_{e1}^{B,III}$ and $x_{e1}^{C,III}$ (say $x_{e1}^{B,III} < x_{e1}^{C,III}$) that fulfill the conditions

$$x_{e1}^{B,III} < u_1 - \frac{a}{c} \cdot \frac{b_2 \cdot u_0}{a_2 - u_0}$$

and

$$u_1 - \frac{a}{c} \cdot \frac{b_2 \cdot u_0}{a_2 - u_0} < x_{e1}^{C,III} < u_1$$

the system possesses four physical equilibrium points. These are

- the wash-out equilibrium point $y_e^{A,III}$, that is locally asymptotically stable.
- the equilibrium point $y_e^{B,III}$, corresponding with only nitrite formation, that is now unstable with index 1: only trajectories on the y_3 -axis on the right of $y_e^{C,III}$ converge to $y_e^{B,III}$.
- an equilibrium point $y_e^{C,III}$ (Eq. 4.226), also corresponding with only nitrite formation, that is also unstable with index 1: only trajectories parallel to the y_4 -axis and with $y_{e3}^{C,III}$ as y_3 -coordinate converge to $y_e^{C,III}$. These trajectories separate the regions of attraction of the equilibrium points $y_e^{A,III}$ and $y_e^{D,III}$.
- an equilibrium point $y_e^{D,III}$ (Eq. 4.231), in which nitrate is formed. This equilibrium point is locally asymptotically stable.

6. For moderately low dilution rates u_0 and even higher influent ammonium concentrations:

$$u_0 < \frac{a_1 \cdot d_1}{(\sqrt{b_1} + \sqrt{d_1})^2}$$

and in case the equation

$$a_1 \cdot \frac{x_{e1}^{\alpha,III}}{b_1 + x_{e1}^{\alpha,III}} \cdot \frac{d_1}{d_1 + x_{e1}^{\alpha,III}} = u_0$$

yields solutions $x_{e1}^{B,III}$ and $x_{e1}^{C,III}$ (say $x_{e1}^{B,III} < x_{e1}^{C,III}$) that fulfill the conditions

$$x_{e1}^{B,III} < u_1 - \frac{a}{c} \cdot \frac{b_2 \cdot u_0}{a_2 - u_0}$$

and

$$x_{e1}^{C,III} < u_1 - \frac{a}{c} \cdot \frac{b_2 \cdot u_0}{a_2 - u_0}$$

the system possesses five physical equilibrium points. These are

- the wash-out equilibrium point $y_e^{A,III}$, that is locally asymptotically stable.

- the equilibrium point $y_e^{B,III}$, corresponding with only nitrite formation, that is now unstable with index 1: only the trajectory to the right of $y_e^{C,III}$ converges to $y_e^{B,III}$.
- an equilibrium point $y_e^{C,III}$ (Eq. 4.226), also corresponding with only nitrite formation, that is unstable with index 2: the only trajectory that converges to $y_e^{C,III}$, is this point itself.
- an equilibrium point $y_e^{D,III}$ (Eq. 4.231), in which nitrate is formed. This equilibrium point is locally asymptotically stable.
- an equilibrium point $y_e^{E,III}$ (Eq. 4.231), in which nitrate is formed. This equilibrium point is unstable with index 1. The trajectories that converge to this point also constitute the stability boundary, that separates the regions of attraction of the equilibrium points $y_e^{A,III}$ and $y_e^{D,III}$.

4.7.6 Practical implications

The results from section 4.7 can be translated into some implications for practice. For good operation of a SHARON reactor, stable nitrite formation is pursued. Qualitatively, this is achieved by applying a dilution rate that is high enough to wash-out nitrite oxidizers, but low enough to ensure growth of ammonium oxidizers. This rule of thumb has been confirmed by the results in section 4.7. However, from Figure 4.6, it is clear that the influent ammonium concentration also plays a role in finding an appropriate dilution rate, starting with designing a reactor volume for a given reject water flow rate. The desired operating region is the one in which the equilibrium points $y_e^{A,I}$ and $y_e^{B,I}$ are both physical equilibrium points, with $y_e^{B,I}$ being quasi globally asymptotically stable. For decreasing influent ammonium concentrations, the dilution rate should, on the one hand, be kept lower to prevent biomass wash-out and, on the other hand, is also allowed to be kept lower and still prevent nitrate formation. For an influent ammonium concentration of about 30 mole m^{-3} , the range of dilution rates that guarantee stable nitrite formation is the largest, i.e. the designed reactor volume is most robust against variations of the influent flow rate. If the range of influent ammonium concentrations to be treated is known in advance, Figure 4.6 can be used to determine the range of dilution rates $u_0 = \frac{\Phi_{in}}{V}$ that guarantee stable nitrite formation. This information can as well be used to control the influent flow rate Φ_{in} (this will probably require

a buffer tank in front of the SHARON reactor or work with variable volume). It can also be used during the design phase, to determine the reactor volume V that guarantees stable nitrite formation for an expected range of influent ammonium concentrations and influent flow rates. However, Figure 4.6 reveals that the boundaries, that separate the operating regions in which $y_e^{A,I}$, $y_e^{B,I}$ or $y_e^{C,I}$ is the (quasi) globally asymptotically stable equilibrium point, depend on the microbial characteristics (a_1 , a_2 , b_1 , b_2 , a and c), that can only be estimated at the design stage.

Microbial characteristics clearly have a large impact on the operating conditions for which stable nitrite formation is obtained. It is known from practice that the operating region in which stable nitrite formation is obtained, becomes larger when the difference between the maximum growth rates of ammonium oxidizers (a_1) and nitrite oxidizers (a_2) becomes larger, e.g. when the temperature increases. However in this chapter, it has been shown that also the values of the substrate affinity constants ($b_1 = K_{TNH}^{amm}$ and $b_2 = K_{TNO_2}^{nit}$) play a role, as well as the value of the yield coefficient of ammonium oxidizers ($a = \frac{1}{Y_1}$) and even the nitrogen content of ammonium oxidizing biomass (as $c = \frac{1}{Y_1} - n$), although the influence of the latter will probably be negligible.

Inhibition effects, although not considered in section 4.7.3 clearly will also affect the operating conditions for which stable nitrite formation is achieved. The influence of nitrite inhibition has been considered explicitly in section 4.7.3. Figure 4.6 reveals that the region of dilution rates that result in stable nitrite formation for given influent ammonium concentrations, becomes broader if the ammonium oxidation is inhibited by nitrite. The reason for this must be sought in the lower nitrite concentration that corresponds with $y_e^{B,II}$ in comparison with $y_e^{B,I}$. In other words, nitrite inhibition of ammonium oxidation leads to substrate limitation of the subsequent nitrite oxidation step.

The effect of ammonium inhibition is even more drastic, as it affects not only the position but also the number of equilibrium points. However, if the ammonium inhibition is not too strong (inhibition constant d_1 rather high), this effect is not noticeable for low influent ammonium concentrations: Figure 4.10 (for $d_1 = 1000 \text{ mole m}^{-3}$) hardly differs from Figure 4.8 for influent ammonium concentrations up to about 80 mole m^{-3} . For larger influent ammonium concentrations or stronger inhibition kinetics (smaller d_1 -values), even two locally asymptotically stable equilibrium points can occur at the same time (case 3, 5 and 6),

in contrast to the situations without nitrite inhibition. In view of stable nitrite formation, especially case 3 is interesting. In this case, both the wash-out point $y_e^{A,III}$ and $y_e^{B,III}$, with only nitrite formation, are locally asymptotically stable. Depending on the initial conditions, one or the other equilibrium point is reached. The stability boundary, that separates their attraction regions is formed by the trajectories that are attracted to the unstable equilibrium point $y_e^{B,III}$: trajectories starting from initial states y with $y_3 < y_{e3}^{C,III}$ converge to $y_e^{A,III}$, while trajectories starting from initial states y for which $y_3 > y_{e3}^{C,III}$ converge to $y_e^{B,III}$. Whether the system converges to the wash-out state or to a steady state in which only nitrite is formed, thus only depends on the initial concentration of ammonium oxidizers in the system, compared to the value of $y_{e3}^{C,III}$ (Eq. 4.226). The latter value depends on the influent ammonium concentration u_1 : $y_{e3}^{C,III}$ increases for increasing influent ammonium concentrations, so the attraction region of the equilibrium point with stable nitrite formation ($y_e^{B,III}$) becomes smaller in favour of the attraction region of the wash-out state ($y_e^{A,III}$), which can be explained by increasing ammonium inhibition. The value of $y_{e3}^{C,III}$ is further determined by microbial characteristic parameters a , a_1 , b_1 and d_1 (see 4.227).

For future research, it is suggested to further exploit the effect of microbial characteristics on the operating conditions under which stable nitrite formation is achieved. In particular, it would be interesting to study how these conditions are affected by the reactor temperature, and moreover, pH. Besides, it could also be investigated under which conditions an Anammox-optimal nitrite:ammonium ratio is obtained in the SHARON reactor.

4.8 Discussion and conclusions

In this chapter, the existence, uniqueness, and stability of the equilibrium points of a SHARON reactor model have been studied on theoretical grounds. The model under study is a simple two-step nitrification model, in which the growth rate of ammonium oxidizers is larger than the growth rate of nitrite oxidizers. The reactor volume is assumed constant. It is further assumed that the reactor is continuously aerated and that the biomass is not limited by oxygen. The reactor pH and temperature are assumed to be controlled on a constant value.

From an operating point of view, it is interesting to work in a region where the system possesses only one equilibrium point. In order to identify such regions, the contraction mapping theorem has been applied. However, only the wash-out equilibrium point could be identified as a unique equilibrium point, occurring at high values of the dilution rate. This wash-out point is clearly not an interesting operating point.

Subsequently, the equilibrium points of the SHARON reactor model have been calculated directly in a number of simplified cases. This theoretical study is useful to determine exactly how many equilibrium points occur under which circumstances. This approach is preferred over the identification of equilibrium points through a simulation study, performing steady state simulations for different initial conditions. Indeed, the latter approach does not guarantee that all equilibrium points will be identified. In particular, it would not be easy to identify unstable equilibrium points. Besides, it would be difficult to determine the boundary conditions for which the model possesses a certain number of equilibrium points.

Three equilibrium points have been found in case the influent does not contain nitrite, ammonium oxidizers or nitrite oxidizers, nitrite oxidizers are not limited by ammonium and no inhibition takes place. For high dilution rates, only the equilibrium point corresponding with biomass wash-out occurs and is globally asymptotically stable. For moderately low dilution rates and at the same time sufficiently high influent ammonium concentrations, a second equilibrium point, corresponding with only nitrite formation, occurs and is now quasi globally asymptotically stable, while the wash-out point now becomes unstable and cannot be reached from within the physical boundaries of the system, unless it is the system's initial condition. If the dilution becomes even lower and the influent ammonium concentration is sufficiently high, a third equilibrium point, corresponding with nitrate formation, appears and is locally asymptotically stable. Under these conditions, the wash-out equilibrium point is still unstable in the same way as mentioned above. Besides, the equilibrium point corresponding with only nitrite formation also becomes unstable. The only way the latter equilibrium is reached, is for initial conditions in which no nitrite oxidizers are present in the system. These findings agree with what is expected from practice. From an operating point of view, the second situation, in which the equilibrium point with only nitrite formation is quasi globally asymptotically stable, is clearly the most interesting.

If nitrite inhibition of ammonium oxidation is taken up in the model, as for the simulation work described in chapters 5 and 8, it has been found that the number of equilibrium points, as well as their stability, is not affected. On the other hand, the position of the equilibrium points corresponding with biomass growth does change: less ammonium is converted as nitrite becomes a more severe inhibitor of the process. The condition for the occurrence of an equilibrium point with only nitrite production remains the same, while the condition for the occurrence of an additional equilibrium point, corresponding with nitrate formation, becomes more stringent: it occurs at lower dilution rates and higher influent ammonium concentrations than in case of no nitrite inhibition. These effects of nitrite inhibition are only minor for the value of the nitrite inhibition constant, applied in the SHARON reactor model in this thesis, as the effect of nitrite inhibition is not so strong at the prevailing pH (= 7) for which the reactor model has been evaluated. It is expected that for lower pH-values, when the fraction of nitrite in the inhibiting – uncharged – form is higher and inhibition effects are thus also higher, the differences between the models with and without nitrite inhibition become larger.

Subsequently, the effect of changing parameter and input values on the number of equilibrium points and their stability has been examined for the SHARON reactor model with nitrite inhibition of ammonium oxidation. Although the position of the equilibrium points is only slightly affected, the equilibrium points on the physical system boundaries now shift outside these boundaries under certain conditions. As a result, only one equilibrium point occurs at a time.

The influence of microbial growth kinetics on the number of equilibrium points has also been addressed in this chapter. While the results indicate that product inhibition does not affect the number of equilibrium points of a (bio)reactor model, it has been shown that substrate inhibition is clearly a source of additional equilibrium points. It has been found that taking up ammonium inhibition of ammonium oxidation in a simple two-step nitrification model leads to the occurrence of up to five equilibrium points: one wash-out point, two equilibrium points corresponding with only nitrite formation and two equilibrium points corresponding with nitrate formation.

Finally, the results from the theoretical analysis have been translated into some practical implications. The theoretical analysis has been proven a useful tool and is recommended by the author to be applied more frequently to practical cases.

Chapter 5

Controlling a SHARON reactor with fixed design

A summarized version of this chapter is currently in press:

Volcke E.I.P., van Loosdrecht M.C.M. and Vanrolleghem P.A. (2006). Controlling the nitrite:ammonium ratio in a SHARON reactor in view of its coupling with an Anammox process. Water Science and Technology, 53, 4-5.

The usefulness of controlling a SHARON reactor in view of its coupling with an Anammox process is the focus of this chapter. Partial nitrification in the SHARON reactor should be performed to such an extent that a nitrite:ammonium ratio is generated that is optimal for full conversion in an Anammox process. In the simulation studies performed in this contribution, the nitrite:ammonium ratio produced in a SHARON process with fixed volume, as well as its effect on the subsequent Anammox process, is examined for realistic influent conditions and considering both direct and indirect pH effects on the SHARON process. Several possible operating modes for the SHARON reactor, differing in control strategies for O_2 , pH and the produced nitrite:ammonium ratio and based on regulating the air flow rate and/or acid/base addition, are systematically evaluated. The results are quantified through an operating cost index (OCI). Best results are obtained by means of cascade feedback control of the SHARON effluent nitrite:ammonium ratio through setting an O_2 -setpoint that is tracked by adjusting the air flow rate, combined with single loop pH-control through acid/base addition.

5.1 Introduction

The combined SHARON-Anammox process for treating wastewater streams with high ammonia load, is discussed. In the SHARON process, nitrification of ammonium to nitrite (nitritation) without nitrate formation is achieved by working at high temperature (30-40°C), neutral pH (about 7.5) and maintaining an appropriate sludge retention time (SRT). In the last few years, the coupling of the SHARON process with a so-called Anammox process, in which ammonium and nitrite are converted to nitrogen gas, has gained a lot of interest (van Dongen et al., 2001). Compared to conventional nitrification/denitrification, the combined SHARON-Anammox process allows large savings on aeration energy (up to 63%) and carbon source addition costs (up to 100%), while sludge production is low. One application of the SHARON-Anammox process is to treat sludge digestion reject water in order to relieve the main wastewater treatment plant (WWTP) with limited aeration capacity. For normal sludge digestion reject water, it can be reasonably assumed that the SHARON influent contains approximately equimolar amounts of ammonium and bicarbonate. Due to alkalinity destruction only partial nitritation will occur: typically approximately half of the ammonium will be converted to nitrite (van Dongen et al., 2001). Hence, the SHARON effluent will approximately contain the required nitrite:ammonium ratio of 1:1 that is needed to feed the Anammox reactor (Figure 5.1). In practice, the actual nitrite:ammonium ratio *needed* for full conversion by the Anammox process will depend on the biomass yield and is typically somewhat higher. Also, the nitrite:ammonium ratio *produced* by the SHARON process depends upon a number of factors, e.g. influent alkalinity.

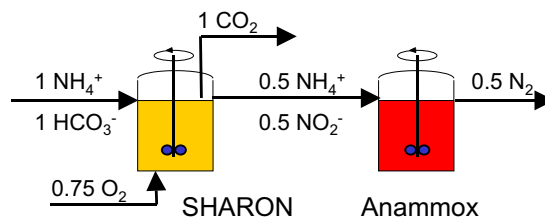


Figure 5.1: Simplified scheme of the SHARON-Anammox process

In this chapter, possible control handles of the SHARON process with fixed reactor volume are identified and several operating modes are evaluated in a systematic way and quantified by means of an ope-

rating cost index (OCI). The operating modes under study differ in the applied control strategies for O_2 and pH, in a single loop configuration or combined with cascade control of the produced nitrite:ammonium ratio.

5.2 Simulation study

5.2.1 Influent conditions

In order to obtain a realistic influent file, daily averaged on-line measurements for flow rate and ammonium concentrations, as well as weekly lab analyses for bicarbonate alkalinity and pH from the full-scale SHARON process in Rotterdam were used. Figure 5.2 gives the resulting influent flow rate, ammonium and bicarbonate concentrations and load profiles, as well as the influent pH profile.

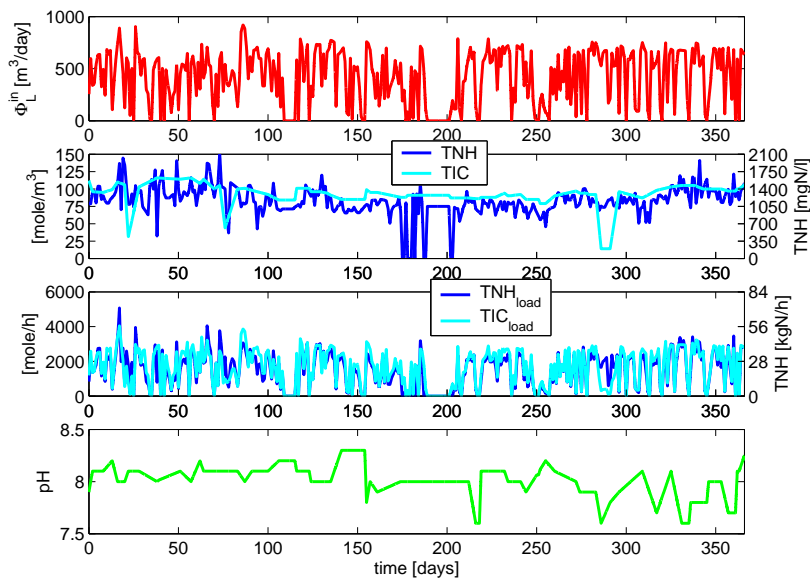


Figure 5.2: Typical yearly SHARON influent characteristics

The influent flow rate varies between 0 and 921 m^3/day (mean 422). The influent ammonium concentration varies between 32 and 152 $mole/m^3$ (mean 85 $mole/m^3$), the influent bicarbonate concentration between 14 and 116 $mole/m^3$ (mean 93 $mole/m^3$) and the influent bicarbonate:ammonium molar ratio between 0.16 and 3.59 (mean 1.1).

The influent pH varies between 7.6 and 8.3 (mean 8.0). The liquid influent stream was assumed not to contain oxygen, its nitrogen concentration was set to 0.44 mole/m^3 , the equilibrium concentration with air for atmospheric pressure and 35°C .

5.2.2 The SHARON and Anammox reactor models

The SHARON reactor model, described in chapter 3, and the Anammox reactor model, described in appendix D, have been used in this study.

The SHARON reactor is a continuously stirred tank reactor (CSTR), operated without sludge retention. Hence, the hydraulic retention time (HRT) equals the sludge retention time (SRT). In steady state the SRT (=HRT) equals the inverse of the growth rate of the microorganisms:

$$\begin{aligned} \frac{1}{SRT} &= \mu^{amm} & (5.1) \\ &= \mu_{max}^{amm} \cdot \frac{C_{NH_3}}{K_{NH_3}^{amm} + C_{NH_3}} \cdot \frac{C_{O_2}}{K_{O_2}^{amm} + C_{O_2}} \cdot \frac{K_{I,HNO_2}^{amm}}{K_{I,HNO_2}^{amm} + C_{HNO_2}} \end{aligned}$$

The actual growth rate (μ^{amm}) is determined by the (aerobic) SRT. The corresponding ammonia (NH_3) concentration (and in this way also the total ammonium conversion) is determined by the concentrations of oxygen and nitrous acid (HNO_2) (also related to the total ammonium conversion) and by temperature and pH. Temperature determines the value of μ_{max}^{amm} and the equilibrium constants of the HNO_2/NO_2^- and NH_4^+/NH_3 equilibria. The actual growth rate μ^{amm} comprises direct and indirect effects of the reactor pH. The direct effect is described in the model through the pH-dependency of the growth rate of ammonium oxidizers as determined by Van Hulle et al. (2004) (Figure 3.1). The pH also plays an indirect role through the fractions of total ammonium and total nitrite that are in the uncharged state (NH_3 , HNO_2). The pH itself decreases due to ammonia conversion and increases by bicarbonate stripping in the form of CO_2 . As the SHARON reactor model takes into account these different effects, it is well suited for scenario analysis, as performed in this chapter.

The SHARON reactor volume is set constant at 528 m^3 (reactor height 4 m), corresponding with a mean retention time of 1.25 days for the given influent conditions (cfr. $1/\mu_{max}^{amm} \approx 0.5$ days). A constant reactor temperature of 35°C is assumed. The Anammox reactor is modelled as a CSTR of 75 m^3 with almost complete (99.5%) biomass retention, operated at 35°C .

5.2.3 SHARON reactor operating modes under study

In this chapter, a SHARON reactor with fixed and constant volume, operated without sludge retention, is considered. Consequently, the SRT (=HRT) varies with varying influent flow rate (no buffer tank is considered). The influent ammonium and bicarbonate concentrations vary as well (see Figure 5.2). In order to control the ammonium conversion and in this way the produced nitrite:ammonium ratio, the following control handles and their constraints are identified from Eq. 5.1:

- Acid/base addition: this directly influences the pH. As the pH increases, the substrate (NH_3) concentration increases and the inhibitor (HNO_2) concentration decreases, enhancing ammonia conversion. However, the pH should stay in a range that guarantees acceptably high values of μ_{max}^{amm} (see Figure 3.1).
- Adjusting the air flow rate: an increasing air flow rate results in a higher O_2 -level in the reactor, increasing the ammonium conversion as long as the Monod term is not approaching one. If the (aerobic) SRT is too high, the air flow rate can be turned off periodically in order to prevent nitrate formation. The air flow rate doesn't only effect the O_2 -concentration but also the pH due to a combined effect of CO_2 -stripping and ammonium conversion. As the air flow rate increases, more CO_2 is stripped from the reactor, resulting in a pH-increase. At the same time, an increasing air flow rate enhances the ammonium conversion, resulting in a pH-decrease.

In this chapter, several control strategies, based on acid/base addition and/or regulating the air flow rate, are systematically evaluated. Table 5.1 summarizes the different operating modes of the SHARON reactor that have been studied. O_2 is controlled by adjusting the air flow rate between almost zero ($3.6e-7$) and $20,000 \text{ m}^3/\text{h}$. The O_2 -setpoint is either fixed (O_2 -control), or set between zero and the prevailing saturation concentration (8.96 mg/l) by a master controller that aims at reaching the setpoint R^{sp} for the nitrite:ammonium ratio (cascade O_2 -control). The pH is controlled by addition of acid (96% H_2SO_4) or base (50% NaOH) at a flow rate of maximum 50 l/h . The pH-setpoint is either fixed (pH-control), or set between 6.23 and 8.23 (around pH^{opt} according to Eq. 3.14) by a master controller in order to reach the setpoint R^{sp} for the nitrite:ammonium ratio (cascade pH-control). For both cascade O_2 -control and cascade pH-control, the setpoint for the nitrite:am-

monium ratio is set at $R^{sp}=1.23$, corresponding to the ratio of their stoichiometric coefficients in the Anammox reactor model (appendix D). Finally, the different O_2 - and pH-control strategies can be combined, resulting in 8 different operating modes.

Table 5.1: SHARON reactor operating modes under study (details, see text)

control variables	O_2	pH	$(TNO_2/TNH)^{sp} = R^{sp}$ (master)
control handle	air flow rate $\Phi_{G,in}$	acid/base addition	O_2^{sp} (slave) or pH^{sp} (slave)
1. no control	constant $\Phi_{G,in}$	-	-
2. O_2 -control	constant O_2^{sp}	-	-
3. cascade O_2 -control	O_2^{sp} set by master	-	constant R^{sp}
4. pH-control	constant $\Phi_{G,in}$	constant pH^{sp}	-
5. cascade pH-control	constant $\Phi_{G,in}$	pH^{sp} set by master	constant R^{sp}
6. O_2 -control + pH-control	constant O_2^{sp}	constant pH^{sp}	-
7. cascade O_2 -control + pH-control	O_2^{sp} set by master	constant pH^{sp}	constant R^{sp}
8. cascade pH-control + O_2 -control	constant O_2^{sp}	pH^{sp} set by master	constant R^{sp}

All controllers are proportional controllers, tuned under short-term conditions for a constant influent, using the ISE and ITAE criteria and preventing saturation of the actuators (that occurs when the controller gain would be too high). Oxygen sensors and pH-sensors are described as first order systems with a time constant of 20 s. The on-line measurements of ammonium and nitrite are modelled as being ideal, but with a delay of 0.5 h. Ideal valves for acid and base addition are assumed.

5.3 Economic evaluation by means of an operating cost index (OCI)

The optimal design and operating mode of a process is a trade-off between effluent quality and the associated investment and operating costs. An operating cost index (OCI) is a useful tool in simplifying this cost analysis. It includes the most important operating cost factors and indicates possible cost savings that can be made with control. Information on investment costs for the necessary equipment will then only

be gathered for those control strategies that promise substantial operational cost savings. Vanrolleghem and Gillot (2002) have previously demonstrated the use of an OCI to compare control strategies through the COST benchmark (Copp, 2002).

In this chapter, an OCI is defined on the basis of the following considerations. As the Anammox effluent doesn't comply with prevailing legislation, it will be most likely recycled to the main wastewater treatment plant (WWTP). It can be reasonably assumed that nitrite and nitrate in the Anammox effluent will be denitrified in the recycle stream, where they are mixed with other streams, containing COD. Ammonium that is recycled to the main plant, that is assumed here to have a lack of aeration capacity, will end up in the effluent and will be fined by the effluent quality term EQ (in kg Pollution Units/day). This term is calculated as in the benchmark approach (Copp, 2002), but in this study only covers ammonium. The differences in the SHARON reactor air flow rates for the different scenarios are accounted for through the aeration energy term AE (in kWh/day), that is also calculated as in the benchmark approach. For the operating mode with acid and base addition, the costs for addition of these chemicals (96% H₂SO₄ and 50% NaOH) are taken into account as well. The resulting OCI (in € /year) is written as follows:

$$OCI = \gamma_1 \cdot EQ + \gamma_2 \cdot AE + \alpha_{acid} \cdot \Phi_{acid} + \alpha_{base} \cdot \Phi_{base} \quad (5.2)$$

in which

$$EQ = \frac{1}{T \cdot 1000} \int_T \beta_{TNH} \cdot C_{TNH,An} \cdot \Phi_{An}^{out} dt \quad (5.3)$$

$$AE = \frac{24}{T} \int_T \frac{V_{SH}}{V_{BSM}} \cdot [0.0007 \cdot k_L a_{SH}^2 + 0.3267 \cdot k_L a_{SH}] dt \quad (5.4)$$

with $T=366$ days the evaluation period and $\beta_{TNH}=20$ a scaling coefficient. The cost coefficients for the pollution units, aeration energy and acid and base additions are summarized in Table 5.2, based on Vanrolleghem and Gillot (2002) (for EQ and AE terms) and <http://ed.icheme.org/costchem.html> (for acid and base addition). Note that the OCI only includes the operating costs that differ between the scenarios under study. As the volume of the SHARON reactor is considered fixed on a predefined value and is constant throughout the operation, reactor investment costs are the same for all scenarios examined. Savings in operating costs between two operating modes thus equal the investment costs that can be supported for additional control equipment.

Table 5.2: Cost multiplication factors

economic weight	value	unit
γ_1	50	€/EQ/year (EQ in kgPU/d)
γ_2	25	€/AE/year (AE in kWh/d)
α_{acid}	62.3	€/m ³
α_{base}	93.4	€/m ³

5.4 Simulation results

The behaviour of the SHARON reactor under the operating modes corresponding with the different control strategies of Table 5.1, and their effect on the subsequent Anammox process have been simulated. The results are summarized in Table 5.3 and discussed in the following paragraphs.

Table 5.3: Simulation results for the different SHARON reactor operating modes under study

Operating mode			OCI [€/year]				
			EQ	AE	acid	base	total
1. no control	$\Phi_G^{in} = 3000 \text{ m}^3/\text{h}$	-	492,420	34,270	0	0	526,690
2. O ₂ -control	$O_2^{sp, opt} = 3 \text{ mg/l}$	-	248,010	40,400	0	0	288,410
3. cascade O ₂ -control	O_2^{sp} set by master $R^{sp} = 1.23$	-	478,630	121,310	0	0	608,930
4. pH-control	$\Phi_G^{in} = 3000 \text{ m}^3/\text{h}$	$pH^{sp, opt} = 6.25$	227,150	34,270	17,840	2,190	281,450
5. cascade pH-control	$\Phi_G^{in} = 3000 \text{ m}^3/\text{h}$	pH^{sp} set by master $R^{sp} = 1.23$	443,580	34,270	12,120	2,640	492,610
6. O ₂ -control + pH-control	$O_2^{sp, opt} = 3 \text{ mg/l}$	$pH^{sp, opt} = 7.23$	140,830	65,080	540	31,030	237,480
7. cascade O ₂ -control + pH-control	O_2^{sp} set by master $R^{sp} = 1.23$	$pH^{sp, opt} = 7.23$	56,300	59,330	5,200	4,740	125,570
8. O ₂ -control + cascade pH-control	$O_2^{sp, opt} = 4 \text{ mg/l}$	pH^{sp} set by master $R^{sp} = 1.23$	231,760	48,430	7,110	9,180	296,480

5.4.1 SHARON operating mode 1: no control

In case the SHARON reactor is operated with a fixed air flow rate (no control), periods of high influent flow rates (lowered SRT) cause a pH-increase because of decreasing ammonium conversion combined with CO₂-stripping, eventually resulting in biomass wash-out. Air flow rates from 1000 up to 8000 m³/h all resulted in complete wash-out of the ammonium oxidizers after less than 30 days. Consequently,

hardly any ammonium conversion occurs in the Anammox-reactor. Figure 5.3 shows typical concentration profiles (for $\Phi_G^{in} = 3000 \text{ m}^3/\text{h}$).

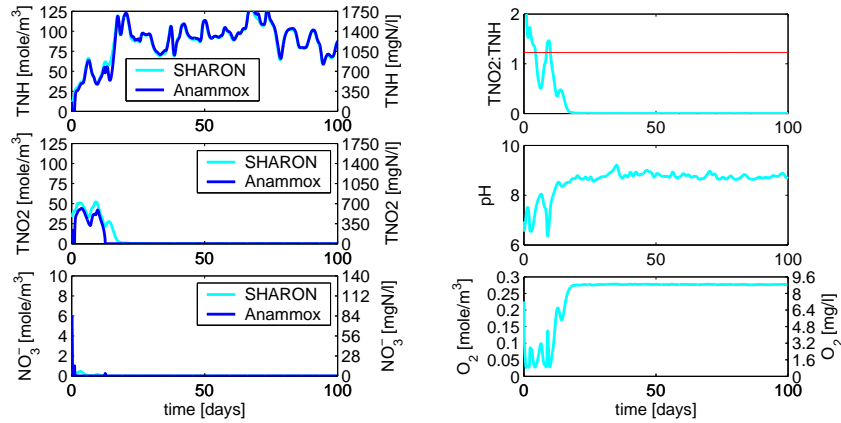


Figure 5.3: (from top to bottom) Concentration profiles of total ammonium (TNH), total nitrite (TNO₂) and nitrate in SHARON reactor and in subsequent Anammox reactor (left). Profiles of nitrite:ammonium ratio (TNO₂:TNH), pH and O₂ concentration (right). Operating mode of SHARON reactor with fixed air flow rate ($\Phi_G^{in} = 3000 \text{ m}^3/\text{h}$)

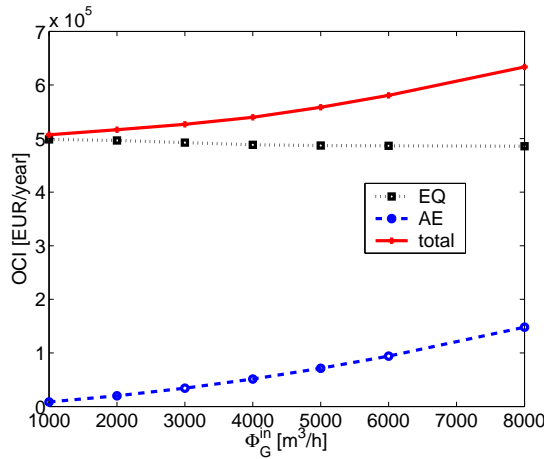


Figure 5.4: OCI in terms of Φ_G^{in} (no control)

Figure 5.4 shows the OCI in terms of the air flow rate applied. As biomass is washed out and there is no more conversion, the OCI term for effluent quality is very high, although a slight decrease for higher

air flow rates is noticeable as biomass wash-out occurs a little later as the air flow rate increases. In any case, this operating mode is not an option, since there is no conversion in the SHARON and Anammox reactors and the permit of the wastewater treatment plant may be in jeopardy when the maximum discharge limit is not reached.

5.4.2 SHARON operating mode 2: O_2 -control

In this operating mode, the oxygen concentration in the SHARON reactor (expressed in mole/m³) is controlled at a fixed level by adjusting the air flow rate (in m³/s through a proportional controller with gain $K=1000$. The best results (smallest OCI) are obtained for $O_2^{sp} = 3$ mg/l and are shown in Figure 5.5. Under these conditions, during most of the time ammonium is converted in the SHARON reactor, while there are also periods -corresponding with high influent flow rates and corresponding low SRT- without ammonium conversion and showing concomitantly high pH-values. When ammonium is converted in the SHARON reactor, too much ammonium is converted, resulting in an unfavourable nitrite:ammonium ratio that leads to nitrite inhibition of the Anammox process. As a result, hardly any Anammox conversion is realized. Some nitrite conversion is realized in the Anammox reactor, but this is due to denitrification (using hydrolysed products from biomass decay as a COD source).

When the O_2 -setpoint is increased from $O_2^{sp} = 1$ to 4.5 mg/l (results not shown), ammonium conversion becomes possible for lower SRT-values. Hence more and longer periods with ammonium conversion in the SHARON reactor occur, but in each of these cases too much ammonium is converted, causing nitrite inhibition of the Anammox process. This indicates that the O_2 -setpoint can only be used to control the ammonium conversion in a sense that it allows ammonium conversion (for the prevailing SRT) or not, but it cannot be used to control the extent of ammonium conversion. These results agree with steady state simulation results (not shown), that show an almost discontinuous profile of the amount of ammonium conversion in terms of the oxygen setpoint for a fixed SRT. In order to control the extent of ammonium conversion and thus the nitrite:ammonium ratio, one could change the O_2 -setpoint on a lower time scale (faster) than the hydraulic retention time, i.e. use it as kind of on/off controller. This is realized through cascade O_2 -control in operating mode 3.

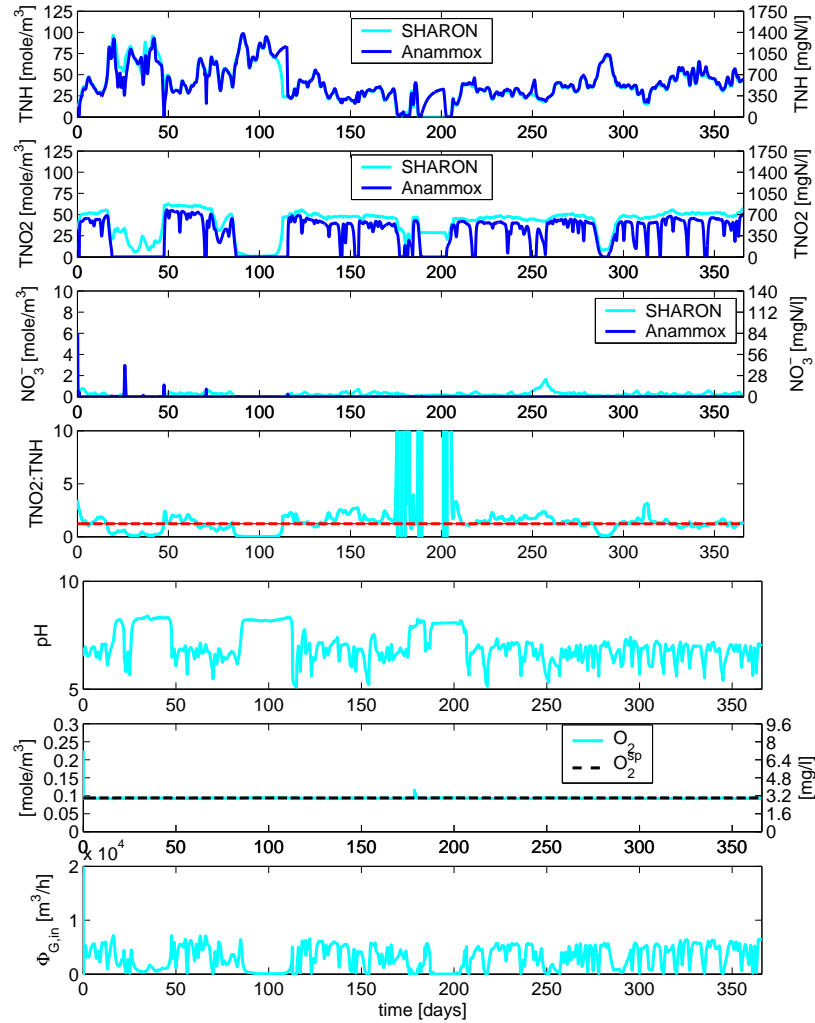


Figure 5.5: (from top to bottom) Concentration profiles of total ammonium (TNH), total nitrite (TNO2) and nitrate in SHARON reactor and in subsequent Anammox reactor. Profiles of nitrite:ammonium ratio (TNO2:TNH), pH, acid/base addition, O_2 concentration vs. O_2^{sp} and air flow rate in SHARON reactor. Operating mode of SHARON reactor with O_2 -control (at $O_2^{sp}=3$ mg/l)

As the O_2 -setpoint increases beyond 4.5 mg/l (results not shown), more periods appear again without ammonium conversion and concomitantly high pH-values. This is probably due to increased CO_2 -stripping because of the increased air flow rate and results in a worse effluent quality, that now plays a dominant role.

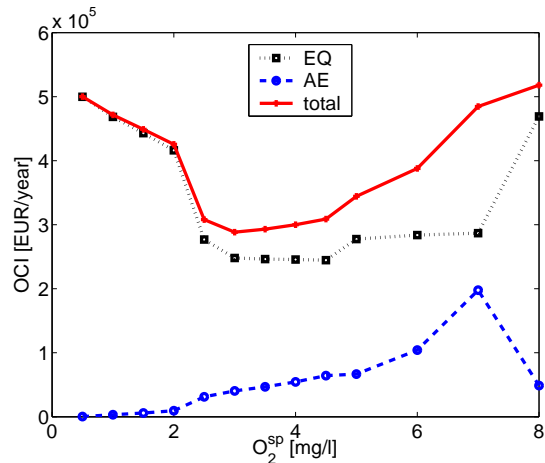


Figure 5.6: OCI in terms of O_2^{sp} for O_2 -control

Figure 5.6 shows the different OCI contributions for the different O_2 -setpoints examined. The effluent quality term makes up the largest fraction of the costs. As in all cases hardly any Anammox conversion occurs, the effluent quality term corresponds with the amount of ammonium converted in the SHARON reactor: its value increases up to $O_2^{sp} = 4.5$ mg/l and decreases for higher oxygen setpoint values. The aeration energy required increases as the oxygen setpoint increases up till $O_2^{sp} = 7$ mg/l. For $O_2^{sp} = 8$ mg/l less aeration energy is required, as substantially less ammonium is converted in this case, and therefore less aeration is required to maintain the oxygen level in the reactor.

It is clear that a fixed oxygen setpoint for the SHARON process does not guarantee the realization of a fixed nitrite:ammonium ratio (and certainly not the optimal one). The mean air flow rate corresponding with the best results (for $O_2^{sp} = 3$ mg/l) is about $\Phi_{G,in} = 3000$ m³/h. For this reason, this value is further used in the operating modes with constant air flow rate (4, 5 and 8).

5.4.3 SHARON operating mode 3: cascade O_2 -control

This strategy, schematically presented in Figure 5.7, consists of increasing the oxygen setpoint when the produced nitrite:ammonium ratio is too low, in order to increase ammonium conversion. The (varying) oxygen setpoint is met by adjusting the air flow rate. The gain of the sec-

ondary controller was kept at 1000, the gain of the primary controller was tuned at 0.01 (for concentrations expressed in mole m^{-3}).

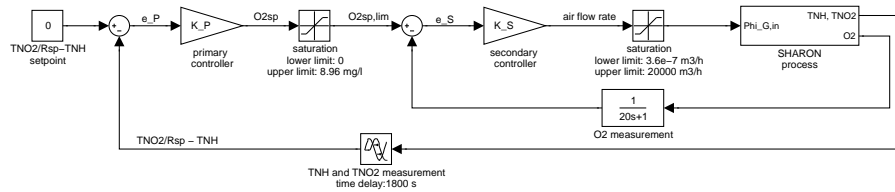


Figure 5.7: Control scheme for cascade O_2 -control

Figure 5.8 gives the simulation results for this operating mode. All ammonium oxidizers are washed out within 20 days. This is caused by the fact that during a period of high influent flow rates (short SRT), the resulting decrease in ammonium conversion is leading to an increase in the oxygen setpoint, that is met by increasing the air flow rate. As a result, however, more CO_2 is stripped from the reactor too, increasing the pH to such an extent that the growth rate of the ammonium oxidizers decreases even further and the biomass is eventually washed out. For this reason, it seems advisable to combine cascade O_2 -control with pH-control (operating mode 7).

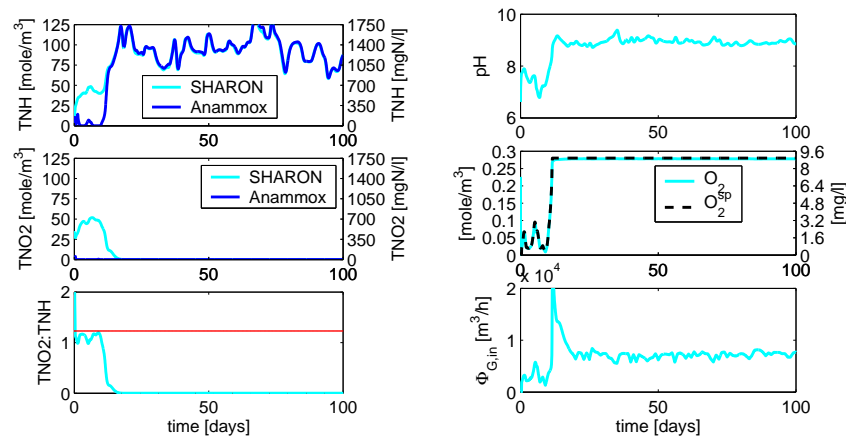


Figure 5.8: (from top to bottom) Concentration profiles of total ammonium (TNH), total nitrite (TNO2) in SHARON reactor and in subsequent Anammox reactor, nitrite:ammonium ratio in SHARON reactor (left). Profiles of pH, O_2 concentration vs. O_2^{sp} and air flow rate in SHARON reactor (right). Operating mode of SHARON reactor with cascade O_2 -control

5.4.4 SHARON operating mode 4: pH-control

In this operating mode, the pH in the SHARON reactor is controlled at a fixed value by adding acid or base (in eq/m^3) through a proportional controller with gain $K=1$. The best results (smallest OCI) are obtained for $pH^{sp} = 6.25$ and are shown in Figure 5.10. However, the setpoint is not well tracked, because of insufficient control authority (limitation on amount of acid/base added). The nitrite:ammonium ratio produced in the SHARON reactor is not constant and most of the time lower than the optimal ratio, so a large quantity of ammonium remains unconverted in the Anammox-reactor.

As the pH-setpoint increases, the nitrite:ammonium ratio produced in the SHARON reactor exceeds the optimal value more often, resulting in more nitrite inhibition of the Anammox reactor (results not shown). For $pH^{sp} = 6.75$ and higher, hardly any Anammox conversion takes place. As a result, the effluent quality is now almost completely determined by the amount of ammonium produced in the SHARON reactor. This amount of ammonium is related to the pH-dependency of the biomass growth rate, that is optimal at $pH=7.23$. This optimum is slightly reflected in Figure 5.9, that shows the different OCI contributions in terms of the pH-setpoint. The effluent quality clearly accounts for the largest fraction of the costs.

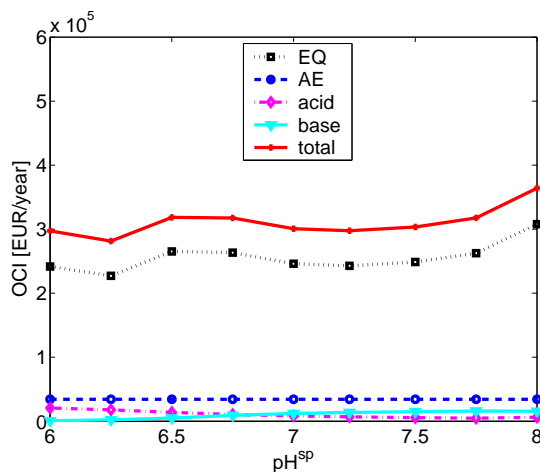


Figure 5.9: OCI in terms of pH^{sp} for pH-control

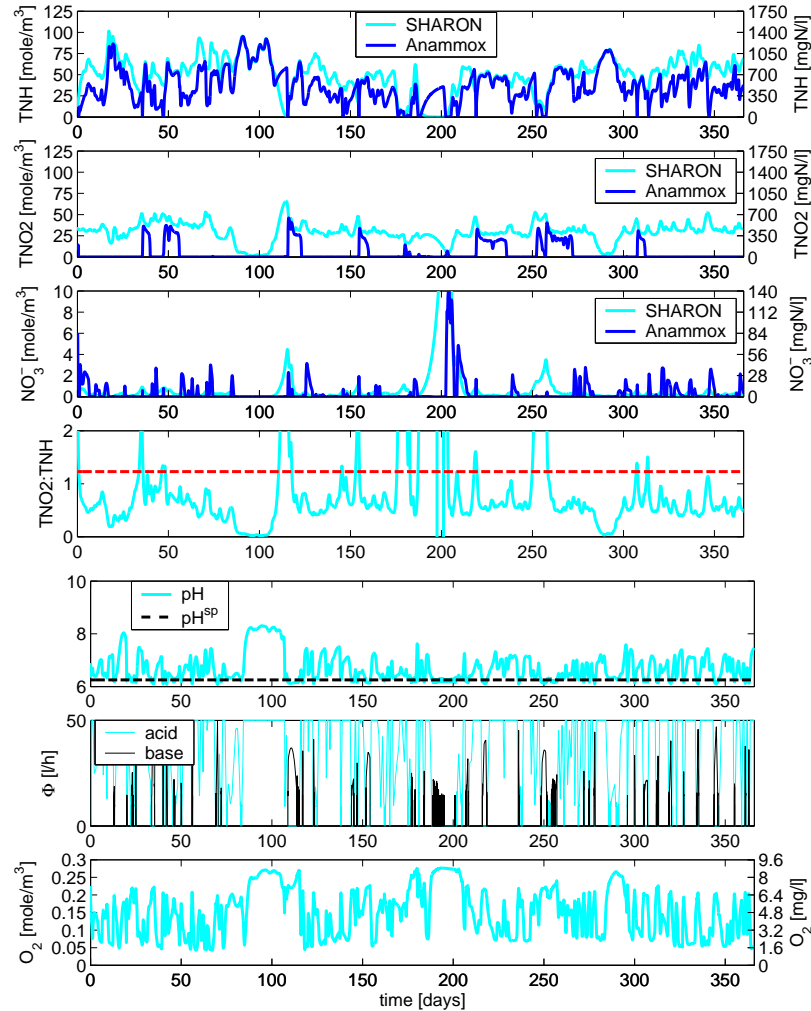


Figure 5.10: (from top to bottom) Concentration profiles of total ammonium (TNH), total nitrite (TNO2) and nitrate in SHARON reactor and in subsequent Anammox reactor. Profiles of nitrite:ammonium ratio (TNO2:TNH), pH vs. pH^{sp} , acid/base addition and O_2 concentration in SHARON reactor. Operating mode of SHARON reactor with fixed air flow rate ($\Phi_{G,in} = 3000 \text{ m}^3/\text{h}$) and pH-control (at $pH^{sp}=6.25$)

5.4.5 SHARON operating mode 5: cascade pH-control

Cascade pH-control is based on increasing the pH-setpoint when the produced nitrite:ammonium ratio is too low (van Dongen et al., 2001), in order to increase the conversion due to an increasing substrate (NH_3)

concentration and a decreasing concentration of HNO_2 , that inhibits conversion. The control scheme is given in Figure 5.11. The gain of the secondary controller was kept at 1, the gain of the primary controller was tuned at 1.5 (for concentrations expressed in mole m^{-3}).

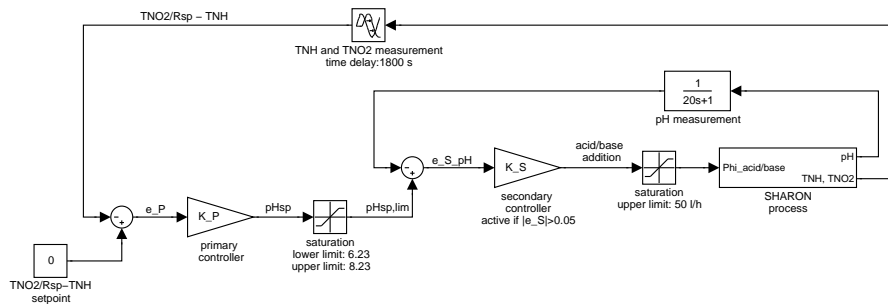


Figure 5.11: Control scheme for cascade pH-control

Figure 5.12 gives the corresponding simulation results. The cascade pH-control strategy does not perform well because the maximum growth rate of the ammonium oxidizers decreases at higher pH-levels. This direct pH-effect is not accounted for in the applied control strategy, that is based on the indirect pH-dependency of the biomass growth rate only. As a result, very little nitrite is produced in the SHARON reactor and only little Anammox conversion takes place in the subsequent Anammox-reactor, resulting in a very bad effluent quality.

5.4.6 SHARON operating mode 6: O_2 -control + pH-control

Numerous combinations of fixed oxygen setpoints (ranging from 1 to 7 mg/l) and fixed pH-setpoints (from 6.5 to 7.5) have been examined. The best results (minimum OCI) have been obtained for $O_2^{sp}=3$ mg/l and $pH^{sp} = 7.23$. Note that the value for the oxygen setpoint corresponds to the optimal value that has been found for operating mode 2 with oxygen control, while the value for the pH-setpoint differs from the optimal value found for operating mode 4 with only pH-control. The optimal combination of an oxygen- and a pH-setpoint thus appears to be different from the combination of an optimal oxygen setpoint and an optimal pH-setpoint. Figure 5.13 shows the simulation results for $O_2^{sp}=3$ mg/l and $pH^{sp} = 7.23$. In this 'optimal' case, too much ammonium is converted in the SHARON reactor, leading to complete inhibition of the Anammox conversion by nitrite. Consequently, no ammonium conversion occurs in the Anammox reactor.

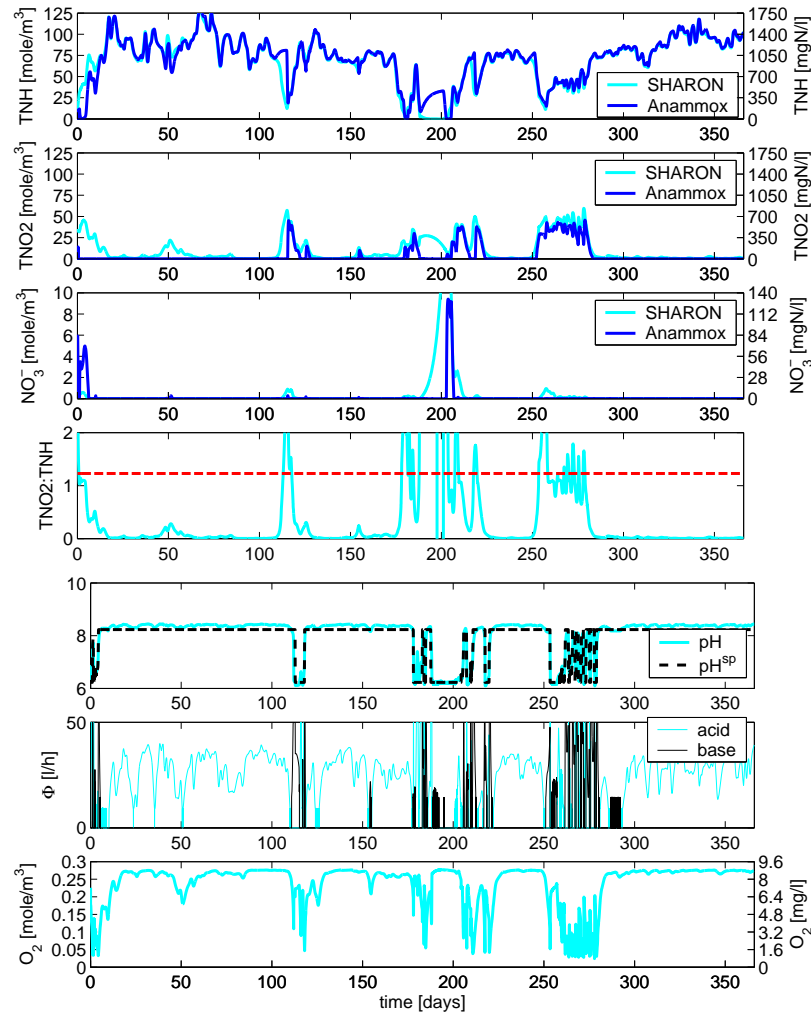


Figure 5.12: (from top to bottom): Concentration profiles of total ammonium (TNH), total nitrite (TNO2) and nitrate in SHARON reactor and in subsequent Anammox reactor. Profiles of nitrite:ammonium ratio (TNO2:TNH), pH vs. pH^{sp}, acid/base addition and O₂ concentration in SHARON reactor. Operating mode of SHARON reactor with fixed air flow rate ($\Phi_{G,in} = 3000 \text{ m}^3/\text{h}$) and cascade pH-control

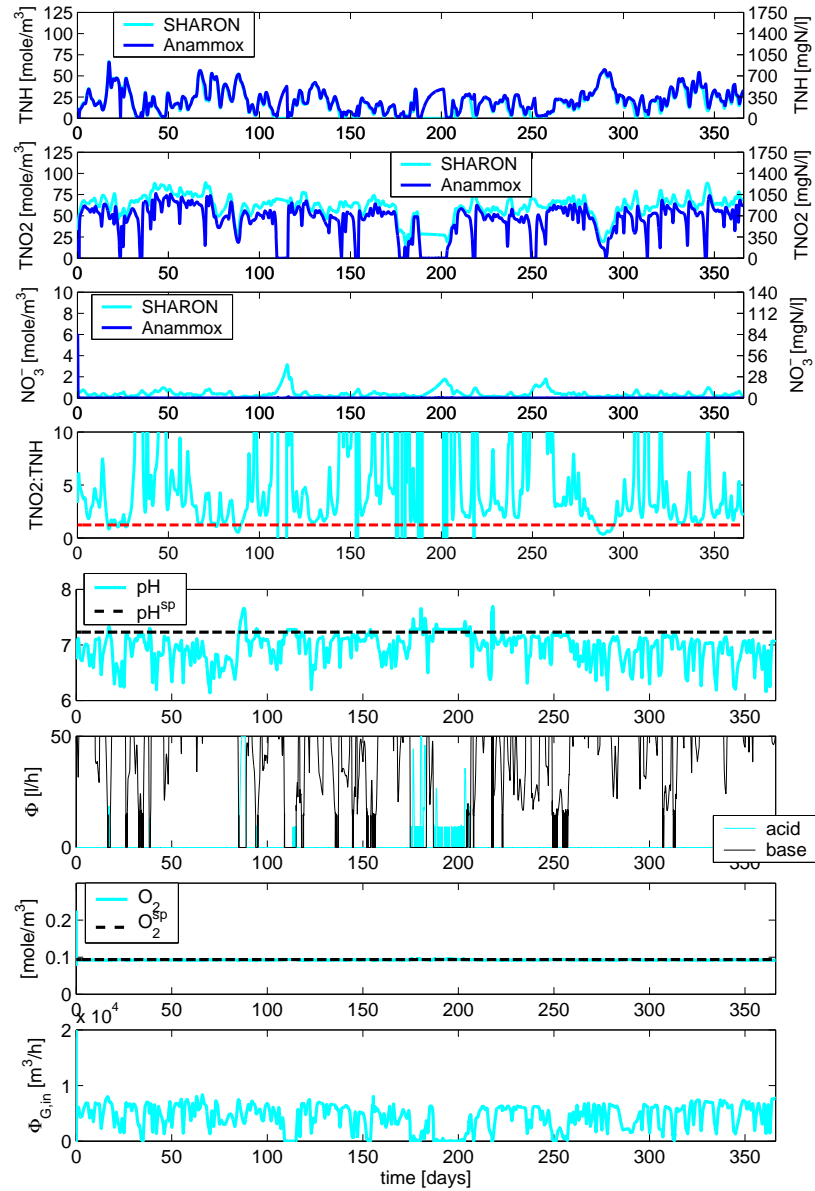


Figure 5.13: (from top to bottom): Concentration profiles of total ammonium (TNH), total nitrite (TNO2) and nitrate in SHARON reactor and in subsequent Anammox reactor. Profiles of nitrite:ammonium ratio (TNO2:TNH), pH vs. pH^{sp} , acid/base addition, O_2 concentration vs. O_2^{sp} and air flow rate in SHARON reactor. Operating mode of SHARON reactor with O_2 -control ($O_2^{sp}=3$ mg/l) and pH-control ($pH^{sp}=7.23$)

5.4.7 SHARON operating mode 7: cascade O_2 -control + pH-control

In order to avoid an unacceptable pH-increase due to CO_2 -stripping at high air flow rates (see operating mode 3), cascade O_2 -control is combined with pH-control to a fixed setpoint (Figure 5.14).

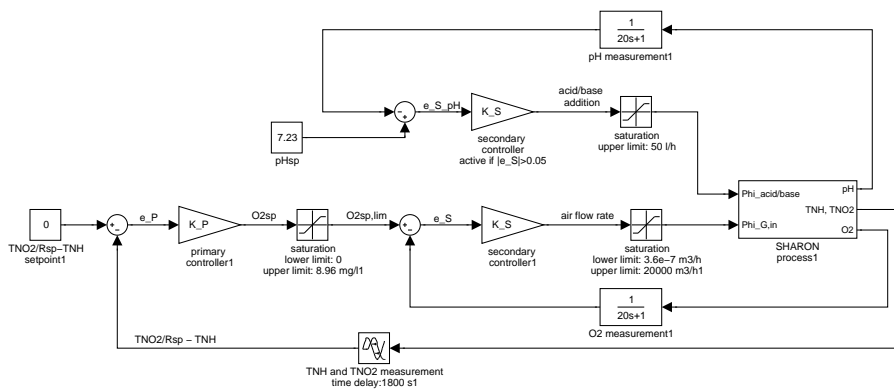


Figure 5.14: Control scheme for cascade O_2 -control + pH-control

The optimum value of the pH-setpoint, giving rise to the minimum OCI-value (Figure 5.15) has been found at 7.23. Note that this value corresponds with the maximum growth rate of ammonium oxidizers (Figure 3.1).

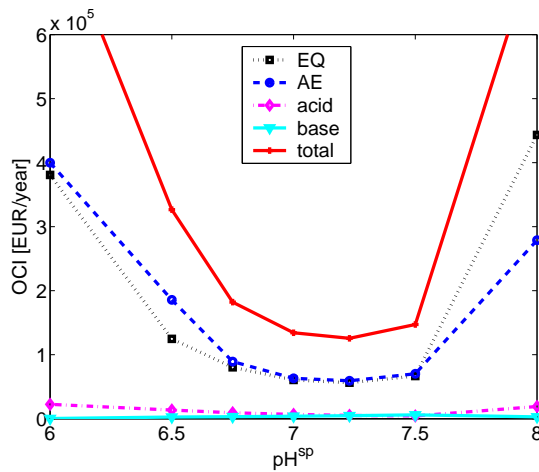


Figure 5.15: OCI in terms of pH^{sp} for cascade O_2 -control + pH-control

Figure 5.16 shows the corresponding reactor performance. Although the individual nitrite and ammonium concentrations in the SHARON reactor still vary, the produced nitrite:ammonium ratio remains quite constant, without nitrite excess produced. As a result, the Anammox reactor performs very well and a very good effluent quality is obtained, reflected in an OCI-value as low as 125,570 € /year. From the operating cost savings, compared to e.g. the scenario with stand-alone O_2 -control, it should be possible to support the investment costs for on-line ammonium and nitrite analysers (assumed to cost about 2x25,000 €). Also, it must be stressed that this is the only operating mode so far, for which a good Anammox-conversion takes place. The fact that biomass only grows between certain pH-limits, necessitates pH-control on top of cascade O_2 -control, at least for the given reactor configuration.

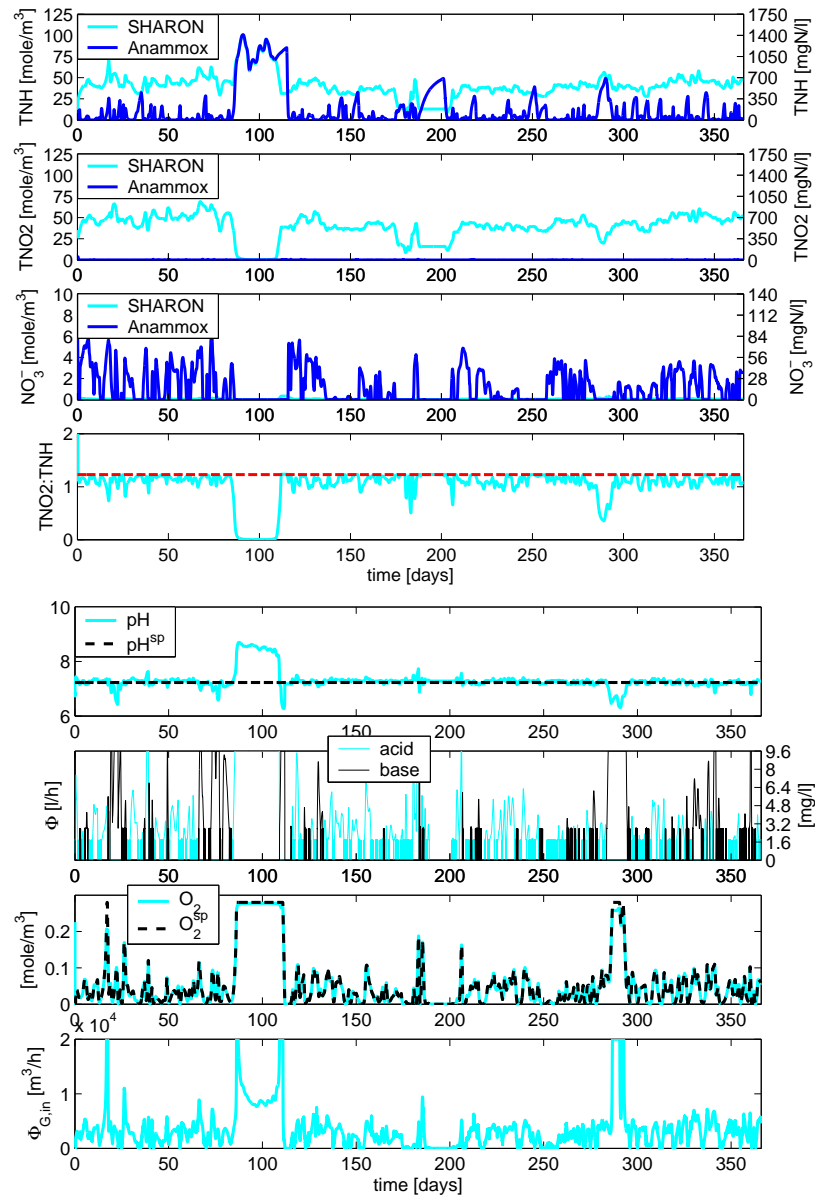


Figure 5.16: (from top to bottom): Concentration profiles of total ammonium (TNH), total nitrite (TNO2) and nitrate in SHARON reactor and in subsequent Anammox reactor. Profiles of nitrite:ammonium ratio (TNO2:TNH), pH vs. pH^{sp} , acid/base addition, O_2 concentration vs. O_2^{sp} and air flow rate in SHARON reactor. Operation mode of SHARON reactor cascade O_2 -control + pH control (at $pH^{sp}=7.23$)

5.4.8 SHARON operating mode 8: O_2 -control + cascade pH-control

In this operating mode, cascade pH-control is combined with O_2 -control, as shown schematically in Figure 5.17.

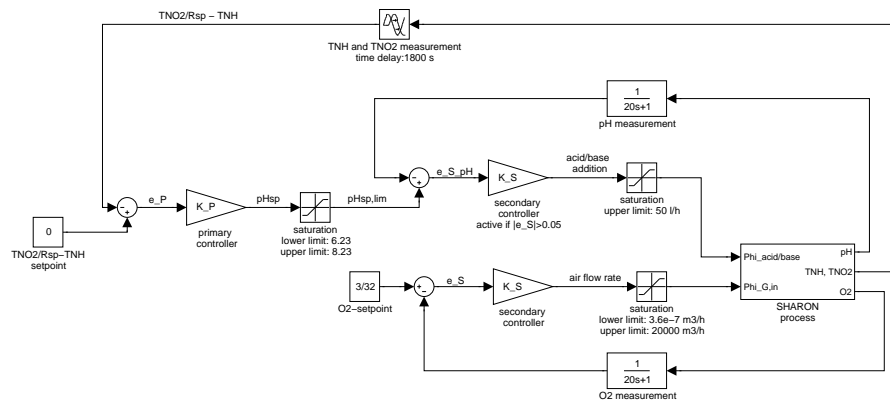


Figure 5.17: Control scheme for O_2 -control + cascade pH-control

Figure 5.18 summarizes the simulation results in terms of costs for this operating mode. The best results are obtained for $O_2^{sp} = 4$ mg/l

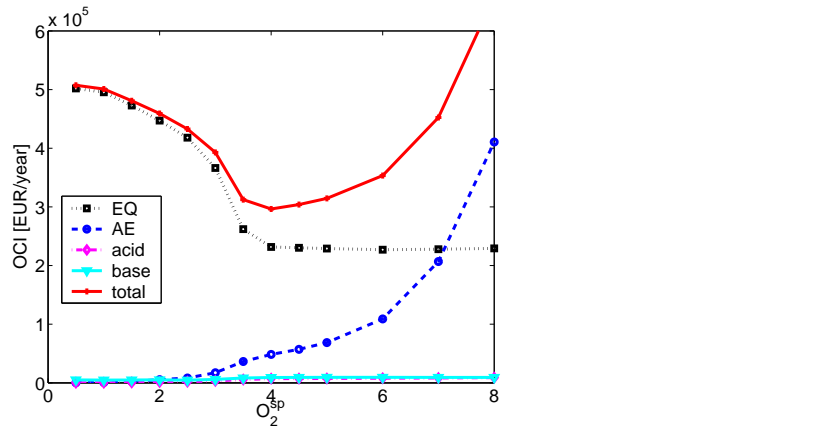


Figure 5.18: OCI in terms of O_2^{sp} for O_2 -control + cascade pH-control

and are given in Figure 5.19. However, even for this best case scenario the nitrite:ammonium setpoint is not well tracked, resulting in nitrite inhibition in the Anammox reactor. Hence, no consistent Anammox-conversion takes place.

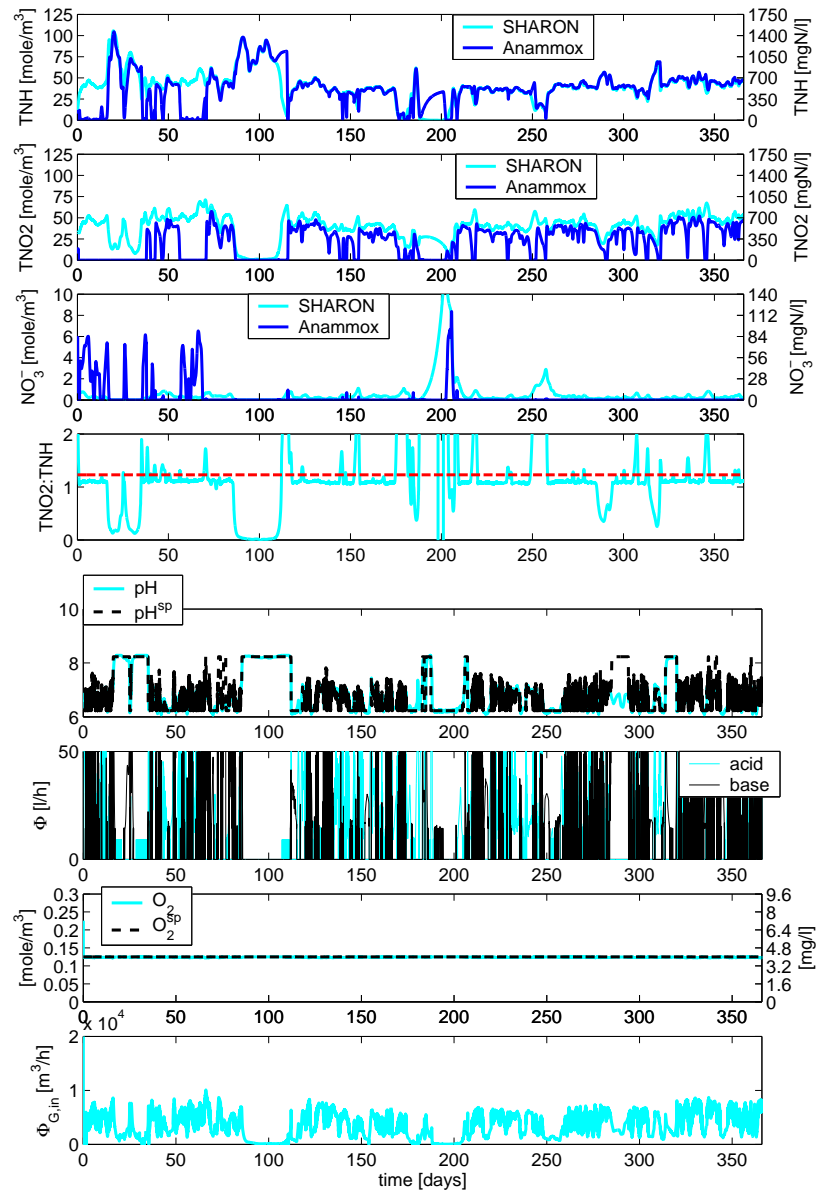


Figure 5.19: (from top to bottom): Concentration profiles of total ammonium (TNH), total nitrite (TNO2) and nitrate in SHARON reactor and in subsequent Anammox reactor. Profiles of nitrite:ammonium ratio (TNO2:TNH), pH vs. pH^{sp} , acid/base addition, O_2 concentration vs. O_2^{sp} and air flow rate in SHARON reactor. Operation mode of SHARON reactor with O_2 -control ($O_2^{sp} = 4\text{mg/l}$) and cascade pH-control

5.5 Discussion and conclusions

By means of a simulation study, different operating modes for a SHARON reactor with fixed volume have been evaluated in view of their effect on a subsequent Anammox process. The operating modes differ in the applied control strategies for the produced nitrite:ammonium ratio, the O_2 -concentration and the pH in the SHARON reactor, in order to cope with varying influent conditions. Control of the nitrite:ammonium ratio produced by the SHARON reactor is essential to avoid toxic nitrite concentrations, that inhibit the Anammox conversion.

Control of O_2 and/or pH in the SHARON reactor is in the first place necessary to avoid wash-out of ammonium oxidizers from the SHARON reactor, due to retention time and process condition changes. For the given reactor volume, corresponding with a mean retention time of 1.25 days, satisfying results have been obtained only with cascade O_2 -control, in which the O_2 -setpoint is set by a master controller tracking a fixed nitrite:ammonium ratio, combined with pH-control that avoids an excessive pH-increase under high oxygen supply conditions due to concomitant CO_2 stripping. At all times the Anammox process remains active under this operating mode.

All results have been quantified in an economic way by means of an operating cost index (OCI) for a wastewater plant with limited aeration capacity. The operating cost savings realized with the cascade O_2 -control combined with pH-control compared to e.g. the scenario with stand-alone O_2 -control, warrant the investments costs for the necessary on-line ammonium and nitrite sensors (payback time less than 1 year).

The simulation results presented in this chapter reveal some limitations of the controllers applied, as well as problems arising from the chosen (small) reactor volume.

As for oxygen controllers, it was found that the oxygen level in the reactor mainly determines whether ammonium is converted or not rather than the amount of ammonium that is converted. The extent of ammonium conversion can be controlled by changing the oxygen setpoint fast, so by using the oxygen controller as a kind of on/off controller. This can be seen as controlling the aerobic retention time. In some conditions the ammonium conversion may be too low because the reactor volume is too small and consequently the maximum aerobic retention time that can be applied (which equals the SRT) is too low. A larger reactor is expected to cope better with periods of high influent flows and for this reason to need less control.

The cascade O_2 -controller for the given reactor volume resulted in complete biomass wash-out after a period of high influent flow rates (short SRT). This was caused by the resulting decrease in ammonium conversion, that was met by an increasing oxygen setpoint, resulting in an increased air flow rate that also caused a high pH due to CO_2 -stripping, preventing further biomass growth. This problem was overcome here by combining the cascade O_2 -controller with a pH-controller, that controlled the pH at a fixed level. The influence of the reactor volume on the pH-fluctuations requires further investigation. A larger reactor volume may lead to less pH-fluctuations and in this way may improve the performance of stand-alone cascade O_2 -control.

Regarding pH-control strategies, it appeared to be difficult, if not impossible, for the given reactor volume, to control the pH at a fixed level. It will probably be easier to control the pH for a larger reactor volume.

It is clear that the chosen volume for the SHARON reactor will influence the usefulness of control. The relationship between reactor design and control is addressed in chapter 8.

Chapter 6

Continuity-based model interfacing for plant-wide simulation - inclusion of reject water treatment

A summarized version of this chapter has been accepted for publication as: Volcke E.I.P., van Loosdrecht M.C.M. and Vanrolleghem P.A. (2006). Continuity-based model interfacing for plant-wide simulation: a general approach. Water Research.

In plant-wide simulation studies of wastewater treatment facilities, often existing models from different origin need to be coupled. However, as these submodels are likely to contain different state variables, their coupling without 'leakage' or 'production' of elements or components is not straightforward. The Continuity-Based Interfacing Method (CBIM) provides a general framework to construct model interfaces for models of wastewater systems described by Petersen matrices, taking into account conservation principles. In this chapter, the CBIM approach is applied to study the effect of sludge digestion reject water treatment with a SHARON-Anammox process on a plant-wide scale. Separate models were available for the SHARON process and for the Anammox process. The Benchmark Simulation Model no. 2 (BSM2) is used to simulate the behaviour of the complete WWTP including sludge digestion. The CBIM approach is followed to develop three different model interfaces. At the same time, the generally applicable

CBIM approach is further refined and particular issues when coupling models in which pH is considered as a state variable, are pointed out.

6.1 Introduction

The usefulness of modelling and simulation to gain insight into and evaluate the behaviour of wastewater treatment facilities is nowadays widely acknowledged. The Activated Sludge Models (ASM, Henze et al. 2000), the River Water Quality Model no. 1 (RWQM1, Reichert et al. 2001) and the Anaerobic Digestion Model (ADM1, Batstone et al. 2002), developed by the respective IWA task groups, are generally accepted. Besides, different user groups have adapted these models or have built specific models for specific unit processes. Although these different types of models are very suitable to evaluate the behaviour of the processes for which they have been developed, the coupling of these models to evaluate the behaviour of a wastewater treatment plant (WWTP) in a plant-wide context is often a source of problems. Typically, each model contains its own state variables with their own meanings and their own elemental composition, which makes their coupling not straightforward, as mass conservation needs to be maintained. One solution is to adapt and extend the individual models to create a 'super-model' that comprises all state variables of all submodels, as has been done by Jones and Takacs (2004). However, this is often not desirable because it increases model complexity as the behaviour of all state variables must be described in each subsystem and it results in the addition of unused state variables to submodels. In addition, the adaptation of state variables that have a similar meaning but e.g. a different composition, may require complete rewriting of some submodels. Also, the supermodel needs to be adapted each time a new submodel is added. Alternatively, model interfaces can be developed to link the state variables of one submodel to the state variables of another submodel. These model interfaces are placed between the two models considered, leaving the individual models unchanged. As a result, differences in model state variables, composition and units are accounted for in the model interfaces and not in the models themselves. Figure 6.1 illustrates the two approaches.

In the last few years, the issue of model interfacing has already been addressed in several specific cases, e.g. the coupling of ASM1 with RWQM1 (Meirlaen et al. 2001; Benedetti et al. 2004) and the coupling of ASM1 to ADM1 and vice versa (Copp et al. 2003; Zaher et al. 2006).

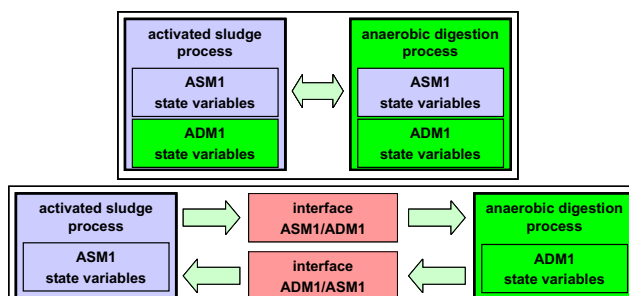


Figure 6.1: Supermodel approach (top) versus model interfacing (bottom) for the coupling of ASM1 and ADM1

A more generally applicable framework for constructing model interfaces has been proposed by Vanrolleghem et al. (2005) in the form of the continuity-based interfacing method (CBIM), a further development of the method proposed by Meirlaen et al. (2001). The CBIM approach is a way to construct model interfaces between subsystems considered in wastewater treatment, maintaining continuity of e.g. C, H, O, N, P, charge and COD.

In this chapter, the CBIM approach is applied to three different interfacing cases. The individual models, describing the subprocesses, are left unchanged. The CBIM approach is further refined and particular points of attention when dealing with one or more submodels with varying pH, are pointed out. Although the interfaces are developed for a specific case, the followed methodology is generally applicable and should be easily extrapolated to other cases.

6.2 Case study: implementation of a SHARON and Anammox model in BSM2

The model interfaces developed in this study serve to evaluate the effect of treatment of sludge digestion reject water with a SHARON-Anammox process on a plant-wide scale. The reject water stream, originating from sludge digestion and dewatering, typically represents only 2% of the volume of the influent wastewater stream but can contribute up to 25% of the influent nitrogen load of the main plant, to which it is typically recycled. This is especially problematic in case the latter has a limited aeration/nitrification/denitrification capacity. In order to relieve the main plant, it can be decided to treat the reject water

stream before recirculation, e.g. through a SHARON-Anammox process (van Dongen et al., 2001). For this purpose, in the SHARON reactor half of the ammonium is nitrified to nitrite, while nitrate formation is suppressed. In the subsequent Anammox reactor, almost equimolar amounts of ammonium and nitrite are combined to form nitrogen gas in the anaerobic ammonium oxidation (anammox) reaction. With the combined SHARON-Anammox process, that is fully autotrophic, substantial savings on aeration costs (up to 63%) and external carbon addition costs (up to 100%) are realized in comparison with conventional nitrification-denitrification over nitrate, while CO₂-production is low and sludge production is also decreased. To evaluate the influence of reject water with SHARON-Anammox on the performance of the activated sludge tanks, it was decided to implement the existing SHARON and Anammox models in the Benchmark Simulation Model no. 2 (BSM2, Jeppsson et al. 2006), developed by the IWA task group on Benchmarking. The BSM2 is a simulation platform for testing plant-wide control strategies, proposed by Jeppsson et al. (2006). Its layout is given in Figure 6.2. The BSM2 itself already contains sub-models: besides primary and secondary clarifier models, the activated sludge plant is modelled according to the Activated Sludge Model no. 1 (ASM1, Henze et al. 2000), while the anaerobic digester is modelled following the Anaerobic Digester Model no. 1 (ADM1) of Batstone et al. (2002). Consequently, the BSM2 also contains model interfaces between ASM1 and ADM1, as indicated in Figure 6.2. Note that the current interfaces (Copp et al., 2003) are not CBIM-based but only ensure conservation of COD and N. As the treatment of reject water with the SHARON and Anammox processes is located behind the dewatering facility, additional interfaces will be required

- from ASM1 to the SHARON model,
- between the SHARON and the Anammox model and
- from the Anammox model to the ASM1 model

The ASM1/SHARON interface is applied to the stream that comes from the sludge dewatering, in order to connect it to the SHARON process (see Figure 6.2) This approach was preferred over the removal of the existing ADM1/ASM1 interface before sludge dewatering in the BSM2 and replacing it by an ADM1/SHARON interface. The latter would also require rewriting the dewatering model and is not in accordance with the starting-point of not changing the models, as stated above.

Leaving the existing ADM1/ASM1 interface in the BSM2 unchanged, also allows a more fair comparison with operating strategies in which the reject water is not treated with a SHARON-Anammox process.

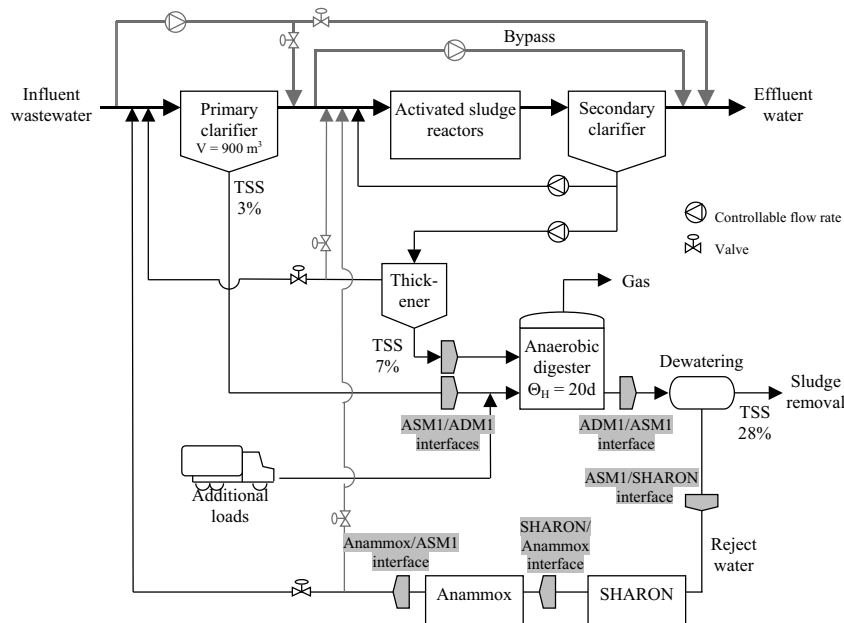


Figure 6.2: Extended benchmark plant with anaerobic sludge digestion and reject water recirculation, adapted from Jeppsson et al. (2006). The location for inclusion of the SHARON and Anammox process is indicated, as well as the model interfaces

6.3 Application of the CBIM approach

In order to couple the models taking into account conservation principles, the Continuity-Based Interfacing Method (CBIM) approach, proposed by Vanrolleghem et al. (2005), is followed. This interfacing method comprises the development of a set of algebraic transformation equations based on a description of the two models to be interfaced through their Petersen and composition matrices that modellers are familiar with. The methodology consists of the following steps:

1. Formulation of elemental mass fractions and charge density
2. Set-up of the composition matrices

3. Definition of the transformation matrix
4. Implementation of the transformation equations

6.3.1 Step 1: Elemental mass fractions and charge density

The state variables of the ASM1, SHARON and Anammox models, that are to be coupled, are listed in Tables 6.1, 6.2 and 6.3. The coupling of these models is not straightforward, as each model has its own state variables, only partly overlapping with the ones of the other models. For state variables that have the same meaning, their dimensions and even the elemental composition can differ between the models. Besides, in the SHARON model the pH is a state variable, as the pH is highly influenced by the conversion of high ammonium concentrations, as well as by CO_2 -stripping, while the conversion processes themselves depend on pH. In the Anammox and in the ASM models, on the other hand, pH is considered constant and the model parameter values are valid for a pH of 7-8.

Table 6.1: State variables of ASM1

component description	symbol	unit	composition (mass fractions in g/g component)					
			α^C	α^N	α^H	α^O	α^P	α^{ch}
soluble inert organic matter	S_I	gCOD m ⁻³	0.65 ^a	0 ^c	0.07 ^b	0.28 ^b	0 ^c	0
readily biodegradable substrate	S_S	gCOD m ⁻³	0.62 ^a	0 ^c	0.08 ^b	0.28 ^b	0.02 ^c	0
particulate inert organic matter	X_I	gCOD m ⁻³	0.56 ^a	0.09 ^e	0.06 ^e	0.28 ^c	0.01 ^c	0
slowly biodegradable substrate	X_S	gCOD m ⁻³	0.62 ^a	0	0.08 ^b	0.28 ^b	0.02 ^c	0
heterotrophic biomass	X_{BH}	gCOD m ⁻³	0.516 ^a	0.114 ^f	0.06 ^d	0.28 ^d	0.03 ^c	0
autotrophic biomass	X_{BA}	gCOD m ⁻³	0.516 ^a	0.114 ^f	0.06 ^d	0.28 ^d	0.03 ^c	0
particulate products from biomass decay	X_P	gCOD m ⁻³	0.5575 ^a	0.0925 ^d	0.06 ^d	0.28 ^d	0.01 ^c	0
oxygen (O_2)	S_O	g m ⁻³	0	0	0	1	0	0
nitrate + total nitrite (NO_3^-)	S_{NO}	gN m ⁻³	0	0.2258	0	0.7742	0	-0.0161
total ammonium (NH_4^+)	S_{NH}	gN m ⁻³	0	0.7778	0.2222	0	0	0.0556
soluble biodegradable organic nitrogen (NH_3^*)	S_{ND}	gN m ⁻³	0	0.8235	0.1765	0	0	0
particulate biodegradable organic nitrogen (NH_3^*)	X_{ND}	gN m ⁻³	0	0.8235	0.1765	0	0	0
alkalinity (HCO_3^-)	S_{alk}	mole m ⁻³	0.1967	0	0.0164	0.7869	0	-0.0164

Table 6.2: State variables of the SHARON model

component description	symbol	unit	composition
total ammonium	TNH	mole m^{-3}	$NH_3(pH) + NH_4^+(pH)$
total nitrite	TNO_2	mole m^{-3}	$HNO_2(pH) + NO_2^-(pH)$
total inorganic carbon	TIC	mole m^{-3}	$CO_2(pH) + HCO_3^-(pH) + CO_3^{2-}(pH)$
total inorganic phosphorus	TIP	mole m^{-3}	$H_2PO_4^-(pH) + HPO_4^{2-}(pH)$
nitrate	NO_3^-	mole m^{-3}	NO_3^-
oxygen	O_2	mole m^{-3}	O_2
nitrogen gas	N_2	mole m^{-3}	N_2
ammonium oxidizing biomass	X_{amm}	mole m^{-3}	$CH_{1.8}O_{0.5}N_{0.2}P_p^{**}$
nitrite oxidizing biomass	X_{nit}	mole m^{-3}	$CH_{1.8}O_{0.5}N_{0.2}P_p^{**}$
heterotrophic biomass	X_{het}	mole m^{-3}	$CH_{1.8}O_{0.5}N_{0.2}P_p^{**}$
methanol	CH_3OH	mole m^{-3}	CH_3OH
protons	H^+	mole m^{-3}	H^+

Table 6.3: State variables of the Anammox model

component description	symbol	unit	composition (mass fractions in g/g component)					
			α^C	α^N	α^H	α^O	α^P	α^{ch}
oxygen	S_O	$gO_2 m^{-3}$	0	0	0	1	0	0
readily biodegradable substrate	S_S	$gCOD m^{-3}$	0.62 ^a	0 ^c	0.08 ^b	0.28 ^b	0.02 ^c	0
total ammonium (NH_4^{+*})	S_{NH}	$gN m^{-3}$	0	0.7778	0.2222	0	0	0.0556
total nitrite (NO_2^{-*})	S_{NO_2}	$gN m^{-3}$	0	0.3043	0	0.6957	0	-0.0217
nitrate (NO_3^-)	S_{NO_3}	$gN m^{-3}$	0	0.2258	0	0.7742	0	-0.0161
nitrogen gas (N_2)	S_{N_2}	$gN m^{-3}$	0	1	0	0	0	0
heterotrophic biomass	X_H	$gCOD m^{-3}$	0.516 ^a	0.114 ^f	0.06 ^d	0.28 ^d	0.03 ^c	0
ammonium oxidizing biomass	X_{NH}	$gCOD m^{-3}$	0.516 ^a	0.114 ^f	0.06 ^d	0.28 ^d	0.03 ^c	0
nitrite oxidizing biomass	X_{NO}	$gCOD m^{-3}$	0.516 ^a	0.114 ^f	0.06 ^d	0.28 ^d	0.03 ^c	0
anammox biomass	X_{AN}	$gCOD m^{-3}$	0.4830 ^g	0.0845 ^g	0.0805 ^g	0.3220 ^g	0.03 ^g	0
slowly biodegradable substrate	X_S	$gCOD m^{-3}$	0.62 ^a	0	0.08 ^b	0.28 ^b	0.02 ^c	0
particulate products from biomass decay	X_P	$gCOD m^{-3}$	0.5575 ^a	0.0925 ^d	0.06 ^d	0.28 ^d	0.01 ^c	0
alkalinity	S_{alk}	mole m^{-3}	0.1967	0	0.0164	0.7869	0	-0.0164

a: calculated as the remaining mass fraction after the assignment of other element fractions

b: taken from RWQM1 (Reichert et al., 2001)

c: assumed fraction

d: according to stoichiometric formula $C_5H_7O_2N$, also used by Henze et al. (2000) and Batstone et al. (2002)

e: similar to ADM1

f: in agreement with the ASM1 nitrogen fraction used in BSM2

g: corresponding with stoichiometric formula determined by Strous et al. (1999), and an assumed phosphorus content of $\alpha^P=0.03$ gP/g biomass, i.e. $CH_2O_{0.5}N_{0.15}P_p$, with $p = 0.0240$

*: in agreement with the model stoichiometry and the (major) form in which the state variable occurs

** A value of $p = 0.02454$ is found for an assumed phosphorus content $\alpha^P=0.03$ gP/g biomass

*** The equilibrium forms H_3PO_4 and PO_4^{3-} are negligible in a pH operating range of 5-9.

According to the general CBIM approach, elemental mass fractions are formulated for all state variables, relying on the hypothesis that the mass of each component is made up of constant mass fractions of the elements C, H, O, N, and P. Note that no other elements (e.g. S) are considered here, but an extension would be straightforward. The elemental mass fractions, $\alpha^C, \alpha^H, \alpha^O, \alpha^N$ and α^P are expressed in gram element per gram component. As a result, the sum of all elemental mass fractions of each component k must be unity:

$$\alpha_k^C + \alpha_k^H + \alpha_k^O + \alpha_k^N + \alpha_k^P = 1 \quad (6.1)$$

Besides, also the charge density (α^{ch} , expressed in equivalents per gram component) and the COD content (α^{COD} , expressed in gCOD per g component) of each state variable are identified. Once the elemental mass fractions and the charge density have been assigned, one gram of any model component k is represented by the following molecular formula:

$$\left[C_{(\alpha_k^C/12)} H_{\alpha_k^H} O_{(\alpha_k^O/16)} N_{(\alpha_k^N/14)} P_{(\alpha_k^P/31)} \right]^{\alpha_k^{ch}} \quad (6.2)$$

From the composition of a component, also its molecular weight is known. The COD content of a component is defined here as the amount of oxygen (expressed in g) that is consumed during oxidation of a mass unit of this component to NH_4^+, CO_2, H_2O, H^+ and PO_4^{3-} . It is the conservative quantity that effectively accounts for the electrons involved in the biological redox processes, denoted as Theoretical Oxygen Demand (ThOD) in Henze et al. (2000). The COD content of a component is related to the mass fractions of the elements and charge through the relationship

$$\alpha^{COD} = 32 \cdot \frac{\alpha^C}{12} + 8 \cdot \alpha^H - 16 \cdot \frac{\alpha^O}{16} - 24 \cdot \frac{\alpha^N}{14} + 40 \cdot \frac{\alpha^P}{31} - 8 \cdot \alpha^{ch} \quad (6.3)$$

For state variables that represent components of which the molecular formula is known a priori in terms of all elements considered (in this case C, H, O, N, P), charge and COD content, the assignment of elemental fractions is straightforward. One can even decide to start immediately by setting up the composition (in terms of gram C, H, O, N, P, charge equivalents and gCOD) of these components per stoichiometric mass unit (step 2) instead of first defining its composition per gram component, in this way skipping step 1.

ASM1 model (Table 6.1)

The composition of S_I , S_S , X_I , X_S , X_{BH} , X_{BA} and X_P in terms of elemental mass fractions and charge density was based on descriptions of the activated sludge model ASM1 (Henze et al., 2000), the anaerobic digestion model ADM1 (Batstone et al., 2002) and the river water quality model RWQM1 (Reichert et al., 2001), in an analogous way as this was done by Zaher et al. (2006). Note that the biomass composition (both heterotrophic and autotrophic) is based on the empirical formula $C_5H_7O_2N$, as for ASM1 (Henze et al., 2000) and suggested in the IWA ADM1 report (Batstone et al., 2002), adjusted with addition of an assumed phosphorus mass fraction of 3%. Although phosphorus is not considered in the original models, it is necessary to take it into account to ensure a complete implementation of the elemental mass balances.

The remaining components are associated with a known molecular formula. The composition of oxygen (S_O) is straightforward. Although S_{NO} represents the sum of nitrate (NO_3^-) and total nitrite ($HNO_2 + NO_2^-$), the stoichiometry of the ASM1 is written as if it were all NO_3^- , as this is the major form occurring in traditional activated sludge plants. For this reason, the composition of S_{NO} should also be the one for NO_3^- . An analogous reasoning holds for S_{NH} , representing total ammonium ($NH_4^+ + NH_3$), but expressed in terms of NH_4^+ , as this is the major form under which this component occurs and also agrees with the ASM1 stoichiometry. S_{ND} and X_{ND} , representing soluble and particulate biodegradable organic nitrogen respectively, are expressed as NH_3 since the degree of reduction and thus the COD content of the associated proteins is typically equal to the one of NH_3 (that is zero for the given definition of COD). By expressing S_{ND} and X_{ND} as NH_3 rather than NH_4^+ , alkalinity is produced during hydrolysis to S_{NH} (NH_4^+), which corresponds with reality. Alkalinity (S_{alk}) is expressed as HCO_3^- , again corresponding with the ASM1 stoichiometry.

SHARON model (Table 6.2)

Most state variables of the SHARON model are components with known composition in terms of C, H, O, N, P and charge. Consequently, also their COD content is known. For these components, the corresponding elements of the composition matrix can be calculated immediately. The composition of the state variables representing biomass is somewhat less straightforward. In the SHARON model, all biomass is assumed to have the composition $CH_{1.8}O_{0.5}N_{0.2}$.

The phosphorus content of the biomass is not considered in the model, neither is the effect on the inorganic phosphorus concentration in the system during biomass growth. However, it is necessary to assume a certain phosphorus content of the biomass in the SHARON reactor when taking into account a P-balance in the model interfaces. For this purpose, the same phosphorus content on mass basis ($\alpha^P=0.03$ gP/g biomass) is assumed as has been done for state variables representing biomass in the ASM and Anammox model. As a result, the biomass molecular formula becomes $CH_{1.8}O_{0.5}N_{0.2}P_p$ with $p = 0.02454$.

The state variables TNH (total ammonium), TNO_2 (total nitrite), TIC (total inorganic carbon) and TIP (total inorganic phosphorus) represent sums of components involved in chemical equilibria, exchanging protons, and require special attention. The composition of these state variables is the weighed composition of the constituting equilibrium components, of which the proportions change with pH. For instance, total ammonium (TNH) represents the sum of ionized ammonium (NH_4^+) and uncharged ammonia (NH_3), of which the proportions vary with varying pH. As the pH varies with time, the composition of these lumped state variables is also time-varying (Figure 6.3). For this reason, no fixed composition can be written down for these state variables.

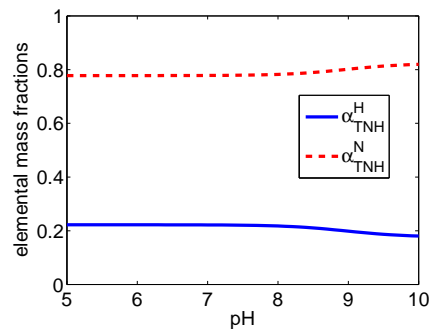


Figure 6.3: Elemental hydrogen and nitrogen mass fractions of total ammonium as a function of pH

Anammox model (Table 6.3)

The state variables S_S , X_S and X_P are the same as in the ASM1, so their composition is also the same. The biomass composition of both X_{BH} and X_{BA} , was applied for heterotrops (X_H), ammonium oxidizers

(X_{NH}) and nitrite oxidizers (X_{NO}) in the Anammox model. For the Anammox biomass however, its molecular formula $CH_2O_{0.5}N_{0.15}S_{0.05}$ determined by Strous et al. (1998) was used as a starting point. Ignoring its sulphur content and assuming the same phosphorus content on mass basis as for all other types biomass ($\alpha^P=0.03$ gP/g biomass), the molecular formula $CH_2O_{0.5}N_{0.15}P_p$ with $p = 0.0240$ was used to represent the composition of Anammox bacteria. The remaining components are again associated with a known molecular formula. In contrast with the ASM1 model, separate components are considered for total nitrite and for nitrate (S_{NO_3}). The state variable S_{NO_2} , representing total nitrite, is expressed as NO_2^- , in accordance with the model stoichiometry.

Inclusion of P-balances

The inclusion of P-balances in the model interfaces is not self-evident in the given case study. The ASM1, SHARON and Anammox models do not consider any biological conversion reactions involving phosphorus. Only the effect of the phosphorus dissociation reactions on the pH is considered in the SHARON model. However, it has been decided to incorporate the P-balances in the interfaces to anticipate for future inclusion of conversion reactions involving phosphorus. One could indeed decide to use ASM2 instead of ASM1 and in this way consider biological P-removal and P-uptake during biomass growth. Another incentive to take up P-balances is the ongoing development of anaerobic digestion models involving the fate of phosphorus (e.g. Jones and Takacs 2004; Ekama et al. 2005). For this purpose, all components have been assigned a certain phosphorus content (that of course can be zero). Note that in case it would be decided not to include the P-balances, the formulation of elemental mass fractions should be done without considering P (as it is done now, for instance, by not considering S). In particular, the COD content of each component should then also be calculated without considering phosphorus.

6.3.2 Step 2: Set-up of composition matrices

Once the complete composition of all components is known in terms of elements, charge and COD, a composition matrix is set up for each model. A composition matrix element i_k^E represents the elemental, charge or COD fraction of a component (expressed in gram for E=C, H, O, N,

P, in equivalents for E=charge and in gCOD for E=COD) per stoichiometric mass unit of this component. It is related to α_k^E through

$$i_k^E = \alpha_k^E \cdot M_k \tag{6.4}$$

where M_k stands for the mass of components expressed in g per stoichiometric mass unit (e.g. gCOD, gN or mole). The composition matrices for the ASM1 model, the SHARON model and the Anammox model are calculated straightforwardly and are given in Tables 6.4, 6.5 and 6.6 respectively.

Table 6.4: Composition matrix ASM1 for BSM2

i_k^E	composition matrix												
	1	2	3	4	5	6	7	8	9	10	11	12	13
	S_I	S_S	X_I	X_S	X_BH	X_BA	X_P	S_O	S_NO	S_NH	S_ND	X_ND	S_alk
COD (gCOD/stoich mass unit)	1	1	1	1				-1	-4.57	0	0	0	0
C (g/stoich mass unit)	0.32	0.30	0.36	0.30	0.36	0.36	0.36	0	0	0	0	0	12
N (g/stoich mass unit)	0	0	0.058	0	0.080	0.080	0.060	0	1	1	1	1	0
H (g/stoich mass unit)	0.035	0.039	0.039	0.039	0.042	0.042	0.039	0	0	0.29	0.21	0.21	1
O (g/stoich mass unit)	0.14	0.14	0.18	0.14	0.20	0.20	0.18	1	3.43	0	0	0	48
P (g/stoich mass unit)	0	0.0089	0.0064	0.0089	0.021	0.021	0.0065	0	0	0	0	0	0
charge (eq/stoich mass unit)	0	0	0	0	0	0	0	0	-0.071	0.071	0	0	-1

Table 6.5: Composition matrix SHARON model (CNC: composition not constant)

i_k^E	composition matrix											
	1	2	3	4	5	6	7	8	9	10	11	12
	TNH	TNO2	TIC	TIP	NO3-	O2	N2	Xamm	Xnitr	Xhet	CH3OH	H+
COD (gCOD/stoich mass unit)	CNC	CNC	CNC		-64	-32	-48	34.58	34.58	34.58	48	0
C (g/stoich mass unit)					0	0	0	12	12	12	12	0
N (g/stoich mass unit)					C 14	0	28	2.8	2.8	2.8	0	0
H (g/stoich mass unit)					N 0	0	0	1.8	1.8	1.8	4	1
O (g/stoich mass unit)					C 48	32	0	8	8	8	16	0
P (g/stoich mass unit)					0	0	0	0.76	0.76	0.76	0	0
charge (eq/stoich mass unit)					-1	0	0	0	0	0	0	0

Table 6.6: Composition matrix Anammox model

i_k^E	composition matrix														
	1	2	3	4	5	6	7	8	9	10	11	12	13	14	15
	S_O	S_S	S_NH	S_NO2	S_NO3	S_N2	X_H	X_NH	X_NO	X_AN	X_S	X_P	S_alk	S_I	X_I
COD (gCOD/stoich. mass unit)	-1	1	0	-3.43	-4.57	-1.71	1	1	1	1	1	1	0	1	1
C (g/stoich mass unit)	0	0.30	0	0	0	0	0.36	0.36	0.36	0.32	0.30	0.36	12	0.32	0.36
N (g/stoich mass unit)	0	0	1	1	1	1	0.080	0.080	0.080	0.056	0	0.060	0	0	0.058
H (g/stoich mass unit)	0	0.039	0.29	0	0	0	0.042	0.042	0.042	0.054	0.039	0.039	1	0.035	0.039
O (g/stoich mass unit)	1	0.14	0	2.29	3.43	0	0.20	0.20	0.20	0.21	0.14	0.18	48	0.14	0.18
P (g/stoich mass unit)	0	0.0089	0	0	0	0	0.021	0.021	0.021	0.020	0.0089	0.0065	0	0	0.0064
charge (eq/stoich mass unit)	0	0	0.071	-0.071	-0.071	0	0	0	0	0	0	0	-1	0	0

6.3.3 Step 3: Definition of transformation matrices

General procedure

Once the composition of all state variables is listed in the form of composition matrices, transformation processes are defined from the state variables of the origin model to those of the destination model. The definition of these transformations is done by the user, who takes a decision based on process knowledge and insight. The number of transformations is typically equal to the number of state variables of the origin model, that need to be transformed (see step 4). All proposed transformations must guarantee continuity:

$$\sum_k \nu_{jk} \cdot i_k^E = 0 \quad (6.5)$$

for each $E = C, H, O, N, P$, charge and COD. Note that one of these 7 equations can be omitted because of the relationship given by Eq.6.3, resulting in 6 linear constraints that need to be fulfilled for each transformation process. ν_{jk} represents the 'stoichiometric' coefficient of component k for transformation j . The summation is made over all components k of both the source and destination model. The stoichiometric coefficients should be negative for components of the origin model, that are 'consumed' in the interface and positive for components of the destination model, that are 'produced'. In this way the transformation is maintained in the right direction.

For state variables that have the same composition in both models to be interfaced, e.g. O_2 , the transformation is straightforward and the corresponding stoichiometric coefficients can be written down immediately, only taking into account the possible difference in units in which these components are expressed. Regarding the transformation of other components of the origin model, in this chapter the following general procedure is followed to determine the stoichiometric coefficients for each transformation j :

1. Each transformation reaction j corresponds with the transformation of a component of the origin model. The stoichiometric coefficient of this component is set to an arbitrary value, e.g. -1, with a negative sign to express that this component is consumed in the interface. The coefficients of the destination component(s), to which the source component is mapped on the basis of process insight, are set in such a way that the transformation conserves the

COD content. For components with COD content zero (i.e. NH_4^+ , CO_2 , H_2O , H^+ and PO_4^{3-}), transformation is usually straightforward (based on N-, C-, O-, H- and P-content, respectively).

2. So-called compensation components (Meirlaen et al., 2001) are used to close the remaining balances. The user is free to choose which of the 7 balances (COD, C, H, O, N, P, charge) will be omitted (as one balance is linearly dependent on the others, see Eq. 6.3) and to choose which components will be used for compensation. After closing the COD-balance, the following choice has been made:

- (a) The C-balance is closed with HCO_3^-
- (b) The N-balance is closed with NH_4^+
- (c) The P-balance is closed with HPO_4^{2-}
- (d) The charge balance is closed with H^+
- (e) The O-balance is closed with H_2O
- (f) The H-balance is then automatically fulfilled, since the balances are linearly dependent on each other (see Eq. 6.3).

Noteworthy is that if this procedure is followed in the order as described, every step is independent of the previous ones. For instance, HCO_3^- , NH_4^+ , HPO_4^{2-} , H^+ and H_2O , of which the stoichiometric coefficients are determined under point 2, do not have a COD content and in this way will not affect the coefficients determined in point 1. In the same way, the components of which the stoichiometric coefficients are calculated under (d), (e) and (f) do not contain COD, N or P. Note that, in this respect, the order of (a), (b) and (c), as well as the one of (d) and (e) may be switched as these components do not influence the balance(s) closed by using the other component.

The stoichiometric coefficients $\nu_{j,m}$ (for all components m involved in point 1), ν_{j,HCO_3^-} , ν_{j,NH_4^+} , $\nu_{j,HPO_4^{2-}}$, ν_{j,H^+} and ν_{j,H_2O} are calculated one by one in the given order. Note that it is also possible to calculate all stoichiometric coefficients at once, by solving the matrix equation

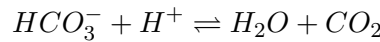
$$\begin{aligned}
& \begin{bmatrix} i_{HCO_3^-}^C & 0 & 0 & 0 & 0 \\ 0 & i_{NH_4^+}^N & 0 & 0 & 0 \\ 0 & 0 & i_{HPO_4^{2-}}^P & 0 & 0 \\ i_{HCO_3^-}^{charge} & i_{NH_4^+}^{charge} & i_{HPO_4^{2-}}^{charge} & i_{H^+}^{charge} & 0 \\ i_{HCO_3^-}^O & 0 & i_{HPO_4^{2-}}^O & 0 & i_{H_2O}^O \end{bmatrix} \cdot \begin{bmatrix} \nu_{j,HCO_3^-} \\ \nu_{j,NH_4^+} \\ \nu_{j,HPO_4^{2-}} \\ \nu_{j,H^+} \\ \nu_{j,H_2O} \end{bmatrix} \\
& = \begin{bmatrix} -\sum_m i_m^C \cdot \nu_{j,m} \\ -\sum_m i_m^N \cdot \nu_{j,m} \\ -\sum_m i_m^P \cdot \nu_{j,m} \\ -\sum_m i_m^{charge} \cdot \nu_{j,m} \\ -\sum_m i_m^O \cdot \nu_{j,m} \end{bmatrix} \quad (6.6)
\end{aligned}$$

where the summations are made over all components m for which stoichiometric coefficients have been determined under point 1. Of course this yields the same result as when calculating the stoichiometric coefficients ν_{j,HCO_3^-} , ν_{j,NH_4^+} , $\nu_{j,HPO_4^{2-}}$, ν_{j,H^+} and ν_{j,H_2O} one by one. Following this procedure, the number of compensation components is minimized, as well as the resulting values of their stoichiometric coefficients. Note that taking up the elemental H-balance in addition to the other balances, aiming to determine the stoichiometric coefficient of an additional component, would result in a matrix of stoichiometric coefficients in Eq. 6.6 that is singular (i.e. with determinant zero), which would make matrix inversion, necessary to obtain the values of the stoichiometric coefficients, impossible, indicating that the system is overdetermined. It is advisable to check the accuracy of the performed calculations by calculating the H-balance, that should be fulfilled.

The number of balances to be considered can be reduced when certain components are not considered in the destination model. For instance, the O-balance can be omitted when H_2O is not considered in the destination model, without influencing the stoichiometric coefficients of the remaining components. In the same way, the charge balance can be omitted when H^+ is not taken up in the destination model. Even if the destination model would consider H_2O but not H^+ , the charge balance can still be omitted since the order of (d) and (e) may be switched, so the stoichiometric coefficient of H^+ determined by the charge balance does not influence the stoichiometric coefficient

of H_2O . In this chapter however, all balances are considered in every case to illustrate the principle of maintaining continuity of all elements, charge and COD.

The protons that are produced or consumed in the model interfaces and are modelled by the compensation state variable H^+ , require special attention. As these protons do not represent 'free' protons but will immediately take part in the water equilibrium and other chemical equilibria, they cannot be passed on by summing up like the other state variables. For this reason, the pH of the anaerobic digester effluent (assumed to remain unchanged by the dewatering process) is passed on unaltered as the SHARON model influent pH, while the protons produced in the ASM1/SHARON interface are passed on separately to the SHARON model, where they take part in the chemical equilibria and in this way influence the pH (Figure 6.4). Protons produced in the SHARON/Anammox and Anammox/ASM1 interface should also be accounted for. However, since the destination models (Anammox and ASM1, respectively) do not consider pH as a state variable, protons that are produced or consumed in these model interfaces should be accounted for in their pH-related state variable S_{alk} , representing alkalinity. As S_{alk} is represented as bicarbonate, continuity of elemental and charge balances is ensured by considering the reaction



in the interface. In this way, the protons that are produced/consumed are transformed into an equivalent amount of HCO_3^- , H_2O and CO_2 . HCO_3^- is then passed on as S_{alk} , while H_2O and CO_2 are not passed on.

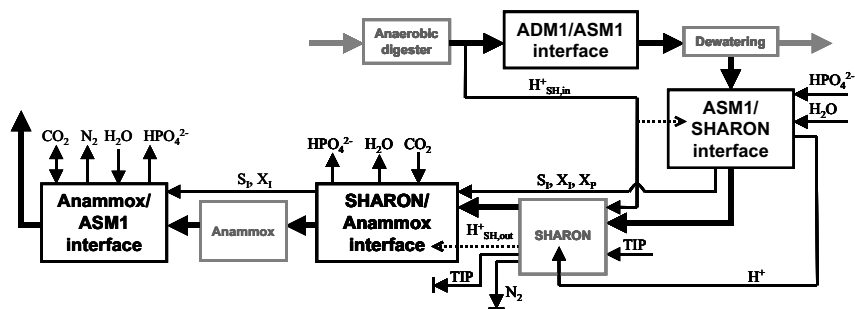


Figure 6.4: Construction of the ASM1/SHARON, SHARON/Anammox and Anammox/ASM1 model interfaces: direct pass-through of variables and fate of compensation state variables

Figure 6.4 gives a general scheme of the interfaces constructed in this study. The set-up of the transformation matrices for the three model interfaces constructed, is addressed in detail in the following paragraphs. Seven types of transformations are distinguished:

1. Direct transformation of state variables
2. Transformation of state variables that have the same meaning in the two models to be connected, while their composition differs (slightly).
3. Splitting up or merging lumped state variables.
4. Transformation of state variables of the origin model that are not included in the destination model, or exhibit a different behaviour.
5. Incoming values for state variables of the destination model that are not included in the origin model.
6. Direct pass-through of state variables of the origin model that are not included in the destination model and do not influence the behaviour of the destination model
7. Some state variables are not passed on.

Note however that not all types of transformations occur in each interface.

ASM1 to SHARON transformation matrix (Table 6.7)

Type 1 : Direct transformation processes: The ASM1 component S_O is passed on as O_2 , including unit conversion.

Type 2: Transformation of state variables with the same meaning but a different composition: The state variable X_{BH} for heterotrophic biomass is mapped to the corresponding state variable X_{het} of the destination model on a COD-basis. The state variables S_{alk} , S_{NH} , TIP , H^+ and H_2O are used as compensation components to close the C-, N-, P-, charge and O-balances respectively. Note that it is not likely that sludge digester effluent still contains viable heterotrophic or autotrophic biomass, that is able to perform conventional C- and/or N-removal (Salem et al., 2006) in a SHARON-process or in the main WWTP. However, the transformation of biomass is taken up in the model interface in case

new insights in this matter should be gained, e.g. when it would be shown that a (small) biomass fraction can survive the anaerobic digester when the latter is operated with a relatively short retention time.

Type 3: Splitting up or merging lumped state variables The ASM1 state variable S_{NH} is mapped to TNH on a N-basis (as this component does not contain COD). However, when the lumped state variable TNH enters the SHARON reactor, it is split up into NH_4^+ and NH_3 , in proportions that depend on the incoming pH. This means that S_{NH} , expressed as all NH_4^+ , is in fact transformed partly to NH_4^+ and partly to NH_3 . In order to ensure continuity, protons are released in the interface, equivalent with the amount of NH_3 that corresponds with the amount of S_{NH} transformed and the incoming pH:

$$\nu_{2,H^+}^{AS}(pH_{SH,in}) = \frac{NH_3}{NH_4^+ + NH_3} \cdot \left(-\frac{\nu_{S_{NH}}^{AS}}{14} \right) = \frac{K_{e,NH_4^+}}{H_{SH,in}^+ + K_{e,NH_4^+}} \cdot 1$$

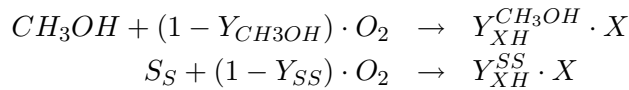
As the coefficient ν_{2,H^+}^{AS} depends on the incoming pH of the SHARON model, in this case the anaerobic digester effluent pH, it should be recalculated at every time step. Indeed, for the incoming pH, that changes from 7.17 to 7.33, the coefficient ν_{2,H^+}^{AS} changes from 0.01666 to 0.02391, so it cannot be considered constant.

The ASM1 state variable S_{NO} represents both nitrite and nitrate but is expressed in terms of nitrate. For this reason, this component is passed on as if it were all nitrate. This will not give rise to large mistakes as the anaerobic digester effluent is not expected to contain nitrite or nitrate.

The ASM1 does not distinguish between ammonium and nitrite oxidizers, as does the SHARON model. The state variable X_{BA} for autotrophic biomass is mapped on a COD-basis to 75% ammonium oxidizers (X_{amm}) and 25% nitrite oxidizers (X_{nit}), corresponding with the number of electrons involved in the oxidation of ammonium and nitrite and in this way with the biomass yield coefficients. Compensation state variables are needed to close the remaining balances, as the biomass composition differs between the ASM1 and the SHARON model. Again, little chance exists that there is much autotrophic biomass present in the anaerobic digester effluent.

Type 4: Transformation of state variables of the origin model into state variables of the destination model The effluent of the anaerobic

digester contains (small amounts of) easily biodegradable substrate S_S , that should be sent to the SHARON reactor. However, the only form of easily biodegradable substrate that is considered in the SHARON reactor model is methanol, the degradation of which shows a significantly lower biomass yield than the degradation of 'regular' S_S components:



where $Y_{XH}^{CH_3OH} = 0.20$ gCOD/gCOD (Hellings et al., 1999) and $Y_{XH}^{SS} = 0.67$ gCOD/gCOD (Henze et al., 2000), which means that degradation of methanol yields significantly less biomass but consumes significantly more oxygen than degradation of S_S . To compensate for this in the interface, 1 gCOD S_S is transformed into $(1 - \alpha)$ gCOD heterotrophic biomass (X_{het}) and α gCOD methanol in such a way that the overall oxygen consumption and biomass production remains the same (see Figure 5). One finds:

$$\alpha = \frac{1 - Y_{XH}^{SS}}{1 - Y_{XH}^{CH_3OH}} = 0.4125$$

The compensation state variables are used to close the C-, N-, P-, charge and O-balance.

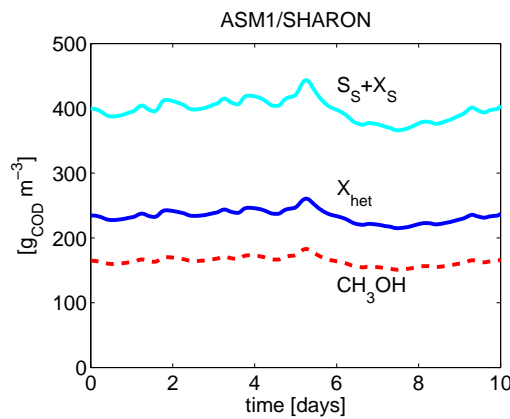


Figure 6.5: Transformation of S_S and X_S to CH_3OH and X_{het} in ASM1/SHARON interface

Slowly biodegradable substrate, X_S , is treated in the interface as if it were hydrolysed instantaneously to S_S , thereby neglecting the time

needed for this reaction. This is a reasonable assumption since the hydraulic retention time in the SHARON reactor (typically > 1.25 days) is long compared to the time constant for hydrolysis ($1/k_H = 0.333$ days, Henze et al. 2000) and regarding the fact that the SHARON reactor is operated as a CSTR, which means that the reactor concentrations are equal to its effluent concentrations. The hydrolysed X_S is further split up into X_{het} and CH_3OH in the same way as S_S , using compensation state variables to close the remaining balances.

Soluble biodegradable organic matter, S_{ND} , is ammonified to S_{NH} instantaneously in the model interface. In the same way, particulate biodegradable organic nitrogen, X_{ND} , is hydrolysed and ammonified to S_{NH} instantaneously. During ammonification, protons are consumed in the same (molar) amount as the amount of S_{ND} or X_{ND} converted. The formed S_{NH} is directly passed on as T_{NH} (with the same correction for protons) and for this reason does not appear in the interface.

The ASM1 state variable S_{alk} for alkalinity, lumping HCO_3^- , CO_3^{2-} as well as fatty acid ions, is expressed as if it were all HCO_3^- . Fatty acids components (e.g. acetate, propionate, butyrate) are state variables of the ADM1. Unfortunately, information on the amount of fatty acids is lost in the existing ADM1/ASM1 interface in the BSM2, as the ASM1 does not contain any state variables representing fatty acids but only contains alkalinity, expressed as bicarbonate. However, for a well-operated anaerobic digester, the amount of fatty acids should be small anyway (Zaher et al., 2006). In this way, it is assumed that the ASM1 state variable S_{alk} can be written as

$$S_{alk} = HCO_3^- + 2CO_3^{2-}$$

On the other hand, the SHARON state variable TIC represents total inorganic carbon:

$$TIC = CO_2 + HCO_3^- + CO_3^{2-}$$

Consequently, these two state variables are related by (see section 3.4.2)

$$\begin{aligned} \nu_{13,TIC}^{AS}(pH_{SH,in}) &= \frac{CO_2 + HCO_3^- + CO_3^{2-}}{HCO_3^- + 2CO_3^{2-}} \cdot (-\nu_{S_{alk}}^{AS}) \\ &= \frac{H_{SH,in}^+ + H_{SH,in}^+ \cdot K_{eCO_2} + K_{eCO_2} \cdot K_{eHCO_3^-}}{H_{SH,in}^+ \cdot K_{eCO_2} + 2K_{eCO_2} \cdot K_{eHCO_3^-}} \cdot 1 \end{aligned}$$

It is important to note that the transformation of S_{alk} to TIC depends on the incoming pH of the SHARON model, in this case the anaerobic

digester effluent pH. As a result, the coefficient $\nu_{13,TIC}^{AS}$ is not constant (it changes from 1.1370 for pH=7.17 to 1.0941 for pH=7.33), so it needs to be recalculated at every time step.

Type 5: Influent values for state variables of the destination model, not included in the origin model While pH plays an important role in anaerobic digestion and consequently is taken up in the ADM1 model, it is not considered in the ASM and for this reason was left out of the ADM1-ASM1 interface, that was already implemented in BSM2. However, in the SHARON process, pH also plays an important role. For this reason, it was decided for pH to bypass the existing ADM1-ASM1 interface – as well as the subsequent dewatering process – and to pass its value directly from the anaerobic digester to the SHARON process. In this way, it is assumed that the pH is not affected during dewatering. This pH-value still must be corrected for the proton production/consumption in the model interface. However, this cannot be done by just adding up the latter to the proton concentration corresponding with the pH-value coming from the anaerobic digester, as the protons produced/consumed in the interface are not all free protons but will participate in chemical equilibrium reactions. For this reason, the protons originating from the model interfacing, are sent separately to the pH-calculation module of the SHARON reactor model, where these equilibria shifts are taken care of. Alternatively, one could include a pH-calculation module into the interface.

Inorganic phosphorus (*TIP*) is only considered in the SHARON model, and only regarding its effect on chemical equilibria, which is important for pH-calculation. None of the ASM1, SHARON or Anammox models consider the fate of phosphorus in biological conversion reactions. Since the ASM1 does not contain inorganic phosphorus, it was decided to 'add' a realistic concentration of inorganic phosphorus to the SHARON reactor influent, to include the effect of inorganic phosphorus on the chemical equilibria. From influent data of the full-scale SHARON reactor in Rotterdam, an influent concentration of 1.5 mole m^{-3} *TIP* has been selected as a reasonable assumption.

Type 6: Direct pass-through of state variables of the origin model that are not included in the destination model and do not influence the behaviour of the destination model. X_P , S_I and X_I do not participate in any of the SHARON model reactions. However, it is important to pass on these state variables to the subsequent models in which they

are considered: X_P is a state variable of the Anammox model, and S_I and X_P are state variables of the ASM model. Care must be taken that these state variables do not disappear in model interfaces, e.g. to correctly simulate build-up of these state variables in the activated sludge tanks. Note that by direct pass-through, the retention time of X_P , S_I and X_I in the SHARON reactor is ignored. However, their dynamics are so slow that this results in only small errors.

Type 7: State variables not passed on to the destination model. The compensation state variables HPO_4^{2-} and H_2O are not passed on to the SHARON model.

SHARON to Anammox transformer (Table 6.8)

It is realistically assumed that the SHARON effluent is passed completely to the Anammox reactor, without biomass settling in between.

Type 1 : Direct transformation processes: Oxygen and nitrate are passed directly, after unit conversion. The state variable X_P that has been directly passed through in the ASM1/SHARON interface, is mapped to this state variable in the Anammox model.

Type 2: Transformation of state variables with the same meaning but a different composition: Ammonium oxidizers of the SHARON model, X_{amm} , are mapped to the corresponding component in the Anammox model, X_{NH} on the basis of their COD content. TIC , TNH , HPO_4^{2-} , H^+ and H_2O are used as compensation components to close the C-, N-, P-, charge and O-balance, respectively. The transformation reaction for nitrite oxidizing (X_{nit} , X_{NO}) and heterotrophic biomass (X_{het} , X_H) in the SHARON-Anammox interface is defined in an identical way, as the biomass composition of ammonium oxidizers, nitrite oxidizers and heterotrophs is the same in both models. It is important to note that it is assumed here that all biomass in the SHARON reactor survives as active biomass in the Anammox reactor.

Type 3: Splitting up or merging lumped state variables The SHARON state variable TNH is mapped to the ASM1 state variable S_{NH} . However, as S_{NH} is expressed as all NH_4^+ , protons need to be consumed in the interface to ensure continuity. The amount of protons taken up are equivalent with the amount of NH_3 that corresponds with

the amount of TNH transformed and the outgoing pH ($\sim H_{SH,out}^+$) from the SHARON reactor:

$$\nu_{1,H^+}^{SA}(pH_{SH,out}) = -\frac{K_{e,NH_4^+}}{H_{SH,out}^+ + K_{e,NH_4^+}}$$

An analogous reasoning holds for the SHARON state variable TNO_2 , that is mapped to the ASM1 state variable S_{NO} . As S_{NO} is expressed as all NO_2^- , protons are released in the interface to ensure continuity. The amount of protons released are equivalent with the amount of HNO_2 for the given amount of TNO_2 transformed and the outgoing pH from the SHARON reactor:

$$\nu_{2,H^+}^{SA}(pH_{SH,out}) = \frac{H_{SH,out}^+}{H_{SH,out}^+ + K_{eHNO_2}}$$

Type 4: Transformation of state variables of the origin model into state variables of the destination model Methanol, added to the SHARON reactor as an external carbon source in case of denitrification, is passed on as easily biodegradable substrate S_S . The higher biomass yield and lower oxygen consumption on S_S compared to CH_3OH , is accounted for completely analogously to the ASM1/SHARON interface.

From the same reasoning as in the ASM1/SHARON interface, TIC is passed on as the state variable S_{alk} to the Anammox model according to

$$\nu_{12,S_{alk}}^{SA}(pH_{SH,out}) = \frac{H_{SH,out}^+ \cdot K_{eCO_2} + 2 K_{eCO_2} \cdot K_{eHCO_3^-}}{H_{SH,out}^{+2} + H_{SH,out}^+ \cdot K_{eCO_2} + K_{eCO_2} \cdot K_{eHCO_3^-}}$$

Type 6: Direct pass-through of state variables of the origin model that are not included in the destination model and do not influence the behaviour of the destination model. Soluble and particulate inert organic matter, S_I and X_I , respectively, are no state variables of the Anammox model and are passed directly to ASM1, after taking into account the retention of particulates in the Anammox reactor.

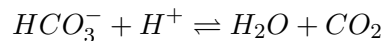
Type 7: State variables of the origin model that are not passed on Although N_2 is taken up as a state variable in both the SHARON and the Anammox model, it was decided not to pass this component in the

SHARON/Anammox interface. This does not give rise to continuity problems as N_2 is not consumed in any reaction but is only a denitrification product. As no N_2 enters the SHARON model through the interface, all N_2 leaving the reactor originates from denitrification. The fact that N_2 is not passed from the SHARON to the Anammox model ensures that the amount of N_2 produced in the Anammox model is directly related to the amount of ammonium and nitrite converted in the Anammox reactor through the anaerobic ammonium oxidation (anammox) reaction and some denitrification.

The state variable TIP , representing inorganic phosphorus, is not passed on from the SHARON model as it was only added to the incoming stream of the SHARON reactor to simulate its effect on the chemical equilibria in the SHARON reactor. The ASM1 and Anammox model do not contain a state variable representing inorganic phosphorus.

Note that state variables of the origin model that are not passed on, are omitted from the transformation matrix, as they would result in a singular (non-invertible) matrix T_{orig} .

As the proton concentration is not included as a state variable in the Anammox model or ASM1, it is not passed on from the SHARON effluent. However, the protons produced/consumed in the interface are taken into account to calculate the buffer capacity, represented by the state variable S_{alk} and expressed as if it was all HCO_3^- , passed on to the Anammox model, through the reaction



The compensation state variables HPO_4^{2-} , H_2O and CO_2 are not passed to the Anammox model.

Anammox to ASM1 transformer (Table 6.9)

Type 1 : Direct transformation processes: The Anammox model and ASM1 have most of their state variables in common. These therefore can be passed easily: S_O , S_S , S_{NH} , X_H (which is the same as X_{BH}), X_S , X_P and S_{alk} . The mapping of nitrate (S_{NO_3}) to S_{NO} , that represents both nitrite and nitrate, but is expressed as if it were all nitrate, is also straightforward.

Type 3: Splitting up or merging lumped state variables Passing nitrite (S_{NO_2}) requires extra attention, as nitrite is not included as a separate component in ASM, but as a lumped component S_{NO} , that is ex-

pressed as nitrate. It was decided to map S_{NO_2} to S_{NO} on a COD-basis. As a result, the biomass yield during denitrification will not be affected. This means that the amount of $NO_3^- - N$ in the destination model will be lower than the amount of $NO_2^- - N$ in the source model. In order to fulfill the N-balance, N_2 (and not NH_4^+ !) is added to the destination model, accounting for the lower N_2 -production associated with the denitrification of a lower amount of $NO_3^- - N$ compared to $NO_2^- - N$ (see Figure 6.6). Note however that N_2 is not passed to the ASM1, as it is

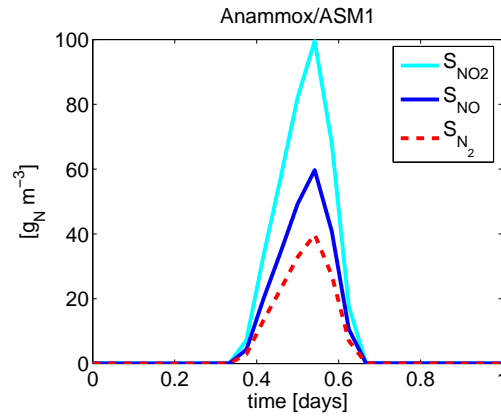


Figure 6.6: Transformation of S_{NO_2} (nitrite) to S_{NO} (nitrite+nitrate) and S_{N_2} in Anammox/ASM1 interface

not a state variable in the latter model. Stoichiometric coefficients are determined for H^+ and H_2O as compensation state variables to fulfill the charge and the O-balance, respectively. This approach is preferred over an alternative one, in which S_{NO_2} would be mapped to S_{NO} on a N-basis, adding S_S as a COD-source to compensate for the extra COD that would be required to denitrify the same amount (on N-basis) of nitrate compared to nitrite. However, in this case also a biomass compensation term should be added to account for the additional biomass production during denitrification of nitrate compared to nitrite. As the latter approach would lead to more compensation terms with larger stoichiometric coefficients, the transformation of nitrite to nitrate on COD-basis is preferred to the one on N-basis.

Type 4: Transformation of state variables of origin model into state variables of destination model. Concerning the fate of ammonium and nitrite oxidizers (X_{amm} , resp. X_{nit}), there are no indications so far

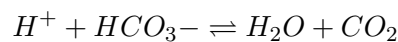
that nitrifying biomass coming from the SHARON reactor – that we have assumed to survive in the Anammox reactor – will survive in the main wastewater plant and in this way will have an augmentation effect. Also the Anammox biomass, performing the autotrophic conversion of ammonium and nitrite to nitrogen gas is assumed to decay completely in the main WWTP. The decay process to which the autotrophic biomass is subjected, is the one defined in ASM1:

$$X_{NH/NO/AN} \rightarrow f_P \cdot X_P + (1 - f_P) \cdot X_S + \nu_{X_{ND}}^{AA} \cdot X_{ND}$$

in which $f_P = 0.08$ (Henze et al., 2000). X_{ND} accounts for the different N-contents of the components involved. In this way, the N-balance is closed besides the COD balance. Subsequently, the compensation state variables S_{alk} , $S_{HPO4(2-)}$, S_{H+} and S_{H2O} are used to close the C-, P-, charge and O-balances. By implementing the decay process of autotrophs in the Anammox/ASM1 interface, it is assumed that this process takes place instantaneously, thereby neglecting the time constant for this reaction and making slowly biodegradable substrate X_S immediately available for hydrolysis to readily biodegradable substrate S_S . Although the time constant for the decay of biomass is larger (slower process) than the time constant for hydrolysis ($b_A = 0.05 \text{ day}^{-1}$ vs. $k_H = 3 \text{ day}^{-1}$, Henze et al. 2000), the load of X_S released by decay of autotrophic biomass in the interface is very small compared to the load of X_S in the influent (about 0.035%), so the assumption of instantaneous decay of autotrophic biomass in the interface is considered acceptable.

Type 6: Direct pass-through of state variables of the origin model that are not included in the destination model and do not influence the behaviour of the destination model. S_I and X_I are no state variables of the SHARON or Anammox models. Their value from the ASM1/SHARON interface is passed directly, at least after taking into account the biomass retention by the Anammox reactor. This will cause only a small fraction of X_I to eventually be passed in the Anammox/-ASM1 interface.

Type 7: State variables of the origin model that are not passed on
The compensation state variable H^+ is not passed on as such, but the protons produced/consumed in the interface are taken into account through the equilibrium reaction



in which S_{alk} , H_2O and CO_2 are involved.

The state variable S_{N_2} , representing nitrogen gas, is not passed on as it is not taken up in the ASM1.

The compensation state variables HPO_4^{2-} , H_2O and CO_2 are not passed on either.

Table 6.7: ASM1-SHARON Transformation matrices. Top: Petersen section ASM1 model ('origin'). Bottom: Petersen section SHARON model ('destination'). Important note: the pH from the anaerobic digester effluent is directly passed to the SHARON model but is not taken up here as it is no ASM1 state variable. Columns in grey correspond with compensation state variables that are not passed on in the interface.

components →	S_I	S_S	X_I	X_S	X_BH	X_BA	X_P	S_O	comp. N			comp. C	
									S_NO	S_NH	S_ND	X_ND	S_alk
transformations ↓	gCOD/m3	gCOD/m3	gCOD/m3	gCOD/m3	gCOD/m3	gCOD/m3	gCOD/m3	gO2/m3	gN/m3	gN/m3	gN/m3	gN/m3	mole/m3
1. S_O to O2	0	0	0	0	0	0	0	-32	0	0	0	0	0
2. S_NH to TNH	0	0	0	0	0	0	0	0	0	-14	0	0	0
3. S_NO to NO3	0	0	0	0	0	0	0	0	-14	0	0	0	0
4. X_BH to Xhet	0	0	0	0	-34.5817	0	0	0	0	-0,0223	0	0	0,0477
5. X_BA to Xamm/Xnit	0	0	0	0	0	-34.5817	0	0	0	-0,0223	0	0	0,0477
6. S_S to CH3OH/Xhet	0	-1	0	0	0	0	0	0	0	-0,0476	0	0	-0,0002
7. X_S to CH3OH/Xhet	0	0	0	-1	0	0	0	0	0	-0,0476	0	0	-0,0002
8. S_ND to TNH	0	0	0	0	0	0	0	0	0	0	-14	0	0
9. X_ND to TNH	0	0	0	0	0	0	0	0	0	0	0	-14	0
10. Direct pass S_I	-1	0	0	0	0	0	0	0	0	0	0	0	0
11. Direct pass X_I	0	0	-1	0	0	0	0	0	0	0	0	0	0
12. Direct pass X_P	0	0	0	0	0	0	-1	0	0	0	0	0	0
13. S_alk to TIC	0	0	0	0	0	0	0	0	0	0	0	0	-1

components →	TNH	TNO2	TIC	TIP	NO3-	O2	N2	Xamm	Xnitr	Xhet	CH3OH	S_I	X_I	X_P	comp. P			comp. ch	comp. O
															HPO4(2-)	H+	H2O	H+	
transformations ↓	mole/m3	mole/m3	mole/m3	mole/m3	mole/m3	mole/m3	mole/m3	mole/m3	mole/m3	mole/m3	mole/m3	gCOD/m3	gCOD/m3	gCOD/m3	mole/m3	mole/m3	mole/m3		
1. S_O to O2	0	0	0	0	0	1	0	0	0	0	0	0	0	0	0	0	0	0	
2. S_NH to TNH	1	0	0	0	0	0	0	0	0	0	0	0	0	0	0	0	0	0	
3. S_NO to NO3	0	0	0	0	1	0	0	0	0	0	0	0	0	0	0	0	0	0	
4. X_BH to Xhet	0	0	0	0	0	0	0	0	0	1	0	0	0	0	0	-9,63E-04	0,0474	-0,2129	
5. X_BA to Xamm/Xnit	0	0	0	0	0	0	0	0,75	0,25	0	0	0	0	0	0	-9,63E-04	0,0474	-0,2129	
6. S_S to CH3OH/Xhet	0	0	0	0	0	0	0	0	0	0,0170	0,0086	0	0	0	0	-1,31E-04	0,0029	-0,0074	
7. X_S to CH3OH/Xhet	0	0	0	0	0	0	0	0	0	0,0170	0,0086	0	0	0	0	-1,31E-04	0,0029	-0,0074	
8. S_ND to TNH	1	0	0	0	0	0	0	0	0	0	0	0	0	0	0	0	-1+v _{2,H+} ^{AS}	0	
9. X_ND to TNH	1	0	0	0	0	0	0	0	0	0	0	0	0	0	0	0	-1+v _{2,H+} ^{AS}	0	
10. Direct pass S_I	0	0	0	0	0	0	0	0	0	0	0	1	0	0	0	0	0	0	
11. Direct pass X_I	0	0	0	0	0	0	0	0	0	0	0	0	1	0	0	0	0	0	
12. Direct pass X_P	0	0	0	0	0	0	0	0	0	0	0	0	0	1	0	0	0	0	
13. S_alk to TIC	0	0	v _{13,TIC} ^{AS}	0	0	0	0	0	0	0	0	0	0	0	0	0	0	0	

$$\text{in which } v_{13,TIC}^{AS} = \frac{H_{SH,in}^+ + H_{SH,in}^+ \cdot K_{eCO_2} + K_{eCO_2} \cdot K_{eHCO_3^-}}{H_{SH,in}^+ \cdot K_{eCO_2} + 2K_{eCO_2} \cdot K_{eHCO_3^-}}; v_{2,H+}^{AS} = \frac{K_{eNH_4^+}}{H_{SH,in}^+ + K_{eNH_4^+}}$$

Table 6.8: SHARON-Anammox interface. Top: Petersen section SHARON model ('origin'). Bottom: Petersen section Anammox model ('destination'). Columns in grey correspond with (compensation) state variables that are not passed on in the interface.

components →	TNH	TNO2	TIC	NO3-	O2	Xamm	Xnitr	Xhet	CH3OH	S_I	X_I	X_P
transformations ↓	mole/m3	gCOD/m3	gCOD/m3	gCOD/m3								
1. TNH to S_NH	-1	0	0	0	0	0	0	0	0	0	0	0
2. TNO2 to S_NO2	0	-1	0	0	0	0	0	0	0	0	0	0
3. NO3- to S_NO3	0	0	0	-1	0	0	0	0	0	0	0	0
4. O2 to S_O	0	0	0	0	-1	0	0	0	0	0	0	0
5. Xamm to X_NH	0	0	0	0	0	-1	0	0	0	0	0	0
6. Xnit to X_NO	0	0	0	0	0	0	-1	0	0	0	0	0
7. Xhet to X_H	0	0	0	0	0	0	0	-1	0	0	0	0
8. CH3OH to S_S	0	0	0	0	0	0	0	-0.0170	-0.0086	0	0	0
9. Direct pass S_I	0	0	0	0	0	0	0	0	0	-1	0	0
10. Direct pass X_I	0	0	0	0	0	0	0	0	0	0	-1	0
11. Direct pass X_P	0	0	0	0	0	0	0	0	0	0	0	-1
12. TIC to S_alk	0	0	-1	0	0	0	0	0	0	0	0	0

components →	comp. N												comp. H			comp. P		comp. ch.		
	S_O	S_S	S_NH	S_NO2	S_NO3	S_N2	X_H	X_NH	X_NO	X_AN	X_S	X_P	S_alk	S_I	X_I	H2O	HPO4(2-)	CO2	H+	
transformations ↓	gO2/m3	gCOD/m3	gN/m3	gN/m3	gN/m3	gN/m3	gCOD/m3	gCOD/m3	gCOD/m3	gCOD/m3	gCOD/m3	gCOD/m3	mole/m3	gCOD/m3	gCOD/m3	mole/m3	mole/m3	mole/m3	mole/m3	
1. TNH to S_NH	0	0	14	0	0	0	0	0	0	0	0	0	0	0	0	0	0	0	0	0
2. TNO2 to S_NO2	0	0	0	14	0	0	0	0	0	0	0	0	0	0	0	0	0	0	0	0
3. NO3- to S_NO3	0	0	0	0	14	0	0	0	0	0	0	0	0	0	0	0	0	0	0	0
4. O2 to S_O	32	0	0	0	0	0	0	0	0	0	0	0	0	0	0	0	0	0	0	0
5. Xamm to X_NH	0	0	0.0223	0	0	0	0	34.5817	0	0	0	0	-0.0003	0	0	0.1655	9.63E-04	-0.04739	-0.0474	
6. Xnit to X_NO	0	0	0.0223	0	0	0	0	0	34.5817	0	0	0	-0.0003	0	0	0.1655	9.63E-04	-0.04739	-0.0474	
7. Xhet to X_H	0	0	0.0223	0	0	0	34.5817	0	0	0	0	0	-0.0003	0	0	0.1655	9.63E-04	-0.04739	-0.0474	
8. CH3OH to S_S	0	1	0.0476	0	0	0	0	0	0	0	0	0	0.0031	0	0	0.0045	1.31E-04	-0.00294	-0.0029	
9. Direct pass S_I	0	0	0	0	0	0	0	0	0	0	0	0	0	1	0	0	0	0	0	
10. Direct pass X_I	0	0	0	0	0	0	0	0	0	0	0	0	0	0	1	0	0	0	0	
11. Direct pass X_P	0	0	0	0	0	0	0	0	0	0	0	1	0	0	0	0	0	0	0	
12. TIC to S_alk	0	0	0	0	0	0	0	0	0	0	0	0	V12,Salk	0	0	0	0	0	0	

with

$$V_{1,H+}^{SA} = -\frac{K_{e,NH_4^+}}{H_{SH,out}^+ + K_{e,NH_4^+}}; V_{2,H+}^{SA} (pH_{SH,out}) = \frac{H_{SH,out}^+}{H_{SH,out}^+ + K_{eHNO_2}};$$

$$V_{12,Salk}^{SA} = \frac{H_{SH,out}^+ \cdot K_{eCO_2} + 2K_{eCO_2} \cdot K_{eHCO_3^-}}{H_{SH,out}^+{}^2 + H_{SH,out}^+ \cdot K_{eCO_2} + K_{eCO_2} \cdot K_{eHCO_3^-}}$$

Table 6.9: Anammox-ASM1 interface. Top: Petersen section Anammox model ('origin'). Bottom: Petersen section ASM1 model ('destination'). Columns in grey correspond with (compensation) state variables that are not passed on in the interface.

components →	S_O	S_S	S_NH	S_NO2	S_NO3	S_N2	X_H	X_NH	X_NO	X_AN	X_S	X_P	S_alk	S_I	X_I
transformations ↓	gO2/m3	gCOD/m3	gN/m3	gN/m3	gN/m3	gN/m3	gCOD/m3	gCOD/m3	gCOD/m3	gCOD/m3	gCOD/m3	gCOD/m3	mole/m3	gCOD/m3	gCOD/m3
1. S_O	-1	0	0	0	0	0	0	0	0	0	0	0	0	0	0
2. S_S	0	-1	0	0	0	0	0	0	0	0	0	0	0	0	0
3. S_NH	0	0	-1	0	0	0	0	0	0	0	0	0	0	0	0
4. S_N2	0	0	0	0	0	-1	0	0	0	0	0	0	0	0	0
5. X_H to X_BH	0	0	0	0	0	0	-1	0	0	0	0	0	0	0	0
6. X_S	0	0	0	0	0	0	0	0	0	0	-1	0	0	0	0
7. X_P	0	0	0	0	0	0	0	0	0	0	0	-1	0	0	0
8. S_NO3 to S_NO	0	0	0	0	-1	0	0	0	0	0	0	0	0	0	0
9. S_NO2 to S_NO	0	0	0	-1	0	0	0	0	0	0	0	0	0	0	0
10. X_NH to X_S/P	0	0	0	0	0	0	0	-1	0	0	0	0	0	0	0
11. X_NO to X_S/P	0	0	0	0	0	0	0	0	-1	0	0	0	0	0	0
12. X_AN to X_S/P	0	0	0	0	0	0	0	0	0	-1	0	0	0	0	0
13. Direct pass S_I	0	0	0	0	0	0	0	0	0	0	0	0	0	-1	0
14. Direct pass X_I	0	0	0	0	0	0	0	0	0	0	0	0	0	0	-1
15. S_alk	0	0	0	0	0	0	0	0	0	0	0	0	-1	0	0

components →	S_I	S_S	X_I	X_S	X_BH	X_BA	X_P	S_O	S_NO	S_NH	S_NO2	X_NO2	S_alk	comp. O	comp. P	comp. ch.		
transformations ↓	gCOD/m3	gO2/m3	gN/m3	gN/m3	gN/m3	gN/m3	mole/m3	S_H2O	S_HPO4 ²⁻	S_N2	CO2	H+						
1. S_O	0	0	0	0	0	0	0	1	0	0	0	0	0	0	0	0	0	0
2. S_S	0	1	0	0	0	0	0	0	0	0	0	0	0	0	0	0	0	0
3. S_NH	0	0	0	0	0	0	0	0	0	1	0	0	0	0	0	0	0	0
4. S_N2	0	0	0	0	0	0	0	0	0	0	0	0	0	0	0	1	0	0
5. X_H to X_BH	0	0	0	0	1	0	0	0	0	0	0	0	0	0	0	0	0	0
6. X_S	0	0	0	1	0	0	0	0	0	0	0	0	0	0	0	0	0	0
7. X_P	0	0	0	0	0	0	1	0	0	0	0	0	0	0	0	0	0	0
8. S_NO3 to S_NO	0	0	0	0	0	0	0	0	1	0	0	0	0	0	0	0	0	0
9. S_NO2 to S_NO	0	0	0	0	0	0	0	0	0,6	0	0	0	0,028571	-0,0143	0	0,4	-0,029	-0,03
10. X_NH to X_S	0	0	0	0,92	0	0	0,08	0	0	0	0	0,0755	-0,0008	-0,0063	0,012	0	0,0053	0,005
11. X_NO to X_S/P	0	0	0	0,92	0	0	0,08	0	0	0	0	0,0755	-0,0008	-0,0063	0,012	0	0,0053	0,005
12. X_AN to X_S/P	0	0	0	0,92	0	0	0,08	0	0	0	0	0,0514	-0,00073	0,0019	0,011	0	0,0017	0,002
13. Direct pass S_I	1	0	0	0	0	0	0	0	0	0	0	0	0	0	0	0	0	0
14. Direct pass X_I	0	0	1	0	0	0	0	0	0	0	0	0	0	0	0	0	0	0
15. S_alk	0	0	0	0	0	0	0	0	0	0	0	0	1	0	0	0	0	0

6.3.4 Step 4: Implementation of the transformation equations

Besides the stoichiometric coefficients ν_{jk} , defined in the previous step, also transformation 'rates' ρ_j need to be identified for full definition of the interfaces. These transformation rates must fulfill the following equations (Vanrolleghem et al., 2005):

$$\phi_k^{in} = - \sum_{j=1}^N \nu_{jk} \cdot \rho_j \quad k = 1, \dots, P \quad (6.7)$$

$$\phi_k^{out} = \sum_{j=1}^N \nu_{jk} \cdot \rho_j \quad k = P + 1, \dots, P + Q \quad (6.8)$$

in which ϕ_k^{in} represents the known (positive) influx of a component $k=1, \dots, P$ of the source model, while ϕ_k^{out} stands for the unknown outflux of component $k=P+1, \dots, P+Q$ of the destination model. Equation 6.7 enables the calculation of the transformation rates ρ_j in terms of the known stoichiometric components and influxes, the latter being time-varying. These expressions are subsequently substituted in Eq. 6.8 to calculate the outflux of destination components at every time step:

$$\begin{aligned} \begin{bmatrix} \phi_{P+1}^{out} \\ \vdots \\ \phi_{P+Q}^{out} \end{bmatrix} &= - \begin{bmatrix} \nu_{1,P+1} & \cdots & \nu_{N,P+1} \\ \vdots & \ddots & \vdots \\ \nu_{1,P+Q} & \cdots & \nu_{N,P+Q} \end{bmatrix} \begin{bmatrix} \nu_{1,1} & \cdots & \nu_{N,1} \\ \vdots & \ddots & \vdots \\ \nu_{1,P} & \cdots & \nu_{N,P} \end{bmatrix}^{-1} \begin{bmatrix} \phi_1^{in} \\ \vdots \\ \phi_P^{in} \end{bmatrix} \\ &\triangleq - T_{dest} \cdot T_{orig}^{-1} \cdot \begin{bmatrix} \phi_1^{in} \\ \vdots \\ \phi_P^{in} \end{bmatrix} \end{aligned} \quad (6.9)$$

Note that inversion of the second matrix is only possible unambiguously when $N = P$, i.e. if the number of transformation reactions defined is equal to the number of components of the origin model, as long as the matrix does not contain any rows or columns only containing zeros and if these transformation reactions are linearly independent of each other. So, care must be taken to define independent transformation reactions for all components of the origin model (step 1).

By implementing the transformation matrices between influxes and outfluxes, coupling of the resulting models maintaining continuity is realized at every time step. During the interfacing, it is important to check that all transformation rates ρ_j are positive, to ensure that the transformation is carried out in the right direction, i.e. from the source to the destination model (Vanrolleghem et al., 2005).

6.4 Temperature and time in model interfacing

The CBIM approach considers conservation of elements, charge and COD during model coupling. Besides these elements, also temperature needs to be passed between the models to be connected. In this case, a constant temperature of 35°C is assumed for the anaerobic digester and it is assumed not to be effected by the dewatering process. The SHARON and Anammox reactors were also operated at 35°C and this temperature value has been passed to the main plant.

When coupling different models, one must also take care of the time units in which the models are expressed. In the given case study, the BSM2 model is expressed in days, while the SHARON and Anammox models were originally expressed in seconds. Coupling an 'origin' and a 'destination' model, working with different time units is not a problem when they do not have to be coupled physically, i.e. when they are implemented as separate models and the output of the origin model is passed to the destination model as a file. In this case one can first run the 'origin' model, save the output and send it to the destination model after passing through the model interface and after additionally converting the time units, e.g. for the flow rates. However, when both models need to be implemented in the same file, the same time units have to be used. This is the case here because the sludge reject water that comes from the BSM2 model and is treated in the SHARON-Anammox process needs to be recirculated to the BSM2 model afterwards (see Figure 6.2). For this reason, the SHARON and Anammox models were rewritten for days instead of seconds as time unit.

6.5 Conclusions

In this chapter, the use of the Continuity-Based Interfacing Method (CBIM) is illustrated for a plant-wide simulation case study, in which the effect of sludge digestion reject water treatment by means of the combined SHARON-Anammox process is evaluated on plant-wide scale, using the Benchmark Simulation Model no. 2 (BSM2) model to simulate the behaviour of a complete WWTP including sludge digestion. For this case study, model interfaces have been constructed between the models ASM1/SHARON, SHARON/Anammox and Anammox/ASM1, in such a way that the continuity of COD, C, N, H, O, P and charge is maintained. Avoiding leaks of elements is indeed essential in model coupling. In this respect, the authors also want to stress the desirability

to check the existing BSM2 model interfaces and revise them where necessary, so that not only continuity of COD and N, but also of all other elements is guaranteed.

Special points of attention during the construction of model interfaces in general and more specifically when using the CBIM approach were pointed out, e.g. how the order in which the elemental balances are closed and the choice of sink/source components can minimize the number of compensation components required, as well as the values of their stoichiometric coefficients. Besides, special attention was given to the construction of interfaces between models in which pH is considered as a state variable and lumped state variables are used to represent the sum of concentrations of different equilibrium components. Although the method was illustrated for a specific case, it was described in such way that it can easily be generalized and used in other applications.

Chapter 7

Plant-wide (BSM2) evaluation of reject water treatment with a SHARON-Anammox process

A summarized version of this chapter has been accepted for oral presentation (long platform presentation) at the IWA World Water Congress in Beijing as: Volcke E.I.P., Gernaey K.V., Vrecko D., Jeppsson U., van Loosdrecht M.C.M. and Vanrolleghem P.A. (2006). Plant-wide (BSM2) evaluation of reject water treatment with a SHARON-Anammox process. IWA biennial conference, Beijing (China), 10-15 September 2006.

In wastewater treatment plants (WWTPs) equipped with sludge digestion and dewatering systems, the reject water originating from these facilities contributes significantly to the load of the activated sludge tanks, to which it is typically recycled. In this chapter, the impact of reject water streams on the performance of a WWTP is assessed in a simulation study, using the Benchmark Simulation Model no. 2 (BSM2), that includes not only the activated sludge process, but also the processes describing sludge treatment and in this way allows for plant-wide evaluation. Comparison of performance of a WWTP without reject water with a WWTP where reject water is recycled to the primary clarifier, i.e. the BSM2 plant, shows that the ammonium load of influent to the primary clarifier is 28% higher in case of reject water recycling. In the considered BSM2 plant, this results in violation of the effluent total ni-

trogen limit. In order to relieve the main wastewater treatment plant, reject water treatment with a combined SHARON-Anammox process seems a promising option. The simulation results indicate that significant improvements of the effluent quality of the main wastewater treatment plant can be realized. An economic evaluation of the different scenarios is performed using an operating cost index (OCI).

7.1 Introduction

The influent nitrogen load of wastewater treatment plants (WWTPs) is increased considerably when reject water, originating from sludge digestion and dewatering systems, is recycled to it. The reject water stream, representing typically only 2% of the volume of the influent wastewater stream, can contribute up to 25% of the nitrogen load of the influent to the activated sludge process. This is especially problematic in case the latter has a limited aeration/nitrification/denitrification capacity. In order to relieve the main plant, it can be decided to treat the reject water stream before recirculation, e.g. through the SHARON-Anammox process (van Dongen et al., 2001). In this process, half of the ammonium in the reject water is nitrified to nitrite in the SHARON reactor. Nitrate formation is suppressed by working at high temperatures combined with maintaining an appropriate sludge retention time, that is equal to the hydraulic retention time as a SHARON reactor is typically operating without sludge retention. In the subsequent Anammox reactor, almost equimolar amounts of ammonium and nitrite are combined to form nitrogen gas in the anaerobic ammonium oxidation (Anammox) reaction. With the combined SHARON-Anammox process, that is fully autotrophic, substantial savings on aeration costs (up to 63%) and external carbon addition costs (up to 100%) are realized in comparison with conventional nitrification-denitrification over nitrate, minimizing CO_2 and sludge productions.

In this chapter, model simulations are used as a tool for evaluating the impact of the recirculation of a reject water stream and to examine the effect of reject water treatment with SHARON-Anammox on the activated sludge process. For this purpose, a preliminary version of the COST/IWA Benchmark Simulation Model no. 2 (BSM2, Jeppsson et al. 2006) is used. This model includes pre-treatment of wastewater as well as the processes describing sludge treatment and is in this way suitable for plant-wide evaluation. In order to also include the effect of reject water treatment, models of the SHARON and Anammox pro-

cesses have been implemented in the existing BSM2. A scenario without sludge treatment and therefore without reject water is compared with one in which untreated reject water is recycled to the main plant and one in which the reject water is treated with a combined SHARON-Anammox process before recirculation. An economic evaluation is performed on the basis of an operating cost index (OCI).

7.2 The BSM2, SHARON and Anammox models

The layout of the BSM2, representing a 80 000 PE WWTP, as proposed by Jeppsson et al. (2006), is given in Figure 7.1. The predenitrifying activated sludge system (2 anoxic reactors followed by 3 aerobic reactors) and the secondary clarifier are identical to the ones in the benchmark simulation model no 1 (BSM1, Copp 2002). The BSM2 plant further contains a primary clarifier, a sludge thickener, an anaerobic digester and a dewatering unit. Influent data from Gernaey et al. (2005), are used. The model is initialized by running a steady state simulation over 200 days, before simulating the dynamic plant behaviour over 609 days. Plant performance evaluation is based on a one-year simulation period (the last 365 days of dynamic simulation).

For the simulation study described in this work, the BSM2 plant is operated with the default closed-loop strategy, as proposed by Vrecko et al. (2006). However, adjustments have been made regarding the maximum internal recycle flow rate as well as the external carbon dosing. This results in the following operating strategy:

- While the oxygen transfer rate is kept constant at 240 d^{-1} in the first two aerobic tanks (i.e. tanks 3 and 4), the oxygen concentration in the last aerobic tank (tank 5) is controlled to a constant set point of $2 \text{ gO}_2 \text{ m}^{-3}$ by adjusting the $k_L a$, as for the closed-loop BSM1 (Copp, 2002).
- Nitrate in the second (anoxic) tank is controlled to a constant set point of 1 gN m^{-3} by changing the internal recycle flow (Φ_{int}), as for the closed-loop BSM1 (Copp, 2002). In contrast to the default closed-loop strategy, the internal recycle flow rate is limited to three times the average value of the influent flow rate during dry weather in BSM1 ($3 \cdot \Phi_{in0} = 55338 \text{ m}^3 \text{ d}^{-1}$) instead of allowing up to five times this value ($5 \cdot \Phi_{in0} = 92230 \text{ m}^3 \text{ d}^{-1}$). In this way, very high internal recycle flow rates in case of low nitrate concentrations in the second tank (this is the case if no reject water

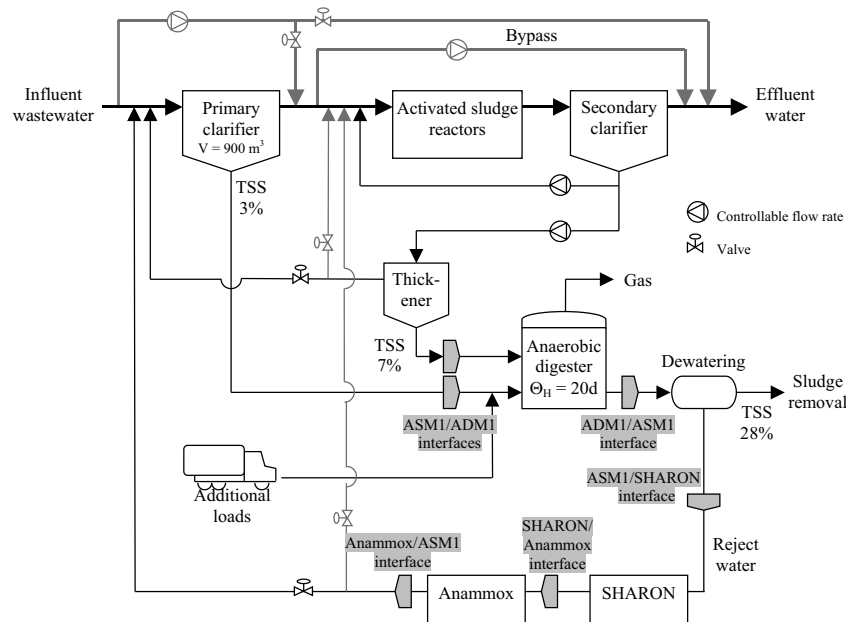


Figure 7.1: Extended benchmark plant with anaerobic sludge digestion and reject water recirculation, adapted from Jeppsson et al. (2006). The inclusion of the SHARON and Anammox process is indicated, as well as the model interfaces

is recycled or when the reject water is treated before recirculation) are avoided.

- The total suspended solids concentration in the last aerobic tank is controlled through the waste sludge flow rate (Φ_w). The TSS set point amounts 3400 gSS m^{-3} for a wastewater temperature above 15°C and 4400 gSS m^{-3} for a temperature below this value.
- The external recycle flow rate (Φ_r) is manipulated proportional (by factor 1.5) to the influent flow rate.
- The external carbon flow rate (Φ_{EC}) is adjusted in such a way that a constant nitrate set point of 10 gN m^{-3} is obtained in the last reactor, instead of applying an external carbon flow rate proportional to the influent flow rate as in the default BSM2 closed loop control strategy. As a result, savings on external carbon flow dosage are realized in case of reject water treatment.

7.3 Economic evaluation by means of an operating cost index 209

- All thickener and dewatering overflows (the latter being the so-called reject water) are sent to the inlet of the primary clarifier and not directly to the activated sludge plant.
- No bypassing of the primary settler and/or activated sludge reactors and secondary settler was used.
- No additional sludge loads have been sent to the anaerobic digester.

The SHARON and Anammox reactor models, described in chapter 3 and in appendix D respectively, have been used. The SHARON reactor volume was set constant at 338 m³ (height = 4 m), a value that corresponds to a hydraulic retention time of 1.25 days for the 95-percentile value of the reject water flow rate, i.e. the value that is only exceeded 5% of the time. The SHARON reactor is cyclically operated with aerobic/anoxic periods in such a way that an aerobic sludge retention time of 1.25 days is maintained, despite the varying influent flow rate. Note, however, that no significant denitrification takes place, as the reject water stream contains almost no carbon source. During the aerobic periods, the oxygen concentration is controlled to a fixed set point of 1.5 g m⁻³ by adjusting the air flow rate. This operating mode is comparable to the one that is applied to the full-scale SHARON reactor at Sluisjesdijk. The Anammox reactor volume has been set to 75 m³ and almost complete (99.5%) biomass retention has been applied. A constant reactor temperature of 35°C has been assumed for both reactors. The different state variables in the BSM2 and the SHARON and Anammox models have been taken into account using the model interfaces described in chapter 6. All models have been implemented in Matlab-Simulink.

7.3 Economic evaluation by means of an operating cost index

As in chapter 5, an operating cost index (OCI), taking into account the most important operating cost factors that differ between the applied operating strategies, has been used for economic evaluation. The resul-

ting OCI (in € /year) is defined as follows:

$$\begin{aligned}
 OCI = & \gamma_1 \cdot EQ_{BSM2} + \gamma_2 \cdot (AE_{BSM2} + AE_{SH} + ME_{BSM2} + ME_{SH} \\
 & + PE_{BSM2} + PE_{SH,An}) + \max(0, \gamma_2 \cdot HE^{net}) \\
 & + \gamma_3 \cdot SP_{BSM2} + \gamma_3 \cdot (SP_{SH} + SP_{An}) + \gamma_4 \cdot EC - \gamma_5 \cdot MP \quad (7.1)
 \end{aligned}$$

This OCI differs from the ‘standard’ one for BSM2 (Vrecko and Ger-naey, 2005) by including the effluent quality (EQ) as a cost factor and by considering costs associated to the SHARON and Anammox reactor. The applied weights γ_i also differ from the standard ones, although their relative values are the same (see below).

The effluent quality term EQ_{BSM2} (kgPU d⁻¹, Copp 2002) takes into account suspended solids (TSS), COD, BOD, Kjeldahl-N (TKN) and nitrate (NO) in the effluent of the main WWTP:

$$\begin{aligned}
 EQ_{BSM2} = & \frac{1}{T \cdot 1000} \int_{245 \text{ days}}^{609 \text{ days}} [\beta_{TSS} \cdot TSS_e(t) + \beta_{COD} \cdot COD_e(t) \\
 & + \beta_{BOD} \cdot BOD_e(t) + \beta_{TKN} \cdot TKN_e(t) + \beta_{NO} \cdot NO_e(t)] \cdot Q_e dt \quad (7.2)
 \end{aligned}$$

with weights $\beta_{TSS} = 2$; $\beta_{COD} = 1$; $\beta_{BOD} = 2$; $\beta_{TKN} = 20$; $\beta_{NO} = 20$. The definitions of composite variables as in BSM1 (Copp, 2002) have been used:

$$TSS = 0.75 \cdot (X_S + X_{BH} + X_{BA} + X_P + X_I) \quad (7.3)$$

$$COD = S_S + S_I + X_S + X_{BH} + X_{BA} + X_P + X_I \quad (7.4)$$

$$BOD = 0.25 \cdot (S_S + X_S + (1 - f_P) \cdot (X_{BH} + X_{BA})) \quad (7.5)$$

$$\begin{aligned}
 TKN = & S_{NH} + S_{ND} + X_{ND} + i_{XB}^N \cdot (X_{BH} + X_{BA}) \\
 & + i_{XP}^N \cdot X_P + i_{XI}^N \cdot X_I \quad (7.6)
 \end{aligned}$$

$$NO = S_{NO} \quad (7.7)$$

Aeration energy (in kWh d⁻¹) is calculated for the main plant as

$$\begin{aligned}
 AE_{BSM2} = & \frac{24}{T} \int_{245 \text{ days}}^{609 \text{ days}} \sum_{i=1}^5 \left(\frac{V_i}{V_{ref}} \right) \cdot \\
 & [0.0007 \cdot (k_L a_i)^2 + 0.3267 \cdot k_L a_i] dt \quad (7.8)
 \end{aligned}$$

7.3 Economic evaluation by means of an operating cost index 211

in which $V_{ref} = 1333 \text{ m}^3$ and $k_L a$ is expressed in days. This expression differs from the one used in BSM1 (Copp, 2002) by taking into account the dependency of the aeration energy of the reactor volume (Jeppsson, 2005). The aeration energy for the SHARON reactor (AE_{SH}) is calculated analogously.

The mixing energy term ME_{BSM2} (in kWh d⁻¹) combines energy for mixing the activated sludge tanks during non-aerated periods (i.e. when $k_L a$ is smaller than 20 d⁻¹) and for mixing the anaerobic digester (Vrecko and Gernaey, 2005):

$$ME_{BSM2} = ME_{as} + ME_{ad} \quad (7.9)$$

in which

$$ME_{as} = \frac{24}{T} \int_{245 \text{ days}}^{609 \text{ days}} \sum_{i=1}^5 \left[\begin{array}{ll} ME^{unit} \cdot V_i & \forall t : k_L a_i(t) < 20 \\ 0 & \forall t : k_L a_i(t) \geq 20 \end{array} \right] dt \quad (7.10)$$

$$ME_{ad} = 24 \cdot ME^{unit} \cdot V_{ad} \quad (7.11)$$

with $ME^{unit} = 0.005 \text{ kW m}^{-3}$. The mixing energy consumed in the SHARON reactor (ME_{SH}) during non-aerated periods is calculated in an identical way as in Eq. 7.10. No mixing device is installed in the Anammox reactor, as mixing is established by the produced nitrogen gas.

Pumping energy (in kWh d⁻¹) is calculated as described by Vrecko and Gernaey (2005) for the internal (Φ_{int}) and external recycle flow (Φ_r), the waste sludge flow (Φ_w), the primary settler underflow (Φ_{pu}), the thickener underflow (Φ_{tu}) and the dewatering overflow (Φ_{do}), all flows are expressed in m³ d⁻¹:

$$PE_{BSM2} = \frac{0.04}{T} \int_{245 \text{ days}}^{609 \text{ days}} [\phi_{int}(t) + \phi_r(t) + \phi_w(t) + \phi_{pu}(t) + \phi_{tu}(t) + \phi_{do}(t)] dt \quad (7.12)$$

Note that the same weight of 0.04 kWh m⁻³ is used for all flow rates. The pumping energy associated with the flow from the SHARON to the Anammox reactor ($PE_{SH,An}$) is calculated in the same way. Gravitational flow (no pumping energy required) is assumed for the remaining flows.

The heating energy term, defined as $\max(0, \gamma_2 \cdot HE^{net})$ (Jeppsson et al., 2005), takes into account the energy demand HE to heat the anaerobic digester, which is met by the heat generated from the gas motor used for electricity production from biogas, at least in case of good operation of the anaerobic digester. Assuming that 1 kg CH_4 produces about 7 kWh of heat, the net heating energy demand amounts to

$$HE^{net} = HE - 7MP \quad (7.13)$$

A correction is made as this term can never be negative: the surplus heat that may be produced during electricity generation and that is not used for heating the anaerobic digester, is not valued elsewhere. The average energy HE needed to heat the flow of sludge fed to the anaerobic digester is calculated from Vrecko and Gernaey (2005)

$$HE = \frac{24}{T \cdot 86400} \int_{245 \text{ days}}^{609 \text{ days}} \rho_{H2O} \cdot c_{p,H2O} \cdot [T_{ad} - T_{ad}^{in}(t)] \cdot \Phi_{ad}(t) dt \quad (7.14)$$

for a constant anaerobic digester temperature of 35°C.

The sludge production SP_{BSM2} (in kgTSS d⁻¹) includes solids that have been accumulated in activated sludge unit (TSS_{as}), settler (TSS_s), primary clarifier (TSS_p), and anaerobic digester (TSS_{ad}), as well as disposed solids in the dewatering underflow (TSS_{du}) (Vrecko and Gernaey, 2005):

$$SP_{BSM2} = \frac{1}{T \cdot 1000} \left[(TSS_{as} + TSS_s + TSS_p + TSS_{ad})_{245 \text{ days}}^{609 \text{ days}} + \int_{245 \text{ days}}^{609 \text{ days}} TSS_{du} dt \right] \quad (7.15)$$

in which the total solids concentration is calculated as in Eq. 7.3. For the scenario without reject treatment, disposed solids are calculated from the concentrations in the primary clarifier and the settler underflows. The terms SP_{SH} and SP_{An} for solids accumulation in the SHARON and Anammox reactors, respectively, are calculated analogously.

External carbon addition is represented by the term EC (kgCOD d^{-1}) (Vrecko and Gernaey, 2005):

$$EC = \frac{C_{EC}}{T \cdot 1000} \int_{245 \text{ days}}^{609 \text{ days}} \Phi_{EC}(t) dt \quad (7.16)$$

for an external carbon concentration C_{EC} of $4 \cdot 10^5$ gCOD m^{-3} .

The term MP denotes the amount of methane produced (in kg CH_4 d^{-1}) in the anaerobic digester (Vrecko and Gernaey, 2005):

$$MP = \frac{16}{T} \int_{245 \text{ days}}^{609 \text{ days}} \frac{1}{R \cdot T_{ad}} \cdot p_{CH_4}(t) \cdot \Phi_{gas}(t) dt \quad (7.17)$$

The weights for the pollution units ($\gamma_1=50$), energy ($\gamma_2=25$) and sludge disposal ($\gamma_3=75$) are taken from Vanrolleghem and Gillot (2002). The weights for external carbon addition ($\gamma_4=75$) and methane production ($\gamma_5=150$) were set in such a way that their relative value compared to γ_1 , γ_2 and γ_3 is the same as in the OCI proposed for BSM2 (Vrecko et al., 2006).

The OCI includes the operating costs that differ between the scenarios under study. Savings in operating costs between two operating modes thus equal the investment costs that can be supported for establishing a SHARON/Anammox reactor and for purchase and installation of extra equipment to establish a control strategy.

For each scenario, also the percentage of time of effluent limits for ammonium, total nitrogen ($N_{tot} = TKN + NO$), BOD, COD and TSS (Copp, 2002) are violated, as well as the 95 percentiles of the effluent concentrations for ammonium, total nitrogen and TSS (i.e. the effluent concentrations for these components that are exceeded 5% of the time), are registered.

7.4 Simulation results and discussion

Plant-wide performance was assessed for three different scenarios:

1. The 'standard' BSM2 layout, with recirculation of reject water to the inlet of the primary clarifier.

2. A WWTP consisting of a primary settler, an activated sludge process and a secondary settler, without sludge treatment and thus without reject water.

3. A WWTP in which the reject water is treated with a SHARON-Anammox process before recycling to the main WWTP.

Figure 7.2 compares the ammonium load of the influent to the primary clarifier (including the recycled reject water stream) with the ammonium load of the reject water stream in case the reject water is recycled to the primary clarifier.

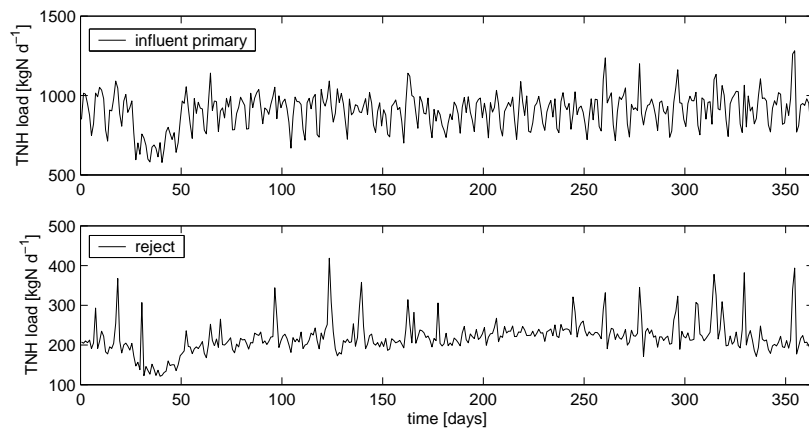


Figure 7.2: Ammonium load of influent stream to primary clarifier versus ammonium load of reject water (daily mean values) in case of recycling of untreated reject water.

The reject water stream (mean flow rate $172 \text{ m}^3 \text{ day}^{-1}$) only represents 0.8% of the total flow (mean flow rate $21138 \text{ m}^3 \text{ day}^{-1}$) to the primary clarifier, but it contains such high ammonium concentrations (mean 1372 gN m^{-3}), that the ammonium load of the reject water stream represents a significant part (mean: 21%) of the influent ammonium load to the primary clarifier (mean: $1122 \text{ kgN day}^{-1}$). When comparing the influent ammonium load to the primary clarifier in case of recirculation of untreated reject water with the scenario without reject water (results not shown), it is clear that the ammonium load of the influent to the primary clarifier increases by 28% when reject water is recycled.

In case of reject water treatment with a SHARON-Anammox process, the ammonium load to the primary clarifier is reduced by 25% (mean ammonium load 901 kgN day^{-1} , results not shown) for the operating mode suggested in this chapter. Note that this value may even be

further improved by optimizing the operation of the SHARON-Anammox process, as the nitrite:ammonium ratio produced in the SHARON reactor is suboptimal, resulting in incomplete ammonium conversion in the Anammox reactor (see chapter 8).

Table 7.1: Effluent quality

		BSM2	no reject water	reject water treatment with SHARON-Anammox
ammonium limit: 4 gN m ⁻³	95% percentile (g m ⁻³)	9.89	6.64	6.96
	% of time limit violation	30.73	16.86	18.54
total N limit: 18 gN m ⁻³	95% percentile (gN m ⁻³)	20.78	15.47	15.94
	% of time limit violation	20.72	0.45	0.82

The effluent quality of the WWTP is compared for the three scenarios under study. In Figure 7.3, daily mean values of the effluent concentrations are plotted. Table 7.1 gives the 95 percentiles of the effluent concentrations, i.e. the effluent concentrations that are exceeded 5% of the time, as well as the percentage of time the effluent limits are violated. As the effluent concentrations of COD, BOD and TSS do not differ much between the three treatment options and the corresponding effluent limits are met nearly the whole time, only the results for total nitrogen and ammonium are shown. The increased ammonium load due to recirculation of untreated reject water causes frequent violations of the effluent total nitrogen limit: 21% of the time, compared with less than 1% for the case without reject water. When treating the reject water with a SHARON-Anammox process before recirculation, the effluent quality improves significantly, also exceeding the total nitrogen effluent limit less than 1% of the time. For all three scenarios, the effluent ammonium limit is exceeded a significant part of the time. However, the percentage of time the limit is violated is reduced from 31% to 19% by treatment of the reject water with SHARON-Anammox before recirculation, which is comparable to the case without reject water (17% of the time). The latter situation serves as a reference case for what can be obtained by ideal reject water treatment. Low temperature during the winter period ($t=100$ to $t=250$ days) is one of the main reasons for the poor performance of the nitrification process. It is clear that this should be remedied by optimizing the control of the main WWTP rather than

the reject water treatment, for example by allowing aeration in one of the denitrification tanks when temperatures are low. Another option to meet the ammonium limits would be to use a bio-augmentation process for reject water treatment.

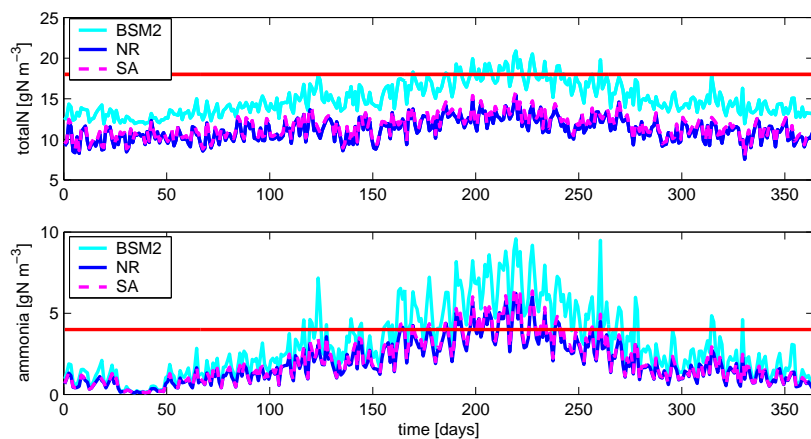


Figure 7.3: Effluent quality in terms of total nitrogen and ammonium; NR: scenario without reject water; SA: scenario with treatment of reject water with SHARON-Anammox.

The operating cost index defined above has been used to compare the three scenarios under study on an economic basis. Table 7.2 summarizes the results.

Regarding the effluent quality, main differences are established in terms of Kjeldahl-N (TKN) and nitrate (NO): in case the reject water is treated before recirculation, the concentration of nitrogen compounds in the effluent is significantly reduced, to values that approach the ones in case the reject water is not recycled. In case of recirculation of reject water, the WWTP effluent contains considerably more COD. This is explained almost completely by an increased amount of soluble inert material (S_I), which is not biodegradable.

The aeration energy needed in the activated sludge tanks is decreased in case of treatment of reject water compared to the scenario with recirculation of untreated reject water. When also taking into account the aeration energy consumed in the SHARON reactor, the total aeration energy is comparable, but it is important to note here that a higher overall amount of ammonium has been oxidized. Indeed, ammonium removal from the reject water stream with the SHARON-Anammox processes would consume relatively less oxygen than in the

Table 7.2: Economic evaluation

cost factors		BSM2	no reject water	SHARON- Anammox
effluent quality (EQ_{BSM2}) [kgPU day ⁻¹]	TSS	711	683	707
	COD	1 595	1 025	1 592
	BOD	143	133	137
	TKN	2 339	1 775	1 871
	NO	3 960	2 727	2 887
	total	8 748	6 342	7 194
aeration energy (AE) [kWh day ⁻¹]	BSM2	7 773	7 198	7 243
	SHARON	-	-	538
mixing energy (ME) [kWh day ⁻¹]	BSM2	648	240	648
	SHARON	-	-	15
pumping energy (PE) [kWh day ⁻¹]	BSM2	2 311	2 699	2 658
	SHARON	-	-	7
sludge production (SP) [kg TSS day ⁻¹]	BSM2	3 187	5 979	3 067
	SHARON	-	-	0.005
	Anammox	-	-	13
external carbon addition (EC) [kgCOD day ⁻¹]		585	20	27
heating energy (HE) [kWh day ⁻¹]		4 304	0	4 215
methane production (MP) [kgCH ₄ day ⁻¹]		858	0	820
net heating energy (HE^{net}) [kWh day ⁻¹]		0	0	0
associated costs [€/year]				
effluent quality (EQ)		437 419	317 105	359 683
aeration energy (AE)		194 333	179 949	194 526
mixing energy (ME)		16 200	6 000	16 571
pumping energy (PE)		57 764	67 474	66 623
net heating energy (HE^{net})		0	0	0
sludge production (SP)		239 002	448 422	230 975
external carbon addition (EC)		43 889	1 491	2 016
methane production (MP)		-128 766	0	- 122 973
TOTAL		859 842	1 020 442	747 422
savings		160 600	0	273 020
savings		0	-160 600	112 420

activated sludge reactors as typically half of the ammonium is oxidized to nitrite only in the SHARON process and the other half is converted without oxygen consumption in the Anammox process.

As the Anammox process converts ammonium and nitrite to nitrogen gas in an autotrophic way, external carbon source addition has been made almost redundant in case of reject water treatment, still realizing a much better effluent quality in terms of nitrate.

Sludge disposal costs (SP) are very high for the scenario without on-site sludge treatment (no reject water). For the scenario with recirculation of reject water, treated with SHARON-Anammox, less sludge is produced than in the case the reject water is not treated. This is due to the ammonium oxidation to nitrite only in the SHARON reactor and to the very low yield of the Anammox biomass.

The smaller sludge production in case of reject treatment before recirculation is the reason why a little less methane is produced during anaerobic digestion in comparison to recirculation of non-treated reject water. Note that the heat generated during methane production is more than sufficient for heating the anaerobic digester ($HE^{net} = 0$).

Comparing the total cost indices for the three scenarios, the case with external sludge treatment (no reject water) clearly has the largest operating costs. Still, one might jump to the conclusion that the yearly extra costs of 160 600 € do not counterbalance investment costs for sludge treatment (digester, thickener and dewatering equipment) and for this reason it may seem economically more feasible to treat the sludge externally. However, it is important to note that the sludge treatment costs are calculated on TSS basis, but do not consider the TSS concentration of the sludge. Sludge transportation costs are not included. For the relatively large WWTP (80 000 PE) represented by BSM2, it seems unrealistic to transport the large sludge volumes with very low solids concentration from the primary and secondary clarifier for external treatment. Therefore, this scenario should be considered as a reference case for ideal reject water treatment rather than as a realistic treatment option.

Comparing the scenario with recirculation of untreated reject water with the one in which the reject water is treated by SHARON-Anammox before recycling, it is not clear whether the yearly operating costs savings of 112 420 € /year will warrant the investment costs for installing a SHARON and Anammox reactor. The aeration capacity of the activated sludge tanks of the BSM2 plant has shown to be still sufficient to oxidize at least part of the ammonium load originating from the reject water stream. For this reason, not as much is gained by implementing a SHARON-Anammox process as when the aeration capacity of the activated sludge tanks would already be fully utilized. However, one must keep in mind that a considerable effluent quality improvement is realized by treatment of the reject stream before recirculation and that the permit of the WWTP may be in danger when effluent standards are not met.

7.5 Conclusions

The effect of reject water originating from sludge treatment on the performance of the activated sludge process, to which this stream is typically recycled was examined in a plant-wide simulation study using the Benchmark Simulation Model no. 2, developed by the IWA Task Group on Benchmarking. A scenario without sludge treatment and therefore without reject water was compared with one in which untreated reject water is recycled to the main plant and one in which the reject water is treated with a combined SHARON-Anammox process before recirculation.

It was shown that recirculation of the untreated reject water stream, representing 21% of the total influent ammonium load, unacceptably worsens the total nitrogen concentration in the effluent of the WWTP for the BSM2 plant. The effluent quality in terms of Kjeldahl-nitrogen and nitrate was improved significantly by treatment of the reject water stream with a SHARON-Anammox process before recirculation. Moreover, in case of reject water treatment, external carbon source addition was made almost redundant and less sludge was produced, while more ammonium was converted for about the same aeration energy consumption. In this way, the benefits of reject water treatment with a SHARON partial nitrification process, combined with an Anammox process, have been demonstrated well.

A plant-wide economic analysis has been performed using an operating cost index (OCI), taking into account the operating cost factors that differ between the different operating modes. For the given BSM2 plant, of which the aeration capacity has not yet fully been utilized, the yearly operating cost savings resulting from reject water treatment with a SHARON-Anammox process as such only partly warrant the associated investment costs. However, it was clearly shown that reject water treatment with a SHARON-Anammox process is a promising option to meet the required effluent limits and to prevent the WWTP from losing its permit.

Chapter 8

Interaction between control and design of a SHARON reactor

8.1 Introduction

In chapter 7, the effect of reject water treatment for the Benchmark Simulation Model no. 2 (BSM2) through a SHARON-Anammox process has been investigated. However, the applied control strategy in the SHARON reactor was rather arbitrary, and so was the reactor design. The question arises whether better results could be obtained with different control strategies, similar to what has been investigated in chapter 5 for realistic influent conditions as observed at the full-scale SHARON reactor at Sluisjesdijk. Further, it would also be interesting to know to which extent the usefulness of a certain control strategy is influenced by the reactor design (volume). These issues are dealt with in this chapter for the BSM2 case.

8.2 BSM2 reject water characteristics

Figure 8.1 illustrates the characteristics (daily mean values) of the BSM2 reject water, which is fed to the SHARON reactor, in terms of flow rate (mean $172 \text{ m}^3 \text{ d}^{-1}$, total ammonium concentration (mean¹ 97 mole m^{-3}), total inorganic carbon concentration (mean 102 mole m^{-3}), pH

¹given mean concentrations are all load-averaged values

222 Interaction between control and design of a SHARON reactor

(mean 7.2) as well as COD concentration (mean 373 gCOD m^{-3}) translated into CH_3OH equivalents (mean 3.2 mole m^{-3}). For the given BSM2 reject water, the mean $TIC : TNH$ ratio amounts to 1.06, which is comparable to the Sluisjesdijk case (see section 3.8 and chapter 5). However, the influent pH is rather low in comparison to the Sluisjesdijk case, for which the mean pH is about 8-8.3.

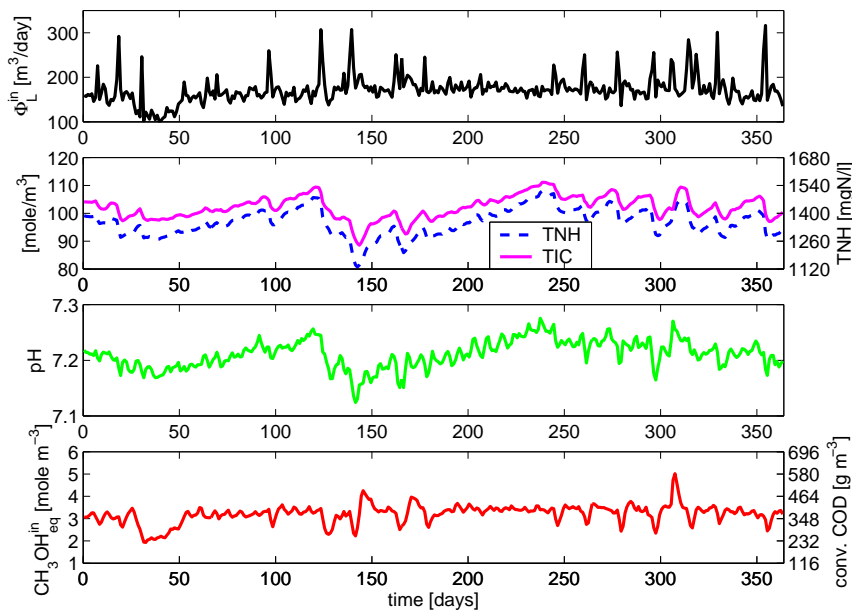


Figure 8.1: BSM2 reject water characteristics (from top to bottom): flow rate, concentrations of total ammonium (TNH) and total inorganic carbon (TIC), pH, influent COD translated into methanol equivalents ($\text{CH}_3\text{OH}_{\text{eq}}$).

8.3 SHARON reactor operating modes under study

The simulations have again been performed with the SHARON and Anammox reactor models, described in chapter 3 and in appendix D respectively. For their implementation in the BSM2, the model interfaces described in chapter 6 have been used.

The SHARON reactor volume has been taken constant for each operating mode. However, simulations have been performed for different values of the reactor volume and its effect on the usefulness of the applied control strategies has been studied. The following control strate-

gies have been applied to the SHARON reactor, as stand-alone strategies or combined with each other:

1. Aerobic retention time control by working with aerobic/anoxic periods. It is important to note here that – for a high influent flow rate or a small reactor volume – the hydraulic retention time may be smaller than the set point for the aerobic retention time, during certain periods or even the whole time. In this case, the aeration will be kept on so the resulting aerobic retention time will equal the hydraulic retention time but will be lower than the set point for the aerobic retention time.
2. Oxygen control by adjusting the air flow rate (between 0 and 5000 $\text{m}^3 \text{h}^{-1}$) through a proportional controller (with gain $K = 5e8$).
3. Cascade oxygen control, adjusting the oxygen setpoint (between 0 and 4 g m^{-3}) to maintain a constant nitrite:ammonium ratio in the SHARON reactor. Both primary (master) and secondary (slave) controllers are proportional controllers, with gains $K_p = 0.1$ and $K_s = 5e8$, respectively.
4. pH-control within a certain range around a setpoint, at $\text{pH}^{sp} \pm \text{pH}^{threshold}$, by acid or base addition through a proportional controller (with gain $K = 1e4$). Both acid (96% H_2SO_4) and base (50% NaOH) addition have been limited to 50 liter h^{-1} .

As acid or base addition should be avoided as much as possible, because the consumption of chemicals is costly and does not contribute to sustainable operation, it has been decided not to use stand-alone pH-control or cascade pH-control. Instead, the air flow rate will be used as much as possible as a control handle. In chapter 5, it was concluded that the oxygen level in the reactor mainly determines whether ammonium is converted or not, while the extent of ammonium conversion can be controlled by switching between high and low oxygen levels, which can be seen as controlling the aerobic retention time. The aerobic sludge retention time (aerSRT) determines the actual growth rate μ^{amm} of the ammonium oxidizers; the corresponding ammonium conversion is higher for higher μ^{amm} . However, as the actual growth rate of ammonium oxidizers, μ^{amm} , cannot increase beyond its maximum value, μ_{max}^{amm} , increasing the aerobic retention time beyond this point will not lead to increasing ammonium conversion. If still a higher ammonium conversion is desired, this can be achieved by increasing pH, through

base addition. Besides, pH-control has also been applied to maintain the reactor pH within a range that allows sufficiently high maximum specific growth rates (see Figure 3.1).

Although optimizing the Anammox reactor design would also be an interesting research topic, the Anammox reactor volume has been set to a constant value of 75 m³ throughout this chapter. Almost complete (99.5%) biomass retention has been applied. A constant reactor temperature of 35°C has been assumed for both reactors.

8.4 Economic evaluation by means of OCIs

Two types of operating cost indices (OCIs, in €/year) have been used to evaluate the simulation results. The first OCI is the one of chapter 5 and only considers the operating cost factors of the SHARON and Anammox processes that differ between the different operating modes:

$$OCI_{SH,An} = \gamma_1 \cdot EQ_{An} + \gamma_2 \cdot AE_{SH} + \alpha_{acid} \cdot \Phi_{SH,acid} + \alpha_{base} \cdot \Phi_{SH,base} \quad (8.1)$$

The effluent quality term (EQ) comprises the amount of ammonium in the effluent of the Anammox reactor:

$$EQ_{An} = \frac{1}{T \cdot 1000} \int_{245 \text{ days}}^{609 \text{ days}} \beta_{TNH} \cdot C_{TNH,An} \cdot \Phi_{An}^{out} dt \quad (8.2)$$

The aeration energy term for the SHARON reactor is defined as in chapters 5 (Eq. 5.4) and 7. Further, also costs for acid and base addition in the SHARON reactor have been taken into account (see Table 5.2).

The second OCI considers the plant-wide operating cost factors that differ between the applied operating strategies, as in chapter 7, but now also including possible acid or base addition in the SHARON reactor:

$$\begin{aligned} OCI_{PW} = & \gamma_1 \cdot EQ_{BSM2} + \gamma_2 \cdot (AE_{BSM2} + AE_{SH} + ME_{BSM2} + ME_{SH} \\ & + PE_{BSM2} + PE_{SH,An}) + \max(0, \gamma_2 \cdot HE^{net}) \\ & + \gamma_3 \cdot SP_{BSM2} + \gamma_3 \cdot (SP_{SH} + SP_{An}) + \gamma_4 \cdot EC - \gamma_5 \cdot MP \\ & + \alpha_{acid} \cdot \Phi_{SH,acid} + \alpha_{base} \cdot \Phi_{SH,base} \quad (8.3) \end{aligned}$$

The OCIs are used to indicate possible costs savings that can be made with control. Savings in operating costs between two operating modes equal the investment costs that can be supported. The results obtained with both OCIs will be compared to each other.

8.5 Simulation results

8.5.1 Operation of a SHARON reactor with $V=338 \text{ m}^3$

In a first series of simulations, it is examined what can be achieved with a moderately large SHARON reactor. The reactor volume has been set to 338 m^3 , a value that corresponds to a hydraulic retention time of 1.25 days for the 95-percentile value of the reject water flow rate, i.e. the value that is only exceeded 5% of the time. An operating mode with fixed air flow rate is compared to one with fixed oxygen set point, both cases with setting aerobic/anoxic periods in such a way that an aerobic sludge retention time of 1.25 days is maintained, despite the varying influent flow rate. The influence of the oxygen set point and the applied aerobic sludge retention time is studied. Further, it is examined whether the results can be improved by applying cascade O_2 -control.

Table 8.1 summarizes the results of the economic evaluation, which are discussed below. The behaviour of the SHARON and Anammox reactors is also investigated in detail.

aerSRT control at 1.25 days ; $\Phi_G^{\text{in}} = 2500 \text{ m}^3 \text{ h}^{-1}$

Figure 8.2 illustrates the behaviour of the SHARON and Anammox reactors in case the SHARON reactor is operated with a fixed aerobic retention time of 1.25 days, while maintaining a constant air flow rate of $2500 \text{ m}^3 \text{ h}^{-1}$ during the aerobic periods. The figure shows daily mean values for the ammonium and nitrite concentrations in both reactors, as well as for the nitrite:ammonium ratio and the pH in the SHARON reactor over the complete evaluation period. The oxygen concentration in the SHARON reactor varies, concentrations up to $7.3 \text{ gO}_2 \text{ m}^{-3}$ are reached during the aerobic periods (results not shown).

Although the influent ammonium load to the SHARON reactor varies widely (between 129 and 445 kgN d^{-1} , mean 233 kgN d^{-1}), the percentage of ammonium conversion remains almost constant over the whole simulation period. This is due to the fixed aerobic retention time that is maintained despite the varying influent flow rate, as well as to the quite constant $TIC:TNH$ ratio ($1.02 \rightarrow 1.11$). Nitrite inhibition of ammonium conversion, which is expected to lead to a decreasing conversion efficiency for increasing incoming ammonium concentrations, appears not to play a major role in the given range of influent ammonium concentrations.

Table 8.1: Economic evaluation for a SHARON reactor with $V=338 \text{ m}^3$

cost factors [€/year]		aerSRT=1.25 days $\Phi_G^{in} = 2500 \text{ m}^3/\text{h}$	aerSRT=1.25 days $O_2^{sP} = 1.5 \text{ g/m}^3$	aerSRT=1.25 days $O_2^{sP} = 4 \text{ g/m}^3$	aerSRT=1.75 days $O_2^{sP} = 1.5 \text{ g/m}^3$	aerSRT=2.5 days $O_2^{sP} = 1.5 \text{ g/m}^3$	cascade O_2 $R^{sP} = 1.1$ $pH^{sP} = 7.23 \pm 1$	cascade O_2 $R^{sP} = 1.1$
effluent quality (EQ)	TSS _{BSM2}	35 348	35 350	35 345	35 347	35 342	35 337	35 343
	COD _{BSM2}	79 580	79 587	79 579	79 582	79 575	79 571	79 576
	BOD _{BSM2}	6 830	6 840	6 837	6 838	6 835	6 831	6 835
	TKN _{BSM2}	93 528	93 558	93 361	93 456	93 268	93 122	93 263
	NO _{BSM2}	142 023	144 347	142 385	143 221	141 753	139 517	141 737
	EQ _{BSM2}	357 309	359 683	357 506	358 443	356 775	354 379	356 754
	EQ _{An}	15 794	21 268	16 593	18 490	14 781	9 230	14 707
aeration energy (AE)	BSM2	180 805	181 079	180 867	180 951	180 776	180 530	180 772
	SHARON	33 888	13 446	24 482	12 421	20 765	20 740	20 380
mixing energy (ME)	BSM2	16 200	16 200	16 200	16 200	16 200	16 200	16 200
	SHARON	371	371	371	182	71	0	0
pumping energy (PE)	BSM2	67 092	66 451	67 013	66 777	67 181	67 832	67 183
	SHARON	172	172	172	172	172	172	172
sludge produc- tion (SP)	BSM2	230 628	230 024	229 963	229 982	229 924	229 846	229 920
	SHARON	0.34	0.34	0.34	0.29	0.27	0.27	0.27
	Anammox	253	950	950	948	951	955	954
external carbon addition (EC)		1 739	2 016	1 780	1 863	1 699	1 394	1 695
methane production (MP)		-122 970	-122 972	-122 925	-122 940	-122 895	-122 838	-122 893
net heating energy (HE ^{net})		0	0	0	0	0	0	0
acid addition		0	0	0	0	0	0	0
base addition		0	0	0	0	0	1 131	0
OCI _{SH,An}		49 683	34 715	41 075	30 911	35 546	31 102	35 087
OCI _{PW}		765 488	747 422	756 380	745 001	751 622	750 342	751 138

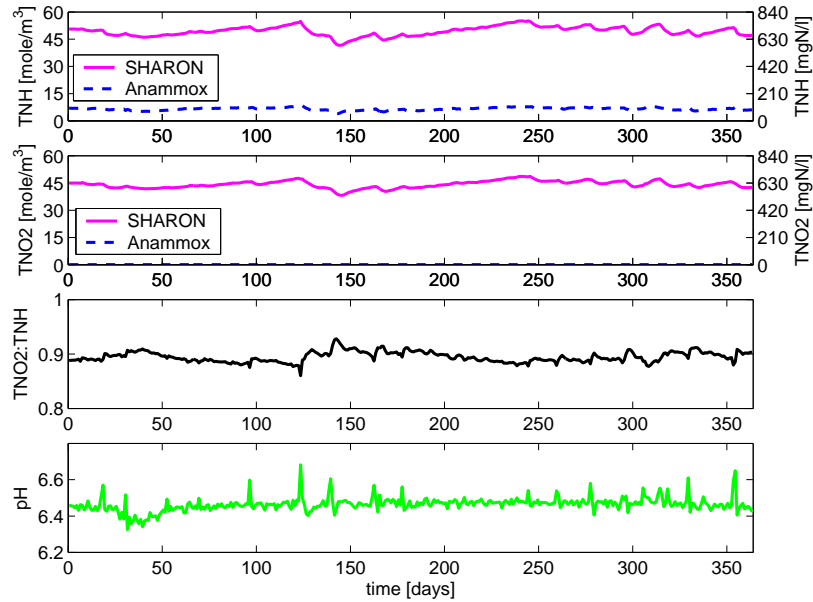


Figure 8.2: (from top to bottom, daily mean values) Concentrations of total ammonium (TNH) and total nitrite (TNO₂) in SHARON reactor and Anammox reactor. Nitrite:ammonium ratio (TNO₂:TNH), pH, in SHARON reactor. Operating mode of SHARON reactor ($V = 338 \text{ m}^3$) with aerSRT=1.25 days and fixed air flow rate $\Phi_G^{in} = 2500 \text{ m}^3/\text{h}$.

As a result, the nitrite:ammonium ratio produced in the SHARON reactor remains quite constant, at 0.89. The mean reactor pH is 6.5. The amount of TIC that remains in the reactor is 1.78 mole m^{-3} . As expected for the given aerobic sludge retention time applied, nitrate production in the SHARON reactor is negligible at all times (mean value 0.4 mole m^{-3} or 6 gN m^{-3} , results not shown). According to the Anammox stoichiometry, a nitrite:ammonium ratio of 1.23 would be optimal to feed the Anammox reactor. Consequently, some ammonium (mean 6.5 mole m^{-3} or 92 gN m^{-3}) remains unconverted in the Anammox reactor.

aerSRT control ; O_2 -control

The behaviour of a SHARON reactor, operated with a fixed aerobic retention time of 1.25 days by switching the air flow rate on/off and with oxygen control on 1.5 g m^{-3} during the aerobic periods, is displayed in

Figure 8.3. For the applied value of the proportional oxygen controller, the oxygen set point is tracked very well (results not shown).

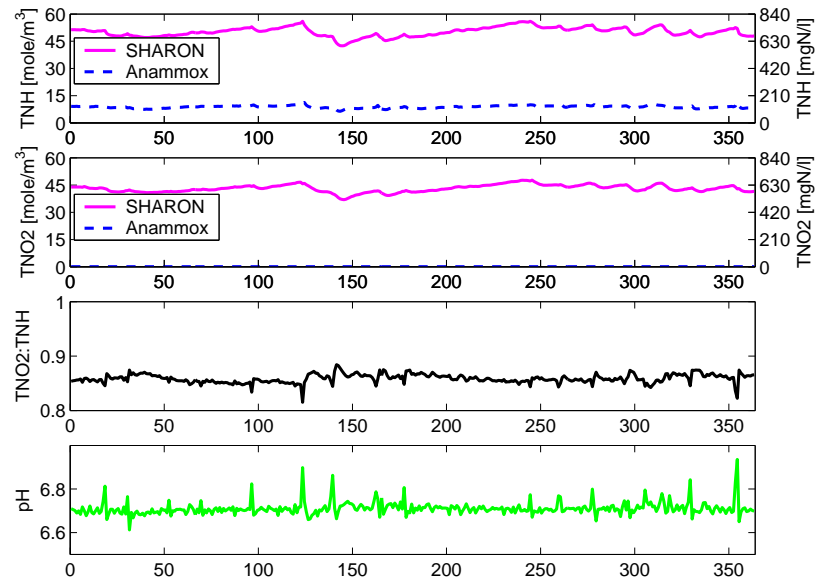


Figure 8.3: (from top to bottom, daily mean values) Concentrations of total ammonium (TNH) and total nitrite (TNO₂) in SHARON reactor and Anammox reactor. Nitrite:ammonium ratio (TNO₂:TNH), pH, in SHARON reactor. Operating mode of SHARON reactor ($V = 338 \text{ m}^3$) with aerSRT=1.25 days and oxygen control $O_2^{sp} = 1.5 \text{ g m}^{-3}$.

The mean nitrite:ammonium ratio produced in the SHARON reactor (0.86) is again suboptimal, resulting in incomplete ammonium conversion in the Anammox reactor: the mean ammonium concentration in the Anammox reactor amounts to 8.8 mole m^{-3} or 123 gN m^{-3} . Nitrate production in the SHARON reactor is negligible (mean value $0.2 \text{ mole NO}_3^- \text{ m}^{-3}$ or 3 gN m^{-3}). Although the increase of ammonium concentration in the Anammox effluent is significant in comparison to the previous scenario ($\Delta EQ_{An} = 21268 - 15794 = 5474\text{€ /year}$, respectively), the overall effluent quality of the plant only increases slightly ($\Delta EQ_{BSM2} = 359683 - 357309 = 2374\text{€ /year}$), as can be seen from Table 8.1. Apparently, the activated sludge tanks of the BSM2 plant still possess sufficient aeration capacity to convert this additional amount of ammonium in the reject water. In this way, the additional aeration energy that has been supplied to the SHARON reactor in the previous scenario (with fixed air flow rate $\Phi_G^{in} = 2500 \text{ m}^3 \text{ h}^{-1}$) does not yield any

added value in terms of overall effluent quality and is thus lost. As a result, the overall operating cost index is significantly lower for the current scenario, in which the oxygen level in the SHARON reactor is controlled at a constant value of $O_2^{sp} = 1.5 \text{ g m}^{-3}$.

It can be noted that an oxygen set point of $O_2^{sp} = 1.5 \text{ g m}^{-3}$ is rather low, compared to the oxygen affinity constant of ammonium oxidizers $K_{O_2}^{amm} = 1 \text{ g m}^{-3}$. For this reason, it has also been tested whether better results are obtained by increasing the oxygen set point to $O_2^{sp} = 4 \text{ g m}^{-3}$, while keeping the aerobic sludge retention time at 1.25 days. In this case, a little more ammonium is converted in the SHARON reactor (mean $TNO_2 : TNH = 0.89$, results not shown), and therefore less ammonium remains in the Anammox reactor (mean 6.9 mole m^{-3} or 96 gN m^{-3} , results not shown) in comparison with the scenario with $O_2^{sp} = 1.5 \text{ g m}^{-3}$ ($\Delta EQ_{An} = 16593 - 21268 = -4675 \text{ €/year}$, see Table 8.1), however this level of effluent quality improvement is not warranted by the significant increase in aeration costs needed to achieve the higher oxygen level in the SHARON reactor ($\Delta EQ_{An} = 24482 - 13446 = 11036 \text{ €/year}$, see Table 8.1). This is also true for the plant-wide effluent quality, the improvement of which is even less ($\Delta EQ_{BSM2} = 357506 - 359683 = -2177 \text{ €/year}$, see Table 8.1) as the activated sludge tanks of the BSM2 still have some aeration capacity left.

As increasing the oxygen set point does not seem to be a good option, the effect of increasing the aerobic retention time has been tested as an alternative to increase the ammonium conversion.

The aerobic retention time is prolonged to 1.75 days, while keeping the oxygen at $O_2^{sp} = 1.5 \text{ g m}^{-3}$. Note that 1.75 days corresponds to the *maximum* aerobic retention time in the reactor. In case the hydraulic retention time is too low to meet this set point, the reactor remains aerated and the resulting aerobic retention time equals the prevailing hydraulic retention time. Still little or no nitrate formation occurs in the SHARON reactor: 0.3 mole m^{-3} or 4.5 gN m^{-3} , while the produced nitrite:ammonium ratio (mean 0.88) increases in comparison with the scenario in which the aerobic retention time was controlled at 1.25 days. As a result, less ammonium remains unconverted in the Anammox reactor (7.7 mole m^{-3} or 107 gN m^{-3}), although the effect on the overall effluent quality of the plant is hardly noticeable.

It is surprising that less aeration energy is required in the SHARON reactor for aerSRT=1.75 days than in case the aerobic retention time is kept lower, to 1.25 days. This may be attributed to the fact that switch-

ing from anoxic to aerobic periods is always accompanied with large air flow rates (using a proportional controller to meet the oxygen set point), that are very energy-consuming. When an aerSRT of 1.75 days is applied, the reactor remains aerated for longer periods than for an aerSRT of 1.25 days, so there are less energy-consuming switches.

When prolonging the (maximum) aerobic retention time further to 2.5 days, still not much nitrate is formed in the SHARON reactor (0.73 mole m^{-3} or 10 gN m^{-3}), in fact only slightly more than in case aerSRT is controlled to 1.25 days. However, one should keep in mind that the value of 2.5 days is in fact the *maximum* aerobic retention time, which only equals the actual aerobic retention time in case the SRT(=HRT) is at least as long. To obtain an HRT of 2.5 days or more during at least half of the time, the reactor volume should be at least 430 m^3 , which is obviously not the case. The additional ammonium conversion in the SHARON reactor, resulting in a mean $TNO_2 : TNH$ of 0.89, (remaining ammonium concentration in the Anammox reactor: 6.1 mole m^{-3} or 86 gN m^{-3}) is hardly noticeable and certainly does not warrant the additional aeration costs.

Even for high oxygen set points and long aerobic retention times, the obtained nitrite:ammonium ratio in the SHARON reactor remains below the Anammox-optimal value, which results in incomplete ammonium conversion in the Anammox reactor. This contrasts with the findings of chapter 5, where oxygen control on a constant set point either resulted in incomplete ammonium conversion, or in a too high nitrite:ammonium ratio and consequent inhibition of the Anammox reactor. This difference is attributed to the relatively lower alkalinity of the BSM2 reject water compared to the reject water of chapter 5, based on measurements at Sluisjesdijk. Although the $TIC : TNH$ ratio is about the same in both cases, the pH of the BSM2 reject water is lower (mean pH = 7.2) than the pH of the Sluisjesdijk reject water (mean pH = 8.2). In the first case, more than 10% of the inorganic carbon (TIC) is present as CO_2 and has no buffering capacity.

cascade O_2 -control; pH-control

As good results have been obtained with cascade O_2 -control, combined with pH-control in chapter 5, it has been tested if a more optimal nitrite:ammonium ratio could be obtained through this control strategy.

The $TNO_2 : TNH$ set point has first been set to the stoichiometric optimum of 1.23. However, this resulted in nitrite inhibition of

the Anammox reactor during periods of increasing influent flow rate. It was concluded that the optimal nitrite:ammonium ratio should be lower and a value of $R^{sp} = 1.1$ has been chosen. Figure 8.4 summarizes the simulation results. The mean nitrite:ammonium ratio pro-

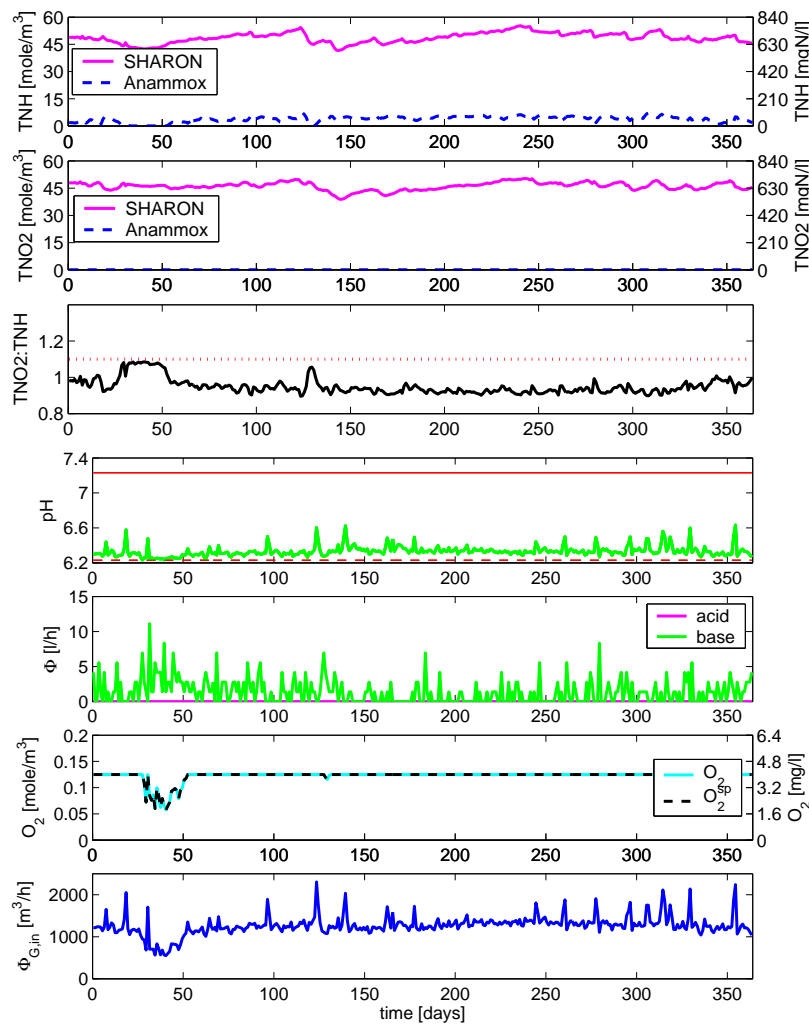


Figure 8.4: (from top to bottom, daily mean values) Concentrations of total ammonium (TNH) and total nitrite (TNO2) in SHARON reactor and Anammox reactor. Nitrite:ammonium ratio (TNO2:TNH), pH, acid/base addition, O_2 concentration vs. set point, air flow rate, in SHARON reactor. Operating mode of SHARON reactor ($V = 338 \text{ m}^3$) with cascade oxygen control ($R^{sp} = 1.1$) and pH-control ($pH^{sp} = 7.23 \pm 1$)

232 Interaction between control and design of a SHARON reactor

duced in the SHARON reactor amounts 0.94, resulting in an unconverted amount of ammonium in the Anammox reactor of 3.9 mole m^{-3} or 54 gN m^{-3} on average. The set point $R^{sp} = 1.1$ is not reached most of the time because of saturation of the oxygen set point at $4 \text{ gO}_2 \text{ m}^{-3}$. The effluent quality obtained in the Anammox reactor is clearly the best of all scenarios that have been examined so far, and so is the overall effluent quality of the main plant, even if the latter is less pronounced. Note that, even though the oxygen set point is set to $4 \text{ gO}_2 \text{ m}^{-3}$ nearly the whole time, significantly less aeration energy is needed as in case a fixed oxygen set point of 4 g m^{-3} is applied during aerobic periods for an aerSRT=1.25 days. This may also be attributed to the abovementioned peaks in aeration intensity at the start of an aerobic phase. It could be prevented by further limiting the maximum air flow rate to be applied.

cascade O_2 -control

As base addition comprises an additional operating cost factor, it has been examined whether a good reactor performance is still obtained with stand-alone cascade O_2 -control. The results are similar to the ones of the previous scenario, but due to the absence of base addition the nitrite:ammonium ratio produced in the SHARON reactor is lower (mean 0.89). This ratio is further almost constant over the whole period (min: 0.87; max: 0.92). Because of the suboptimal nitrite:ammonium ratio produced in the SHARON reactor, the oxygen set point in the SHARON reactor is kept at its maximum value of 4 g m^{-3} the whole time, which means that the same results would have been obtained with stand-alone oxygen control at $O_2^{sp} = 4 \text{ g m}^{-3}$. In comparison to the scenario with pH-control on top of cascade O_2 -control, the effluent quality improvement that is achieved by additional pH-control ($\Delta EQ_{BSM2} = 354379 - 356754 = -2375 \text{ € /year}$, see Table 8.1) clearly warrants the base addition costs (1131 € /year).

8.5.2 Operation of a SHARON reactor with $V=220 \text{ m}^3$

Secondly, a relatively small SHARON reactor is considered, with a volume of 220 m^3 , corresponding with a mean retention time of 1.25 days for the given influent flow rate, as in chapter 5. Table 8.2 summarizes the simulation results.

Table 8.2: Economic evaluation for a SHARON reactor with $V=220 \text{ m}^3$

cost factors [€/year]		aerSRT=1.25 days $O_2^{sp} = 1.5 \text{ g m}^{-3}$	cascade O_2 $R^{sp} = 1.1$ $pH^{sp} = 7.23 \pm 0.2$	cascade O_2 $R^{sp} = 1.23$ $pH^{sp} = 7.23 \pm 1$
effluent quality (EQ)	TSS _{BSM2}	35 367	35 327	35 345
	COD _{BSM2}	79 609	79 581	79 579
	BOD _{BSM2}	6 867	6 824	6 836
	TKN _{BSM2}	94 305	92 719	93 420
	NO _{BSM2}	151 426	135 984	142 590
	EQ _{BSM2}	367 573	350 437	357 770
	EQ _{An}	42 751	338	16 847
aeration energy (AE)	BSM2	182 290	180 125	180 876
	SHARON	12 394	25 788	23 904
mixing energy (ME)	BSM2	16 200	16 200	16 200
	SHARON	99	188	0
pumping energy (PE)	BSM2	64 861	68 822	66 964
	SHARON	172	172	172
sludge production (SP)	BSM2	230 352	229 728	229 950
	SHARON	2.9	0.18	0.24
	Anammox	1 164	960	947
external carbon addition (EC)		5 130	1 122	1 736
methane production (MP)		-123 342	-122 730	-122 918
net heating energy (HE ^{net})		0	0	0
acid addition		0	0.24	0
base addition		0	5 557	39
OCI _{SH,An}		55 146	31 684	40 790
OCI _{PW}		756 896	756 369	755 643

aerSRT control; O₂-control

It has been tested whether the given small SHARON reactor performs well with combined control of the aerobic retention time (aerSRT=1.25 days) and oxygen control at a constant set point ($O_2^{sp} = 1.5 \text{ g m}^{-3}$) during the aerobic periods. Figure 8.5 shows the simulation results. During the first 45 days of the evaluation period, only little ammonium (about 10 mole m^{-3}) is converted to nitrite in the SHARON reactor, while the pH increases up to 8. The reactor performance is recovered, but only after a period of low influent flow rates. As a result, the mean ammonium concentration in the Anammox reactor is very high (mean 18 mole m^{-3} or 255 gN m^{-3}). It is clear that the reactor volume is too small to be operated with oxygen control, at least for an oxygen set point of $1.5 \text{ gO}_2 \text{ m}^{-3}$. However, again the plant-wide operating cost

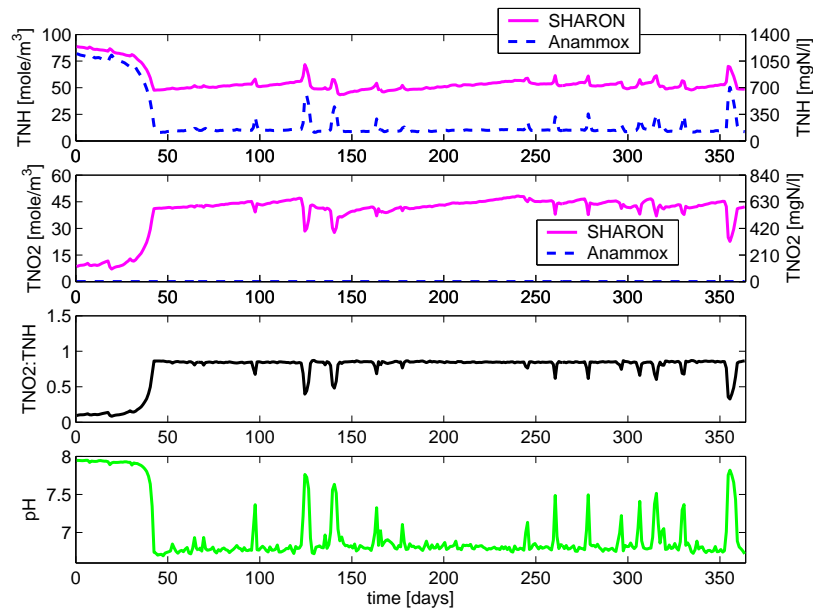


Figure 8.5: (from top to bottom, daily mean values) Concentrations of total ammonium (TNH) and total nitrite (TNO₂) in SHARON reactor and Anammox reactor. Nitrite:ammonium ratio (TNO₂:TNH) and pH in SHARON reactor. Operating mode of SHARON reactor ($V = 220 \text{ m}^3$) with aerSRT=1.25 days and oxygen control $O_2^{sp} = 1.5 \text{ g m}^{-3}$

index does not differ much from the previous operating modes for this reactor volume, due to the fact that the aeration capacity of the activated sludge tanks of the BSM2 plant has not been fully utilized.

Prolonging the (maximum) aerobic retention time is not expected to improve the performance much, since the aerobic retention time can never exceed the hydraulic retention time, which is clearly too short. It is advised to take the reactor volume in such a way that the desired aerobic retention time can be obtained during most of the time, say 95%, instead of only 50% of time, as in this case.

cascade O₂-control + pH-control

As the simulation results obtained in chapter 5 for a comparable small reactor volume indicate that good results are obtained with cascade O₂-control, combined with pH-control at a fixed set point, this operating mode has been examined subsequently. As in section 8.5.1, the

Anammox reactor showed nitrite inhibition for a nitrite:ammonium set point of $R^{sp} = 1.23$, so this value has been lowered, to 1.1. The performance of the SHARON and the Anammox reactor is displayed in Figure 8.6. The nitrite:ammonium set point is tracked very well in the

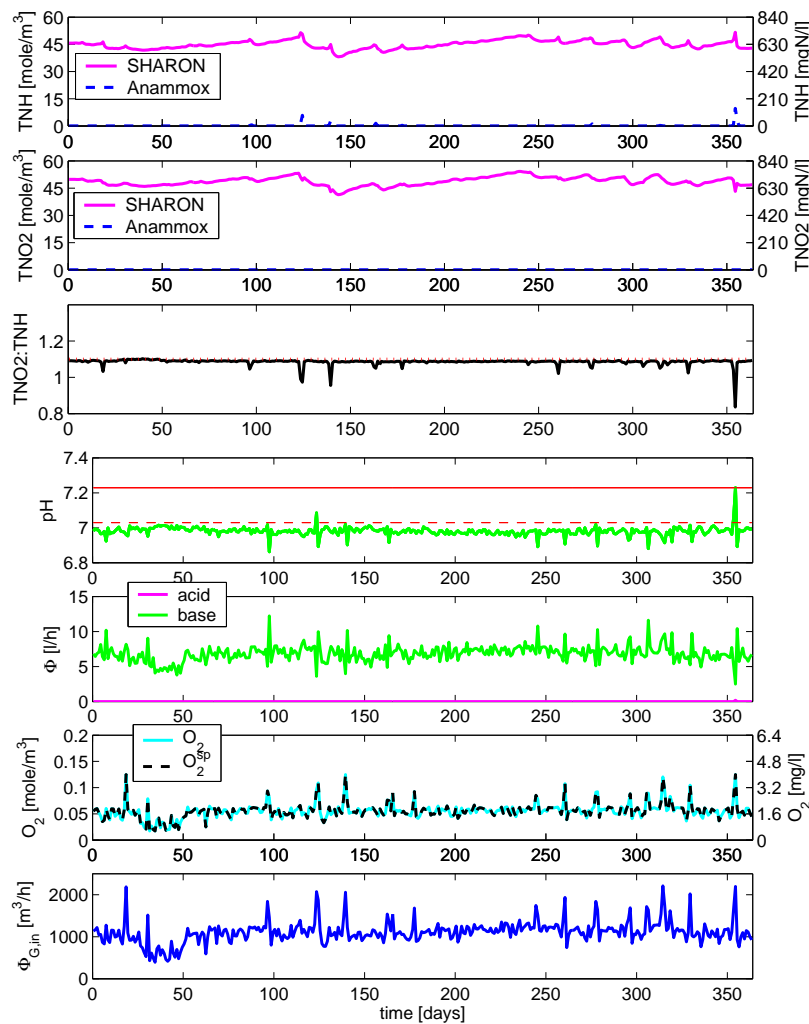


Figure 8.6: (from top to bottom, daily mean values) Concentrations of total ammonium (TNH) and total nitrite (TNO2) in SHARON reactor and Anammox reactor. Nitrite:ammonium ratio (TNO2:TNH), pH, acid/base addition, O_2 concentration vs. set point, air flow rate, in SHARON reactor. Operating mode of SHARON reactor ($V = 220 \text{ m}^3$) with cascade oxygen control ($R^{sp} = 1.1$) and pH-control ($pH^{sp} = 7.23 \pm 0.2$)

SHARON reactor (mean $TNO_2 : TNH = 1.08$). The value of the set point, $R^{sp} = 1.1$ appears to be well chosen, as very little ammonium remains unconverted in the Anammox reactor (mean 0.14 mole m^{-3} or 2 gN m^{-3}). This results in the lowest value for EQ_{An} that has been obtained so far. However, because of the high base addition costs, the operating cost index for the SHARON-Anammox system ($OCI_{SH,An}$) is not significantly better and the overall operating costs of the plant (OCI_{BSM2}) are even higher than in the scenarios that have been examined for $V = 338 \text{ m}^3$.

When widening the range for pH-control (scenario with cascade O_2 -control for $R^{sp} = 1.23$ and pH-control at 7.23 ± 1 , see Table 8.2), not enough ammonium can be converted in the small reactor (mean $TNO_2 : TNH = 0.89$). As a result, quite some ammonium ends up in the effluent of the Anammox reactor (mean 7 mole m^{-3} or 98 gN m^{-3}), resulting in a high value for $OCI_{SH,An}$. However, as the remaining ammonium is converted in the activated sludge tanks, the operating cost index on a plant-wide level, OCI_{PW} , does not increase and is even slightly lower than for strict pH-control. For this reason, and also regarding the sustainability of this operating strategy (only a small amount of base addition is needed), this operating mode is judged the best one for the given reactor volume.

When comparing the best operating modes for both reactor volumes studied so far, it is clear that significant operating cost savings can be realized by building a SHARON reactor of 338 m^3 instead of 220 m^3 . In case a SHARON reactor of 338 m^3 is operated with combined aerSRT (at 1.75 days) and oxygen control (at $O_2^{sp} = 1.5 \text{ g m}^{-3}$), the operating cost savings amount $\Delta OCI_{PW} = 745001 - 755643 = 10642 \text{ € /year}$ in comparison with operation of a 220 m^3 SHARON reactor with combined cascade O_2 -control (for $R^{sp} = 1.23$) and pH-control (at $pH^{sp} = 7.23 \pm 1$). The additional annual investment costs (depreciation period: 30 years; interest rate: 5%) needed to build a reactor of 338 m^3 instead of 220 m^3 are estimated at 1570 € /year , on the basis of a cost function given by Bohn (1993). It can be concluded that the investment costs to build a reactor of 338 m^3 clearly warrant the operating cost savings that are realized in comparison with a reactor of 220 m^3 .

8.5.3 Operation of a SHARON reactor with $V=460 \text{ m}^3$

Finally, it is studied whether the SHARON reactor performance can be improved when the reactor volume is increased to 460 m^3 , a value

that corresponds to a hydraulic retention time of 1.75 days for the 95-percentile value of the reject water flow rate, which seems rather overdimensioned. The results of the economic evaluation are summarized in Table 8.3.

Table 8.3: Economic evaluation for a SHARON reactor with $V=460 \text{ m}^3$

cost factors [€/year]		aerSRT=1.25 days $O_2^{sP} = 1.5 \text{ g m}^{-3}$	aerSRT=1.75 days $O_2^{sP} = 1.5 \text{ g m}^{-3}$	cascade O_2 $R^{sP} = 1.1$ $pH^{sP} = 7.23 \pm 1$
effluent quality (EQ)	TSS _{BSM2}	35 350	35 346	35 328
	COD _{BSM2}	79 586	79 581	79 576
	BOD _{BSM2}	6 840	6 838	6 821
	TKN _{BSM2}	93 521	93 402	92 622
	NO _{BSM2}	144 115	142 877	136 419
	EQ _{BSM2}	359 412	358 045	350 766
	EQ _{An}	20 780	17 741	277
aeration energy (AE)	BSM2	181 058	180 918	180 091
	SHARON	13 268	12 303	17 658
mixing energy (ME)	BSM2	16 200	16 200	16 200
	SHARON	779	482	0.16
pumping energy (PE)	BSM2	66 516	66 870	68 605
	SHARON	172	172	172
sludge production (SP)	BSM2	230 025	229 978	229 686
	SHARON	0.34	0.30	0.14
	Anammox	948	950	959
external carbon addition (EC)		1 996	1 838	1 178
methane production (MP)		-122 971	-122 937	- 122 688
net heating energy (HE ^{net})		0	0	0
acid addition		0	0	0
base addition		0	0	3 921
OCI _{SH,An}		34 049	30 045	21 856
OCI _{PW}		747 404	744 820	746 549

aerSRT control ; O_2 -control

aerSRT = 1.25 days For this operating mode, the results of the economic evaluation hardly differ from the same operating mode in a SHARON reactor with volume $V = 338 \text{ m}^3$. This is not surprising, since a reactor volume of $V = 338 \text{ m}^3$ is already sufficient to maintain an aerobic retention time of 1.25 days during 95% of the time. The advantages associated with maintaining the desired aerSRT the whole time are rather small: the mean ammonium conversion in the SHARON reactor is a lit-

238 Interaction between control and design of a SHARON reactor

tle higher (mean $TNO_2 : TNH = 0.86$), so the mean ammonium concentration remaining in the Anammox reactor (8.6 mole m^{-3} or 121 gN m^{-3}) is a little lower, resulting in somewhat lower aeration energy requirements and external carbon addition in the activated sludge tanks. The overall effluent quality is hardly influenced by increasing the reactor volume from 338 to 460 m^3 , although the difference would be larger if the aeration capacity of the activated sludge tanks would already be fully utilized. As the SHARON reactor remains unaerated during a large fraction of the time, more mixing energy is consumed. It is clear that a larger reactor should only be considered if one wants to establish a higher mean aerobic sludge retention time. Whether this is beneficial, is examined by prolonging the aerobic retention time to 1.75 days.

aerSRT = 1.75 days Increasing the applied aerobic retention time from 1.25 to 1.75 days results in a slightly higher nitrite:ammonium ratio produced in the SHARON reactor (mean $TNO_2 : TNH = 0.88$, results not shown), resulting in a slightly lower amount of unconverted ammonium in the Anammox reactor (mean 7.4 mole m^{-3} or 103 gN m^{-3}). Despite the high aerobic retention time, almost no nitrate is formed in the SHARON reactor (mean 0.36 mole m^{-3} or 5 gN m^{-3}), which is attributed to the low oxygen concentration and the low pH (mean 6.5).

Although the obtained operating cost indices for this scenario are slightly lower than for the same operating mode (aerSRT=1.75 days; $O_2^{sp} = 1.5 \text{ g m}^{-3}$) in a SHARON reactor with volume 338 m^3 , the resulting small savings in operating costs ($\Delta OCI_{SH,An} = 30911 - 30045 = 866 \text{ € / year}$; $\Delta OCI_{PW} = 745001 - 744820 = 181 \text{ € / year}$) will not warrant the investment costs to build a larger reactor.

cascade O_2 -control + pH-control

Finally, it has also been examined which results are obtained with cascade O_2 -control, combined with pH-control. The performance of the SHARON and the Anammox reactor is displayed in Figure 8.7.

In contrast to what has been obtained for smaller reactor volumes, the nitrite:ammonium set point is now tracked quite well in the SHARON reactor (mean $TNO_2 : TNH = 1.06$). As a result, quasi complete conversion is realized in the Anammox reactor. However, mainly because of the increased aeration energy costs and costs for base addition in the SHARON reactor, the plant-wide operating cost index is higher than for the operating mode with aerSRT control (at 1.75 days) and

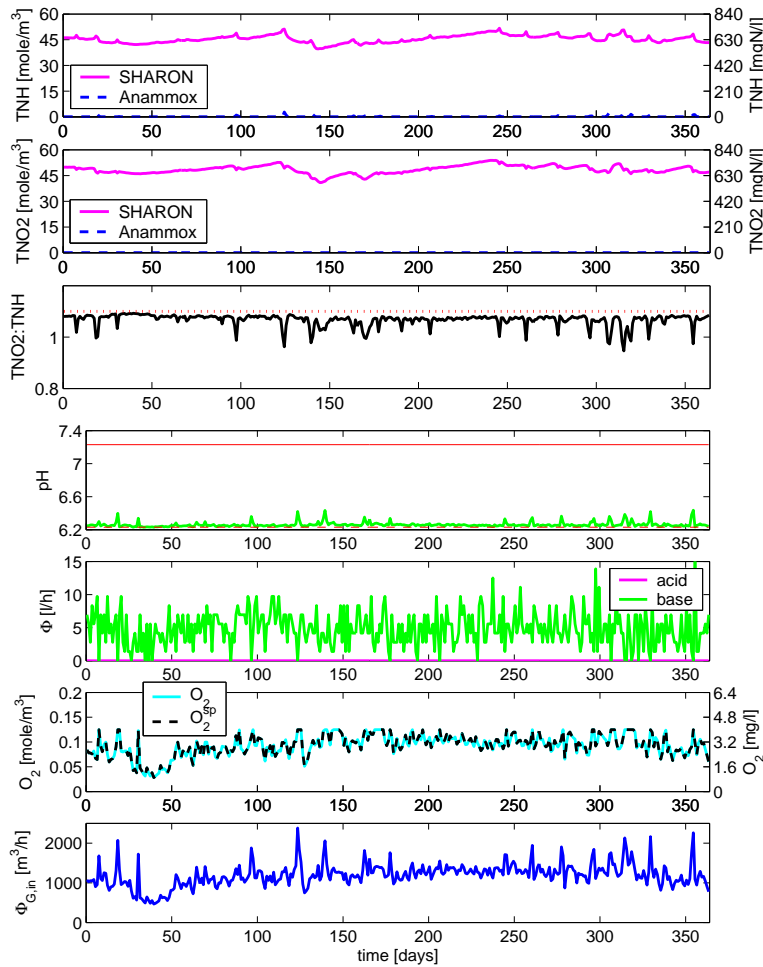


Figure 8.7: (from top to bottom, daily mean values) Concentrations of total ammonium (TNH) and total nitrite (TNO2) in SHARON reactor and Anammox reactor. Nitrite:ammonium ratio (TNO2:TNH), pH, acid/base addition, O_2 concentration vs. set point, air flow rate, in SHARON reactor. Operating mode of SHARON reactor ($V = 460 \text{ m}^3$) with cascade oxygen control ($R^{sp} = 1.1$) and pH-control ($pH^{sp} = 7.23 \pm 1$)

oxygen control (at $O_2^{sp} = 1.5 \text{ g m}^{-3}$). Note that results would be different when the aeration capacity of the activated sludge plants would already have been fully utilized, so the improved Anammox effluent quality would result in an even more pronounced effluent quality of the plant.

8.6 Discussion and conclusions

In this chapter, the operating strategy for BSM2 reject water treatment has been optimized. Different operating modes have been examined, also considering the effect of reactor volume. Figure 8.8 summarizes the best results for the different reactor volumes in terms of the plant-wide operating cost index OCI_{PW} , which is a measure of the overall operating costs, and in terms of the effluent quality of the Anammox reactor (EQ_{An}), which indicates to which extent a good conversion efficiency is realized in the SHARON and Anammox reactors.

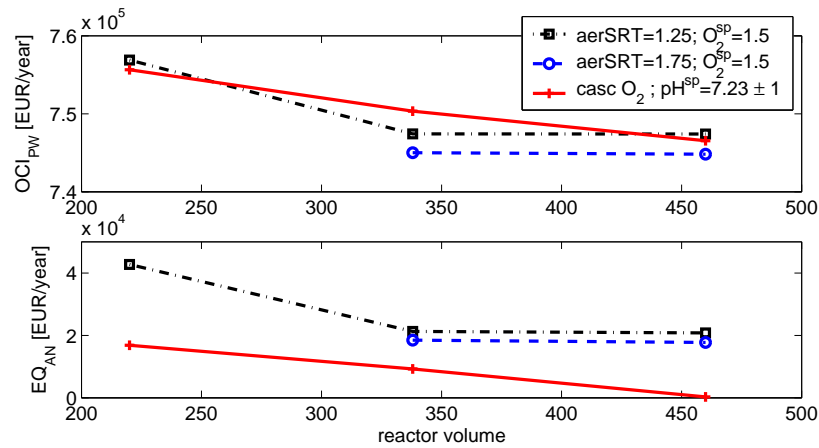


Figure 8.8: Plant-wide operating cost index (OCI_{PW}) and Anammox reactor effluent quality (EQ_{An}) for different operating modes in terms of reactor volume

The best performance of the SHARON and Anammox reactor (lowest EQ_{An}) is obtained with combined cascade O_2 -control and pH-control in the SHARON reactor. This operating mode ensures the production of a favourable nitrite:ammonium ratio in the SHARON reactor, which leads to a good conversion efficiency in the Anammox reactor. As the SHARON reactor volume increases from $V = 220 \text{ m}^3$ to $V = 460 \text{ m}^3$, the Anammox-optimal nitrite:ammonium set point is tracked better in the SHARON reactor, so the conversion efficiency of the Anammox reactor increases.

When comparing the effluent quality of the Anammox reactor, expressed in terms of EQ_{An} , with the plant-wide operating cost index, OCI_{PW} , it is clear that a better conversion efficiency of the combined

SHARON-Anammox process does not necessarily result in lower operating costs on a plant-wide scale. This is mainly attributed to the increased aeration energy needed to meet higher oxygen set points and to the base addition costs to maintain a minimal pH level in the SHARON reactor. The spare aeration capacity of the BSM2 activated sludge tanks also plays an important role: it is the reason why an improved effluent quality of the Anammox reactor does not result in an equivalent improvement of the effluent quality of the plant. It appears to be cheaper to remove residual ammonia in the main plant, provided it still has some aeration capacity left, rather than in the dedicated SHARON-Anammox reactor system.

The best results in terms of the lowest plant-wide operating cost index (OCI_{PW}) have been obtained for an operating mode of the SHARON reactor in which the aerobic retention time is controlled through cyclic reactor operation at an aerobic SRT (aerSRT) of 1.75 days (maximum) and a fixed oxygen set point of $O_2^{sp} = 1.5 \text{ g m}^{-3}$ is applied during the aerobic phases. The behaviour of a SHARON reactor under this operating scenario has been evaluated both for a moderately large reactor with volume $V = 338 \text{ m}^3$, corresponding with a HRT of at least 1.25 days during 95% of the time, and for an even larger reactor with volume $V = 460 \text{ m}^3$, corresponding with a HRT of at least 1.75 days during 95% of the time. The yearly operating costs were only slightly lower (difference: 181€/year) for a reactor of 460 m^3 compared to a reactor of 338 m^3 and did not warrant the additional investment costs.

When further decreasing the SHARON reactor volume to 220 m^3 , corresponding with a mean HRT of 1.25 days, the lowest operating costs were obtained with cascade O_2 -control, combined with pH-control between wide ranges. However, the investment costs savings for building a reactor of 220 m^3 instead of 338 m^3 (estimated at 1570 €/year) did not warrant the increased operating costs (difference: 10642 €/year). As a result, operating a SHARON reactor of 338 m^3 with combined aerSRT (at 1.75 days) and O_2 -control (at 1.5 $\text{gO}_2 \text{ m}^{-3}$) was judged as the best way to treat the BSM2 reject water.

It is interesting to note that, for the different scenarios examined in this chapter, the optimal nitrite:ammonium ratio of 1.1-1.23 needed to feed the Anammox reactor is never reached without pH-control. For the scenarios in which only (cascade) O_2 -control is applied in the SHARON reactor, the highest mean nitrite:ammonium ratios obtained in the SHARON reactor typically amount only 0.89. The necessity of base addition to enhance ammonium conversion in such a way that the

242 Interaction between control and design of a SHARON reactor

nitrite:ammonium set point is reached in the SHARON reactor, which results in a good Anammox effluent quality, was attributed to the relatively low alkalinity(bicarbonate):ammonium ratio in the BSM2 reject water. However, in the given case study, it appeared to be no problem when a (slightly) suboptimal nitrite:ammonium ratio (lower than 1.1) was produced in the SHARON reactor. The amount of unconverted ammonium that remained in the Anammox reactor could indeed be handled easily by the activated sludge tanks of the BSM2 plant, in which the aeration capacity was not fully utilized. For this reason, controlling the nitrite:ammonium ratio in the SHARON reactor more closely to the set point of 1.1 by adding base, also implying the implementation of a measurement system for ammonium and nitrite to monitor the produced nitrite:ammonium ratio, appears a waste of money. This situation is different from the one examined in chapter 5, where monitoring of the produced nitrite:ammonium ratio is necessary, as the alkalinity:ammonium ratio in the reject water considered is so high that it would lead to a too high nitrite:ammonium ratio produced. It is clear that the optimal operating strategy for a SHARON reactor depends on the reject water composition, in particular its alkalinity(bicarbonate):ammonium ratio.

Chapter 9

General discussion, conclusions and perspectives

In this thesis, modelling, analysis and control of partial nitritation in a SHARON reactor for coupling with an Anammox process have been studied. Several research aspects have been addressed and are discussed hereafter, also indicating opportunities for future research.

Applicability of the SHARON partial nitritation process for reject water treatment

The influent nitrogen load of wastewater treatment plants (WWTPs) is increased considerably when reject water, originating from sludge digestion and dewatering systems, is recycled to it. This is especially problematic in case the latter has a limited aeration/nitrification/denitrification capacity. In chapter 7, a plant-wide simulation study has been carried out to study the effect of reject water on the performance of the activated sludge process for the BSM2 (Benchmark Simulation Model no. 2) plant. It has been shown that recirculation of the untreated reject water stream, representing 21% of the total influent ammonium load, unacceptably worsens the total nitrogen concentration in the effluent of the WWTP.

The main plant can be relieved by treatment of the reject water stream before recirculation. From the literature review (chapter 2), in which different biological techniques for reject water treatment are compared on the basis of their underlying principles, it is clear that the

process selection strongly depends on site-specific conditions and requirements in terms of efficiency, effluent quality, process compactness and associated operating and investment costs. The best option is mostly found among either bio-augmentation techniques or processes based on nitrification. Bio-augmentation techniques combine reject water treatment with the supply of additional nitrifiers to the activated sludge tanks in the main line and are essentially applied when the aerobic retention time in the activated sludge process is insufficient for nitrification or its anoxic retention time is insufficient for denitrification. Other reject water treatment techniques only reduce the nitrogen load that is recirculated to the main line and are especially suitable in case the retention time in the main line is sufficient, but its aeration capacity or the supply of carbon source is limited. In comparison with processes based on nitrification/denitrification over nitrate, techniques establishing nitrification/denitrification over nitrite or combining partial nitrification and Anammox, the SHARON partial nitrification process for coupling with the Anammox process being an example of the latter, realize significant cost savings in terms of aeration (up to 63%) and carbon source addition (up to 100%), while sludge production and CO_2 -emission are minimized.

The simulation results of chapter 7 clearly showed that treatment of the reject water stream with a SHARON-Anammox process before recirculation results in a significant effluent quality improvement in terms of Kjeldahl-nitrogen and nitrate. The results are comparable to the case without reject water, which can be seen as a reference case for ideal reject water treatment. Other advantages of a combined partial nitrification-Anammox process, such as a lower aeration energy consumption per amount of ammonium converted, quasi redundancy of external carbon source addition and a decreased sludge production were also well demonstrated.

Nevertheless, meeting the ammonium effluent limit still remains a bottleneck for the BSM2 plant, especially during the winter period. It is clear that this should be remedied by optimizing the control of the main WWTP rather than the reject water treatment, for example by allowing aeration in one of the denitrification tanks when temperatures are low. Another interesting option to meet the ammonium limits would be to use a bio-augmentation process for reject water treatment.

Modelling the SHARON process in a plant-wide context

The SHARON reactor model A detailed model has been developed to describe the dynamics of a SHARON reactor. Both the liquid phase and the gas phase as well as interphase transport have been modelled. Special attention has been devoted to pH calculation, for which a general procedure has been put forward. This model has been used in the simulation study carried out in this thesis.

In the work presented in this thesis, not all features of the model have been fully utilized yet. For instance, although a heat balance has been set up and reaction enthalpies have been calculated rigorously, the simulations described in this work have been performed for a reactor of which the temperature is kept constant. However, the model could also be used to study the interaction between biological conversion rates and reactor temperature. For a specific case in which e.g. the heat transfer coefficients are known, one could study the difference between a SHARON reactor operated with nitrification-denitrification over nitrite and a SHARON reactor in which partial nitritation is established in terms of possible autothermal reactor operation or requirement for external heating. Another model option that has not yet been exploited, is the possibility to vary the reactor volume during operation, e.g. to provide a constant flow rate for the subsequent Anammox reactor despite varying influent flow rates to the SHARON reactor. Finally, in the simulation study described in this work, the SHARON reactor model has been used for long-term simulations (several weeks-months). Nevertheless, the model is also very suitable for describing short-term dynamics, e.g. to simulate the reactor behaviour within one aerobic-anoxic cycle of 2 hours, for which no simulation results have been taken up in this thesis.

The resulting model has been validated at a full-scale SHARON reactor in Sluisjesdijk. Although the simulation results didn't quantitatively reproduce the measurements, in particular concerning the denitrification process, the model was judged sufficiently accurate to qualitatively represent the behaviour of an actual SHARON reactor. For further optimization of the simulation model, it will be needed to first investigate the nature of denitrification occurring in the SHARON process in more detail. However, it is clear that, taking into account a combined effect of several of the hypotheses that have been considered to explain the differences, it will be possible to calibrate the model. Such model calibration is an interesting future research topic too, although it is very dependent on the availability of frequent and reliable data.

Continuity-based model interfacing for plant-wide evaluation In order to simulate the effect of reject water treatment with a SHARON-Anammox process on a plant-wide (BSM2) scale, as well as to evaluate the impact of different control strategies in the SHARON reactor and the interaction with the reactor volume, chapter 6 addresses the issue of coupling models with different state variables. The general continuity-based model interfacing method (CBIM) has been followed for the construction of model interfaces between the models ASM1/-SHARON, SHARON/Anammox and Anammox/ASM1 in such a way that continuity of COD, C, N, H, O, P and charge is maintained.

It has been pointed out how the order in which the elemental balances are closed and the choice of sink/source components can minimize the number of compensation components required, as well as the values of the stoichiometric coefficients in the transformations. Besides, special attention was given to the construction of interfaces between models in which pH is considered as a state variable and in which lumped state variables are used to represent the sum of concentrations of different equilibrium components (e.g. NH_3 and NH_4^+). Although the method was illustrated for a specific case, it was described in such way that it can easily be generalized and used in other applications.

Avoiding leaks of elements is indeed essential in model coupling. The desirability to check the existing BSM2 model interfaces and revise them where necessary, so that not only continuity of COD and N, but also of all other elements is guaranteed, has been stressed. Although this may seem a laborious and cumbersome task at first sight, advantage can be taken of the possible reduction of the number of balances when certain components are not considered in the destination model. For instance, the O-balances can be omitted as it is closed with H_2O , which is not explicitly taken up as a component of interest in the composing models. Also the P-balance can be left out as phosphorus is not taken up in any of the models that make part of the BSM2. This means that, besides the COD- and N-balance, which are currently fulfilled, the only two additional balances that should still be checked for the BSM2 interfaces are the C-balance and the charge balance. The work described in chapter 6 for the coupling of the ASM1, with lumped state variables, and the ADM, in which H^+ is taken up as a state variable, can serve as a guideline.

Finally, it seems also advisable to move the ADM1/ASM1 interface in the BSM2 from the outlet of the anaerobic digester to the outlet of the dewatering equipment. In this way, more accurate information on

pH and on state variables that take part in chemical equilibria would be available for the study of reject water treatment, where they play an important role. One direct ADM1/SHARON interface would indeed be preferred over the current two ADM1/ASM1 and ASM1/SHARON interfaces.

Equilibrium points of a two-step nitrification model

A good knowledge of the SHARON process dynamics is essential for control purposes. From this point of view, it is interesting to know if multiple equilibrium states occur for different regions in the input space, i.e. whether the reactor's steady state(s) differ(s) between operating conditions (e.g. possible combinations of influent ammonium concentration and applied dilution rates) or even different steady states may be reached for the same operating conditions, dependent on the reactor's initial state.

The existence, uniqueness, and stability of the equilibrium points of a simplified two-step nitrification model, in which the growth rate of ammonium oxidizers is larger than the growth rate of nitrite oxidizers, oxygen is always present in excess and pH is controlled at a constant value, have been studied on theoretical grounds. The contraction mapping theorem has been applied to identify regions in the input space where the system possesses only one equilibrium point, but only the wash-out equilibrium point at high values of the dilution rate could be identified, which is clearly not an interesting operating point.

Subsequently, the equilibrium points of such SHARON reactor model have been calculated directly for a number of simplified cases. Three equilibrium points have been found in case nitrite oxidizers are not limited by ammonium and no inhibition takes place. For high dilution rates, the equilibrium point corresponding with biomass wash-out is globally asymptotically stable. For moderately low dilution rates and at the same time sufficiently high influent ammonium concentrations, a second equilibrium point, corresponding with only nitrite formation, occurs and is now (quasi) globally asymptotically stable. If the dilution becomes even lower and the influent ammonium concentration is sufficiently high, a third equilibrium point, corresponding with nitrate formation, becomes (quasi) globally asymptotically stable. These findings agree with what is expected from practice. From an operating point of view, the second situation, in which the equilibrium point with only

nitrite formation is quasi globally asymptotically stable, is clearly the most interesting.

Particular attention has been paid to the influence of microbial properties. If nitrite inhibition of ammonium oxidation is taken up in the model, as for the simulation work described in chapters 5 and 8, it has been found that the number of equilibrium points, as well as their stability, is not affected. However, the position of the equilibrium points corresponding with biomass growth does change: less ammonium is converted as nitrite becomes a more severe inhibitor of the process. The condition for the occurrence of an equilibrium point with only nitrite production remains the same, while the condition for the occurrence of an additional equilibrium point, corresponding with nitrate formation, becomes more stringent: as nitrite inhibition becomes stronger, the additional equilibrium point occurs at lower dilution rates and higher influent ammonium concentrations than in case of no nitrite inhibition.

While the results indicate that product inhibition does not affect the number of equilibrium points of a (bio)reactor model, it has been shown that substrate inhibition is clearly a source of additional equilibrium points. It has been found that addition of ammonium inhibition of ammonium oxidation to a simple two-step nitrification model leads to the occurrence of up to five equilibrium points: one wash-out point, two equilibrium points corresponding with only nitrite formation and two equilibrium points corresponding with nitrate formation.

Finally, the results from the theoretical analysis have been translated into some practical implications, regarding reactor design and operation. For instance, it has been demonstrated that the range of dilution rates that guarantee stable nitrite formation depends on the influent ammonium concentration. If the range of influent ammonium concentrations to be treated is known in advance, information on the allowable range of dilution rates can be used for reactor design or for controlling the influent flow rate to the SHARON reactor.

For future research, it is suggested to further exploit the effect of microbial characteristics on the operating conditions under which stable nitrite formation is achieved. In particular, it would be interesting to study how these conditions are affected by the reactor temperature, and moreover, pH. Besides, it could also be investigated under which conditions an Anammox-optimal nitrite:ammonium ratio is obtained in the SHARON reactor. The influence of control on the number of equilibrium points and their stability could be discussed in more detail. The investigation of the number of equilibrium points and their stability for

a SHARON reactor model with varying pH, would also be a very interesting research topic, although analysis of the corresponding model will not be straightforward. The evaluation of stability in a dynamic system, e.g. starting with slowly varying inputs, is another option.

Controlling the nitrite:ammonium ratio in a SHARON reactor for coupling with an Anammox process

Operating a SHARON reactor in such a way that an Anammox-optimal nitrite:ammonium ratio is produced at all times is important to assure complete conversion and, more critically, to avoid nitrite inhibition of the Anammox reactor.

Controlling a SHARON reactor with fixed design In chapter 5, the usefulness of controlling a SHARON reactor for coupling with an Anammox process has been examined for realistic influent conditions, based on measurements of the full-scale SHARON reactor at Sluisjesdijk. The given reactor volume has been calculated to obtain a mean HRT (=SRT) of 1.25 days. In this case, no good results could be obtained with oxygen control on a fixed set point, as the oxygen level appeared either too low to allow ammonium conversion in the SHARON reactor, or it led to too much nitrite formation, resulting in inhibition of the subsequent Anammox reactor. Stand-alone cascade O_2 -control, adjusting the oxygen set point to meet the desired nitrite:ammonium ratio in the SHARON reactor, appeared not to be a good option either. In the latter case, high air flow rates, aiming to meet an increasing oxygen set point during a period of decreasing ammonium conversion, cause so much CO_2 -stripping from the reactor that the pH increases to such an extent that the growth rate of ammonium oxidizers decreases further, eventually leading to their wash-out. This problem was overcome by combining the cascade O_2 control with pH control at the optimal value ($pH^{opt} = 7.23$) corresponding with maximum microbial growth rates. This operating mode was the only one for which a good Anammox-conversion took place.

All results of chapter 5 have been quantified in an economic way by means of an operating cost index (OCI), that takes into account the operating costs for the SHARON reactor that differ between the different operating modes under study, as well as the costs associated with the Anammox effluent quality. The operating cost savings realized with the cascade O_2 -control combined with pH-control compared to e.g. the

scenario with stand-alone O_2 -control, warrant the investments costs for the necessary on-line ammonium and nitrite sensors (payback time less than 1 year).

Ammonium and nitrite measurements can be realized in a relatively cheap way using a titrimetric set-up. Van Hulle et al. (2006) have demonstrated the reliability of this method for the measurement of ammonium and nitrite concentrations in a SHARON-reactor for partial nitrification: the titrimetric results could not be distinguished (with 95% confidence) from the ones obtained with conventional colorimetric methods.

It can be remarked that the maximum oxygen set point allowed by the cascade O_2 -controller in chapter 5, being the prevailing saturation concentration (9 g m^{-3}), is rather high compared to the oxygen affinity constant of ammonium oxidizers $K_{O_2}^{amm} = 1 \text{ g m}^{-3}$ and will not increase the microbial growth rate much more than when choosing for instance a maximum value of $O_2 = 4 \text{ g m}^{-3}$ (Monod term 0.9 versus 0.8), while consuming much more aeration energy. Besides, the associated high air flow rates may induce biomass wash-out due to high pH-values. It could be examined whether better results would be obtained with the stand-alone cascade O_2 -controller by lowering the maximum oxygen set point and maybe also by further limiting the maximum air flow rate supplied to the process. In the mean time, a lower maximum oxygen set point has been applied in the simulations on the BSM2 reject water, described in chapter 8.

Finally, as the implementation of pH-control on top of cascade O_2 -control apparently only serves at maintaining acceptable maximum microbial growth rates, keeping the pH within a broader range around the optimal value (e.g. 1 pH unit below or above) instead of controlling it at a fixed value is expected to yield good results as well and at the same time reduce costs for acid/base addition. This strategy has consequently been applied for the simulations in chapter 8 and indeed resulted in a satisfying nitrite:ammonium ratio produced in the SHARON reactor and consequently a good conversion efficiency of the Anammox reactor.

Influence of the influent bicarbonate:ammonium ratio The obtained result that, under the conditions studied in chapter 5, a fixed oxygen set point either hardly allows ammonium conversion, or results in a too high nitrite:ammonium ratio produced, is striking. However, steady state results (Villez, personal communication) have confirmed the steep

profile of the ammonium conversion as function of the oxygen concentration for operation with O_2 -control.

In case the oxygen concentration allows ammonium conversion, the extent of ammonium conversion and thus the produced nitrite:ammonium ratio are mainly determined by the alkalinity:ammonium ratio in the influent. The influent conditions of chapter 5 are characterized by a rather high amount of inorganic carbon, of which bicarbonate is the dominant form. This leads to a too high nitrite:ammonium ratio produced in the SHARON reactor. The BSM2 reject water, for which a SHARON reactor with corresponding control strategy has been designed in chapter 8, contains a relatively low alkalinity(bicarbonate):ammonium ratio. As a result, in the latter case the optimal nitrite:ammonium ratio needed to feed the Anammox reactor is never reached without pH-control.

In case the alkalinity:ammonium ratio of the reject water is so high that it would cause a nitrite:ammonium ratio in the SHARON reactor that is higher than the Anammox-optimum, controlling the SHARON reactor is clearly more critical than in case the alkalinity:ammonium ratio of the reject water would lead to a suboptimal nitrite:ammonium ratio. Indeed, a too high nitrite:ammonium ratio produced by the SHARON process will cause nitrite inhibition of the Anammox reactor, leading to its failure: no conversion will take place in the Anammox reactor. On the other hand, if the nitrite:ammonium ratio in the SHARON effluent is too low, this will lead to incomplete ammonium conversion in the Anammox reactor, but all the nitrite in the SHARON effluent will be converted.

Discrepancy between Anammox effluent quality and plant-wide operating costs In chapter 8, different operating strategies for a SHARON reactor have been evaluated in terms of the corresponding conversion efficiency of the SHARON and Anammox reactor, reflected by the effluent quality (ammonium) of the Anammox reactor, as well as in terms of operating costs on a plant-wide scale, expressed in terms of a plant-wide operating cost index. It has been demonstrated that a better conversion efficiency of the combined SHARON-Anammox process does not necessarily result in lower operating costs on a plant-wide scale. Indeed, although more sophisticated control strategies such as combined cascade O_2 -control, combined with pH-control, mostly lead to a nitrite:ammonium ratio produced in the SHARON reactor that is more close to the Anammox-optimal value, they also give rise to increased

operating costs in terms of increased aeration energy needed to meet higher oxygen set points and base addition costs to maintain a minimal pH-level in the SHARON reactor (besides increased investment costs). Besides, in case the activated sludge tanks in the main line still possess some spare aeration capacity (as is the case for the BSM2 plant), an improved effluent quality of the Anammox reactor does not result in an equivalent improvement of the effluent quality of the plant. If the nitrite:ammonium ratio produced in the SHARON reactor is only slightly suboptimal to feed an Anammox reactor, the ammonium concentrations that remain unconverted in the Anammox reactor are rather low and are to a large extent further removed in the activated sludge tanks of the BSM2 plant, of which the aeration capacity is not fully utilized. In this case, it appears to be cheaper to remove residual ammonia in the main plant rather than in the dedicated SHARON-Anammox reactor system.

Influence of SHARON reactor design on its optimal control strategy

The interaction between reactor design and the usefulness of control has been assessed in chapter 8. It has been shown that the requirements of the SHARON-Anammox system can be fulfilled in different volumes, applying different control strategies.

The best performance of the SHARON and Anammox reactor in terms of Anammox effluent quality is obtained with combined cascade O_2 -control and pH-control in the SHARON reactor. This operating mode ensures the production of a favourable nitrite:ammonium ratio in the SHARON reactor, which leads to a good conversion efficiency in the Anammox reactor. As the SHARON reactor volume increases, the Anammox-optimal nitrite:ammonium set point is tracked better in the SHARON reactor, so the conversion efficiency of the Anammox reactor increases.

However, the operating scenarios with the best effluent Anammox effluent quality are not necessarily the ones with the lowest operating costs on a plant-wide scale. Besides, at different SHARON reactor volumes, different control strategies may be optimal. The best results in terms of the lowest plant-wide operating cost index (OCI_{PW}) have been obtained for an operating mode of the SHARON reactor in which the aerobic retention time is controlled through cyclic reactor operation at an aerobic SRT (aerSRT) of 1.75 days and a fixed oxygen set point of $O_2^{sp} = 1.5 \text{ g m}^{-3}$ is applied during the aerobic phases. The use of a moderately large SHARON reactor, which volume corresponds

with a HRT of at least 1.25 days during 95% of the time, was preferred over using an even larger reactor, as yearly operating costs were only slightly lower and did not warrant the additional investment costs in the latter case. When further decreasing the SHARON reactor volume, to a value corresponding with a mean HRT of 1.25 days, the lowest operating costs were obtained with cascade O_2 -control, combined with pH-control between wide ranges. However, the investment costs savings for building this smaller reactor did not warrant the increased operating costs.

Perspectives in controlling a SHARON-Anammox system In this thesis, the focus in controlling a SHARON-Anammox system has been on the SHARON reactor, aiming to produce the Anammox-optimal nitrite:ammonium ratio, either directly through cascade controller configurations, that rely on ammonium and nitrite measurements in the SHARON reactor, or indirectly through O_2 - and/or pH-control on a fixed set point. In all cases, it has been assumed that the optimal nitrite:ammonium ratio to feed the Anammox process is constant.

In practice, it will be important to adjust the desired nitrite:ammonium to the performance of the Anammox reactor, especially to avoid nitrite inhibition. In case the Anammox reactor is not controlled, a substantial amount of nitrite entering the Anammox reactor during a period of non-optimal control of the SHARON reactor will slow down the growth of the Anammox biomass. Even if the performance of the SHARON reactor is immediately restored afterwards, producing an Anammox-optimal nitrite:ammonium ratio, the Anammox biomass will not be able to convert this mixture when still suffering from the past nitrite overload, but will be further inhibited by the nitrite entering the reactor. To detect this, installing a nitrite sensor in the Anammox reactor is essential. If too high nitrite concentrations are frequently monitored in the Anammox reactor, the setpoint for the nitrite:ammonium ratio that is to be produced by the SHARON reactor, can be decreased. In case ammonium is measured in the Anammox reactor as well, the setpoint for the nitrite:ammonium ratio, which may vary e.g. due to varying microbial characteristics, can be increased if too much ammonium remains unconverted in the Anammox reactor.

Overall, the SHARON-Anammox process shows clear benefits for reject water treatment in case the aeration capacity of the activated sludge tanks is limited. Even for small SHARON reactor volumes, an Anammox-optimal nitrite:ammonium ratio can be produced in the SHARON reactor, using more sophisticated control strategies, that rely on ammonium and nitrite measurements, which can be realized in a relatively cheap way using a titrimetric sensor (Van Hulle et al., 2006). The defined operating cost indices have proven to be a useful tool to determine which control strategy is most suitable for a given SHARON reactor volume, as well as to determine the optimal combination of control strategy and design for a SHARON reactor.

References

- U. Abeling and C.F. Seyfried. Anaerobic-aerobic treatment of high-strength ammonium wastewater - Nitrogen removal via nitrite. *Water Science and Technology*, 26(5-6):1007–1015, 1992.
- A.C. Anthonisen, R.C. Loehr, T.B.S. Prakasam, and E.G. Srinath. Inhibition of nitrification by ammonia and nitrous acid. *Journal of the WPCF*, 48(5):835–852, 1976.
- D.J. Batstone, J. Keller, R.I. Angelidaki, S.V. Kalyuzhnyi, S.G. Pavlostathis, A. Rozzi, W.T.M. Sanders, H. Siegrist, and V.A. Vavilin. *Anaerobic Digestion Model No.1*. IWA Scientific and Technical Report No. 13. IWA Publishing, London, U.K., 2002.
- L. Benedetti, J. Meirlaen, and P. A. Vanrolleghem. *Sewer Networks and Processes within Urban Water Systems*, chapter Model connectors for integrated simulations of urban wastewater systems, pages 13–21. Water and Environment Management Series (WEMS). IWA Publishing, London, U.K., 2004.
- D. Berends, E. van der Zandt, R. van der Kuij, S. Salem, and C. Uijterlinde. De BABE-technologie. *Afvalwaterwetenschap*, april:91–107, 2003.
- N. Bernet, D. Peng, J.P. Delgens, and R. Moletta. Nitrification at low oxygen concentration in biofilm reactor. *Journal of Environmental Engineering*, 127(3):266–271, 2000.
- T. Bohn. *Wirtschaftlichkeit und Kostenplanung von kommunalen Abwasserreinigungsanlagen*. Verlag Stuttgart, 1993.
- H. Chiang, M. Hirsch, and F. Wu. Stability regions of nonlinear autonomous dynamical systems. *IEEE transactions on automatic control*, 33:16–27, 1998.

- J. Copp, editor. *The COST simulation Benchmark: description and simulator manual*. European Communities, 2002.
- J.B. Copp, U. Jeppsson, and C. Rosen. Towards an ASM1-ADM1 state variable interface for plant-wide wastewater treatment modeling. In *Proceedings of the Water Environment Federation Conference WEFTEC 2003*, Los Angeles, California, USA, 11-15 October 2003.
- R. Dams. *Beginselen van de analytische scheikunde*. Syllabus. Universiteit Gent, 1996.
- A. Dapena-Mora, S.W.H. Van Hulle, J.L. Campos, R. Méndez, P.A. Vanrolleghem, and M. Jetten. Enrichment of anammox biomass from municipal activated sludge: experimental and modelling results. *Journal of Chemical Technology and Biotechnology*, 79:1421–1428, 2004.
- B. De heyder, P.A. Vanrolleghem, H. Van Langenhove, and W. Verstraete. Kinetic characterisation of mass transfer limited degradation of a poorly water soluble gas in batch experiments. necessity for multiresponse fitting. *Biotechnology and Bioengineering*, 55:511–519, 1997.
- G.A. Ekama, M.C. Wentzel, and R.E. Loewenthal. Integrated chemical-physical processes kinetic modelling of multiple mineral precipitation problems. In *Proceedings of the IWA conference on nutrient management in wastewater treatment processes and recycle streams*, pages 225–233, Krakow, Poland, 19-21 September 2005.
- C.T.M.J. Frijters, S. Vellinga, T. Jorna, and R. Mulder. Extensive nitrogen removal in a new type of airlift reactor. *Water Science and Technology*, 41(4-5):469–476, 2000.
- C. Fux, K. Lange, A. Faessler, P. Huber, B. Grueniger, and H. Siegrist. Nitrogen removal from digester supernatant via nitrite - SBR or SHARON? *Water Science and Technology*, 48(8):9–18, 2003.
- J.M. Garrido, J.L. Campos, R. Méndez, and J.M. Lema. Nitrous oxide production by nitrifying biofilms in a biofilm airlift suspension reactor. *Water Science and Technology*, 36(1):157–163, 1997a.
- J.M. Garrido, W.A.J. van Benthum, M.C.M. van Loosdrecht, and J.J. Heijnen. Influence of dissolved oxygen concentration on nitrite accumulation in a biofilm airlift suspension reactor. *Biotechnology and Bioengineering*, 53:168–178, 1997b.

- K.V. Gernaey, C. Rosen, L. Benedetti, and U. Jeppsson. Phenomenological modeling of wastewater treatment plant influent disturbance scenarios. In *Proceedings of the 10th International Conference on Urban Drainage*, Copenhagen (Denmark), 21-26 August 2005.
- W. Ghyyoot, S. Vandaele, and W. Verstraete. Nitrogen removal from sludge reject water with a membrane-assisted bioreactor. *Water Research*, 33(1):23–32, 1999.
- H.J. Gijzen and A. Mulder. The nitrogen cycle out of balance. *Water* 21, 8:38–40, 2001.
- J.K. Hale. *Oscillations in nonlinear systems*. McGraw-Hill, 1963.
- X. Hao, J.J. Heijnen, and M.C.M. van Loosdrecht. Model-based evaluation of temperature and inflow variations on a partial nitrification-anammox biofilm process. *Water Research*, 36:4839–4849, 2002a.
- X.-D. Hao, M.C.M. van Loosdrecht, and J.J. Heijnen. Sensitivity analysis of a biofilm model describing a one-stage completely autotrophic nitrogen removal (CANON) process. *Biotechnology and Bioengineering*, 77(3):266–277, 2002b.
- H.C. Helgeson. Complex dissociations in aqueous solution at elevated temperatures. *Journal of Physical Chemistry*, 71(10):3121–3136, 1967. cited by Loewenthal:1989.
- C. Hellinga, A.A.J.C. Schellen, J.W. Mulder, M.C.M. van Loosdrecht, and J.J. Heijnen. The SHARON process: An innovative method for nitrogen removal from ammonium-rich waste water. *Water Science and Technology*, 37(9):135–142, 1998.
- C. Hellinga, M.C.M. van Loosdrecht, and J.J. Heijnen. Model based design of a novel process for nitrogen removal from concentrated flows. *Mathematical and Computer Modelling of Dynamical Systems*, 5 (4):351–371, 1999.
- C. Helmer, S. Kunst, S. Juretschko, M.C. Schmid, K-H. Schleifer, and M. Wagner. Nitrogen loss in a nitrifying biofilm system. *Water Science and Technology*, 39(7):13–21, 1999.
- C. Helmer-Madhok, M. Schmid, E. Filipov, T. Gaul, A. Hippen, K.-H. Rosenwinkel, C.F. Seyfried, M. Wagner, and S. Kunst. Deammonification in biofilm systems: population structure and function. *Water Science and Technology*, 46(1-2):223–231, 2002.

- M. Henze, W. Gujer, T. Mino, and M. van Loosdrecht. *Activated Sludge Models ASM1, ASM2, ASM2d and ASM3*. IWA Scientific and Technical Report No. 9. IWA Publishing, London, U.K., 2000.
- A. Hippen, K.-H. Rosenwinkel, G. Baumgarten, and C.F. Seyfried. Aerobic deammonification: A new experience in the treatment of wastewaters. *Water Science and Technology*, 35(10):111–120, 1997.
- A. Hippen, C. Helmer, S. Kunst, K.-H. Rosenwinkel, and C.F. Seyfried. Six years' practical experience with aerobic/anoxic deammonification in biofilm systems. *Water Science and Technology*, 44(2-3):39–48, 2001.
- H.M. Janus and H.F. van der Roest. Don't reject the idea of treating reject water. *Water Science and Technology*, 35(10):27–34, 1997.
- U. Jeppsson. Aeration energy and mixing energy for BSM1, BSM1_LT and BSM2. 3 September, 2005.
- U. Jeppsson, J. Comas, and D. Aguado. Minutes from the IWA task group on Benchmarking, TG meeting no. 3, 2005.
- U. Jeppsson, C. Rosen, J. Alex, J. Copp, K.V. Gernaey, M.-N. Pons, and P.A. Vanrolleghem. Towards a benchmark simulation model for plant-wide control strategy performance evaluation of WWTPs. *Water Science and Technology*, 53(1):287–295, 2006.
- M.S.M. Jetten, M. Strous, K.T. van de Pas-Schoonen, J. Schalk, U.G.J.M. van Dongen, A.A. Van De Graaf, S. Logemann, G. Muyzer, M.C.M. van Loosdrecht, and J.G. Kuenen. The anaerobic oxidation of ammonium. *FEMS Microbiology Reviews*, 22:421–437, 1999.
- R.M. Jones and I. Takacs. Importance of anaerobic digestion modeling on predicting the overall performance of wastewater treatment plants. In *Proceedings anaerobic digestion 2004, 10th world congress*, pages 1371–1375, Montréal, Canada, 29 August–2 September 2004.
- D.W. Jordan and P. Smith. *Nonlinear ordinary differential equations*. Oxford University Press, 1977.
- S.G. Karsson. Experience with the SBR process at the Linköping WWTP. In *Proceedings conference on upgrading for nitrogen and phosphorus removal*, Eslöv, Sweden, 4–5 May 1994. Cited by Siegrist (1996).

- P. Kos. Short SRT (solids retention time) nitrification process/flow-sheet. *Water Science and Technology*, 38(1):23–29, 1998.
- L. Kuai and W. Verstraete. Ammonium removal by the Oxygen-Limited Autotrophic Nitrification-Denitrification system. *Applied and Environmental Microbiology*, 64(11):4500–4506, 1998.
- G. Ladiges and N.-P. Bertram. Optimisation of Hamburg's WWTPs – three years of experience with the new concept. *Water Science and Technology*, 50(7):45–48, 2004.
- F. Laurich. Combined quantity management and biological treatment of sludge liquor at Hamburg's WWTPs. First experience in operation with the Store And Treat process. *Water Science and Technology*, 50(7):49–52, 2004.
- F. Laurich and C. Günner. The 'Store And Treat' process for sludge liquor management. *Water Science and Technology*, 47(12):269–275, 2003.
- S.F.W. Lochman. *Proceskeuze en -optimalisatie van het SHARON proces voor slibverwerkingsbedrijf Sluisjesdijk*. Afstudeerverslag beroepsopleiding biotechnologie. TU Delft, 1995.
- A. Magri, L. Corominas, H. Lopez, E. Campos, M. Balaguer, J. Colprim, and X. Flotats. A model for the simulation of the SHARON process: pH as a key factor. In *Proceedings IWA conference on nutrient management (BNR)*, Krakow, Poland, 19-21 September 2005.
- J. Meirlaen, B. Huyghebaert, F. Sforzi, L. Benedetti, and P.A. Vanrolleghem. Fast, simultaneous simulation of the integrated urban wastewater system using mechanistic surrogate models. *Water Science and Technology*, 43(8):301–310, 2001.
- A. Mulder. The quest for sustainable nitrogen removal technologies. *Water Science and Technology*, 48(1):67–75, 2003.
- A. Mulder, A.A. van de Graaf, L.A. Robertson, and J.G. Kuenen. Anaerobic ammonium oxidation discovered in a denitrifying fluidized bed reactor. *FEMS Microbiology Ecology*, 16:177–184, 1995.
- J.W. Mulder, M.C.M. van Loosdrecht, C. Hellinga, and R. van Kempen. Full scale application of the SHARON process for treatment of rejection water of digested sludge dewatering. *Water Science and Technology*, 43(11):127–134, 2001.

- A. Muller, M.C. Wentzel, R.E. Loewenthal, and G.A. Ekama. Heterotrophic anoxic yield in anoxic aerobic activated sludge systems treating municipal wastewater. *Water Research*, 37:2435–2441, 2003.
- R.H. Perry and D.W. Green, editors. *Perry's chemical engineer's handbook*. McGraw-Hill, 1984.
- K. Pynaert, B.F. Smets, S. Wyffels, D. Beheydt, S.D. Siciliano, and W. Verstraete. Characterization of an autotrophic nitrogen-removing biofilm from a highly loaded lab-scale rotating biological contactor. *Applied and Environmental Microbiology*, 69:3626–3635, 2003.
- C.W. Randall and D. Buth. Nitrite build-up in activated sludge resulting from temperature effects. *Journal of the WPCF*, 56:1039–1044, 1984.
- P. Reichert, D. Borchardt, M. Henze, W. Rauch, P. Shanahan, L. Somlyódy, and P.A. Vanrolleghem. *River Water Quality Model No. 1*. IWA Scientific and Technical Report No. 12. IWA Publishing, London, U.K., 2001.
- B. Rosén and C. Huijbregsen. The ScanDeNi process could turn an existing under-performing activated sludge plant into an asset. *Water Science and Technology*, 47(11):31–36, 2003.
- C. Rosén, D. Vrecko, K.V. Gernaey, and U. Jeppsson. Implementing ADM1 for benchmark simulations in Matlab/Simulink. *Water Science and Technology*, page Accepted, 2006.
- S. Salem, D. Berends, J.J. Heijnen, and M.C.M. van Loosdrecht. Model-based evaluation of a new upgrading concept for N-removal. *Water Science and Technology*, 45(6):169–176, 2002.
- S. Salem, D. Berends, J.J. Heijnen, and M.C.M. van Loosdrecht. Bio-augmentation by nitrification with return sludge. *Water Research*, 37:1794–1804, 2003.
- S. Salem, M.S. Moussa, and M.C.M. van Loosdrecht. Determination of the decay rate of nitrifying bacteria. *Biotechnology and Bioengineering*, In press, 2006.
- M. Sbarciog, E.I.P. Volcke, M. Loccupier, and E. Noldus. Stability boundaries of a SHARON bioreactor model with multiple equilibrium points. *Nonlinear Dynamics and System Theory*, To appear, 2006.

- H Siegrist. Nitrogen removal from digester supernatant – comparison of chemical and biological methods. *Water Science and Technology*, 34 (1-2):399–406, 1996.
- A.O. Sliemers, K. Third, W. Abma, J.G. Kuenen, and M.S.M. Jetten. CANON and Anammox in a gas-lift reactor. *FEMS Microbiology Letters*, 218:339–344, 2003.
- STOWA. Het gecombineerde Sharon-Anammox proces: een duurzame methode voor N-verwijdering uit slibgistingwater. Rapport 2000-25, STOWA, Utrecht, Nederland, 2000.
- M. Strous, J.J. Heijnen, J.G. Kuenen, and M.S.M. Jetten. The sequencing batch reactor as a powerful tool for the study of slowly growing anaerobic ammonium-oxidizing microorganisms. *Applied Microbiology and Biotechnology*, 50:589–596, 1998.
- M. Strous, J.G. Kuenen, and M.S.M. Jetten. Key physiology of anaerobic ammonium oxidation. *Applied and Environmental Microbiology*, 65: 3248–3250, 1999.
- M. Strous, J.G. Kuenen, Fuerst J.A., M. Wagner, and M.S.M. Jetten. The anammox case - a new experimental manifesto for microbiological eco-physiology. *Antonie van Leeuwenhoek*, 81:693–702, 2002.
- W. Stumm and J.J. Morgan. *Aquatic chemistry*. Environmental science and technology. Wiley-Interscience, 1996.
- R. Stüven and E. Bock. Nitrification and denitrification as a source for NO and NO₂ production in high-strength wastewater. *Water Research*, 35(8):1905–1914, 2001.
- G. Tchobanoglous and F.L. Burton. *Metcalf & Eddy wastewater engineering - treatment, disposal and reuse*. Series in Water resources and environmental engineering. McGraw-Hill, 1991.
- R. van der Lans. *Advanced course on environmental biotechnology. Chapter 21: Gas-liquid interphase transport*. Syllabus. Biotechnological sciences Delft Leiden, 2000.
- U. van Dongen, M.S.M. Jetten, and M.C.M. van Loosdrecht. The SHARON-Anammox process for treatment of ammonium rich wastewater. *Water Science and Technology*, 44(1):153–160, 2001.

- S.W.H. Van Hulle. *Modelling, simulation and optimization of autotrophic nitrogen removal processes*. PhD thesis, Ghent University, Faculty of Bio-engineering. 2005. In Dutch.
- S.W.H. Van Hulle, E.I.P. Volcke, J.L. Teruel, B. Donckels, M.C.M. van Loosdrecht, and P.A. Vanrolleghem. Influence of temperature and pH on the kinetics of the SHARON nitrification process. In *Proceedings 4th IWA World Water Congress*, pages (on CD-ROM), Marrakech, Morocco, September 19-24 2004.
- S.W.H. Van Hulle, U. Zaher, G. Schelstraete, and P.A. Vanrolleghem. Titrimetric monitoring of a completely autotrophic nitrogen removal process. *Water Science and Technology*, 53(4-5):in press, 2006.
- R. van Kempen, J.W. Mulder, C.A. Uijterlinde, and M.C.M. van Loosdrecht. Overview: full scale experience of the SHARON-process for treatment of rejection water of digested sludge dewatering. *Water Science and Technology*, 44(1):145–152, 2001.
- M.C.M. van Loosdrecht and S. Salem. Biological treatment of sludge digester liquids. *Water Science and Technology*, Submitted, 2006.
- P.A. Vanrolleghem and S. Gillot. Robustness and economic measures and control benchmark performance criteria. *Water Science and Technology*, 45(4-5):117–126, 2002.
- P.A. Vanrolleghem, C. Rosen, U. Zaher, J. Copp, L. Benedetti, E. Ayesa, and U. Jeppsson. Continuity-based interfacing of models for wastewater systems described by peterson matrices. *Water Science and Technology*, 52(1-2):493–500, 2005.
- D. Vrecko and K.V. Gernaey. Proposed evaluation criteria for the BSM2. Benchmark internal report, 9 September 2005.
- D. Vrecko, K.V. Gernaey, C. Rosen, and U. Jeppsson. Benchmark simulation model no. 2 in Matlab-Simulink: towards plant-wide WWTP control strategy evaluation. In *IWA World Water Congress and Exhibition*, Beijing, China, 10-14 September 2006. Accepted.
- A. Warakomski, R. van Kempen, and M.C.M. van Loosdrecht. Operating experience in the netherlands with a high rate process for total nitrogen control sharon at rotterdam and utrecht. In *Proc. New England Environment Association Conference*, U.S., 28 January 2003.

- B. Wett and J. Alex. Impacts of separate rejection water treatment on the overall plant performance. *Water Science and Technology*, 48(4): 139–146, 2003.
- B. Wett, R. Rostek, W. Rauch, and K. Ingerle. pH-controlled reject-water-treatment. *Water Science and Technology*, 37(12):165–172, 1998.
- U. Wiesmann. *Advances in biochemical engineering/biotechnology*, volume 51, pages 113–154. Springer-Verlag, Berlin, 1994.
- S. Wyffels, K. Pynaert, P. Boeckx, W. Verstraete, and O. Van Cleemput. Identification and quantification of nitrogen removal in a rotating biological contactor by ^{15}N tracer techniques. *Water Research*, 37(6): 1252–1259, 2003.
- S. Wyffels, P. Boeckx, K. Pynaert, D. Zhang, O. Van Cleemput, G. Chen, and W. Verstraete. Nitrogen removal from sludge reject water by the two-stage oxygen-limited autotrophic nitrification denitrification process. *Water Science and Technology*, 49(5-6):57–64, 2004a.
- S. Wyffels, S. Van Hulle, P. Boeckx, E. Volcke, O. Van Cleemput, P. Vanrolleghem, and W. Verstraete. Modelling and simulation of oxygen-limited partial nitritation in a membrane-assisted bioreactor (MBR). *Biotechnology and Bioengineering*, 86(5):531–542, 2004b.
- U. Zaher, P. Grau, L. Benedetti, E. Ayesa, and P.A. Vanrolleghem. Transformers for interfacing anaerobic digestion models to pre- and post-treatment processes. *Environmental Modelling and Software*, In press, 2006.

Appendices

Appendix A

Equilibrium constants

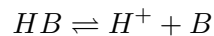
In this appendix, first a definition of equilibrium constants is given. In particular, the difference between absolute and relative equilibrium constants is pointed out. Afterwards, the temperature effect on equilibrium constants is illustrated for the ammonium/ammonia and nitrous acid/nitrite equilibria taken up in the SHARON model.

A.1 Definition of equilibrium constants

The definitions given in this section are based on Dams (1996). Activity coefficients have been replaced with concentrations, an approximation that is essentially only correct for infinitely diluted solutions.

A.1.1 Absolute equilibrium constants

Consider the equilibrium¹



The absolute acidity constant of HB is defined as

$$K_{a,HB}^{abs} = \frac{C_{H^+} \cdot C_B}{C_{HB}}$$

while the absolute basicity constant of B equals

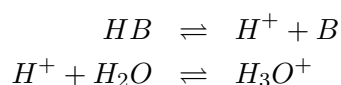
$$K_{b,B}^{abs} = \frac{C_{HB}}{C_{H^+} \cdot C_B} = \frac{1}{K_{a,HB}^{abs}}$$

¹Possible charge of HB and B is not written explicitly

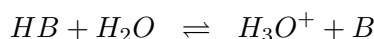
These absolute equilibrium constants don't have a practical use. It makes more sense to define equilibrium constants in comparison with the solution medium, i.e. water.

A.1.2 Relative equilibrium constants in water

Interaction of an acid with water (acting as a base):



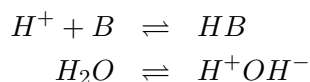
leads to the overall reaction



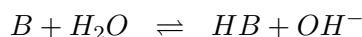
The (relative) acidity constant of an acid HB in water is defined as

$$K_{a,HB} = \frac{C_{H_3O^+} \cdot C_B}{C_{HB}}$$

Interaction of a base with water (acting as an acid):



leads to the overall reaction



from which the (relative) basicity constant of B results as

$$K_{b,B} = \frac{C_{HB}}{C_{OH^-} \cdot C_B}$$

Consequently, between acidity and basicity constants in water, the following relationship holds:

$$K_{a,HB} \cdot K_{b,B} = C_{H_3O^+} \cdot C_{OH^-} = K_w \approx 10^{-14}$$

It is important to note that pH is defined as

$$pH = -\log_{10} H_3O^+ \quad (\text{A.1})$$

although, for reasons of simplicity, it is mostly written as

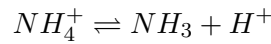
$$pH = -\log_{10} H^+$$

A.2 Temperature dependency of equilibria in the SHARON model

Equilibrium constants depend on temperature, while they are independent of pH or pressure. The temperature dependency of the ammonium/ammonia equilibrium and the nitrous acid/nitrite equilibrium is illustrated below.

A.2.1 The ammonium/ammonia equilibrium

The equilibrium constants (in water) for the ammonium/ammonia equilibrium



are defined as

$$K_{a,NH_4^+} = \frac{C_{H_3O^+} \cdot C_{NH_3}}{C_{NH_4^+}} = \frac{K_w}{K_{b,NH_3}} \quad (A.2)$$

Anthonisen et al. (1976) give the following relationship for the temperature dependency of the equilibrium constant:

$$K_{a,NH_4^+} = \exp\left(\frac{-6344}{T}\right) \quad (A.3)$$

with K_{a,NH_4^+} expressed in mole liter⁻¹ and T in Kelvin. A lumped component, TNH , is defined for which the concentration equals the total concentration of ammonium and ammonia:

$$C_{TNH} = C_{NH_3} + C_{NH_4^+} \quad (A.4)$$

From Eqs. A.1, A.2 and A.4, the fraction of the total ammonium present in the form of free ammonia, can be expressed as

$$\frac{C_{NH_3}}{C_{TNH}} = \frac{1}{1 + 10^{pK_{a,NH_4^+} - pH}} \quad (A.5)$$

This fraction is directly dependent on the pH and dependent on temperature through Eq. A.3. The relationship is illustrated in Figure A.1. Note that a temperature increase of 20°C leads to free ammonium concentrations that are 3 to 4 times higher.

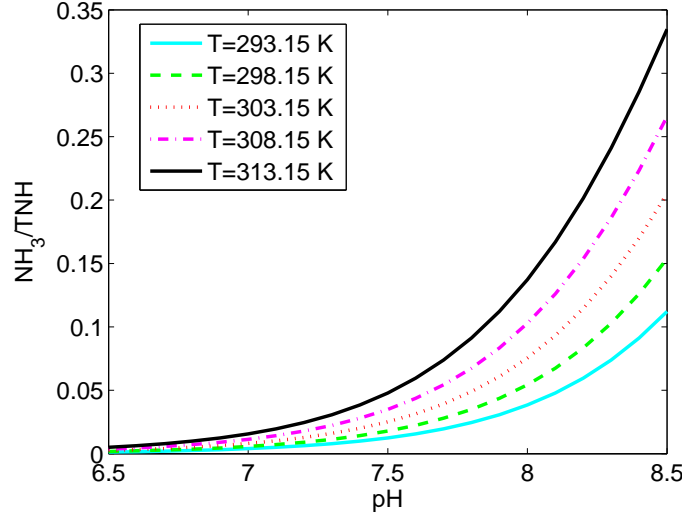
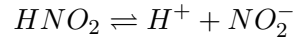


Figure A.1: Free ammonia fraction in function of pH and temperature

A.2.2 The nitrous acid/nitrite equilibrium

The equilibrium constants (in water) for the nitrous acid/nitrite equilibrium



are defined as

$$K_{a,HNO_2} = \frac{C_{H_3O^+} \cdot C_{NO_2^-}}{C_{HNO_2}} = \frac{K_w}{K_{b,NO_2^-}} \quad (A.6)$$

Anthonisen et al. (1976) give the following relationship for the temperature dependency of the equilibrium constant:

$$K_{a,HNO_2} = \exp\left(\frac{-2300}{T}\right) \quad (A.7)$$

with K_{a,HNO_2} expressed in mole liter⁻¹ and T in Kelvin. A lumped component, TNO_2 , is defined for which the concentration equals the total concentration of nitrous acid (HNO_2) and nitrite (NO_2^-):

$$C_{TNO_2} = C_{HNO_2} + C_{NO_2^-} \quad (A.8)$$

From Eqs. A.1, A.6 and A.8, the fraction of the total nitrite present in the form of nitrous acid, can be expressed as

$$\frac{C_{HNO_2}}{C_{TNO_2}} = \frac{1}{1 + 10^{pH - pK_{a,HNO_2}}} \quad (\text{A.9})$$

This fraction is directly dependent on the pH and dependent on temperature through Eq. A.7. The relationship is illustrated in Figure A.2.

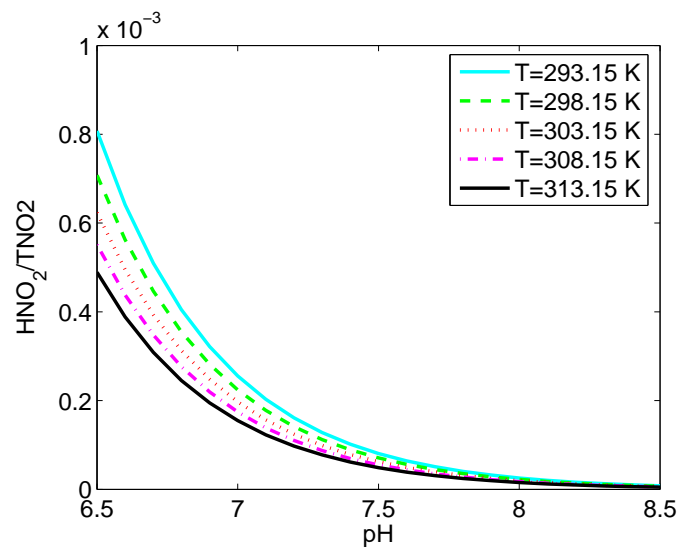


Figure A.2: Free nitrous acid fraction in function of pH and temperature

Appendix B

Source code of Simulink c-mex function for pH calculation

This appendix lists the source code for the Simulink c-mex function for calculation of the pH and equilibrium concentrations (see section 3.4.2). More explanation is given in between text, as code documentation.

```
/*
 * pHeqdisc.c
 */

/*
 * To run this function in Simulink:
 * - create an S-function block
 *   Sfunction name: pHeqdisc
 *   Sfunction parameters: EquiInit
 * - type 'mex pHeqdisc.c' in Matlab command window to create
 * .dll file
 * (make sure this file is in the same directory as model)
 */

#define S_FUNCTION_NAME pHeqdisc
#define S_FUNCTION_LEVEL 2

/*
 * Need to include simstruc.h for the definition of the
 * SimStruct and its associated macro definitions.
 */
#include "simstruc.h"
```

274 Source code of Simulink c-mex function for pH calculation

```
#define Cinit(S) ssGetSFcnParam(S,0)

/* Error handling
 * -----
 *
 * You should use the following technique to report errors
 * encountered within an S-function:
 *
 *     ssSetErrorStatus(S,"Error encountered due to ...");
 *     return;
 *
 * Note that the 2nd argument to ssSetErrorStatus must be
 * persistent memory. It cannot be a local variable.
 * For example the following will cause
 * unpredictable errors:
 *
 *     mdlOutputs()
 *     {
 *         char msg[256];
 *         {ILLEGAL: to fix use "static char msg[256];"}
 *         sprintf(msg,"Error due to %s", string);
 *         ssSetErrorStatus(S,msg);
 *         return;
 *     }
 *
 * See matlabroot/simulink/src/sfuntmpl_doc.c for more details.
 */

/*=====
 * S-function methods *
 *=====*/

/* Function: mdlInitializeSizes =====
 * Abstract:
 *     The sizes information is used by Simulink to determine
 *     the S-function block's characteristics (
 *     number of inputs, outputs, states, etc.).
 */
static void mdlInitializeSizes(SimStruct *S)
{
    /* See sfuntmpl_doc.c for more details on macros below */

    ssSetNumSFcnParams(S, 1); /* Number of expected parameters */
    if (ssGetNumSFcnParams(S) != ssGetSFcnParamsCount(S)) {
        /* Return if number of expected
         * != number of actual parameters */
        return;
    }
}
```

```

ssSetNumContStates(S, 0);
ssSetNumDiscStates(S, 10);

if (!ssSetNumInputPorts(S, 1)) return;
ssSetInputPortWidth(S, 0, 12);
/*(S, port index, port width)*/
/* ssSetInputPortRequiredContiguous(S, 0, false);*/
/*Signal elements entering the specified port must occupy
 * contiguous areas of memory
 * This allows a method to access the elements of the signal
 * simply by incrementing the signal pointer
 * returned by ssGetInputPortSignal*/

/*
 * Set direct feedthrough flag (1=yes, 0=no).
 * A port has direct feedthrough if the input is used in
 * either mdlOutputs or mdlGetTimeOfNextVarHit functions.
 * See matlabroot/simulink/src/sfuntmpl_directfeed.txt.
 */
ssSetInputPortDirectFeedThrough(S, 0, 0);

if (!ssSetNumOutputPorts(S, 1)) return;
ssSetOutputPortWidth(S, 0, 10);

ssSetNumSampleTimes(S, 1); /* ?? */

/* ssSetNumRWork(S, 0); */
/* ssSetNumIWork(S, 0); */
/* ssSetNumPWork(S, 0); */
/* ssSetNumModes(S, 0); */
/* ssSetNumNonsampledZCs(S, 0); */

ssSetOptions(S, SS_OPTION_EXCEPTION_FREE_CODE);
/* p3 sfuntmpl_doc*/
}

/* Function: mdlInitializeSampleTimes =====
 * Abstract:
 * This function is used to specify the sample time(s) for your
 * S-function. You must register the same number of
 * sample times as specified in ssSetNumSampleTimes.
 */
static void mdlInitializeSampleTimes(SimStruct *S)
{
    ssSetSampleTime(S, 0, INHERITED_SAMPLE_TIME);
    /* executes whenever driving block executes */
}

```

276 Source code of Simulink c-mex function for pH calculation

```
        ssSetOffsetTime(S, 0, 0.0);

    }

#define MDL_INITIALIZE_CONDITIONS
/* Change to #undef to remove function */
#if defined(MDL_INITIALIZE_CONDITIONS)
    /* Function: mdlInitializeConditions =====
     * Abstract:
     *   In this function, you should initialize the continuous
     *   and discrete states for your S-function block.
     *   The initial states are placed in the state vector,
     *   ssGetContStates(S) or ssGetRealDiscStates(S).
     *   You can also perform any other initialization
     *   activities that your S-function may require.
     *   Note, this routine will be called at the start of
     *   simulation and if it is present in an enabled subsystem
     *   configured to reset states, it will be called when the
     *   enabled subsystem restarts execution to reset the
     *   states
     */
    static void mdlInitializeConditions(SimStruct *S)
    {
        real_T *x0 = ssGetDiscStates(S); /*x0 is pointer*/
        int_T lp;
        /* get the real_T continuous state vector */
        /* can also be used in mdlstart, misschien beter*/

        for (lp=0;lp<10;lp++)
        {
            x0[lp] = mxGetPr(Cinit(S))[lp];
        }

        /* The initial conditions are passed in as the
         * first S-function parameter */
    }
#endif /* MDL_INITIALIZE_CONDITIONS */

#undef MDL_START /* Change to #undef to remove function */
#if defined(MDL_START)
    /* Function: mdlStart =====
     * Abstract:
     *   This function is called once at start of
     *   model execution. If you have states that should be
     *   initialized once, this is the place to do it.
    */

```

```
    */
    static void mdlStart(SimStruct *S)
    {
    }
#endif /* MDL_START */

/* Function: mdlOutputs =====
 * Abstract:
 *   In this function, you compute the outputs of your
 *   S-function block. Generally outputs are placed
 *   in the output vector, ssGetY(S).
 */
static void mdlOutputs(SimStruct *S, int_T tid)
{
    real_T      *y      = ssGetOutputPortRealSignal(S,0);
    real_T      *x      = ssGetDiscStates(S);
    int_T i;

    /* UNUSED_ARG(tid); not used in single tasking mode */

    for (i=0; i<10; i++)
    {
y[i] = x[i];
/* state variables are passed on as output variables */
    }
}

/* The following functions
 * are used in MdlUpdate
 * and thus need to be defined before */

static real_T Gap(SimStruct *S)
{
    real_T      *x      = ssGetDiscStates(S);
    InputRealPtrsType uPtrs = ssGetInputPortRealSignalPtrs(S,0);
    static real_T TNO2,TNH,TIC,TIP,NO3,Zplus;
    static real_T Kw,KeCO2,KeHCO3,KeHNO2,KeNH4,KeH2PO4;

    Kw      = *uPtrs[0];
    KeNH4   = *uPtrs[1];
    KeHNO2  = *uPtrs[2];
    KeCO2   = *uPtrs[3];
    KeHCO3  = *uPtrs[4];
    KeH2PO4 = *uPtrs[5];
    TNH     = *uPtrs[6];
    TNO2    = *uPtrs[7];
```

278 Source code of Simulink c-mex function for pH calculation

```
TIC      = *uPtrs[8];
TIP      = *uPtrs[9];
NO3      = *uPtrs[10];
Zplus    = *uPtrs[11];

if (TIC<=1E-15)
{
TIC=1E-15;
}

x[6] = TIC/(1+KeHCO3/x[0]+x[0]/KeCO2); /*HCO3*/
x[7] = TIC/(1+x[0]/KeHCO3+x[0]*x[0]/KeHCO3/KeCO2); /*CO3*/
x[4] = TNO2*KeHNO2/(x[0]+KeHNO2); /*NO2*/
x[1] = TNH*x[0]/(x[0]+KeNH4); /*NH4*/
x[8] = TIP*x[0]/(KeH2PO4+x[0]); /*H2PO4*/
x[9] = TIP-x[8]; /*HPO4*/

return x[0]-Kw/x[0]+x[1]-x[4]-x[6]-2*x[7]-x[8]-2*x[9]
      -NO3+Zplus ;
}

static real_T dGapdH(SimStruct *S)
{
    real_T      *x      = ssGetDiscStates(S);
    InputRealPtrsType uPtrs = ssGetInputPortRealSignalPtrs(S,0);
    static real_T TNO2,TNH,TIC,TIP, NO3,Zplus;
    static real_T Kw,KeCO2,KeHCO3,KeHNO2,KeNH4,KeH2PO4;
    static real_T DNH4,DNO2,DTIC,DTIP;

    Kw      = *uPtrs[0];
    KeNH4   = *uPtrs[1];
    KeHNO2  = *uPtrs[2];
    KeCO2   = *uPtrs[3];
    KeHCO3  = *uPtrs[4];
    KeH2PO4 = *uPtrs[5];
    TNH     = *uPtrs[6];
    TNO2    = *uPtrs[7];
    TIC     = *uPtrs[8];
    TIP     = *uPtrs[9];
    NO3     = *uPtrs[10];
    Zplus   = *uPtrs[11];

    if (TIC<=1E-15)
    {
TIC=1E-15;
    }

    DNH4    = x[0]+KeNH4;
    DNO2    = x[0]+KeHNO2;
    DTIC    = x[0]*x[0]+x[0]*KeCO2+KeHCO3*KeCO2;
```

```

DTIP   = KeH2PO4+x[0];

return 1+Kw/x[0]/x[0]
      +TNH*KeNH4/(DNH4*DNH4)
      +TNO2*KeHNO2/(DNO2*DNO2)
      +TIC*KeCO2*(x[0]*x[0]+4*x[0]*KeHCO3+KeCO2*KeHCO3)
      /(DTIC*DTIC)
      +TIP*KeH2PO4/(DTIP*DTIP);
}

static void NewtonRaphson(SimStruct *S)
{
  real_T      *x      = ssGetDiscStates(S);
  InputRealPtrsType uPtrs = ssGetInputPortRealSignalPtrs(S,0);
  real_T      delta;
  static real_T H0;
  static int_T i;
  static const real_T TOL      =1E-12;
  static const real_T MaxSteps= 1000;

  H0=x[0];

  i  =1;
  delta = 1.0;
  while ( (delta>TOL || delta < -TOL) && (i<=MaxSteps) )
  {
    delta=Gap(S);
    x[0]=H0-delta/dGapdH(S);
    if (x[0]<=0)
    { x[0]=1E-12;
    }
    H0  =x[0];
    ++i;
  }
}

#define MDL_UPDATE /* Change to #undef to remove function */
#if defined(MDL_UPDATE)
/* Function: mdlUpdate =====
* Abstract:
*   This function is called once for every major
*   integration time step.
*   Discrete states are typically updated here, but this
*   function is useful for performing any tasks that
*   should only take place once per integration step.
*/

```

280 Source code of Simulink c-mex function for pH calculation

```
static void mdlUpdate(SimStruct *S, int_T tid)
{
real_T      *x      = ssGetDiscStates(S);
    InputRealPtrsType uPtrs = ssGetInputPortRealSignalPtrs(S,0);

    x[0]=1E-12;
    NewtonRaphson(S);
    x[3]= *uPtrs[7]-x[4];      /* HNO2 */
    x[2]= *uPtrs[6]-x[1];      /* NH3 */
    x[5]= *uPtrs[8]-x[6]-x[7]; /* CO2 */
}
#endif /* MDL_UPDATE */

#undef MDL_DERIVATIVES
/* Change to #undef to remove function */
#if defined(MDL_DERIVATIVES)
/* Function: mdlDerivatives =====
 * Abstract:
 *   In this function, you compute the
 *   S-function block's derivatives.
 *   The derivatives are placed in the derivative vector,
 *   ssGetdX(S).
 */
static void mdlDerivatives(SimStruct *S)
{

}
#endif /* MDL_DERIVATIVES */

/* Function: mdlTerminate =====
 * Abstract:
 *   In this function, you should perform any actions
 *   that are necessary
 *   at the termination of a simulation.
 *   For example, if memory was allocated
 *   in mdlStart, this is the place to free it.
 */
static void mdlTerminate(SimStruct *S)
{
}

/*=====
 * Required S-function trailer *
 *=====*/
```

```
#ifndef MATLAB_MEX_FILE
/* Is this file being compiled as a MEX-file? */
#include "simulink.c"
/* MEX-file interface mechanism */
#else
#include "cg_sfun.h"
/* Code generation registration function */
#endif
```


Appendix C

Boundaries for the state variables of the SHARON model for constant pH

In this appendix, upper and lower boundaries are calculated for the state variables of the SHARON reactor model, used in chapter 4, both under dynamic and equilibrium conditions.

C.1 Upper and lower boundaries for the state variables under dynamic conditions

C.1.1 Boundaries for x_1

From Eq. 4.6, one sees that

$$\begin{aligned}x_1 = 0 &\Rightarrow \dot{x}_1 = u_0 \cdot u_1 \geq 0 \\x_1 = u_1 &\Rightarrow \dot{x}_1 = -a \cdot \rho_1 - b \cdot \rho_2 \leq 0\end{aligned}$$

Consequently

$$x_{1,min} = 0 \tag{C.1}$$

$$x_{1,max} = u_1 \tag{C.2}$$

C.1.2 Boundaries for x_3

From Eq. 4.9, one sees that

$$x_3 = u_3 \Rightarrow \dot{x}_3 \geq 0$$

so

$$x_{3,min} = u_3 \quad (C.3)$$

An upper boundary for the reaction rate ρ_1 , (Eq. 4.13), is found as

$$\rho_1 \leq \hat{a}_1 \cdot x_3 \quad (C.4)$$

with

$$\hat{a}_1 \triangleq a_1 \cdot \frac{x_{1,max}}{b_1 + x_{1,max}} = a_1 \cdot \frac{u_1}{b_1 + u_1} \quad (C.5)$$

taking into account the maximum value for x_1 (Eq. C.2 or Eq. C.16 in case of equilibrium conditions, here giving the same result).

Substituting Eq. C.4 in Eq. 4.8 and assuming

$$u_0 > \hat{a}_1 \quad (C.6)$$

a maximum value for x_3 is derived as

$$x_{3,max} = \frac{u_0 \cdot u_3}{u_0 - \hat{a}_1} \quad (C.7)$$

Note that a less stringent (higher value of the) upper boundary for ρ_1 than Eq. C.4 is obtained as

$$\rho_1 \leq a_1 \cdot x_3 \quad (C.8)$$

since

$$\frac{u_1}{b_1 + u_1} \leq 1$$

C.1.3 Boundaries for x_2

From Eq. 4.7, one sees that

$$x_2 = 0 \quad \Rightarrow \quad \dot{x}_2 = u_0 \cdot u_2 + c \cdot \rho_1 \geq 0$$

so

$$x_{2,min} = 0 \quad (C.9)$$

Substituting Eq. C.4 in Eq. 4.7, a maximum value for x_2 is derived as

$$x_{2,max} = u_2 + \frac{c}{u_0} \cdot \hat{a}_1 \cdot x_{3,max} \quad (C.10)$$

For $x_{3,max}$, one can use Eq. C.7 or, in case of equilibrium conditions, its maximum equilibrium value Eq. C.18.

C.1.4 Boundaries for x_4

From Eq. 4.9, one sees that

$$x_4 = u_4 \quad \Rightarrow \quad \dot{x}_4 \geq 0$$

so

$$x_{4,min} = u_4 \quad (C.11)$$

An upper boundary for the reaction rate ρ_2 (Eq. 4.14) results as

$$\rho_2 \leq a_2 \cdot m_1 \cdot m_2 \cdot x_4 \quad (C.12)$$

in which m_1 and m_2 are defined by Eqs. 4.56 and 4.57

Substituting Eq. C.12 in Eq. 4.9 and assuming

$$u_0 > a_2 \cdot m_1 \cdot m_2 \quad (C.13)$$

a maximum value for x_4 is derived as

$$x_{4,max} = \frac{u_0 \cdot u_4}{u_0 - a_2 \cdot m_1 \cdot m_2} \quad (C.14)$$

Note that a less stringent (higher value of the) upper boundary for ρ_2 than Eq. C.12 is obtained as

$$\rho_2 \leq a_2 \cdot x_4 \quad (C.15)$$

since

$$m_1 \leq 1 \quad \text{and} \quad m_2 \leq 1$$

C.2 Upper boundaries for the state variables under equilibrium conditions

From Eq. 4.19 results that

$$u_0 \cdot (u_1 - x_{e1}) \geq 0$$

Consequently, the upper boundary for x_{e1} is

$$x_{e1,max} = u_1 \quad (C.16)$$

which is the same value as obtained for the upper boundary in case of dynamic conditions (Eq. C.2).

Elimination of ρ_{e1} from Eq. 4.19 and Eq. 4.20 results in (for $u_0 \neq 0$)

$$u_0 \cdot (u_2 - x_{e2}) + \frac{c}{a} \cdot u_0 \cdot (u_1 - x_{e1}) - \left(\frac{b \cdot c}{a} + d \right) \cdot \rho_2(\mathbf{x}_e) = 0$$

$$\Rightarrow u_2 - x_{e2} + \frac{c}{a} \cdot (u_1 - x_{e1}) \geq 0$$

Consequently, the upper boundary for x_{e2} is (taking into account $x_{e1} > 0$)

$$x_{e2,max} = u_2 + \frac{c}{a} \cdot u_1 \quad (\text{C.17})$$

From Eqs. 4.62, C.1 and C.17 on the one hand and Eqs. 4.63, C.1 and C.9 on the other hand, upper boundaries for x_{e3} and x_{e4} respectively result as:

$$x_{e3,max} = u_3 + \frac{u_1}{a} \quad (\text{C.18})$$

$$x_{e4,max} = u_4 + \frac{c \cdot u_1 + a \cdot u_2}{a \cdot d + b \cdot c} \quad (\text{C.19})$$

Appendix D

The Anammox reactor model

This appendix briefly describes the Anammox reactor model, that has been used for the simulations described in this thesis. The model stoichiometry and kinetics have been adopted from Hao et al. (2002b) and Van Hulle (2005, Chapter 3.2, sections 3.1-3.3). The Anammox reactor has been modelled as a CSTR with retention of particulates and the resulting model has been implemented in Matlab-Simulink.

D.1 State variables and mass balances

The Anammox model is based on the Activated Sludge Model No. 1 (ASM1) (Henze et al., 2000), completed with two-step nitrification-denitrification and an Anammox reaction, on the basis of Hao et al. (2002b), Van Hulle (2005, Chapter 3.2, sections 3.1-3.3) and Dapena-Mora et al. (2004).

Table D.1 lists the state variables of the Anammox model. Note that insoluble components are given the symbol X , while soluble components are denoted by S .

The Anammox reactor is modelled as a CSTR with a fixed volume. Soluble components are not retained in the reactor, so their outgoing concentration equals their reactor concentration. Insoluble components are retained in the reactor to a given fraction, R_X . Consequently the corresponding mass balances read as:

$$\frac{dS_i}{dt} = \frac{\Phi}{V} \cdot (S_i^{in} - S_i) + r_i \quad (\text{D.1})$$

$$\frac{dX_i}{dt} = \frac{\Phi}{V} \cdot (X_i^{in} - (1 - R_X) \cdot X_i) + r_i \quad (\text{D.2})$$

Table D.1: State variables of the Anammox model

Symbol	Description	Unit
S_O	oxygen	$\text{g O}_2 \text{ m}^{-3}$
S_S	readily biodegradable substrate	g COD m^{-3}
S_{NH}	total ammonium	g N m^{-3}
S_{NO2}	total nitrite	g N m^{-3}
S_{NO3}	nitrate	g N m^{-3}
S_{N2}	nitrogen gas	g N m^{-3}
X_H	heterotrophic biomass	g COD m^{-3}
X_{NH}	ammonium oxidizers	g COD m^{-3}
X_{NO}	nitrite oxidizers	g COD m^{-3}
X_{AN}	Anammox biomass	g COD m^{-3}
X_S	slowly biodegradable substrate	g COD m^{-3}
X_P	particulate products from biomass decay	g COD m^{-3}
S_{alk}	alkalinity	mole m^{-3}

Analogously as for the SHARON model, the volumetric conversion rate of a component i , r_i , is calculated from the process rates ρ_j as

$$r_i = \sum_{j=1}^{11} A_{ij} \cdot \rho_j \quad (\text{D.3})$$

D.2 Biological conversion reactions

Table D.2 summarizes the model's stoichiometric matrix. The corresponding process rates are given in Table D.3. In contrast to Dapena-Mora et al. (2004) and Van Hulle (2005), nitrite inhibition of Anammox bacteria has been taken into account. Note that, unlike Hao et al. (2002b) who used the endogenous respiration concept, biomass decay is modelled according the death-regeneration concept (Henze et al., 2000, ASM1). In this way, the observed activity of heterotrophs in Anammox reactors, without COD being present in the influent, can be simulated.

Table D.2: Stoichiometric (Petersen) matrix of the Anammox model

j	Process	State variables						
		S_O	S_S	S_{NH}	S_{NO_2}	S_{NO_3}	S_{N_2}	
1	Growth of X_H on O_2	$-\frac{1-Y_{H,O}}{Y_{H,O}}$	$-\frac{1}{Y_{H,O}}$	$-i_{NXB}$				
2	Growth of X_H on NO_2^-		$-\frac{1}{Y_{H,NO_2}}$	$-i_{NXB}$	$-\frac{1-Y_{H,NO_2}}{1.71 \cdot Y_{H,NO_2}}$		$\frac{1-Y_{H,NO_2}}{1.71 \cdot Y_{H,NO_2}}$	
3	Growth of X_H on NO_3^-		$-\frac{1}{Y_{H,NO_3}}$	$-i_{NXB}$	$\frac{1-Y_{H,NO_3}}{1.14 \cdot Y_{H,NO_3}}$	$-\frac{1-Y_{H,NO_3}}{1.14 \cdot Y_{H,NO_3}}$		
4	Growth of X_{NH}	$-\frac{3.43-Y_{NH,O}}{Y_{NH,O}}$		$-\frac{1}{Y_{NH,O}} - i_{NXB}$	$\frac{1}{Y_{NH,O}}$			
5	Growth of X_{NO}	$-\frac{1.14-Y_{NO,O}}{Y_{NO,O}}$		$-i_{NXB}$	$-\frac{1}{Y_{NO,O}}$	$\frac{1}{Y_{NO,O}}$		
6	Growth of X_{AN}			$-\frac{1}{Y_{AN}} - i_{NXAN}$	$-1.52 - \frac{1}{Y_{AN}}$	1.52	$\frac{2}{Y_{AN}}$	
7	Decay of X_H			$i_{NXB} - f_P \cdot i_{NXP}$				
8	Decay of X_{NH}			$i_{NXB} - f_P \cdot i_{NXP}$				
9	Decay of X_{NO}			$i_{NXB} - f_P \cdot i_{NXP}$				
10	Decay of X_{AN}			$i_{NXAN} - f_P \cdot i_{NXP}$				
11	Hydrolysis		1					
		X_H	X_{NH}	X_{NO}	X_{AN}	X_S	X_P	S_{atk}
1	Growth of X_H on O_2	1						$-\frac{i_{NXB}}{14}$
2	Growth of X_H on NO_2^-	1						$\frac{1}{14} \cdot \left(-i_{NXB} + \frac{1-Y_{H,NO_2}}{1.71 \cdot Y_{H,NO_2}} \right)$
3	Growth of X_H on NO_3^-	1						$-\frac{i_{NXB}}{14}$
4	Growth of X_{NH}		1					$-\frac{1}{14} \cdot \left(\frac{2}{Y_{NH,O}} + i_{NXB} \right)$
5	Growth of X_{NO}			1				$-\frac{i_{NXB}}{14}$
6	Growth of X_{AN}				1			$-\frac{i_{NXAN}}{14}$
7	Decay of X_H	-1				$1 - f_P$	f_P	$\frac{1}{14} \cdot (i_{NXB} - f_P \cdot i_{NXP})$
8	Decay of X_{NH}	-1				$1 - f_P$	f_P	$\frac{1}{14} \cdot (i_{NXB} - f_P \cdot i_{NXP})$
9	Decay of X_{NO}		-1			$1 - f_P$	f_P	$\frac{1}{14} \cdot (i_{NXB} - f_P \cdot i_{NXP})$
10	Decay of X_{AN}			-1		$1 - f_P$	f_P	$\frac{1}{14} \cdot (i_{NXAN} - f_P \cdot i_{NXP})$
11	Hydrolysis						-1	

Table D.3: Kinetic rate expressions for the Anammox model

$\rho_1 = \mu_H^{max} \cdot \frac{S_O}{K_{O,H} + S_O} \cdot \frac{S_S}{K_{S,H} + S_S} \cdot X_H$
$\rho_2 = \mu_H^{max} \cdot \eta_{NO_2} \cdot \frac{K_{O,H}}{K_{O,H} + S_O} \cdot \frac{S_{NO_2}}{K_{NO_2,H} + S_{NO_2}} \cdot \frac{S_{NO_2}}{S_{NO_2} + S_{NO_3}} \cdot \frac{S_S}{K_{S,H} + S_S} \cdot X_H$
$\rho_3 = \mu_H^{max} \cdot \eta_{NO_3} \cdot \frac{K_{O,H}}{K_{O,H} + S_O} \cdot \frac{S_{NO_3}}{K_{NO_3,H} + S_{NO_3}} \cdot \frac{S_{NO_3}}{S_{NO_2} + S_{NO_3}} \cdot \frac{S_S}{K_{S,H} + S_S} \cdot X_H$
$\rho_4 = \mu_{NH}^{max} \cdot \frac{S_O}{K_{O,NH} + S_O} \cdot \frac{S_{NH}}{K_{NH,NH} + S_{NH}} \cdot X_{NH}$
$\rho_5 = \mu_{NO}^{max} \cdot \frac{S_O}{K_{O,NO} + S_O} \cdot \frac{S_{NO_2}}{K_{NO_2,NO} + S_{NO_2}} \cdot X_{NO}$
$\rho_6 = \mu_{AN}^{max} \cdot \frac{K_{I,O,AN}}{K_{I,O,AN} + S_O} \cdot \frac{S_{NO_2}}{K_{NO_2,AN} + S_{NO_2} + \frac{S_{NO_2}^2}{K_{I,NO_2,AN}}} \cdot \frac{S_{NH}}{K_{NH,AN} + S_{NH}} \cdot X_{AN}$
$\rho_7 = -b_H \cdot X$
$\rho_8 = -b_{NH} \cdot X$
$\rho_9 = -b_{NO} \cdot X$
$\rho_{10} = -b_{AN} \cdot X$
$\rho_{11} = k_H \cdot \frac{\frac{X_S}{X_H}}{K_X + \frac{X_S}{X_H}} \cdot X_H$

Table D.4 lists the stoichiometric parameter values that have been used in this work. Most parameter values have been adopted from Hao et al. (2002b) and Van Hulle (2005). A slightly different value has been used for the nitrogen content of biomass, i_{NXB} to ensure consistency with the values used in the Benchmark Simulation Model (BSM), in view of the plant-wide simulation study described in Chapter 7. Details on the calculation of the nitrogen content for Anammox biomass, i_{NXAN} , are given in Chapter 6.

Literature values for kinetic parameters that are temperature dependent, are often given for temperatures that differ from the one at which the Anammox process is operated (typically 30°C). The temperature dependency of a kinetic parameter k is taken into account by means of an Arrhenius relationship:

$$k(T) = k(T_1) \cdot e^{(\theta_T \cdot (T - T_1))} \quad (D.4)$$

in which θ_T is either calculated as

$$\theta_T = \frac{\ln(k(T_1)/k(T_2))}{T_1 - T_2} \quad (D.5)$$

Table D.4: Stoichiometric parameter values for the Anammox model

Parameter	Description	Value	Unit	Reference
$Y_{H,O}$	heterotrophic yield on oxygen	0.67	gCOD gCOD ⁻¹	Henze et al. (2000) (ASM1)
Y_{H,NO_3}	heterotrophic yield on nitrate	0.54	gCOD gCOD ⁻¹	Muller et al. (2003)
Y_{H,NO_2}	heterotrophic yield on nitrite	0.54	gCOD gCOD ⁻¹	adapted from Muller et al. (2003)
Y_{AN}	Anammox biomass yield	0.159	gCOD gN ⁻¹	Strous et al. (1998)
$Y_{NH,O}$	yield of ammonium oxidizers	0.15	gCOD gN ⁻¹	Wiesmann (1994)
$Y_{NO,O}$	yield of nitrite oxidizers	0.041	gCOD gN ⁻¹	Wiesmann (1994)
f_P	fraction particulates produced from biomass decay	0.08	gCOD gCOD ⁻¹	Henze et al. (2000) (ASM1)
i_{NXP}	nitrogen fraction of particulates	0.06	gN gCOD ⁻¹	Henze et al. (2000) (ASM1)
i_{NXB}	nitrogen fraction of biomass (except Anammox)	0.08	gN gCOD ⁻¹	Copp et al. (2003) (BSM1)
i_{NXAN}	nitrogen fraction of Anammox biomass	0.0562	gN gCOD ⁻¹ (see Chapter 6)	for composition $CH_2O_{0.5}N_{0.15}P_{0.024}$

in case values for the kinetic parameter are given at two different temperatures T_1 and T_2 (Henze et al., 2000), or as

$$\theta_T = \frac{E_a}{R \cdot T_1 \cdot T} \quad (\text{D.6})$$

in case a value for the kinetic parameter is given at a temperature T_1 and at the same time the activation energy of the corresponding reaction (E_a , in J mole⁻¹) is known (Hao et al., 2002a). Table D.5 summarizes the values for temperature dependent kinetic values. The values of the remaining kinetic parameters of the Anammox model, that were assumed independent of temperature, are given in Table D.6

Table D.5: Calculation of the values of temperature dependent kinetic parameters at 35°C according to Eqs. D.4 and D.5 or D.6. All parameters are expressed in d^{-1} , except for K_X that has no dimension.

Parameter	Description	Value at 10°C	Value at 20°C	E_a [kJ·mol ⁻¹]	Value at 35°C
μ_H^{max}	maximum growth rate of heterotrophs	3 ^a	6 ^a	—	16.97
μ_{NH}^{max}	maximum growth rate of ammonium oxidizers	—	0.80 ^b	68 ^c	3.11
μ_{NO}^{max}	maximum growth rate of nitrite oxidizers	—	0.79 ^b	44 ^c	1.90
μ_{AN}^{max}	maximum growth rate of Anammox organisms	—	0.019 ^d	70 ^c	0.0769
b_H	heterotrophic decay rate	—	0.62 ^a	82 ^a	3.18
b_{NH}	decay rate of ammonium oxidizers	—	0.05 ^b	68 ^f	0.1944
b_{NO}	decay rate of nitrite oxidizers	—	0.033 ^b	44 ^f	0.0795
b_{AN}	decay rate of Anammox organisms	—	0.0025 ^e	70 ^f	0.0101
k_H	maximum hydrolysis rate	1 ^a	3 ^a	—	15.59
K_X	saturation constant for slowly biodegradable substrate	0.01 ^a	0.03 ^a	—	0.1559

^a Henze et al. (2000) (ASM1)

^b Wiesmann (1994)

^c Jetten et al. (1999)

^d Strous et al. (1998)

^e Dapena-Mora et al. (2004)

^f assumed equal as for corresponding growth rate

Table D.6: Values of temperature independent kinetic parameters

Parameter	Description	Value	Unit	Reference
$K_{O,H}$	oxygen affinity constant for heterotrophs	0.2	$\text{g O}_2 \text{ m}^{-3}$	Henze et al. (2000) (ASM1)
$K_{S,H}$	substrate affinity constant for heterotrophs	20	g COD m^{-3}	Henze et al. (2000) (ASM1)
$K_{NO_3,H}$	nitrate affinity constant for heterotrophs	0.5	g N m^{-3}	Henze et al. (2000) (ASM3)
$K_{NO_2,H}$	nitrite affinity constant for heterotrophs	0.5	g N m^{-3}	Henze et al. (2000) (ASM3)
$K_{O,NH}$	oxygen affinity constant for ammonium oxidizers	0.6	$\text{g O}_2 \text{ m}^{-3}$	Wiesmann (1994)
$K_{NH,NH}$	ammonium affinity constant for ammonium oxidizers	0.75	g N m^{-3}	Van Hulle et al. (2004)
$K_{O,NO}$	oxygen affinity constant for nitrite oxidizers	1.5	$\text{g O}_2 \text{ m}^{-3}$	Wiesmann (1994)
$K_{NO_2,NO}$	nitrite affinity constant for nitrite oxidizers	5.5	g N m^{-3}	Wiesmann (1994)
$K_{NH,AN}$	ammonium affinity constant for Anammox bacteria	0.07	g N m^{-3}	Strous et al. (1999)
$K_{NO_2,AN}$	nitrite affinity constant for Anammox bacteria	0.05	g N m^{-3}	Strous et al. (1999)
$K_{I,O,AN}$	oxygen inhibition constant for Anammox bacteria	0.01	$\text{g O}_2 \text{ m}^{-3}$	Strous et al. (1999)
$K_{I,NO_2,AN}$	oxygen inhibition constant for Anammox bacteria	15	g N m^{-3}	Strous et al. (1999)
η_{NO_3}	anoxic reduction factor	0.6	—	Henze et al. (2000) (ASM3)
η_{NO_2}	anoxic reduction factor	0.6	—	Henze et al. (2000) (ASM3)

Curriculum vitae

Personal particulars

Eveline Irma Paula Volcke
° Oostende, 29 June 1976

eveline.volcke@biomath.ugent.be

Belgian

married to Bart Moeyersoon (on 14 January 2002)

mother of Kamiel Moeyersoon (° 26 October 2004)

Basic education

1994-1999

Faculty of engineering, Ghent University, Belgium

chemical engineer ('burgerlijk scheikundig ingenieur')

graduated on 9 July 1999 magna cum laude

Extra training

PhD training in Applied Biological sciences

('Doctoraatsopleiding in de Toegepaste Biologische Wetenschappen')

Ghent University, certificate obtained on 19 November 2003

Advanced course on environmental biotechnology

Kluyver Laboratory for Biotechnology, Delft University of Technology

21-30 June 2000

Modern control and automation techniques

(‘Moderne regel- en automatiseringstechnieken’)

Institute for permanent education (IVPV), Ghent University

January-June 2000, certificate obtained on 6 November 2000

Employment

15 August – 15 December 1999

Ghent University, Department of Biochemical and Microbial Technology, Laboratory for Microbial Ecology and Technology (LabMET).

- Research on the possible application of subcritical gasification of wastewater sludge in order to improve the efficiency of subsequent anaerobic digestion.

From 1 February 2000

Ghent University, Department of Applied Mathematics, Biometrics and Process Control, BIOMATH.

Research and teaching assistant:

- Research in view of obtaining PhD degree: ‘Modelling, analysis and control of partial nitrification in a SHARON reactor’.
- Teaching support for courses (partim exercises): Modelling and simulating biosystems (‘Modelleren en simuleren van biosystemen’), Process control (‘Procesregeling’) and Bioprocess control (‘Bioprocessregeling’), among others.
- Supervision of master thesis students, as (co-)supervisor (5) or second promoter (2).

Research stays abroad

3 – 28 November 2003 and 30 August – 7 October 2005

Delft University of Technology (TU Delft),

Department of Biotechnology.

Funding obtained through FWO (scientific research fund Flanders).

Publications

Papers in international journals with reading committee

Volcke E.I.P., van Loosdrecht M.C.M. and Vanrolleghem P.A. (2006). Continuity-based model interfacing for plant-wide simulation: a general approach. *Water Research*, *accepted*.

Sbarciog M., **Volcke E.I.P.**, Loccufier M. and Noldus E.J.L. (2006). Stability conditions and stability boundaries of a SHARON bioreactor model with multiple equilibrium points. *Nonlinear Dynamics and Systems Theory*, *accepted*.

Volcke E.I.P., van Loosdrecht M.C.M. and Vanrolleghem P.A. (2006). Controlling the nitrite:ammonium ratio in a SHARON reactor in view of its coupling with an Anammox process. *Water Science and Technology*, *53(4-5)*, *in press*.

Van Hulle S.W.H., Van Den Broeck S., Maertens J., Villez K., Donckels B.M.R., Schelstraete G., **Volcke E.I.P.** and Vanrolleghem P.A. (2005). Construction, start-up and operation of a continuously aerated laboratory-scale SHARON reactor in view of coupling with an Anammox reactor. *Water SA*, *31*, 327-334.

Volcke E.I.P., Van Hulle S.W.H., Donckels B.M.R., van Loosdrecht M.C.M. and Vanrolleghem P.A. (2005). Coupling the SHARON process with Anammox: Model-based scenario analysis with focus on operating costs. *Water Science and Technology*, *52(4)*, 107-115.

Wyffels S., Van Hulle S.W.H., Boeckx P., **Volcke E.I.P.**, Van Cleemput O., Vanrolleghem P.A. and Verstraete W. (2004). Modeling and simulation of oxygen-limited partial nitrification in a membrane-assisted bioreactor (MBR). *Biotechnology & Bioengineering*, *86(5)* 531-542.

Volcke E.I.P., Villez K., Van Hulle S.W.H., van Loosdrecht M.C.M. and Vanrolleghem P.A. (2004). Wat met rejectiewater? *Afvalwaterwetenschap*, *3(4)*, 297-318.

Verstraete W., Doulami F., **Volcke E.**, Tavernier M., Nollet H. and Roels J. (2002). The importance of anaerobic digestion for global environmental development. *J. Environ. Syst. and Eng., JSCE*, No. 706/VII-23, 97-102, 2002.

Jetten M., Schmid M., Schmidt I., Wubben M., van Dongen U., Abma W., Sliemers O., Revsbech N.P., Beaumont B., Ottosen L., **Volcke E.**

Laanbroek H.J., Campos-Gomez J.L., Cole J., van Loosdrecht M., Mulder J.W., Fuerst J., Richardson D., van de Pas K., Mendez-Pampin R., Third K., Cirpus I., van Spanning R., Nielsen L.P., Op den Camp H., Schultz C., Gundersen J., Vanrolleghem P., Strous M., Wagner M. and Kuenen J.G. (2002). Improved nitrogen removal by application of new nitrogen-cycle bacteria. *Re/Views in Environmental Science & Bio/Technology*, 1, 51-63.

Volcke E.I.P., Clement L., Van De Steene M. and Vanrolleghem P.A. (2001). An overview of the posters presented at Watermatex 2000. II. Sensor/monitoring, control and decision support systems. *Water Science and Technology*, 43(7), 381-386.

Papers in journals without reading committee

Van Den Broeck S., **Volcke E.**, Van Hulle S. and Vanrolleghem P. (2004). 'Kortsluiting leidt tot efficiënte stikstofverwijdering'. *Het ingenieursblad*, 1-2, February 2004.

Papers in conference proceedings

Volcke E.I.P., Gernaey K.V., Vrecco D., Jeppsson U., van Loosdrecht M.C.M. and Vanrolleghem P.A. (2006). Plant-wide (BSM2) evaluation of reject water treatment with a SHARON-Anammox process. *Accepted as a platform paper for oral presentation at the 'IWA biennial conference'*, Beijing (China), 10-15 September 2006.

Villez K., Rosén C., **Volcke E.I.P.** and Vanrolleghem P.A. (2005). PLS-based supervisory control of the SHARON process. *Proc. ICA conference*, Busan (Korea), 29 May-2 June 2005, 895-903.

Van Hulle S.W.H., **Volcke E.I.P.**, López Teruel J., Donckels B., van Loosdrecht M.C.M., and Vanrolleghem P.A. (2004). Influence of temperature and pH on the kinetics of the SHARON nitrification process. *Proc. 4th IWA World Water Congress, Marrakech (Morocco), 19-24 September 2004*, 8 pages (CD-ROM).

Van Hulle S.W.H., **Volcke E.I.P.**, López Teruel J., Donckels B., van Loosdrecht M.C.M. and Vanrolleghem P.A. (2004). The effect of temperature and pH on the kinetics of a partial nitrification process. *Proc. 10th PhD Symposium on Applied Biological Sciences*, Gent, 29 September 2004. *Comm. Appl. Biol. Sci.*, Ghent University, 69(2), 11-14.

Van Hulle S.W.H., Van Den Broeck S., Maertens J., Villez K., Schelstraete G., **Volcke E.I.P.** and Vanrolleghem P.A. (2003). Practical experiences with start-up and operation of a continuously aerated lab-scale SHARON reactor. *Proc. 17th Forum for Applied Biotechnology, Gent*, 18-19 September 2003. *Comm. Appl. Biol. Sci.*, Ghent University, 68(2a), 77-84.

Volcke E.I.P., Van Hulle S.W.H., van Loosdrecht M.C.M. and Vanrolleghem P.A. (2003). Generation of Anammox-optimal nitrite:ammonium ratio with SHARON process: usefulness of process control? *Proc. 9th IWA Specialised Conference on Design, Operation and Economics of Large Wastewater Treatment Plants (poster papers)*. Prague (Czech Republik), 1-4 September, 55-58.

Van Broekhoven E., **Volcke E.**, Georgieva O., De Baets B. (2003). A Mamdani-Assilian controller for the last phase of an operation switch on a distillation unit. In: T. Bilgiç, B. De Baets, and O. Kaynak, editors, *Proc. 10th IFSA World Congress*, 313-317, Istanbul (Turkey), 2003.

Volcke E.I.P., van Loosdrecht M.C.M. and Vanrolleghem P.A. (2002). Influence of operating parameters on the performance of a continuously aerated SHARON reactor. *Proc. 8th PhD Symposium on Applied Biological Sciences, Gent*, 9 October 2002. *Med. Fac. Landbouww. Univ. Gent*, 67(4), 209-212.

Volcke E.I.P., Gillot S. and Vanrolleghem P.A. (2002). Multi-criteria evaluation of control strategies for wastewater treatment processes. *Proc. of the 15th IFAC Triennial World Congress (b'02)*, 21-26 July 2002, Barcelona (Spain), 6 pages.

Volcke E.I.P., Hellinga C., Van Den Broeck S., van Loosdrecht M.C.M. and Vanrolleghem P.A. (2002). Modelling the SHARON process in view of coupling with Anammox. *Proc. 1st IFAC International Scientific and Technical Conference on Technology, Automation and Control of Wastewater and Drinking Water Systems (TiASWiK'02)*, Gdansk-Sobieszewo (Poland), 19-21 June, 65-72.

Abstracts in conference proceedings

Volcke E.I.P., Loccufier M., Vanrolleghem P.A. and Noldus E.J.L. (2004). Existence, uniqueness and stability of the equilibrium points of a SHARON bioreactor model. *Book of Abstracts 23rd Benelux Meeting on Systems and Control*. Helvoirt (The Netherlands), 17-19 March 2004.

Van Hulle S.W.H., **Volcke E.I.P.** and Vanrolleghem P.A. (2004). Simulation of start up and operation of autotrophic nitrogen removal processes. *Proc. IWA conference on upgrading of wastewater treatment plants*. Amsterdam (The Netherlands), 30 September-1 October 2004.

Vanrolleghem P.A., Van Hulle S.W.H., **Volcke E.I.P.** and Sin G.. Modeling, control and optimization of autotrophic nitrogen removal (2004). *Proc. EU 5th framework IcoN symposium on Anammox*. Ghent (Belgium), 21-23 January 2004.

Internal reports

Volcke E.I.P., Van Hulle S.W.H., Deksissa T., Zaher U. and Vanrolleghem P.A. (2005). Calculation of pH and concentration of equilibrium components during dynamic simulation by means of a charge balance. *Biomath technical report*, Ghent University, 61 pages.

Available on http://biomath.ugent.be/~peter/pub_rpirt.html

Sin G., Van Hulle S.W.H., **Volcke E.I.P.** and Vanrolleghem P.A. (2001). Activated sludge model no. 1 extended with Anammox and Sharon processes. *Biomath Technical Report*, Ghent University, 18 pages.

MSc thesis

Volcke E. (1999). *Simulatie van een reverse flow reactor voor de verwijdering van VOS uit afoalgassen*. Scriptie ingediend tot het behalen van de academische graad van burgerlijk scheikundig ingenieur. Vakgroep Technische Chemie en Milieutechniek, Universiteit Gent, 170 pages. Promotor: prof. dr. ir. J. Defrancq.